ABSTRACT

MUELLER MATRIX SPECTROSCOPIC ELLIPSOMETRY OF MULTIFERROICS

by
Roman Basistyy

Multiferroics, materials which possess several ferroic orders, are the focus of research in recent years. Among these materials are oxide crystals, such as, for example, RMnO$_3$, RMn$_2$O$_5$, R_3Fe$_5$O$_{12}$, where R stands for rare earth ions. The most fascinating physics occurs when magnon-lattice coupling reveals itself in the far-IR spectra of multiferroics. The expected optical behavior puts multiferroics into a more general category of bi-anisotropic materials, the properties of which could be only described using anisotropic dielectric $\hat{\varepsilon}(\omega)$, magnetic $\hat{\mu}(\omega)$, and magnetoelectric $\hat{\alpha}(\omega)$, $\hat{\alpha}'(\omega)$ tensors. In the first part of this thesis, general approaches for investigation of optical spectra of bulk and multilayer bi-anisotropic structures are shown. Analytical solutions for the optical spectra of certain crystal symmetries are derived for multilayer structures with both magnetic and magnetoelectric interactions.

The second part of the thesis contains analysis of the experimental data. Initially, Mueller matrix spectroscopic ellipsometry is reviewed. Analysis for optical spectra measured for isotropic Dy$_3$Fe$_5$O$_{12}$ is given, for which contributions from magnetic and electric excitations are identified and the absence of strong magneto-electric effects is explained. In comparison, anisotropic orthorhombic perovskite ME- material, TbMnO$_3$, with a spiral spin structure is investigated and contributions from coupling of different ferroic orders are shown in the far-IR Mueller matrix spectra of electromagnon excitations. Detail studies of optical properties of hexagonal multiferroic oxides RMnO$_3$,

(R = Ho, Er, Tm, Yb, and Lu), are studied in the far-infrared spectral range between 100 and 2000 cm^{-1} and temperatures between 1.5 K and 300 K by means of several experimental techniques: Muller matrix spectroscopic ellipsometry, rotating analyzer ellipsometry, and optical transmission spectroscopy. Spectra of the optical phonons are described in terms of the temperature dependencies of their frequency, damping, and oscillator strength. For all studies, oxide materials' clear signatures of the spin-phonon interaction are found below the temperature of the antiferromagnetic phase transition T_N due to magnetic ordering of Mn^{3+} spins. A decrease of the ionic radius for R^{3+} ions between Ho^{3+} and Lu^{3+} in the corresponding RMnO$_3$ compounds result in systematic variation of the frequency for several optical phonons. A magnetic excitation at ~190 cm^{-1} is observed at low temperatures below T_N and interpreted as resulting from two-magnon absorption.

MUELLER MATRIX SPECTROSCOPIC ELLIPSOMETRY OF MULTIFERROICS

by
Roman Basistyy

A Dissertation
Submitted to the Faculty of
New Jersey Institute of Technology and
Rutgers, The State University of New Jersey - Newark
in Partial Fulfillment of the Requirements for the Degree of
Doctor of Philosophy in Applied Physics

Federated Department of Physics

January 2015

.

APPROVAL PAGE

MUELLER MATRIX SPECTROSCOPIC
ELLIPSOMETRY OF MULTIFERROICS

Roman Basistyy

Dr. Andrei A. Sirenko, Dissertation Advisor Professor of Applied Physics, NJIT	Date

Dr. Michael Kotelyanskii, Dissertation Co-Advisor Senior Executive, Rudolph Technologies, Inc.	Date

Dr. John F. Federici, Committee Member Distinguished Professor of Applied Physics, NJIT	Date

Dr. Martin Schaden, Committee Member Associate Professor of Applied Physics, Rutgers-Newark	Date

Dr. Tao Zhou, Committee Member Associate Professor of Applied Physics, NJIT	Date

Dr. Ken Ahn, Committee Member Assistant Professor of Applied Physics, NJIT	Date

Dr. Vitaly Shneidman, Committee Member Senior Lecturer, NJIT	Date

BIOGRAPHICAL SKETCH

Author: Roman Basistyy

Degree: Doctor of Philosophy

Date: January 2015

Undergraduate and Graduate Education:

- Doctor of Philosophy in Applied Physics,
  New Jersey Institute of Technology, Newark, NJ, 2015

- Master of Science in Electronics and Microelectronics
  Saint-Petersburg Electro-Technical University, Saint-Petersburg, Russia, 2010

- Bachelor of Science in Electronics and Microelectronics,
  Saint-Petersburg Electro-Technical University, Saint-Petersburg, Russia, 2008

Major: Applied Physics

Presentations and Publications:

R. Basistyy, T.N. Stanislavchuk, A.A. Sirenko, A.P. Litvinchuk, M. Kotelyanskii, G.L. Carr, N. Lee, X. Wang, S-W Cheong, "Infrared-active optical phonons and magnetic excitations in the hexagonal manganites $RMnO_3$ (R = Ho, Er, Tm, Yb, and Lu) ", Physical Review B **90**, 024307 (2014).

T.N. Stanislavchuk, T.D. Kang, P.D. Rogers, E. C. Standard, R. Basistyy, A.M. Kotelyanskii, G. Nita, T. Zhou, G.L. Carr, M. Kotelynskii, and A.A. Sirenko, "Synchrotron radiation-based far-infrared spectroscopic ellipsometer with full Mueller Matrix capability," Rev. Sci. Instrum. **84**, 023901 (2013).

R. Basistyy, T.N. Stanislavchuk, A.A. Sirenko, A.P. Litvinchuk, M. Kotelyanskii, G.L. Carr, N. Lee, X. Wang, S-W Cheong, "Ellipsometry studies of the optical phonons in hexagonal manganites $RMnO_3$," American Physical Society (APS) March Meeting, Denver, CO (2014).

ACKNOWLEDGMENT

I would like to thank my advisors, Dr. Andrei Sirenko and Dr. Michael Kotelyanskii for their guidance and support throughout all aspects of my research and dissertation, and committee members: Dr. John Federici, Dr. Martin Schaden, Dr. Ken Ahn, Dr. Tao Zhou and Dr. Vitaly Shneidman.

I would like to thank T.Stanislavchuk for help with measurements, S.-W. Cheong for samples and P. Rogers for help with theory and software development.

TABLE OF CONTENTS

TABLE OF CONTENTS
(Continued)

LIST OF TABLES

LIST OF FIGURES

Figure   **Page**

Figure **Page**

Figure   **Page**

LIST OF SYMBOLS

MM	Mueller Matrix
SE	Spectroscopic Ellipsometry
MMSE	Mueller Matrix Spectroscopic Ellipsometry
ME	Magneto-electric
AOSM	Adjusted Oscillator Strength Matching
RHS	Right Hand Side
LHS	Left Hand Side
DFT	Density Functional Theory
AOI	Angle of Incident
IR	Infrared
PSG	Polarization State Generator
PSA	Polarization State Analyzer
R-IG	Rare Earth Iron Garnett
RAE	Rotating Analyzer Ellipsometry
RCE	Rotating Compensator Ellipsometry
SHO	Simple Harmonic Oscillator
AFM	Antiferromagnetic
TO	Transverse Optical
LO	Longitudinal Optical
c	Speed of Light in Vacuum

CHAPTER 1

MULTIFERROICS AND METAMATERIALS

This chapter is a literature review for the optical properties of multiferroics and other groups of bi-anisotropic optical materials, such as metamaterials. The main source of information is from recent review articles References [1,2,3,4,5].
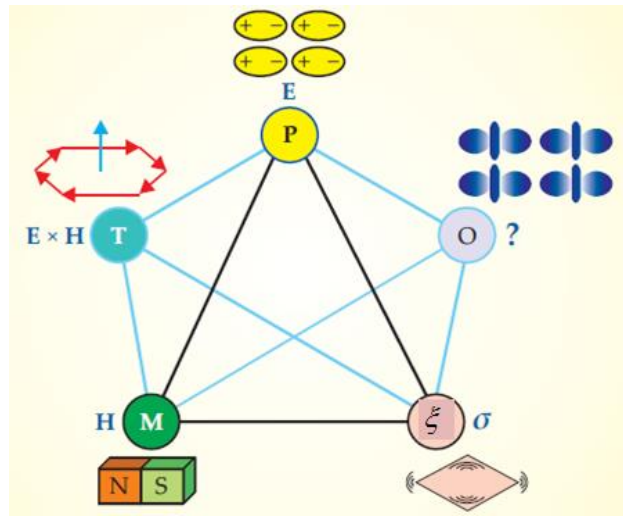
Figure 1.1 Interactions in multiferroics. The established primary ferroic orderings: ferroelectricity P, ferromagnetism M, ferroelasticity ξ can be switched by their conjugate electric E, magnetic H, and stress σ fields. Cross coupling allows those ferroic orderings to be also tuned by fields other than their conjugates; in magnetoelectric multiferroics, for example, E can modify M. Physicists are also exploring the possibility of ferrotoroidics, a promising new ferroic ordering of toroidal moments T, which should be switchable by crossed electric and magnetic fields. The symbol "O" represents other possibilities – such as spontaneous switchable orbital ordering, vortices, and chirality. *Source:*[2].

It is always useful to have materials which allow controlling light propagation based on their unique intrinsic properties. An additional possibility to control the reflected or transmitted light by means of application of external electric and magnetic fields to such materials becomes even more important [8,9,10]. The general class of such materials is called bi-anisotropic. There are many commonly known optical effects in bi-anisotropic

medium such as polarization plane rotation, Kerr effect, Faraday effect, negative index of refraction [4,5]. This bi-anisotropic behavior can be found in materials called multiferroics, which combine several ferroic orders, such as ferroelectric (appearance of electrical polarization), (anti)ferromagnetic (appearance of magnetic polarization), and ferroelastic (appearance of strain). Typical interactions in multiferroics are shown in Figure 1.1. Either electric field E, magnetic field H, or stress σ can control the electric polarization P, magnetization M, and strain ξ. Another class of bi-anisotropic materials includes man-made artificial structures, or metamaterials, which allow for independent control of electric and magnetic field components of reflected/transmitted light.

In multiferroic crystals with certain symmetries it's possible for magnetoelectric effect to occur whereby electric polarization can be induced with application of a magnetic field; and magnetization can be induced with the application of electric field. Further, in the optical spectra of multiferroics (dynamical regime) so-called electromagnon excitations can occur. These electromagnons have magnetic origin, but their oscillator strength is predominantly electrical-dipole active. Optical properties of multiferroics and the corresponding multilayer structures are the focus of the Thesis.

1.1 Metamaterials
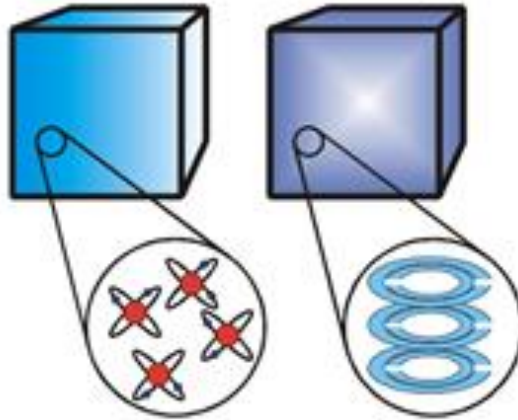
Figure 1.2 Left: in conventional materials ε , μ derive from electrons in the constituent atoms. Right: in metamaterials ε_{eff} , μ_{eff} derive from the elements such as capacitors and current rings, which may contain many atoms. *Source:*[1].

As it was pointed out above, metamaterials are artificial materials, which allow to alter their electromagnetic properties at the macroscopic scale, well above the atomic scale. The idea behind that is the following: electric permittivity ε and magnetic permeability μ of conventional materials originate from the response of constituent atoms to applied fields. Correspondingly, ε, μ represent an average response of the materials system to the external fields. On a length scale much greater than the separation between atoms the optical properties can be well-described by the $\hat{\varepsilon}$, $\hat{\mu}$ tensors [6]. Metamaterials carry this idea one step further: the constituent material is structured into subunits, and the overall optical properties of such metamaterials can be again described by an effective permeability and permittivity. This formalism is valid, of course, only on the length scale greater than the size of the constituent units, which still have to be smaller than the wavelength of electromagnetic radiation. Figure 1.2 illustrates this concept. In this way the properties of a complex metamaterial structure can be described by effective values of

dielectric permittivity ε_{eff} and magnetic permeability μ_{eff} which is a simplification that can provide an easy way for predicting optical properties of artificially developed metamaterials [6]. The flexibility in design of constituent parts enables construction of metamaterials with interesting optical properties: for example to obtain values of ε_{eff}, μ_{eff} which are not encountered in nature and in the present context that will mean either of these parameters being negative. For both $\varepsilon_{eff} < 0$ and $\mu_{eff} < 0$ this phenomenon is known as a negative index of refraction (NIR) [4,5] which is undoubtedly the concept which brought metamaterials into prominence. One of the most exciting sides of NIR is the ability to construct perfect lens, capable of restoring an image with almost unlimited precision [6].

For most natural materials, the magnetic coupling in the far-IR spectral region is weak and magnetic permeability is close to one. In contrast, metamaterials can be made with magnetic resonances with $\mu \neq 1$ in a broad spectral range including far-IR [7].

Note that metamaterials are not in the primary focus of this Thesis. Information on optical properties of metamaterials has been included in this section to highlight their similarity with multiferroics. Also, some of the theoretical formulas developed in this Thesis can be applicable to the light propagation in metamaterials as well as multiferroics.

1.2 Multiferroics

A new class of materials known as multiferroics which possess several ferroic orders simultaneously is discussed in this section. In most of the known multiferroics, the magnetoelectric effects are usually observed at cryogenic temperatures, the spin-lattice coupling is weak, and the magnitude of the electric polarization is small compared to that in classical ferroelectrics, like $BaTiO_3$. This severely limits practical applications of these materials. Nevertheless, several technology applications are intensively discussed in literature, such as alternating current magnetic field sensors, electrically and magnetically tunable filters and resonators [8], and magnetic recording technology [9]. Before going into detail some relevant properties of multiferroicity are discussed. One of them and probably the most important is symmetry. From symmetry considerations, an essential property of ferroelectricity is a broken spatial inverse symmetry, while the magnetic orders usually imply the absence of the time-reverse symmetry [10]. On one hand, spontaneous electric polarization emerges due to the structural distortion in real space. On the other hand,
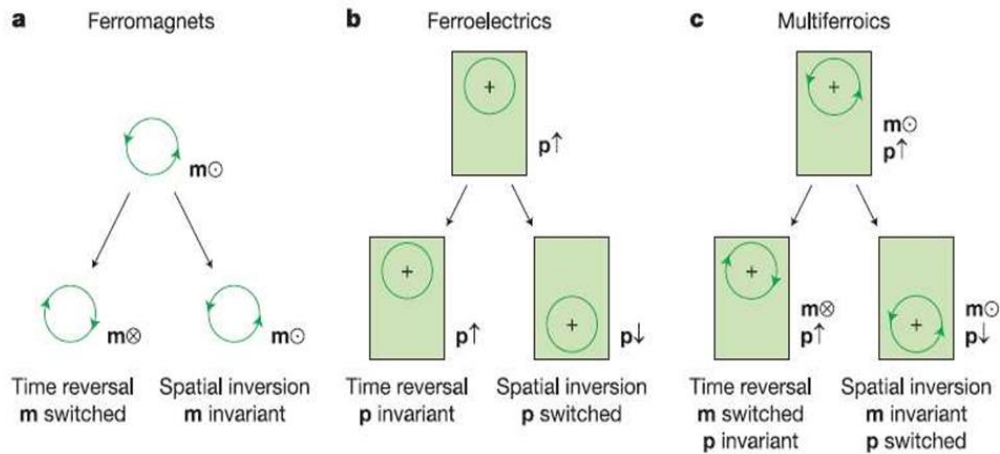
Figure 1.3 Time-reversal and spatial-inversion symmetry: a) Ferromagnets, b) Ferroelectrics, c) Multiferroics. *Source:*[2].

essential property of ferromagnetism is a broken time symmetry while the spatial symmetry is invariant. A reasonable argument for coexisting of ferroelectricity and ferromagnetism is a simultaneous absence of both symmetries. Due to their intrinsic properties, ferroelectric materials are usually good insulators while ferromagnetics are usually metals, like nickel and iron. This is hard to imagine how is it possible to combine these two contradicting properties in one material. Fortunately, there are other subclasses of magnetic materials: antiferromagnetics and ferrimagnetics, both are usually good insulators. Thus, antiferromagnetic and ferrimagnetic oxides are good candidates to possess ferroelectric properties and become multiferroics with magnetoelectric interactions.

In the center of magnetoelectric effects is a magnetoelectric coupling. By representing free energy F in terms of applied fields (E and H), the following expression can be obtained [10]:

$$-F(E,H) = \frac{1}{2}\varepsilon_0\varepsilon_{ij}E_iE_j + \frac{1}{2}\mu_0\mu_{ij}H_iH_j + \alpha_{ij}E_iH_j + \frac{1}{2}\beta_{ijk}E_iH_jH_k + +\frac{1}{2}\gamma_{ijk}H_iE_jE_k + ...$$
(1.1)

Here ε - permittivity tensor, μ - permeability tensor, α - magnetoelectric coupling tensor, γ and further – high order of magnetoelectric coupling tensors. Terms on the RHS (from left to right) represent electrical effect from application electric field, magnetic effect from application magnetic field, electric effect from application magnetic field, magnetic effect from application electric field correspondingly and so on. To establish polarization $P_i(H_j)$ and magnetization $M_i(E_j)$, differentiation of F with respect to E_i and H_i is required:

$$P_i = \alpha_{ij}H_j + \frac{1}{2}\beta_{ijk}H_jH_k + ...$$
$$\mu_0M_i = \alpha_{ji}E_j + \frac{1}{2}\gamma_{ijk}E_jE_k + ...$$
(1.2)

6

It can be pointed out that for thermodynamic reasons, α_{ij} is bounded by the geometric mean of the diagonalized permittivity and permeability tensors [10]:

$$\alpha_{ij}^2 \leq \varepsilon_0 \mu_0 \varepsilon_{ii} \mu_{jj} \tag{1.3}$$

Tensor α_{ij} is a second rank tensor, β_{ijk} and γ_{ijk} are third rank tensors that are functions of temperature T. It changes sign under space inversion or time reversal, and therefore is invariant under simultaneous space and time inversion. Using the definition of α_{ij} and α'_{ij} based on the free energy Equation (1.1), it is easy to assume that $\alpha^T_{ij} = \alpha'_{ij}$. As shown by Dzyaloshinsky, this relationship holds for the static case but may not necessary hold at every particular frequency for the dynamic case, where more complicated interactions of magnons and phonons are involved. This question is still under discussion in literature [11]. To comply with a general possible case, we will keep a different notation for α_{ij} and α'_{ij} tensors. ME effect exists only in materials that do not have a center of inversion and no time-inversion symmetry. In most cases, center of inversion is destroyed by electric polarization in ferroelectrics, while the time-reverse invariance is destroyed by the magnetic order or by external magnetic field. That means, ME crystals allow a simultaneous presence of magnetization (that destroys time reversal) and electric polarization (that destroys the center of inversion). The role of symmetry is extremely important in determining which crystals can display the magneto-electric effect. Crystal symmetry, for example, determines the form of each of the $\varepsilon, \mu, \alpha, \beta, \gamma$ tensors. Neumann's principle states that the symmetry elements of any physical property of a crystal must include the symmetry elements of the point group of the crystal. This principle

7

makes clear connection between the physical properties of a crystal and the material tensor which describes those properties.
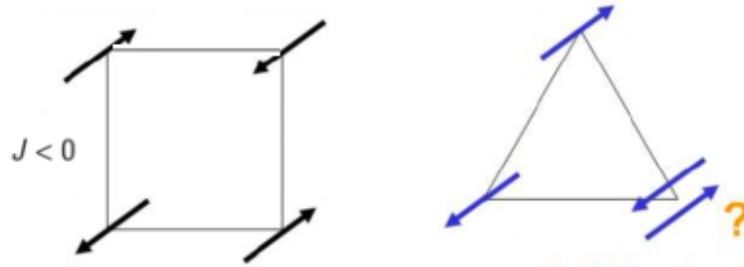
Figure 1.4 Geometrical frustration of spins.

Recently strong coupling between ferroelectricity and antiferromagnetism was observed in spin frustrated systems. Basic principle of frustration is depicted in Figure 1.4. In the simplified case of a triangular spin lattice, which can be realized in a big class of hexagonal materials, such as hexagonal manganites, there is no possibility to satisfy all exchange interactions between all spins involved. As a result, there is no possibility for minimization of magnetic energy. In the left picture of Figure 1.4 it can be seen that antiparallel ordering can be satisfied in a square spin lattice, but in the case of triangular lattice (right panel) it is non-obvious task to predict certain spin arrangement. In both cases there is no chance to minimize energy thus the only way is to form unusual spatial inhomogeneous magnetization (Figure 1.5). In this Thesis the optical properties of hexagonal manganites with spin frustration will be discussed in detail.

Multiferroics can be divided into two big categories: proper and improper. The difference in nomenclature relates to the origin of the ferroic effect in these materials. Proper multiferroics are generally good ferroelectrics but the coupling between magnetism and ferroelectricity is weak [2]. An example of such a system is bismuth ferrite $BiFeO_3$ with the perovskite crystal structure. In this structure, Fe^{3+} has five $3d$ electrons which

account for the magnetism. The Bi^{3+} ion has two electrons on the 6s orbital which form a lonely pair that moves away from the centrosymmetric position with respect to the surrounding oxygen ions. This broken spatial symmetry accounts for ferroelectricity. The fact that these orders arise from two separate and distinct ions accounts for the resultant weak coupling between the two effects of ferroelectricity and magnetism on the level of a crystal unit cell. Ferroelectricity arising from charge ordering and geometric tilting are also included in the category of proper multiferroic materials.
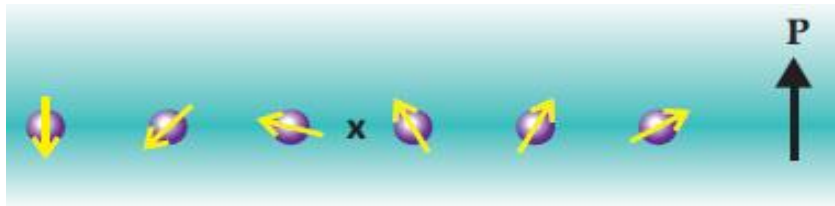
Figure 1.5 Non-centrosymmetric magnetic order produces a net polarization. *Source:* [2].

Improper multiferroics are also referred to as magnetic multiferroics because ferroelectricity exists only in magnetically ordered state at low temperatures; and it is caused by either spiral or collinear magnetic structures, with the spiral spin structure being the most common. In some materials such as rear earth (*RE*) manganites: $TbMnO_3$, $DyMnO_3$, $TbMn_2O_5$, $DyMn_2O_5$ non-centrosymmetric magnetic ordering could produce an electric polarization. Figure 1.5 below shows atoms symmetric about point marked 'x' but the spins are not symmetric, which leads to a net polarization. Non-centrosymmetric magnetic ordering also explains the stronger multiferroicity as in $TbMn_2O_5$, though in this case coupling is mediated by strong superexchange, not weak spin-orbit interactions as in previously mentioned $BiFeO_3$ [2]. The intrinsic magnetoelectric coupling leads to interesting phenomena as electric field control by spin chirality. In $TbMnO_3$ at low temperatures below $T_{N1}= 41$ K, the magnetic structure is sinusoidal [12] which results in

no net magnetic moment and no ferroelectricity. However, below $T_{N2} = 28$ K, the Mn spins change to cycloidal order due to magnetic frustration in which competing interactions between spins preclude simple magnetic order. A polarization is produced in this phase as a result of spin-orbit coupling.
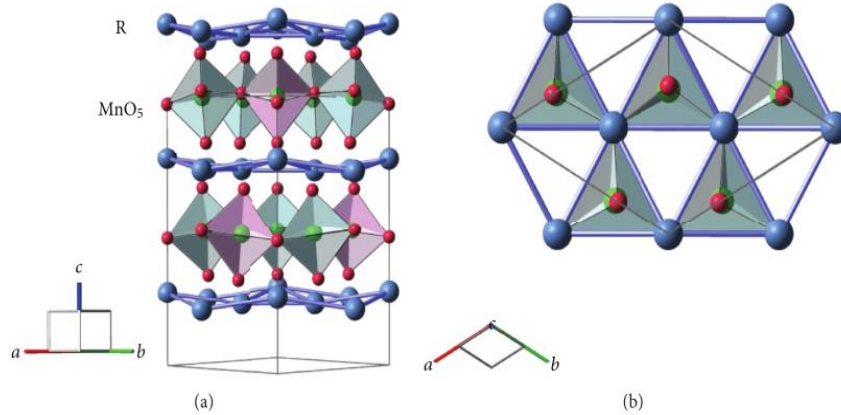
Figure 1.6 Structure of hexagonal rare earth manganite_s RMnO$_3$. (a) view along (110), (b) view along c-axis. *Source:*[13].

One of the most investigated proper class multifferoics are hexagonal (h) rare earth manganites. The crystal structure described by the space group P6$_3$cm with an unusual fivefold and sevenfold coordination polyhedral about the Mn and R ions, respectively [13]. Schematics of the structure is shown in Figure. 1.6. The ferroelectric origin in hexagonal manganites is under debate. It is interesting to note that d-shell is not empty, which leads as we discussed earlier to spatial distortions in perovskite ferroelectrics due to hybridization with the oxygen $2p$ states. All h-manganites possess atiferromagnetic order of manganese ions spins below their Neel temperatures.

Optical properties of hexagonal manganites, such as RMnO$_3$ (R=Ho,Er,Tm,Yb,Lu) will be described in this Thesis.

CHAPTER 2

ELECTROMAGNETIC WAVE PROPAGATION
IN BI-ANISOTROPIC BULK STRUCTURES

Chapter 2 of this Thesis describes the 4×4 matrix formalism applied to bulk structures, which is the most advanced approach for the light propagation problem in bi-anisotropic medium. The main references of this chapter are the original Berreman's paper [14], the Azzam's book [15] and the Thesis of Paul Rogers [16,17]. In addition to the theoretical background, in this chapter we will discuss some analytical solution of Fresnel's coefficients, which describe behavior of light when propagating through an interface between two optical media (Figure 2.1), for general bulk structures with anisotropic $\hat{\varepsilon}(\omega)$, $\hat{\mu}(\omega)$ and magneto-electric interaction which characterizes by magneto-electric (ME) tensor $\hat{\alpha}(\omega)$. Tensors $\hat{\varepsilon}(\omega), \hat{\mu}(\omega), \hat{\alpha}(\omega), \hat{\rho}(\omega)$ are three by three matrices, $\tilde{\Delta}$ matrix which is discussed later is four by four. Also we show which components of the Mueller matrix depends on ME interactions for ME tensors with different symmetries. It is a useful knowledge for measurements to determine for which sample orientation magneto-electric interaction can be observed in optical spectra and exhibit the strongest effect.
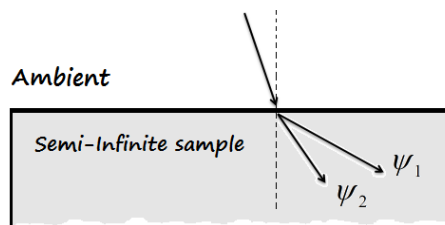
Figure 2.1 Light propagation from isotropic ambient to semi-infinite bi-anisotropic bulk structure.

2.1 Constitutive and Dispersion Relations.

We are concerned with structures which exhibit coupling between electric and magnetic interactions. For such a media different form of constitutive relations should be obtained in order to proper characterize wave propagation in this matter. Dzyaloshinskii obtained constitutive relations in the following form [11]:

$$D_i = \varepsilon_{ij} E_j + \alpha_{ij} H_j$$
$$B_i = \alpha_{ji} E_j + \mu_{ij} H_j$$

(2.1)

Details on these equations were discussed in the Section 1.2 on multiferroics in the previous chapter. Another question, which arises after all relevant relationships are written down, is how to characterize electric, magnetic and electromagnetic interactions with a few measurable quantities in the optical spectra, such as resonant frequencies, broadening, and oscillator strength. One of the most suitable approaches is the Lorentz model (or simple harmonic oscillator) for dispersion relations:

$$\varepsilon(\omega) = \varepsilon_\infty + \sum_{n=1}^{N} \frac{S_{\varepsilon,n} \omega_{\varepsilon,0n}^2}{\omega_{\varepsilon,0n}^2 - \omega^2 - i\gamma_{\varepsilon,n}\omega}$$

(2.2)

$$\mu(\omega) = \mu_\infty + \sum_{n=1}^{N} \frac{S_{\mu,n} \omega_{\mu,0n}^2}{\omega_{\mu,0n}^2 - \omega^2 - i\gamma_{\mu,n}\omega}$$

(2.3)

where ω_{0n} - oscillator resonance phonon or magnon frequency or electronic transition frequency, S_n - corresponding oscillator strength, γ_n - broadening of the nth excitation or electronic transition. The same is valid for treating ME interactions:

$$\alpha(\omega) = \frac{S_{me} \omega_{me,0}^2}{\omega_{me,0}^2 - \omega^2 - i\gamma_{me}\omega}; \quad \alpha(0) = S_{me}; \quad \alpha(\infty) = 0$$

(2.4)

Also we will often assume that the same oscillator that appears in several $\hat{\varepsilon}$, $\hat{\mu}$, $\hat{\alpha}$, and $\hat{\xi}$ tensors has at the same frequency ω_0 and the same value of the decay parameter γ. In the figure below graphs for each type of excitation are shown. Panels (a) and (b) show real and imaginary part of electric excitation respectively, panels (c) and (d) show real and imaginary part of magnetic excitation, panel (e) and (f) show real and imaginary part of magneto-electric excitation. Parameters for each oscillator are presented in Table 2.1.

Table 2.1 Parameters for Electric, Magnetic and Magneto-electric Oscillators as Described by Equations (2.2), (2.3), and (2.4)

	$\varepsilon(\omega)$	$\mu(\omega)$	$\alpha(\omega)$
Infinity value	$\varepsilon_\infty = 10$	$\mu_\infty = 1$	$\alpha_\infty = 0$
Resonant frequency	$\omega_{0,e} = 300$	$\omega_{0,\mu} = 300$	$\omega_{0,\alpha} = 300$
Strength	$S_e = 0.01$	$S_\mu = 0.01$	$S_\alpha = 0.01$
Broadening	$\gamma_e = 1$	$\gamma_\mu = 1$	$\gamma_\alpha = 1$

$$\varepsilon(\omega) \qquad \mu(\omega) \qquad \alpha(\omega)$$
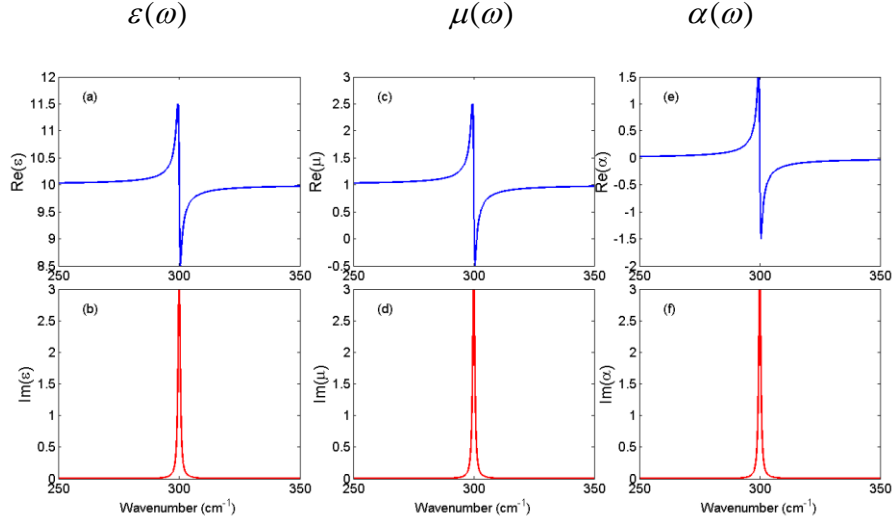
Figure 2.2 Graphs of different types of excitations: (a),(b) – electric; (c),(d) – magnetic; (e),(f) – magneto-electric. Real parts are in blue color, imaginary parts are in red color. Parameters are presented in Table 2.1.

2.2 Basics of the 4x4 Matrix Formalism

The 4×4 matrix formalism developed by Berreman [14] allow to calculate optical properties of stratified bi-anisotropic media if $\hat{\varepsilon}$, $\hat{\mu}$, $\hat{\alpha}$ tensors are known. Figure 2.3 shows the optical matrix M that is composed of the $\hat{\varepsilon}$, $\hat{\mu}$, $\hat{\alpha}$ tensors for a single layer with bi-anisotropic properties. For analysis of experimental data, it is always useful to have analytical solutions for transmittance and reflectance of the media as a function of frequency and angle of incidence to be able to explore phenomena like in the case of the adjusted oscillator strength matching (AOSM), total reflection, skin depth, *etc*. The schematics of the investigated experimental configuration is shown in Figure 2.4. In Berreman formalism, it is assumed that the time variation of fields are harmonic and given by $e^{i\omega t}$, the direction of stratification coincides with the positive direction of the *z*-axis, there is no $\vec{k}_y$ wave vector component of incident light and structures are homogeneous

along x. The theory utilizes the fact that parallel components of the fields are continuous through ought the medium (no surface charges, no surface currents).

$$\hat{\alpha}(\omega), \hat{\alpha}'(\omega)$$
$$\downarrow$$
$$\hat{\varepsilon}(\omega) \longrightarrow \text{Optical Matrix} \longleftarrow \hat{\mu}(\omega)$$
$$\updownarrow$$
$$\begin{pmatrix} \vec{D} \\ \vec{B} \end{pmatrix} = \begin{pmatrix} \hat{\varepsilon} & \hat{\alpha} \\ \hat{\alpha}' & \hat{\mu} \end{pmatrix} \begin{pmatrix} \vec{E} \\ \vec{H} \end{pmatrix}$$

Figure 2.3 Constitutive relations for bi-anisotropic structures. Sample can be described by permittivity $\hat{\varepsilon}(\omega)$, permeability $\hat{\mu}(\omega)$ and ME $\hat{\alpha}(\omega)$ tensors. $\vec{D}$ and $\vec{B}$ relate to $\vec{E}$ and $\vec{H}$ by means of optical matrix.

The advantage of Berreman's formalism is that it deals with the first order Maxwell's equations which allow to easily incorporate the ME tensors. Note that in addition to the Berreman's approach, there are some other ways to investigate electromagnetic wave propagation but they rely on the same physical principles. In comparison, the Yeh's [18] formalism deals with polarization eigenmodes, giving a clearer physical interpretation of boundary conditions, but this approach seems to be more difficult to describe magneto-electric activity and optical activity. We chose Berreman's approach as an established one which allows to obtain all required results for our research.

It is instructive to show derivation of Berreman's matrix wave equation and discuss application of boundary conditions to have clear understanding of incorporating ME effect into structure's interactions.

$$\vec{D} = \hat{\varepsilon}\vec{E} + \hat{\alpha}\vec{H}$$

$$\vec{B} = \hat{\alpha}'\vec{E} + \hat{\mu}\vec{H}$$

$$\begin{pmatrix} \vec{D} \\ \vec{B} \end{pmatrix} = \begin{pmatrix} \hat{\varepsilon} & \hat{\alpha} \\ \hat{\alpha}' & \hat{\mu} \end{pmatrix} \begin{pmatrix} \vec{E} \\ \vec{H} \end{pmatrix}$$

(2.5)
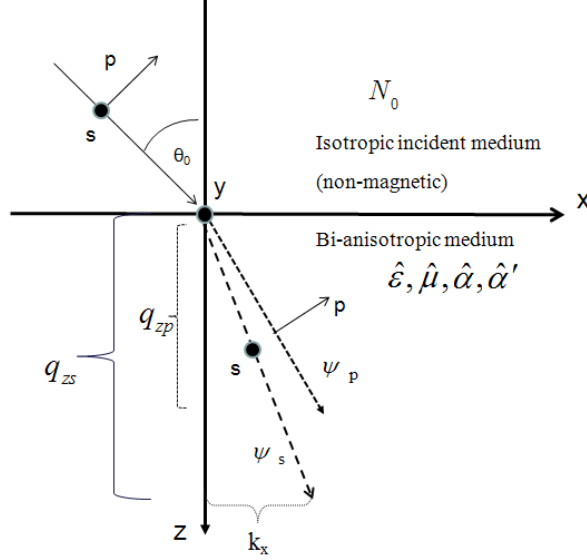
Figure 2.4 Axis orientation and schematics of wave propagation.

For simplicity, we assume that our laboratory x-y-z axes coincide with the symmetry axes of the sample. Such convention determines the diagonal form of both, dielectric permittivity tensor and magnetic permeability tensors. Schematic of the axes notation is shown in Figure 2.4. When this condition does not hold the optical axes should be rotated, transforming correspondingly our optical matrix and it will not have diagonal form anymore. Constitutive relations can be written in the following form:

$$\begin{pmatrix} D_x \\ D_y \\ D_z \\ B_x \\ B_y \\ B_z \end{pmatrix} = \begin{pmatrix} \varepsilon_{xx} & 0 & 0 & \alpha_{xx} & \alpha_{xy} & \alpha_{xz} \\ 0 & \varepsilon_{yy} & 0 & \alpha_{yx} & \alpha_{yy} & \alpha_{yz} \\ 0 & 0 & \varepsilon_{zz} & \alpha_{zx} & \alpha_{zy} & \alpha_{zz} \\ \alpha_{xx}^* & \alpha_{yx}^* & \alpha_{zx}^* & \mu_{xx} & 0 & 0 \\ \alpha_{xy}^* & \alpha_{yy}^* & \alpha_{zy}^* & 0 & \mu_{yy} & 0 \\ \alpha_{xz}^* & \alpha_{yz}^* & \alpha_{zz}^* & 0 & 0 & \mu_{zz} \end{pmatrix} \begin{pmatrix} E_x \\ E_y \\ E_z \\ H_x \\ H_y \\ H_z \end{pmatrix}$$

(2.6)

16

It should be noted that a low-left part of optical matrix $\hat{\alpha}'$ is a conjugate transpose of $\hat{\alpha}$: $\hat{\alpha}' = \hat{\alpha}^\dagger$. In the following discussion, we focus on the cases when non-zero components of ME tensor are $\alpha_{xx}, \alpha_{yy}, \alpha_{zz}, \alpha_{yx} = -\alpha_{xy}, \quad \alpha_{yz} = -\alpha_{zy}, \quad \alpha_{xz} = -\alpha_{zx}$ which corresponds to most common crystal structure.

Maxwell's equations can be written (in the general case of ME tensor each field component is a function of others):

$$\begin{cases} \nabla \times \vec{E} = -\dfrac{\partial \vec{B}}{\partial t} \\[2mm] \nabla \times \vec{H} = \dfrac{\partial \vec{D}}{\partial t} \end{cases} \tag{2.7}$$

It is useful to represent *curl* vector as a matrix and note that our conditions assume that there is no $\vec{k}_y$ component of wave vector and our material is homogeneous as the result $\dfrac{\partial}{\partial y}$ will bring zero and $\dfrac{\partial}{\partial x}$ gives a *x*-component of a wave vector. The curl matrix can be represented as in the following equation:

$$\begin{bmatrix} 0 & 0 & 0 & 0 & -\dfrac{\partial}{\partial z} & \dfrac{\partial}{\partial y} \\[2mm] 0 & 0 & 0 & \dfrac{\partial}{\partial z} & 0 & -\dfrac{\partial}{\partial x} \\[2mm] 0 & 0 & 0 & -\dfrac{\partial}{\partial y} & \dfrac{\partial}{\partial x} & 0 \\[2mm] 0 & \dfrac{\partial}{\partial z} & -\dfrac{\partial}{\partial y} & 0 & 0 & 0 \\[2mm] -\dfrac{\partial}{\partial z} & 0 & \dfrac{\partial}{\partial x} & 0 & 0 & 0 \\[2mm] \dfrac{\partial}{\partial y} & -\dfrac{\partial}{\partial x} & 0 & 0 & 0 & 0 \end{bmatrix} \begin{bmatrix} E_x \\ E_y \\ E_z \\ H_x \\ H_y \\ H_z \end{bmatrix} = \dfrac{1}{c}\dfrac{\partial}{\partial t} \begin{bmatrix} D_x \\ D_y \\ D_z \\ B_x \\ B_y \\ B_z \end{bmatrix} \tag{2.8}$$

Taking into account the discussion above and writing down constitutive relations, our

matrix equation transforms to the following equation:

$$
\begin{bmatrix}
0 & 0 & 0 & 0 & -\dfrac{\partial}{\partial z} & 0 \\
0 & 0 & 0 & \dfrac{\partial}{\partial z} & 0 & ik_x \\
0 & 0 & 0 & 0 & -ik_x & 0 \\
0 & \dfrac{\partial}{\partial z} & 0 & 0 & 0 & 0 \\
-\dfrac{\partial}{\partial z} & 0 & -ik_x & 0 & 0 & 0 \\
0 & ik_x & 0 & 0 & 0 & 0
\end{bmatrix}
\begin{bmatrix}
E_x \\ E_y \\ E_z \\ H_x \\ H_y \\ H_z
\end{bmatrix}
= \frac{1}{c}\begin{pmatrix} \hat{\varepsilon} & \hat{\alpha} \\ \hat{\alpha}' & \hat{\mu} \end{pmatrix}\frac{\partial}{\partial t}
\begin{bmatrix}
E_x \\ E_y \\ E_z \\ H_x \\ H_y \\ H_z
\end{bmatrix}
\tag{2.9}
$$

The most general view can be shown as:

$$
\begin{bmatrix}
0 & 0 & 0 & 0 & -\dfrac{\partial}{\partial z} & 0 \\
0 & 0 & 0 & \dfrac{\partial}{\partial z} & 0 & ik_x \\
0 & 0 & 0 & 0 & -ik_x & 0 \\
0 & \dfrac{\partial}{\partial z} & 0 & 0 & 0 & 0 \\
-\dfrac{\partial}{\partial z} & 0 & -ik_x & 0 & 0 & 0 \\
0 & ik_x & 0 & 0 & 0 & 0
\end{bmatrix}
\begin{bmatrix}
E_x \\ E_y \\ E_z \\ H_x \\ H_y \\ H_z
\end{bmatrix}
= \frac{1}{c}
\begin{pmatrix}
\varepsilon_{xx} & 0 & 0 & \alpha_{xx} & \alpha_{xy} & \alpha_{xz} \\
0 & \varepsilon_{yy} & 0 & \alpha_{yx} & \alpha_{yy} & \alpha_{yz} \\
0 & 0 & \varepsilon_{zz} & \alpha_{zx} & \alpha_{zy} & \alpha_{zz} \\
\alpha'_{xx} & \alpha'_{yx} & \alpha'_{zx} & \mu_{xx} & 0 & 0 \\
\alpha'_{xy} & \alpha'_{yy} & \alpha'_{zy} & 0 & \mu_{yy} & 0 \\
\alpha'_{xz} & \alpha'_{yz} & \alpha'_{zz} & 0 & 0 & \mu_{zz}
\end{pmatrix}
\frac{\partial}{\partial t}
\begin{bmatrix}
E_x \\ E_y \\ E_z \\ H_x \\ H_y \\ H_z
\end{bmatrix}
\tag{2.10}
$$

Looking carefully at the *curl* matrix it should be noted that there is no $\dfrac{\partial}{\partial z}$ dependencies in

third and sixth column. That means E_z and H_z components can be expressed in terms of

E_x, E_y, H_x, H_y. The "reduced" equation looks like:

$$\frac{\partial}{\partial z}\begin{pmatrix} E_x \\ E_y \\ H_x \\ H_y \end{pmatrix} = i\frac{\omega}{c}\begin{pmatrix} \Delta_{11} & \Delta_{12} & \Delta_{13} & \Delta_{14} \\ \Delta_{21} & \Delta_{22} & \Delta_{23} & \Delta_{24} \\ \Delta_{31} & \Delta_{32} & \Delta_{33} & \Delta_{34} \\ \Delta_{41} & \Delta_{42} & \Delta_{43} & \Delta_{44} \end{pmatrix}\begin{pmatrix} E_x \\ E_y \\ H_x \\ H_y \end{pmatrix} \tag{2.11}$$

Calculation of $\tilde{\Delta}$ matrix elements can be found in original Berreman's paper [14]. Though

Berreman's

$$\begin{pmatrix} \Delta_{11} & \Delta_{12} & \Delta_{13} & \Delta_{14} \\ \Delta_{21} & \Delta_{22} & \Delta_{23} & \Delta_{24} \\ \Delta_{31} & \Delta_{32} & \Delta_{33} & \Delta_{34} \\ \Delta_{41} & \Delta_{42} & \Delta_{43} & \Delta_{44} \end{pmatrix}\begin{pmatrix} E_x \\ H_y \\ E_y \\ -H_x \end{pmatrix}$$

Our work

$$\xrightarrow{\ transformation\ }$$

$$\begin{pmatrix} \Delta_{11} & \Delta_{13} & -\Delta_{14} & \Delta_{12} \\ \Delta_{31} & \Delta_{33} & -\Delta_{34} & \Delta_{32} \\ -\Delta_{41} & -\Delta_{43} & \Delta_{44} & -\Delta_{42} \\ \Delta_{21} & \Delta_{23} & -\Delta_{24} & \Delta_{22} \end{pmatrix}\begin{pmatrix} E_x \\ E_y \\ H_x \\ H_y \end{pmatrix}$$

Figure 2.5 Transformation between different bases

Berreman used $\begin{pmatrix} E_x \\ H_y \\ E_y \\ -H_x \end{pmatrix}$ basis (and calculated $\tilde{\Delta}$ elements in this basis), we use $\begin{pmatrix} E_x \\ E_y \\ H_x \\ H_y \end{pmatrix}$ basis.

It is not hard to get expressions for $\tilde{\Delta}$ elements in our basis by slightly modifying

Berreman's matrix as shown in Figure 2.5. There is no principle difference which basis to

choose, but it is more important to work with $\vec{E}$ and $\vec{H}$ because their tangential

components are continuous through interfaces which as was shown earlier lay in the *xy*-

plane.

Finally, one arrives to 4x4 matrix wave equation (we use matrix on the right in

Figure 2.5 but we rename components of $\tilde{\Delta}$):

$$\frac{\partial}{\partial z}\begin{pmatrix} E_x \\ E_y \\ H_x \\ H_y \end{pmatrix} = i\frac{\omega}{c}\begin{pmatrix} \Delta_{11} & \Delta_{12} & \Delta_{13} & \Delta_{14} \\ \Delta_{21} & \Delta_{22} & \Delta_{23} & \Delta_{24} \\ \Delta_{31} & \Delta_{32} & \Delta_{33} & \Delta_{34} \\ \Delta_{41} & \Delta_{42} & \Delta_{43} & \Delta_{44} \end{pmatrix}\begin{pmatrix} E_x \\ E_y \\ H_x \\ H_y \end{pmatrix},$$

(2.12)

or in a more compact form:

$$\frac{\partial \psi}{\partial z} = i\frac{\omega}{c}\tilde{\Delta}\psi$$

(2.13)

For our discussion about wave propagation in the bulk samples, we do not need to solve Equation (2.13). It's enough to solve eigenvalue, eigenvector problem for substrate's $\tilde{\Delta}$ matrix. Further treatment of the Berreman's wave equation will be continued in the chapter on electromagnetic wave propagation in bi-anisotropic multilayer systems.

Because we assume that our structures are homogeneous along z, LHS of the Equation (2.12) yields ik_z multiplier in front of ψ vector. We can rewrite wave equation into the form below, where q_z is an effective refraction index in the z-direction and corresponds to the z-component of wave vector as $q_z = \frac{ck_z}{\omega}$.

$$\begin{pmatrix} \Delta_{11} & \Delta_{12} & \Delta_{13} & \Delta_{14} \\ \Delta_{21} & \Delta_{22} & \Delta_{23} & \Delta_{24} \\ \Delta_{31} & \Delta_{32} & \Delta_{33} & \Delta_{34} \\ \Delta_{41} & \Delta_{42} & \Delta_{43} & \Delta_{44} \end{pmatrix}\begin{pmatrix} E_x(0) \\ E_y(0) \\ H_x(0) \\ H_y(0) \end{pmatrix} = q_z\begin{pmatrix} E_x(0) \\ E_y(0) \\ H_x(0) \\ H_y(0) \end{pmatrix},$$

(2.14)

where we consider field's components at the interface between ambient and structure. For getting analytical solutions it is nice to construct transfer matrix T which relates incident and reflected components to transmitted ones of propagating wave. We desire to have relationship in the form:

$$\begin{pmatrix} E_{is} \\ E_{rs} \\ E_{ip} \\ E_{rp} \end{pmatrix} = T \begin{pmatrix} E_{ts} \\ 0 \\ E_{tp} \\ 0 \end{pmatrix} = \begin{pmatrix} T_{11} & T_{12} & T_{13} & T_{14} \\ T_{21} & T_{22} & T_{23} & T_{24} \\ T_{31} & T_{32} & T_{33} & T_{34} \\ T_{41} & T_{42} & T_{43} & T_{44} \end{pmatrix} \begin{pmatrix} E_{ts} \\ 0 \\ E_{tp} \\ 0 \end{pmatrix}$$

(2.15)

Fresnel's coefficient could be found easily from this equation:

$$r_{pp} = \frac{T_{11}T_{43} - T_{13}T_{41}}{T_{11}T_{33} - T_{13}T_{31}} \qquad\qquad t_{pp} = \frac{T_{11}}{T_{11}T_{33} - T_{13}T_{31}}$$

$$r_{sp} = \frac{T_{11}T_{23} - T_{13}T_{21}}{T_{11}T_{33} - T_{13}T_{31}} \qquad\qquad t_{sp} = -\frac{T_{13}}{T_{11}T_{33} - T_{13}T_{31}}$$

(2.16)

$$r_{ss} = \frac{T_{21}T_{33} - T_{23}T_{31}}{T_{11}T_{33} - T_{13}T_{31}} \qquad\qquad t_{ss} = \frac{T_{33}}{T_{11}T_{33} - T_{13}T_{31}}$$

$$r_{ps} = \frac{T_{33}T_{41} - T_{31}T_{43}}{T_{11}T_{33} - T_{13}T_{31}} \qquad\qquad t_{ps} = -\frac{T_{31}}{T_{11}T_{33} - T_{13}T_{31}}.$$
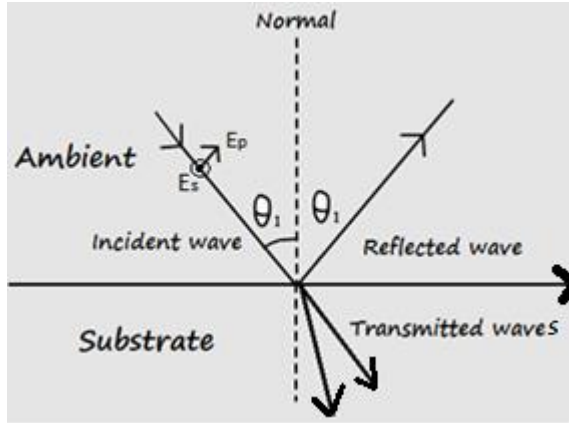
Figure 2.6 Fields near the ambient-substrate interface. Incident and reflected *p*- and *s*-polarized waves in the ambient are shown as well as two transmitted waves corresponding to eigenvectors of substrate's $\tilde{\Delta}$ matrix which are related to eigenvalues with positive real part.

What one needs is to construct matrices which project transmitted waves on *xy*-plane and project *xy*-components on initial and reflected waves. Projecting E_p, E_s

components of incident and reflected waves on the interface and using relationship between

H and E for isotropic medium we get following dependencies for incident light:

$$
\begin{pmatrix} E_x \\ E_y \\ H_x \\ H_y \end{pmatrix}_i = \begin{pmatrix} \cos\theta_0 E_{ip} \\ E_{is} \\ -N_0\cos\theta_0 E_{is} \\ N_0 E_{ip} \end{pmatrix} \tag{2.17}
$$

for reflected light:

$$
\begin{pmatrix} E_x \\ E_y \\ H_x \\ H_y \end{pmatrix}_r = \begin{pmatrix} -\cos\theta_0 E_{rp} \\ E_{rs} \\ N_0\cos\theta_0 E_{rs} \\ N_0 E_{rp} \end{pmatrix}. \tag{2.18}
$$

Total projection on the xy-plane:

$$
\begin{pmatrix} E_x \\ E_y \\ H_x \\ H_y \end{pmatrix} = \begin{pmatrix} \cos\theta_0 E_{ip} \\ E_{is} \\ -N_0\cos\theta_0 E_{is} \\ N_0 E_{ip} \end{pmatrix} + \begin{pmatrix} -\cos\theta_0 E_{rp} \\ E_{rs} \\ N_0\cos\theta_0 E_{rs} \\ N_0 E_{rp} \end{pmatrix} \tag{2.19}
$$

or if we reshape RHS of Equation (2.19) we get:

$$
\begin{pmatrix} E_x \\ E_y \\ H_x \\ H_y \end{pmatrix} = \begin{pmatrix} 0 & 0 & \cos\theta_0 & -\cos\theta_0 \\ 1 & 1 & 0 & 0 \\ -N_0\cos\theta_0 & N_0\cos\theta_0 & 0 & 0 \\ 0 & 0 & N_0 & N_0 \end{pmatrix} \begin{pmatrix} E_{is} \\ E_{rs} \\ E_{ip} \\ E_{rp} \end{pmatrix} \tag{2.20}
$$

In order to get p and s components along, we multiply both parts on the inverse matrix in the RHS of Equation (2.20):

$$
\begin{pmatrix} 0 & 0 & \cos\theta_0 & -\cos\theta_0 \\ 1 & 1 & 0 & 0 \\ -N_0\cos\theta_0 & N_0\cos\theta_0 & 0 & 0 \\ 0 & 0 & N_0 & N_0 \end{pmatrix}^{-1} \begin{pmatrix} E_x \\ E_y \\ H_x \\ H_y \end{pmatrix} = \begin{pmatrix} E_{is} \\ E_{rs} \\ E_{ip} \\ E_{rp} \end{pmatrix} \tag{2.21}
$$

and, finally, following Shubert [19], we obtain matrix L_{in} which project x,y-components of the incident and reflected waves on p,s-components:

$$\begin{pmatrix} E_{is} \\ E_{rs} \\ E_{ip} \\ E_{rp} \end{pmatrix} = L_{in} \begin{pmatrix} E_x \\ E_y \\ H_x \\ H_y \end{pmatrix} = \frac{1}{2} \begin{pmatrix} 0 & 1 & -\dfrac{1}{N_0 \cos\theta_i} & 0 \\ 0 & 1 & \dfrac{1}{N_0 \cos\theta_i} & 0 \\ \dfrac{1}{\cos\theta_i} & 0 & 0 & \dfrac{1}{N_0} \\ -\dfrac{1}{\cos\theta_i} & 0 & 0 & \dfrac{1}{N_0} \end{pmatrix} \begin{pmatrix} E_x \\ E_y \\ H_x \\ H_y \end{pmatrix} \qquad (2.22)$$

Before calculating another matrix which projects the transmitted waves on the xy-plane, let's review Azzam's method of solving wave propagation in bulk materials problem. As we pointed out earlier, in Equation (2.22) a simple relationship can be established between incident and reflected waves and their projections on the xy-plane. We assume that our media is bi-anisotropic in general case and then it's sufficient to assume that propagating waves inside bulk structure will be nothing but linear combination of eigenvectors which corresponds to positive real part eigenvalues (condition for existing only two transmitted waves). This kind of relationship has the form:

$$\begin{cases} (E_{ip} - E_{rp})\cos\theta_0 = C_1\psi_{11} + C_2\psi_{12} \\ N_0(E_{ip} + E_{rp}) = C_1\psi_{21} + C_2\psi_{22} \\ (E_{is} + E_{rs}) = C_1\psi_{31} + C_2\psi_{32} \\ N_0(E_{is} - E_{rs}) = C_1\psi_{41} + C_2\psi_{42} \end{cases} \qquad (2.23)$$

After defining boundary conditions we can introduce transmission coefficients vector $C = \begin{pmatrix} C_1 \\ C_2 \end{pmatrix}$ and rewriting our initial system of equations into more useful form we obtain:

$$\begin{cases} C = S_1(E_i - E_r) \\ C = S_2(E_i + E_r) \end{cases}$$

(2.24)

Where S_1 and S_2 are defined by the following equations:

$$S_1 = \cos\theta_0 \begin{pmatrix} \psi_{11} & \psi_{12} \\ \dfrac{\psi_{41}}{N_0} & \dfrac{\psi_{42}}{N_0} \end{pmatrix}^{-1}$$

$$S_2 = \begin{pmatrix} \dfrac{\psi_{21}}{N_0} & \dfrac{\psi_{22}}{N_0} \\ \psi_{31} & \psi_{32} \end{pmatrix}^{-1}$$

(2.25)

Finally, we get Fresnel's coefficients:

$$R = \begin{pmatrix} r_{pp} & r_{ps} \\ r_{sp} & r_{ss} \end{pmatrix} = (S_1 + S_2)^{-1}(S_1 - S_2)$$

$$T = \begin{pmatrix} t_{pp} & t_{ps} \\ t_{sp} & t_{ss} \end{pmatrix} = S_2(I + R)$$

(2.26)

The disadvantage of such a method is a calculating inverse matrices several times. Shubert [19] proposed slightly different approach. We want to construct matrix which project transmitted waves on *xy*-plane. Let's call it L_{out}. Then we have

$$\begin{pmatrix} E_x \\ E_y \\ H_x \\ H_y \end{pmatrix} = L_{out} \begin{pmatrix} E_{ts} \\ 0 \\ E_{ps} \\ 0 \end{pmatrix}$$

(2.27)

From the system Equation (2.23) it's clear that

$$\begin{pmatrix} E_x \\ E_y \\ H_x \\ H_y \end{pmatrix} = E_{ts} \begin{pmatrix} \psi_{11}^{sub} \\ \psi_{21}^{sub} \\ \psi_{31}^{sub} \\ \psi_{41}^{sub} \end{pmatrix} + E_{ps} \begin{pmatrix} \psi_{12}^{sub} \\ \psi_{22}^{sub} \\ \psi_{32}^{sub} \\ \psi_{42}^{sub} \end{pmatrix} = \begin{pmatrix} \psi_{11}^{sub} & 0 & \psi_{12}^{sub} & 0 \\ \psi_{21}^{sub} & 0 & \psi_{22}^{sub} & 0 \\ \psi_{31}^{sub} & 0 & \psi_{32}^{sub} & 0 \\ \psi_{41}^{sub} & 0 & \psi_{42}^{sub} & 0 \end{pmatrix} \begin{pmatrix} E_{ts} \\ 0 \\ E_{tp} \\ 0 \end{pmatrix}$$

(2.28)

where ψ_{ij}^{sub} are the substrate's $\tilde{\Delta}$ matrix eigenvectors components. As a small remark: when treating semi-infinite bulk structures we simply call it substrates because algorithms are similar to that for a multilayer structure on semi-infinite anisotropic substrate. Eigenvector components of semi-infinite bulk structures we call substrate eigenvector components ψ_{ij}^{sub}. So our L_{out} matrix has the form:

$$L_{out} = \begin{pmatrix} \psi_{11}^{sub} & 0 & \psi_{12}^{sub} & 0 \\ \psi_{21}^{sub} & 0 & \psi_{22}^{sub} & 0 \\ \psi_{31}^{sub} & 0 & \psi_{32}^{sub} & 0 \\ \psi_{41}^{sub} & 0 & \psi_{42}^{sub} & 0 \end{pmatrix} \tag{2.29}$$

Now we can write down transfer matrix T:

$$T = L_{in}L_{out} = \frac{1}{2} \begin{pmatrix} 0 & 1 & -\dfrac{1}{N_0\cos\theta_i} & 0 \\ 0 & 1 & \dfrac{1}{N_0\cos\theta_i} & 0 \\ \dfrac{1}{\cos\theta_i} & 0 & 0 & \dfrac{1}{N_0} \\ -\dfrac{1}{\cos\theta_i} & 0 & 0 & \dfrac{1}{N_0} \end{pmatrix} \begin{pmatrix} \psi_{11}^{sub} & 0 & \psi_{12}^{sub} & 0 \\ \psi_{21}^{sub} & 0 & \psi_{22}^{sub} & 0 \\ \psi_{31}^{sub} & 0 & \psi_{32}^{sub} & 0 \\ \psi_{41}^{sub} & 0 & \psi_{42}^{sub} & 0 \end{pmatrix} \tag{2.30}$$

And, finally, we get explicit formula of Equation (2.30) from which Fresnel's coefficients can be obtained in analytical form. The only thing left is to calculate corresponding eigenvectors of transmitted waves. We consider several symmetries of ME tensor which more often occurs in real materials to simplify our calculation and then we determine which Mueller matrix components depends on ME oscillators.

$$
\begin{pmatrix} E_{is} \\ E_{rs} \\ E_{ip} \\ E_{rp} \end{pmatrix} = T \begin{pmatrix} E_{ts} \\ 0 \\ E_{tp} \\ 0 \end{pmatrix} = \begin{pmatrix} T_{11} & T_{12} & T_{13} & T_{14} \\ T_{21} & T_{22} & T_{23} & T_{24} \\ T_{31} & T_{32} & T_{33} & T_{34} \\ T_{41} & T_{42} & T_{43} & T_{44} \end{pmatrix} \begin{pmatrix} E_{ts} \\ 0 \\ E_{tp} \\ 0 \end{pmatrix} = \begin{pmatrix} \dfrac{\psi_{21}^{sub}}{2} - \dfrac{\psi_{31}^{sub}}{2N_0\cos\theta_0} & 0 & \dfrac{\psi_{22}^{sub}}{2} - \dfrac{\psi_{32}^{sub}}{2N_0\cos\theta_0} & 0 \\[2mm] \dfrac{\psi_{21}^{sub}}{2} + \dfrac{\psi_{31}^{sub}}{2N_0\cos\theta_0} & 0 & \dfrac{\psi_{22}^{sub}}{2} + \dfrac{\psi_{32}^{sub}}{2N_0\cos\theta_0} & 0 \\[2mm] \dfrac{\psi_{41}^{sub}}{2N_0} + \dfrac{\psi_{11}^{sub}}{2\cos\theta_0} & 0 & \dfrac{\psi_{42}^{sub}}{2N_0} + \dfrac{\psi_{12}^{sub}}{2\cos\theta_0} & 0 \\[2mm] \dfrac{\psi_{41}^{sub}}{2N_0} - \dfrac{\psi_{11}^{sub}}{2\cos\theta_0} & 0 & \dfrac{\psi_{42}^{sub}}{2N_0} - \dfrac{\psi_{12}^{sub}}{2\cos\theta_0} & 0 \end{pmatrix} \begin{pmatrix} E_{ts} \\ 0 \\ E_{tp} \\ 0 \end{pmatrix} \quad (2.31)
$$

Fresnel's coefficients for general bulk bi-anisotropic structures with isotropic ambient (coefficients shown as a functions of the eigenvectors components):

$$
r_{pp} = \frac{\left(\dfrac{\psi_{21}^{sub}}{2} - \dfrac{\psi_{31}^{sub}}{2N_0\cos\theta_0}\right)\left(\dfrac{\psi_{42}^{sub}}{2N_0} - \dfrac{\psi_{12}^{sub}}{2\cos\theta_0}\right) - \left(\dfrac{\psi_{41}^{sub}}{2N_0} - \dfrac{\psi_{11}^{sub}}{2\cos\theta_0}\right)\left(\dfrac{\psi_{22}^{sub}}{2} - \dfrac{\psi_{32}^{sub}}{2N_0\cos\theta_0}\right)}{\left(\dfrac{\psi_{21}^{sub}}{2} - \dfrac{\psi_{31}^{sub}}{2N_0\cos\theta_0}\right)\left(\dfrac{\psi_{42}^{sub}}{2N_0} + \dfrac{\psi_{12}^{sub}}{2\cos\theta_0}\right) - \left(\dfrac{\psi_{41}^{sub}}{2N_0} + \dfrac{\psi_{11}^{sub}}{2\cos\theta_0}\right)\left(\dfrac{\psi_{22}^{sub}}{2} - \dfrac{\psi_{32}^{sub}}{2N_0\cos\theta_0}\right)} \quad (2.32)
$$

$$
r_{sp} = \frac{\left(\dfrac{\psi_{21}^{sub}}{2} - \dfrac{\psi_{31}^{sub}}{2N_0\cos\theta_0}\right)\left(\dfrac{\psi_{22}^{sub}}{2} + \dfrac{\psi_{32}^{sub}}{2N_0\cos\theta_0}\right) - \left(\dfrac{\psi_{21}^{sub}}{2} + \dfrac{\psi_{31}^{sub}}{2N_0\cos\theta_0}\right)\left(\dfrac{\psi_{22}^{sub}}{2} - \dfrac{\psi_{32}^{sub}}{2N_0\cos\theta_0}\right)}{\left(\dfrac{\psi_{21}^{sub}}{2} - \dfrac{\psi_{31}^{sub}}{2N_0\cos\theta_0}\right)\left(\dfrac{\psi_{42}^{sub}}{2N_0} + \dfrac{\psi_{12}^{sub}}{2\cos\theta_0}\right) - \left(\dfrac{\psi_{41}^{sub}}{2N_0} + \dfrac{\psi_{11}^{sub}}{2\cos\theta_0}\right)\left(\dfrac{\psi_{22}^{sub}}{2} - \dfrac{\psi_{32}^{sub}}{2N_0\cos\theta_0}\right)} \quad (2.33)
$$

$$
r_{ps} = \frac{\left(\dfrac{\psi_{41}^{sub}}{2N_0} - \dfrac{\psi_{11}^{sub}}{2\cos\theta_0}\right)\left(\dfrac{\psi_{42}^{sub}}{2N_0} + \dfrac{\psi_{12}^{sub}}{2\cos\theta_0}\right) - \left(\dfrac{\psi_{41}^{sub}}{2N_0} + \dfrac{\psi_{11}^{sub}}{2\cos\theta_0}\right)\left(\dfrac{\psi_{42}^{sub}}{2N_0} - \dfrac{\psi_{12}^{sub}}{2\cos\theta_0}\right)}{\left(\dfrac{\psi_{21}^{sub}}{2} - \dfrac{\psi_{31}^{sub}}{2N_0\cos\theta_0}\right)\left(\dfrac{\psi_{42}^{sub}}{2N_0} + \dfrac{\psi_{12}^{sub}}{2\cos\theta_0}\right) - \left(\dfrac{\psi_{41}^{sub}}{2N_0} + \dfrac{\psi_{11}^{sub}}{2\cos\theta_0}\right)\left(\dfrac{\psi_{22}^{sub}}{2} - \dfrac{\psi_{32}^{sub}}{2N_0\cos\theta_0}\right)} \quad (2.34)
$$

$$
r_{ss} = \frac{\left(\dfrac{\psi_{21}^{sub}}{2} + \dfrac{\psi_{31}^{sub}}{2N_0\cos\theta_0}\right)\left(\dfrac{\psi_{42}^{sub}}{2N_0} + \dfrac{\psi_{12}^{sub}}{2\cos\theta_0}\right) - \left(\dfrac{\psi_{41}^{sub}}{2N_0} + \dfrac{\psi_{11}^{sub}}{2\cos\theta_0}\right)\left(\dfrac{\psi_{22}^{sub}}{2} + \dfrac{\psi_{32}^{sub}}{2N_0\cos\theta_0}\right)}{\left(\dfrac{\psi_{21}^{sub}}{2} - \dfrac{\psi_{31}^{sub}}{2N_0\cos\theta_0}\right)\left(\dfrac{\psi_{42}^{sub}}{2N_0} + \dfrac{\psi_{12}^{sub}}{2\cos\theta_0}\right) - \left(\dfrac{\psi_{41}^{sub}}{2N_0} + \dfrac{\psi_{11}^{sub}}{2\cos\theta_0}\right)\left(\dfrac{\psi_{22}^{sub}}{2} - \dfrac{\psi_{32}^{sub}}{2N_0\cos\theta_0}\right)} \quad (2.35)
$$

$$
t_{pp} = \frac{\dfrac{\psi_{21}^{sub}}{2} - \dfrac{\psi_{31}^{sub}}{2N_0\cos\theta_0}}{\left(\dfrac{\psi_{21}^{sub}}{2} - \dfrac{\psi_{31}^{sub}}{2N_0\cos\theta_0}\right)\left(\dfrac{\psi_{42}^{sub}}{2N_0} + \dfrac{\psi_{12}^{sub}}{2\cos\theta_0}\right) - \left(\dfrac{\psi_{41}^{sub}}{2N_0} + \dfrac{\psi_{11}^{sub}}{2\cos\theta_0}\right)\left(\dfrac{\psi_{22}^{sub}}{2} - \dfrac{\psi_{32}^{sub}}{2N_0\cos\theta_0}\right)} \quad (2.36)
$$

$$
t_{sp} = -\frac{\dfrac{\psi_{22}^{sub}}{2} - \dfrac{\psi_{32}^{sub}}{2N_0\cos\theta_0}}{\left(\dfrac{\psi_{21}^{sub}}{2} - \dfrac{\psi_{31}^{sub}}{2N_0\cos\theta_0}\right)\left(\dfrac{\psi_{42}^{sub}}{2N_0} + \dfrac{\psi_{12}^{sub}}{2\cos\theta_0}\right) - \left(\dfrac{\psi_{41}^{sub}}{2N_0} + \dfrac{\psi_{11}^{sub}}{2\cos\theta_0}\right)\left(\dfrac{\psi_{22}^{sub}}{2} - \dfrac{\psi_{32}^{sub}}{2N_0\cos\theta_0}\right)} \quad (2.37)
$$

$$t_{ps} = -\frac{\dfrac{\psi_{41}^{sub}}{2N_0} - \dfrac{\psi_{11}^{sub}}{2\cos\theta_0}}{(\dfrac{\psi_{21}^{sub}}{2} - \dfrac{\psi_{31}^{sub}}{2N_0\cos\theta_0})(\dfrac{\psi_{42}^{sub}}{2N_0} + \dfrac{\psi_{12}^{sub}}{2\cos\theta_0}) - (\dfrac{\psi_{41}^{sub}}{2N_0} + \dfrac{\psi_{11}^{sub}}{2\cos\theta_0})(\dfrac{\psi_{22}^{sub}}{2} - \dfrac{\psi_{32}^{sub}}{2N_0\cos\theta_0})} \qquad (2.38)$$

$$t_{ss} = \frac{\dfrac{\psi_{42}^{sub}}{2N_0} - \dfrac{\psi_{12}^{sub}}{2\cos\theta_0}}{(\dfrac{\psi_{21}^{sub}}{2} - \dfrac{\psi_{31}^{sub}}{2N_0\cos\theta_0})(\dfrac{\psi_{42}^{sub}}{2N_0} + \dfrac{\psi_{12}^{sub}}{2\cos\theta_0}) - (\dfrac{\psi_{41}^{sub}}{2N_0} + \dfrac{\psi_{11}^{sub}}{2\cos\theta_0})(\dfrac{\psi_{22}^{sub}}{2} - \dfrac{\psi_{32}^{sub}}{2N_0\cos\theta_0})}, \qquad (2.39)$$

ψ_{ij}^{sub} calculated for some certain cases are available for download online in the form of

MatLab m-files which are located at *http://web.njit.edu/~sirenko/EllipsNJIT/index1.htm.*
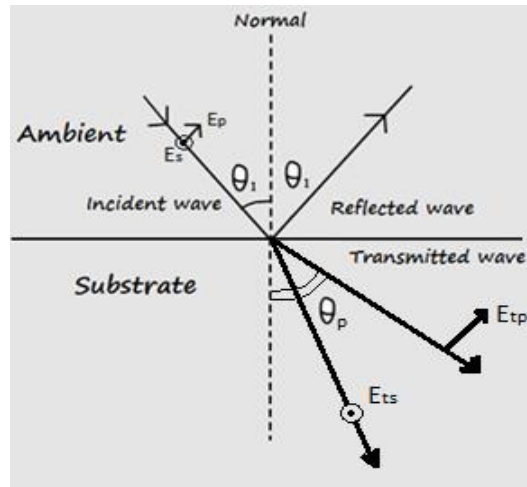
Figure 2.7 Decoupled E_{tp} and E_{ts} wave propagating inside substrate.

When transmitted waves are decoupled, there is a more physical way to show structure of exit matrix. In this case, structure of optical and $\tilde{\Delta}$ matrices look like in the following equations correspondingly.

$$M = \begin{pmatrix} \bullet & 0 & 0 & 0 & 0 & 0 \\ 0 & \bullet & 0 & 0 & 0 & 0 \\ 0 & 0 & \bullet & 0 & 0 & 0 \\ 0 & 0 & 0 & \bullet & 0 & 0 \\ 0 & 0 & 0 & 0 & \bullet & 0 \\ 0 & 0 & 0 & 0 & 0 & \bullet \end{pmatrix} \qquad (2.40)$$

$$\tilde{\Delta} = \begin{pmatrix} 0 & 0 & 0 & \Delta_{14} \\ 0 & 0 & \Delta_{23} & 0 \\ 0 & \Delta_{32} & 0 & 0 \\ \Delta_{41} & 0 & 0 & 0 \end{pmatrix} \tag{2.41}$$

Let's consider separately *p*-polarized and *s*-polarized waves. Rewrite Equation (2.14) into the form and consider *p*-polarized light first:

$$\begin{cases} \Delta_{11}E_x + \Delta_{12}E_y + \Delta_{13}H_x + \Delta_{14}H_y = q_z E_x \\ \Delta_{21}E_x + \Delta_{22}E_y + \Delta_{23}H_x + \Delta_{24}H_y = q_z E_y \\ \Delta_{31}E_x + \Delta_{32}E_y + \Delta_{33}H_x + \Delta_{34}H_y = q_z H_x \\ \Delta_{41}E_x + \Delta_{42}E_y + \Delta_{43}H_x + \Delta_{44}H_y = q_z H_y \end{cases} \tag{2.42}$$

We assume that there is no *y*-component of the electric field thus and substitution all off-diagonal terms of $\tilde{\Delta}$ matrix with zeroes we get:

$$\begin{cases} \Delta_{14}H_y = q_{zp}E_x \\ \Delta_{23}H_x = 0 \\ 0 = q_{zp}H_x \\ \Delta_{41}E_x = q_{zp}H_y \end{cases} \tag{2.43}$$

From first and fourth equations from the we get following dependencies on $\tilde{\Delta}$ matrix components of fields' projections and eigenvalues:

$$H_x = 0; H_y = \frac{q_{zp}}{\Delta_{14}}E_x = \frac{\Delta_{41}}{q_{zp}}E_x, \ q_{zp}^2 = \Delta_{14}\Delta_{41} \tag{2.44}$$

The same system of equations as System (2.43) can be written for *s*-polarized light ($E_x = 0$):

$$\begin{cases} \Delta_{14}H_y = 0 \\ \Delta_{23}H_x = q_{zs}E_y \\ \Delta_{32}E_y = q_{zs}H_x \\ 0 = q_{zs}H_y \end{cases}$$

(2.45)

From second and third equations from the system (2.45), we get following dependencies

on $\tilde{\Delta}$ matrix components of fields' projections and eigenvalues:

$$H_y = 0 \, ; H_x = \frac{q_{zs}}{\Delta_{23}}E_y = \frac{\Delta_{32}}{q_{zs}}E_y \, ; q_{zs}^2 = \Delta_{23}\Delta_{32}$$

(2.46)

We could find projection of fields inside a substrate from eigenvectors. Mode for p-polarized light and mode for s-polarized light become as in following equations correspondently:

$$\begin{pmatrix} E_x \\ 0 \\ H_x \\ H_y \end{pmatrix}_p = \begin{pmatrix} q_{zp} \\ 0 \\ 0 \\ \sqrt{\Delta_{41}} \end{pmatrix} E_{tp}$$

(2.47)

$$\begin{pmatrix} 0 \\ E_y \\ H_x \\ H_y \end{pmatrix}_s = \begin{pmatrix} 0 \\ \sqrt{\Delta_{23}} \\ q_{zs} \\ 0 \end{pmatrix} E_{ts}$$

(2.48)

Total transmitted wave has the form:

$$\begin{pmatrix} E_x \\ E_y \\ H_x \\ H_y \end{pmatrix} = \begin{pmatrix} E_x \\ 0 \\ H_x \\ H_y \end{pmatrix}_p + \begin{pmatrix} 0 \\ E_y \\ H_x \\ H_y \end{pmatrix}_s = \begin{pmatrix} q_{zp}E_{tp} \\ \sqrt{\Delta_{23}}E_{ts} \\ q_{zs}E_{ts} \\ \sqrt{\Delta_{14}}E_{tp} \end{pmatrix} = \begin{pmatrix} 0 & 0 & q_{zp} & 0 \\ \sqrt{\Delta_{23}} & 0 & 0 & 0 \\ q_{zs} & 0 & 0 & 0 \\ 0 & 0 & \sqrt{\Delta_{14}} & 0 \end{pmatrix} \begin{pmatrix} E_{ts} \\ 0 \\ E_{tp} \\ 0 \end{pmatrix}$$

(2.49)

Hence out matrix for this particular case is turned to be:

$$L_{out} = \begin{pmatrix} 0 & 0 & q_{zp} & 0 \\ \sqrt{\Delta_{23}} & 0 & 0 & 0 \\ q_{zs} & 0 & 0 & 0 \\ 0 & 0 & \sqrt{\Delta_{14}} & 0 \end{pmatrix} \qquad (2.50)$$

From practical point of view, substrates are usually made from materials which are isotropic or have anisotropic permittivity tensor, so we will be using Equation (2.50) for out matrix in the next chapter on electromagnetic wave propagation in multilayer systems. Consequently, the dependence of incident, reflected and transmitted wave has the following form:

$$\begin{pmatrix} E_{is} \\ E_{rs} \\ E_{ip} \\ E_{rp} \end{pmatrix} = L_{in} L_{out} \begin{pmatrix} E_{ts} \\ 0 \\ E_{tp} \\ 0 \end{pmatrix} = \frac{1}{2} \begin{pmatrix} 0 & 1 & -\dfrac{1}{N_0 \cos\theta_i} & 0 \\ 0 & 1 & \dfrac{1}{N_0 \cos\theta_i} & 0 \\ \dfrac{1}{\cos\theta_i} & 0 & 0 & \dfrac{1}{N_0} \\ -\dfrac{1}{\cos\theta_i} & 0 & 0 & \dfrac{1}{N_0} \end{pmatrix} \begin{pmatrix} 0 & 0 & q_{zp} & 0 \\ \sqrt{\Delta_{23}} & 0 & 0 & 0 \\ q_{zs} & 0 & 0 & 0 \\ 0 & 0 & \sqrt{\Delta_{14}} & 0 \end{pmatrix} \begin{pmatrix} E_{ts} \\ 0 \\ E_{tp} \\ 0 \end{pmatrix} \qquad (2.51)$$

To sum up, in this part of our work we present detailed discussion of electromagnetic wave propagation in bulk materials with arbitrary symmetry using Berreman's matrix formalism. We calculated Fresnel's coefficients as a function of substrate's $\tilde{\Delta}$ matrix eigenvector components and also presented explicit view of L_{out} matrix when transmitted modes in the substrate are decoupled. In the following Sections we'll continue with the treatment of particular ME tensor symmetries and will determine which components of Mueller matrix are sensitive to ME interaction.

2.3 Fresnel's Coefficients for Materials with Certain ME Tensor Symmetry

In this section, we determine Mueller matrix components dependencies on magneto-electric interaction. First, we consider a symmetry case with the off-diagonal components of the ME tensor $\hat{\alpha}$, as shown in the following optical and $\tilde{\Delta}$ matrices.

$$
M = \begin{pmatrix}
\varepsilon_{xx} & 0 & 0 & 0 & \alpha_{xy} & 0 \\
0 & \varepsilon_{yy} & 0 & -\alpha_{xy} & 0 & 0 \\
0 & 0 & \varepsilon_{zz} & 0 & 0 & 0 \\
0 & -\alpha_{xy}^{*} & 0 & \mu_{xx} & 0 & 0 \\
\alpha_{xy}^{*} & 0 & 0 & 0 & \mu_{yy} & 0 \\
0 & 0 & 0 & 0 & 0 & \mu_{zz}
\end{pmatrix}
\tag{2.52}
$$

$$
\tilde{\Delta} = \begin{pmatrix}
\alpha_{xy} & 0 & 0 & \mu_{yy} - \dfrac{N_0^2 \sin^2 \theta_0}{\varepsilon_{zz}} \\
0 & \alpha_{xy} & -\mu_{xx} & 0 \\
0 & \dfrac{N_0^2 \sin^2 \theta_0}{\mu_{zz}} - \varepsilon_{yy} & \alpha_{xy} & 0 \\
\varepsilon_{xx} & 0 & 0 & \alpha_{xy}
\end{pmatrix}
\tag{2.53}
$$
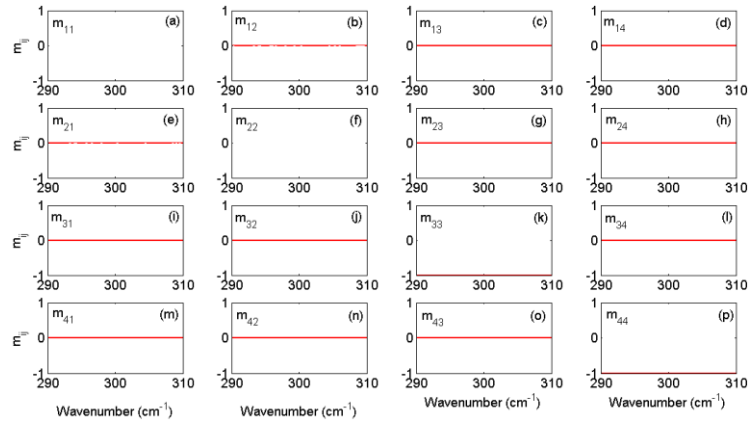
Figure 2.8   Normalized Mueller matrix components for $\begin{pmatrix} 0 & \alpha_{xy} & 0 \\ -\alpha_{xy} & 0 & 0 \\ 0 & 0 & 0 \end{pmatrix}$ ME tensor symmetry. Model contains one oscillator with $S_{\alpha,xy} = 0.01$; $\omega_0 = 300$ cm^{-1}; $\gamma = 2$; dielectric constant $\varepsilon_{xx} = \varepsilon_{yy} = \varepsilon_{zz} = 10$; magnetic permeability $\mu_{xx} = \mu_{yy} = \mu_{zz} = 1$; $AOI = 60°$.

$$M = \begin{pmatrix} \varepsilon_{xx} & 0 & 0 & 0 & 0 & 0 \\ 0 & \varepsilon_{yy} & 0 & 0 & 0 & \alpha_{yz} \\ 0 & 0 & \varepsilon_{zz} & 0 & -\alpha_{yz} & 0 \\ 0 & 0 & 0 & \mu_{xx} & 0 & 0 \\ 0 & 0 & -\alpha_{yz}^* & 0 & \mu_{yy} & 0 \\ 0 & \alpha_{yz}^* & 0 & 0 & 0 & \mu_{zz} \end{pmatrix} \qquad (2.54)$$

$$\tilde{\Delta} = \begin{pmatrix} 0 & -\alpha_{yz} & 0 & \mu_{yy} + \dfrac{N_0 \sin\theta_0 (\alpha_{yz} - N_0 \sin\theta_0)}{\varepsilon_{zz}} \\ 0 & 0 & -\mu_{xx} & 0 \\ \dfrac{\alpha_{yz}(\alpha_{yz} - N_0 \sin\theta_0)}{\mu_{zz}} & -\varepsilon_{yy} - \dfrac{N_0 \sin\theta_0 (\alpha_{yz} - N_0 \sin\theta_0)}{\mu_{zz}} & 0 & 0 \\ \varepsilon_{xx} & 0 & 0 & 0 \end{pmatrix} \qquad (2.55)$$
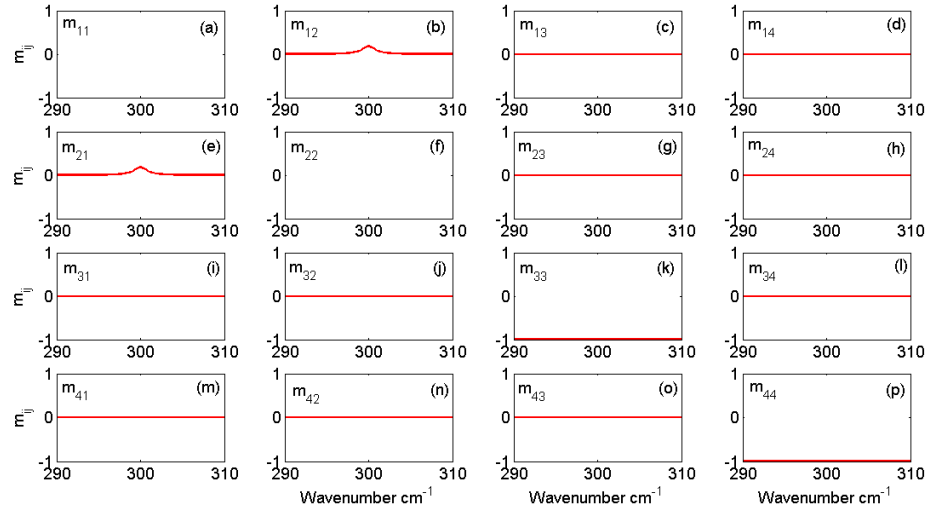
Figure 2.9 Normalized Mueller matrix components for $\begin{pmatrix} 0 & 0 & 0 \\ 0 & 0 & \alpha_{yz} \\ 0 & -\alpha_{yz} & 0 \end{pmatrix}$ ME tensor symmetry.

Model contains one oscillator with $S_{\alpha,yz} = 0.01$; $\omega_0 = 300\,\text{cm}^{-1}, \gamma = 2$; dielectric constant $\varepsilon_{xx} = \varepsilon_{yy} = \varepsilon_{zz} = 10$; magnetic permeability $\mu_{xx} = \mu_{yy} = \mu_{zz} = 1$; $AOI = 60°$.

$$M = \begin{pmatrix} \varepsilon_{xx} & 0 & 0 & 0 & 0 & \alpha_{xz} \\ 0 & \varepsilon_{yy} & 0 & 0 & 0 & 0 \\ 0 & 0 & \varepsilon_{zz} & -\alpha_{xz} & 0 & 0 \\ 0 & 0 & -\alpha_{xz}^{*} & \mu_{xx} & 0 & 0 \\ 0 & 0 & 0 & 0 & \mu_{yy} & 0 \\ \alpha_{xz}^{*} & 0 & 0 & 0 & 0 & \mu_{zz} \end{pmatrix} \tag{2.56}$$

$$\tilde{\Delta} = \begin{pmatrix} 0 & 0 & \dfrac{\alpha_{xz} N_0 \sin\theta_0}{\varepsilon_{zz}} & \mu_{yy} - \dfrac{N_0^2 \sin\theta_0^2}{\varepsilon_{zz}} \\[3mm] 0 & 0 & \dfrac{\alpha_{xz}^2}{\varepsilon_{zz}} - \mu_{xx} & \dfrac{\alpha_{xz} N_0 \sin\theta_0}{\varepsilon_{zz}} \\[3mm] -\dfrac{\alpha_{xz} N_0 \sin\theta_0}{\mu_{zz}} & \dfrac{N_0^2 \sin\theta_0^2}{\mu_{zz}} - \varepsilon_{yy} & 0 & 0 \\[3mm] -\dfrac{\alpha_{xz}^2}{\mu_{zz}} + \varepsilon_{xx} & \dfrac{\alpha_{xz} N_0 \sin\theta_0}{\mu_{zz}} & 0 & 0 \end{pmatrix} \tag{2.57}$$

Figure 2.10 Normalized Mueller matrix components for $\begin{pmatrix} 0 & 0 & \alpha_{xz} \\ 0 & 0 & 0 \\ -\alpha_{xz} & 0 & 0 \end{pmatrix}$ ME tensor symmetry. Model contains one oscillator with $S_{\alpha,xz} = 0.01$; $\omega_0 = 300$ cm^{-1}, $\gamma = 2$; dielectric constant $\varepsilon_{xx} = \varepsilon_{yy} = \varepsilon_{zz} = 10$; magnetic permeability $\mu_{xx} = \mu_{yy} = \mu_{zz} = 1$; $AOI = 60^{\circ}$.

$$M = \begin{pmatrix} \varepsilon_{xx} & 0 & 0 & \alpha_{xx} & 0 & 0 \\ 0 & \varepsilon_{yy} & 0 & 0 & 0 & 0 \\ 0 & 0 & \varepsilon_{zz} & 0 & 0 & 0 \\ \alpha_{xx}^* & 0 & 0 & \mu_{xx} & 0 & 0 \\ 0 & 0 & 0 & 0 & \mu_{yy} & 0 \\ 0 & 0 & 0 & 0 & 0 & \mu_{zz} \end{pmatrix} \tag{2.58}$$

$$\tilde{\Delta} = \begin{pmatrix} 0 & 0 & 0 & \mu_{yy} - \dfrac{N_0^2 \sin\theta_0^2}{\varepsilon_{zz}} \\ -\alpha_{xx} & 0 & -\mu_{xx} & 0 \\ 0 & \dfrac{N_0^2 \sin\theta_0^2}{\mu_{zz}} - \varepsilon_{yy} & 0 & 0 \\ \varepsilon_{xx} & 0 & \alpha_{xx} & 0 \end{pmatrix} \tag{2.59}$$

Figure 2.11 Normalized Mueller matrix components for $\begin{pmatrix} \alpha_{xx} & 0 & 0 \\ 0 & 0 & 0 \\ 0 & 0 & 0 \end{pmatrix}$ ME tensor symmetry. Model contains one oscillator with $S_{\alpha,xx} = 0.01$; $\omega_0 = 300\,\text{cm}^{-1}$, $\gamma = 2$; dielectric constant $\varepsilon_{xx} = \varepsilon_{yy} = \varepsilon_{zz} = 10$; magnetic permeability $\mu_{xx} = \mu_{yy} = \mu_{zz} = 1$; $AOI = 60^\circ$.

$$M = \begin{pmatrix} \varepsilon_{xx} & 0 & 0 & 0 & 0 & 0 \\ 0 & \varepsilon_{yy} & 0 & 0 & \alpha_{yy} & 0 \\ 0 & 0 & \varepsilon_{zz} & 0 & 0 & 0 \\ 0 & 0 & 0 & \mu_{xx} & 0 & 0 \\ 0 & \alpha_{yy}^* & 0 & 0 & \mu_{yy} & 0 \\ 0 & 0 & 0 & 0 & 0 & \mu_{zz} \end{pmatrix} \tag{2.60}$$

$$\tilde{\Delta} = \begin{pmatrix} 0 & \alpha_{yy} & 0 & \mu_{yy} - \dfrac{N_0^2 \sin\theta_0^2}{\varepsilon_{zz}} \\ 0 & 0 & -\mu_{xx} & 0 \\ 0 & \dfrac{N_0^2 \sin\theta_0^2}{\mu_{zz}} - \varepsilon_{yy} & 0 & -\alpha_{yy} \\ \varepsilon_{xx} & 0 & 0 & 0 \end{pmatrix} \tag{2.61}$$
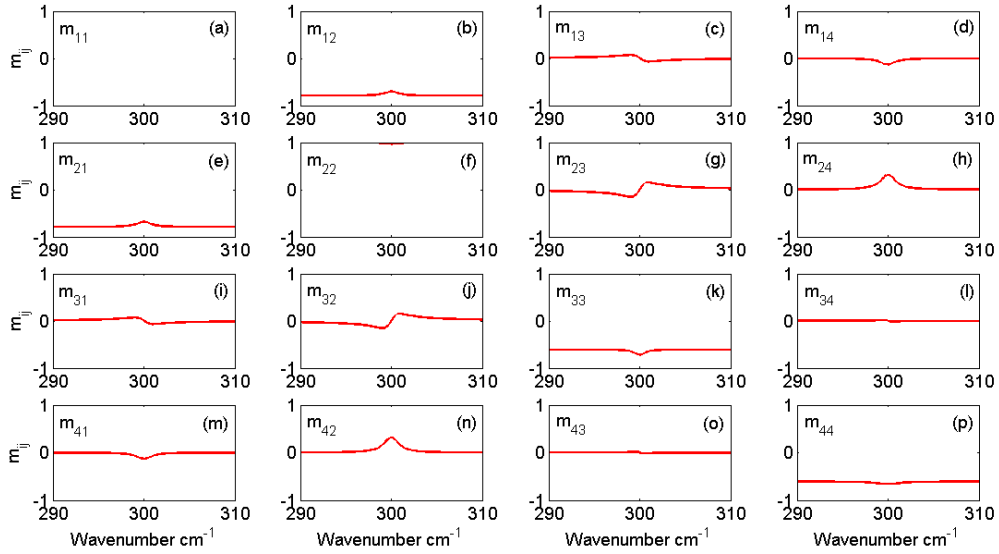
Figure 2.12 Normalized Mueller matrix components for $\begin{pmatrix} 0 & 0 & 0 \\ 0 & \alpha_{yy} & 0 \\ 0 & 0 & 0 \end{pmatrix}$ ME tensor symmetry.

Model contains one oscillator with $S_{\alpha,yy} = 0.01$; $\omega_0 = 300\,\text{cm}^{-1}$, $\gamma = 2$; dielectric constant $\varepsilon_{xx} = \varepsilon_{yy} = \varepsilon_{zz} = 10$; magnetic permeability $\mu_{xx} = \mu_{yy} = \mu_{zz} = 1$; $AOI = 60°$.

$$M = \begin{pmatrix} \varepsilon_{xx} & 0 & 0 & 0 & 0 & 0 \\ 0 & \varepsilon_{yy} & 0 & 0 & 0 & 0 \\ 0 & 0 & \varepsilon_{zz} & 0 & 0 & \alpha_{zz} \\ 0 & 0 & 0 & \mu_{xx} & 0 & 0 \\ 0 & 0 & 0 & 0 & \mu_{yy} & 0 \\ 0 & 0 & \alpha_{zz}^* & 0 & 0 & \mu_{zz} \end{pmatrix} \tag{2.62}$$

$$\tilde{\Delta} = \begin{pmatrix} 0 & -\dfrac{N_0^2 \sin^2\theta_0 \alpha_{zz}}{\varepsilon_{zz}\mu_{zz} - \alpha_{zz}^2} & 0 & \mu_{yy} - \dfrac{N_0^2 \sin^2\theta_0 \mu_{zz}}{\varepsilon_{zz}\mu_{zz} - \alpha_{zz}^2} \\ 0 & 0 & -\mu_{xx} & 0 \\ 0 & \dfrac{N_0^2 \sin^2\theta_0 \varepsilon_{zz}}{\varepsilon_{zz}\mu_{zz} - \alpha_{zz}^2} - \varepsilon_{yy} & 0 & \dfrac{N_0^2 \sin^2\theta_0 \alpha_{zz}}{\varepsilon_{zz}\mu_{zz} - \alpha_{zz}^2} \\ \varepsilon_{xx} & 0 & 0 & 0 \end{pmatrix} \tag{2.63}$$
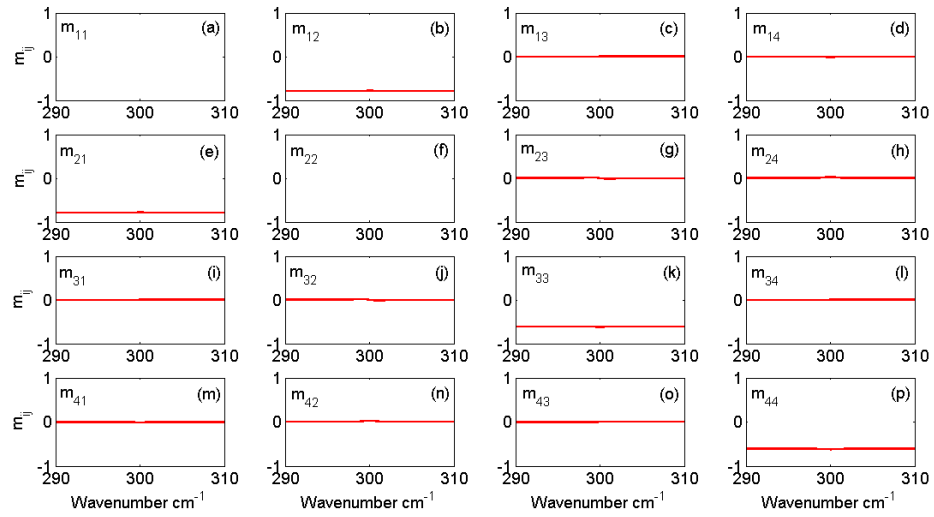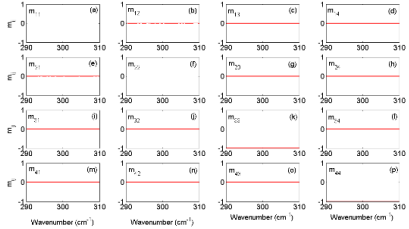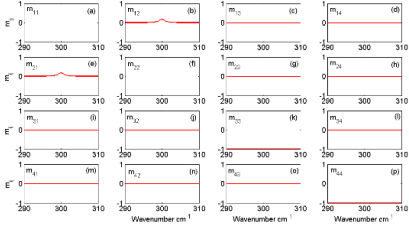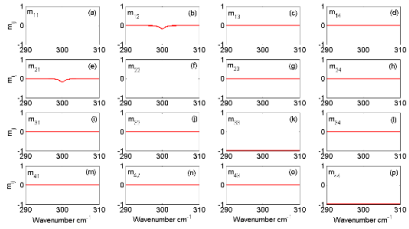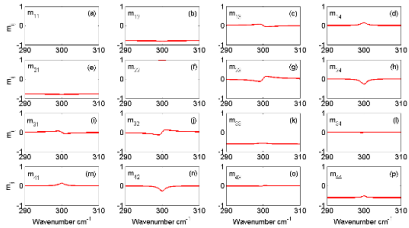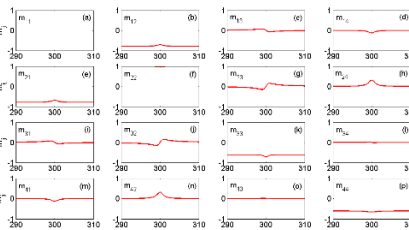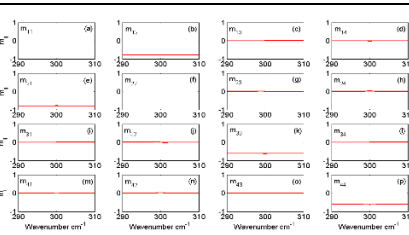
Figure 2.13 Normalized Mueller matrix components for $\begin{pmatrix} 0 & 0 & 0 \\ 0 & 0 & 0 \\ 0 & 0 & \alpha_{zz} \end{pmatrix}$ ME tensor symmetry.

Model contains one oscillator with $S_{\alpha,zz} = 0.01$; $\omega_0 = 300\,\text{cm}^{-1}, \gamma = 2$; dielectric constant $\varepsilon_{xx} = \varepsilon_{yy} = \varepsilon_{zz} = 10$; magnetic permeability $\mu_{xx} = \mu_{yy} = \mu_{zz} = 1$; $AOI = 60°$.

Table 2.2 Dependence of the MM Components on the Symmetry-allowed ME Interaction. The ME tensor Components are in the Left Column, MM Spectra are in the Middle Column, and the Comments are in the Right Column

ME tensor	MM plot	α appearance in MM components
$\begin{pmatrix} 0 & \alpha_{xy} & 0 \\ \alpha_{xy}^* & 0 & 0 \\ 0 & 0 & 0 \end{pmatrix}$		None
$\begin{pmatrix} 0 & 0 & 0 \\ 0 & 0 & \alpha_{yz} \\ 0 & \alpha_{yz}^* & 0 \end{pmatrix}$		m_{12}, m_{21}
$\begin{pmatrix} 0 & 0 & \alpha_{xz} \\ 0 & 0 & 0 \\ \alpha_{xz}^* & 0 & 0 \end{pmatrix}$		m_{12}, m_{21}
$\begin{pmatrix} \alpha_{xx} & 0 & 0 \\ 0 & 0 & 0 \\ 0 & 0 & 0 \end{pmatrix}$		Diagonal weak Off-diagonal strong
$\begin{pmatrix} 0 & 0 & 0 \\ 0 & \alpha_{yy} & 0 \\ 0 & 0 & 0 \end{pmatrix}$		Diagonal weak Off-diagonal strong
$\begin{pmatrix} 0 & 0 & 0 \\ 0 & 0 & 0 \\ 0 & 0 & \alpha_{zz} \end{pmatrix}$		All weak

It should be noted as well that the strength of magneto-electric features in Mueller matrix spectra components depends on the background values of ε and μ. We pointed out earlier that magneto-electric interaction is bounded by the geometric mean of the diagonalized permittivity and permeability tensors. The closer α approaches to this thermodynamic limit the stronger contribution in MM components. Simultaneous increase in values of ε, μ and α, when Equation (1.3) still holds, results in more stronger appearance in MM components of ME contribution.

The main result of simulations presented in Table 2.2 is a demonstration of the fact that MM spectroscopic ellipsometry that measures all spectral components presented in Figures 2.8 – 2.13 can distinguish different symmetries of the α tensor. For example, α_{xx} and α_{yy} peaks have different sign (positive and negative) in the spectra of m_{23} and m_{24}.

2.4 Mueller Matrix Analysis of the Space Group Symmetry in InMnO₃

Another possible application of Mueller Matrix technique using previously developed formalism is the experimental determination of the magnetic symmetries of materials. One of them is hexagonal InMnO₃.

There was a debate in literature about the symmetry of the ground state of InMnO₃: The centrosymmetric, non-polar and ferroelectric space groups have been considered. In the early studies, $P6_3cm$ symmetry [20,21,22] and ferroelectricity under ambient conditions [12] have been reported and supported by theory [23]. However, in more recent studies an absence of ferroelectricity has been found [24] and experimentally confirmed using a combination of x-ray diffraction, piezoresponse force microscopy (PFM), optical

second harmonic generation (SHG), and supported by density functional theory (DFT) calculations. Thus, a centrosymmetric structure with   space group was found, instead of the ferroelectric one. Below we show the four big optical matrices that appear in Equation (2.6) for the three space groups discussed in regard to InMnO₃: $P6_3/mmc$, $P\bar{3}c$ and $P6_3cm$. Examples of some possible magnetic point groups are also shown in brackets. The last two big optical matrices of the right correspond to the same structural group, but two different magnetic symmetries:

$$P6_3/mmc\ (6_z/m_zm_xm_1) \qquad P\bar{3}c\ (\bar{3}_zm_x) \qquad P6_3cm\ (6_zm_xm_1) \qquad P6_3cm\ (6_zm_x{}'m_1{}')$$

$$
\left[
\begin{pmatrix} \varepsilon_\perp & 0 & 0 \\ & \varepsilon_\perp & 0 \\ & & \varepsilon_\parallel \end{pmatrix}
\begin{pmatrix} 0 & 0 & 0 \\ 0 & 0 & 0 \\ 0 & 0 & 0 \end{pmatrix}
\right.
\left.
\begin{pmatrix} 0 & 0 & 0 \\ 0 & 0 & 0 \\ 0 & 0 & 0 \end{pmatrix}
\begin{pmatrix} \mu_\perp & 0 & 0 \\ & \mu_\perp & 0 \\ & & \mu_\parallel \end{pmatrix}
\right]
$$

$$
\left[
\begin{pmatrix} \varepsilon_\perp & 0 & 0 \\ & \varepsilon_\perp & 0 \\ & & \varepsilon_\parallel \end{pmatrix}
\begin{pmatrix} 0 & 0 & 0 \\ 0 & 0 & 0 \\ 0 & 0 & 0 \end{pmatrix}
\right.
\left.
\begin{pmatrix} 0 & 0 & 0 \\ 0 & 0 & 0 \\ 0 & 0 & 0 \end{pmatrix}
\begin{pmatrix} \mu_\perp & 0 & 0 \\ & \mu_\perp & 0 \\ & & \mu_\parallel \end{pmatrix}
\right]
$$

$$
\left[
\begin{pmatrix} \varepsilon_\perp & 0 & 0 \\ & \varepsilon_\perp & 0 \\ & & \varepsilon_\parallel \end{pmatrix}
\begin{pmatrix} 0 & \alpha_{zn} & 0 \\ -\alpha_{zn} & 0 & 0 \\ 0 & 0 & 0 \end{pmatrix}
\right.
\left.
\begin{pmatrix} 0 & -\alpha_{zn} & 0 \\ \alpha_{zn} & 0 & 0 \\ 0 & 0 & 0 \end{pmatrix}
\begin{pmatrix} \mu_\perp & 0 & 0 \\ & \mu_\perp & 0 \\ & & \mu_\parallel \end{pmatrix}
\right]
$$

$$
\left[
\begin{pmatrix} \varepsilon_\perp & 0 & 0 \\ & \varepsilon_\perp & 0 \\ & & \varepsilon_\parallel \end{pmatrix}
\begin{pmatrix} \alpha_\perp & 0 & 0 \\ 0 & \alpha_\perp & 0 \\ 0 & 0 & \alpha_\parallel \end{pmatrix}
\right.
\left.
\begin{pmatrix} \alpha_\perp & 0 & 0 \\ 0 & \alpha_\perp & 0 \\ 0 & 0 & \alpha_\parallel \end{pmatrix}
\begin{pmatrix} \mu_\perp & 0 & 0 \\ & \mu_\perp & 0 \\ & & \mu_\parallel \end{pmatrix}
\right]
$$

Figure 2.14. Possible magnetic symmetries for hexagonal InMnO₃ multiferroic single crystal.

One can see that the diagonal elements of the big optical matrix contain the same set of components $\varepsilon_\perp, \varepsilon_\parallel, \mu_\perp, \mu_\parallel$ for all three structural point groups for this hexagonal system. In contrast, the off-diagonal elements of the big optical matrix can be different depending on the structural and magnetic point groups. For example, the centrosymmetric phase $P6_3/mmc\ (6_z/m_zm_xm_1)$ and $P\bar{3}c(\bar{3}_zm_x)$ are expected to have $\hat{\alpha}=0$, while $P6_3cm\ (6_zm_xm_1)$ phase has non-zero elements of the magneto-electric tensor. For $6_zm_xm_1$, $\alpha_{xy}=-\alpha_{yx}\neq 0$, while for $6_zm_x{}'m_1{}'$ the ME tensor is diagonal with two non-zero elements $\alpha_\perp$ and $\alpha_\parallel$. Thus, the big optical matrix and, hence, MM-SE ellipsometry

are sensitive to the magnetic point groups being able to differentiate, for example, $6_z/m_z m_x m_1$, $6_z m_x m_1$, and $6_z m_x' m_1'$ for the same $P6_3 cm$ structural symmetry. Figure 2.14 shows our model calculations for the diagonal and off-diagonal MM components for three magnetic symmetry cases: $6_z/m_z m_x m_1$, $6_z m_x m_1$ and $6_z m_x' m_1'$. The oscillators in Figure 2.14 (a) correspond to the polar phonon mode polarized along the c-axis in the hexagonal structure. The main contribution originates, of course, from the $\hat{\varepsilon}(\omega)$ tensor.
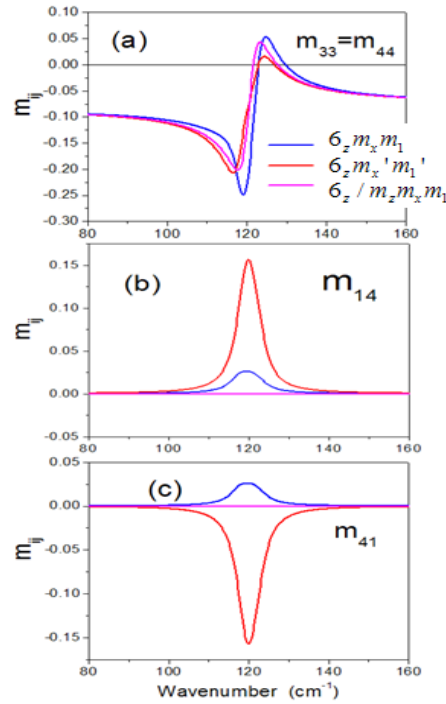
Figure 2.15 Simulated diagonal and off-diagonal MM components for three symmetry cases: $6_z/m_z m_x m_1$, $6_z m_x m_1$ and $6_z m_x' m_1'$: pink, blue, and red curves. The oscillator at 120 cm^{-1} in (a) corresponds to the polar phonon mode polarized along the c-axis in the hexagonal structure. The peaks in the off-diagonal components of the MM in (b) and (c) correspond to the ME tensor components of the same excitation that are allowed by symmetry.

The peaks in the off-diagonal components of the MM in Figure 2.14 (b,c) correspond to the ME tensor components at the phonon frequency. These components are symmetry-sensitive as seen from comparison of the blue and red spectra. Blue spectra are

both positive in $m_{14}(\omega)$ and $m_{41}(\omega)$, while red spectra have opposite sign in $m_{14}(\omega)$ and $m_{41}(\omega)$. Cleary, the MM components are qualitatively different for the different magnetic symmetries, illustrating the power of this approach. While the case of InMnO$_3$ appears to be settled, the symmetries of many other hexagonal compounds discussed here are unknown and will be investigated using ellipsometry. In general, using MMSE, we will be able to measure the parameters of the polar optical phonons, magnons, and electromagnons and compare them for the temperatures above and below the ferroelectric or magnetic transition temperatures. The simultaneous measurements of the off-diagonal components of the MM will provide information about the magneto-electric excitations and the corresponding magnetic group symmetry of the investigated hexagonal samples.

CHAPTER 3

ELECTROMAGNETIC WAVE PROPAGATION IN
BI-ANISOTROPIC MULTILAYER STRUCTURES

In this chapter, original results are shown for calculation techniques for the wave propagation in bi-anisotropic multilayer systems. As shown in the previous chapter, methods for wave propagation in bulk materials were based on the matrices L_{in} and L_{out} in the form of Equation (2.22) and Equation (2.29). For general anisotropic media when transmitted modes are coupled, Equation (2.29) should be used to find the L_{out} matrix. In order to take into account the optical response from thin film layers sandwiched between ambient and substrate one should construct matrices which project xy-components of the fields through all layers, from the top interface to the bottom interface. There are two common strategies of obtaining these matrices. In the first case, which is more detailed but not so desirable for obtaining analytical solutions, we will refer to as a "layer matrix L" method. This approach requires calculations of eigenvectors of each layer's $\tilde{\Delta}$ matrix and,
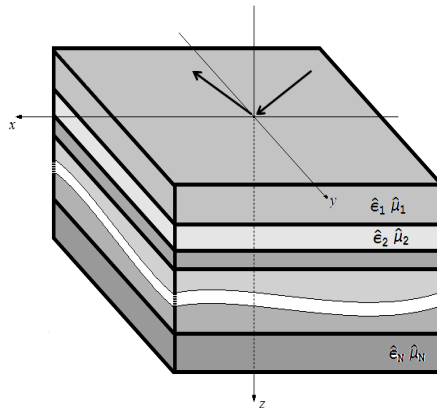
Figure 3.1 General schematics for a bi-anisotropic multilayer system. Incident wave is in the xz-plane. Positive z-direction is vertically down.

based on a trivial solution of the matrix wave equation, constructing propagating matrix K. Second method uses Cayley-Hamilton theorem [25] from linear algebra which provides a faster way to obtaining layer matrix without calculating eigenvectors. We will call layer matrix partial transfer matrix T_p in this case. For discussion of advantages and disadvantages of each method, we solve in the beginning anisotropic double layer system without ME activity problem on isotropic substrate, show consistency with previous developed works and then give general analytical expressions of Fresnel's coefficients for arbitrary systems (Figure 3.1) using second method. We also show simulation of optical response for a single layer, bilayer and a superlattice structure with N bilayers for some cases of certain ME tensor symmetry in terms of MM and reflectance and compare it with numerical calculations. In the final section, we briefly discuss simulating/fitting software developed as a part of this Thesis. Graphical user interface will be presented and some capabilities explained.
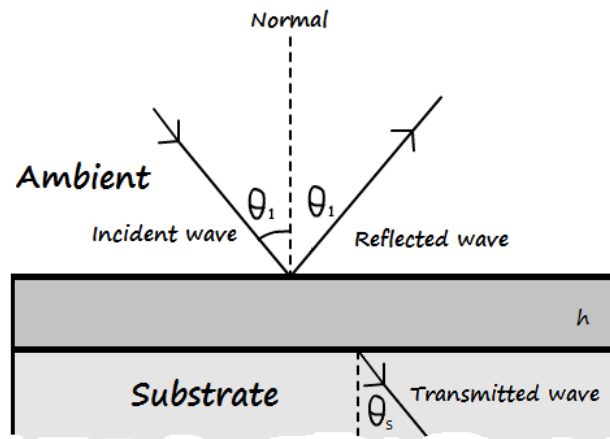
Figure 3.2 Scheme for anisotropic single thin film wave propagation.

3.1 Prior Works for Thin Films

Light propagation in thin films has been studied in a number of theoretical papers. The review can be found in P.Rogers *et al* [16]. Here we present the summary for the most important theoretical developments for single layer systems on isotropic substrate from P. Rogers' Theses and his papers [16,17]. Sketch of the system and wave propagation is shown in Figure 3.2. Fresnel's coefficients solutions are shown below.

$$r_{pp} = \frac{q_{zp}\cos(q_{zp}h)(\frac{N_s}{N_0}k_{z0}-\frac{N_0}{N_2}k_{zs})+i(\frac{N_0 N_2 q_{zp}^2}{\varepsilon_{xx}}-\frac{\varepsilon_{xx}k_{z0}k_{zs}}{N_0 N_2})\sin(q_{zp}h)}{q_{zp}\cos(q_{zp}h)(\frac{N_s}{N_0}k_{z0}+\frac{N_0}{N_2}k_{zs})-i(\frac{N_0 N_2 q_{zp}^2}{\varepsilon_{xx}}+\frac{\varepsilon_{xx}k_{z0}k_{zs}}{N_0 N_2})\sin(q_{zp}h)}$$

$$; r_{ss} = \frac{q_{zs}\cos(q_{zs}h)(k_{z0}-k_{zs})+i(\frac{q_{zp}^2}{\mu_{xx}}-k_{z0}k_{zs}\mu_{xx})\sin(q_{zs}h)}{q_{zs}\cos(q_{zs}h)(k_{z0}+k_{zs})-i(\frac{q_{zp}^2}{\mu_{xx}}+k_{z0}k_{zs}\mu_{xx})\sin(q_{zs}h)}$$

$$t_{pp} = \frac{2k_{z0}q_{zp}}{q_{zp}\cos(q_{zp}h)(\frac{N_s}{N_0}k_{z0}+\frac{N_0}{N_2}k_{zs})-i(\frac{N_0 N_2 q_{zp}^2}{\varepsilon_{xx}}+\frac{\varepsilon_{xx}k_{z0}k_{zs}}{N_0 N_2})\sin(q_{zp}h)}$$

$$; t_{ss} = \frac{2k_{z0}q_{zs}}{q_{zs}\cos(q_{zs}h)(k_{z0}+k_{zs})-i(\frac{q_{zp}^2}{\mu_{xx}}+k_{z0}k_{zs}\mu_{xx})\sin(q_{zs}h)}$$

$$(3.1)$$
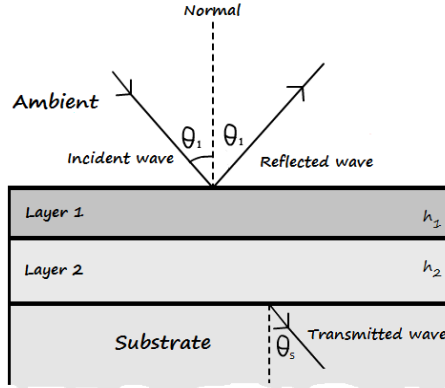
Figure 3.3 Scheme for anisotropic bilayer thin film wave propagation

3.2 Layer Matrix Technique and Analytical Solutions for Bilayer Anisotropic Structure with Zero ME Tensor on Isotropic Substrate

In this section, our original results for bilayer structures are presented. In short, we have increased the number of anisotropic layers compared (Figure 3.3) to that has been done previously by P.Rogers [16]. This step is conceptually important since it leads to the future

development of the theory for multilayers and superlattices. The latter could be considered as 1D metamaterials, thus bringing together several directions of our research. We use layer
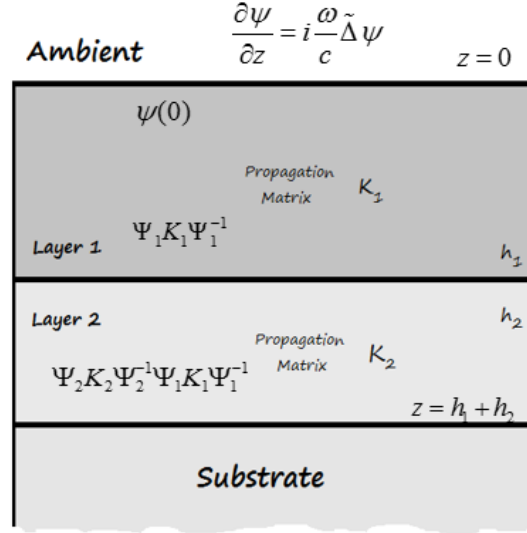
Figure 3.4 Notations for a bilayer structure calculations using a layer matrix L method.

matrix technique in this case.

In the chapter on bulk structures, we got explicit expression for matrix wave Equation (2.13). When $\tilde{\Delta}$ matrix does not depends on z we can integrate it and obtain

$$\psi(z) = e^{i\frac{\omega}{c}\tilde{\Delta}z}\psi(0) \tag{3.2}$$

For each particular mode solution becomes:

$$\psi_i(z) = e^{i\frac{\omega}{c}q_{z,i}z}\psi_i(0) \tag{3.3}$$

Let's consider detail structure of the electromagnetic wave inside the multilayers (Figure 3.4). Each mode variation inside a layer is shown in Equation (3.3). Thus if we want to construct a matrix, which contains all optical modes, such a matrix, which relates modes at the interfaces of the n and n-1 layers, must have the form shown below. It is called a propagation matrix K.

$$\Psi_i = \begin{pmatrix} \psi_1^{(N)} & \psi_2^{(N)} & \psi_3^{(N)} & \psi_4^{(N)} \end{pmatrix} \tag{3.4}$$

$$K_i = \begin{pmatrix} e^{iq_{11}^{(N)}h} & 0 & 0 & 0 \\ 0 & e^{iq_{22}^{(N)}h} & 0 & 0 \\ 0 & 0 & e^{iq_{33}^{(N)}h} & 0 \\ 0 & 0 & 0 & e^{iq_{44}^{(N)}h} \end{pmatrix} \tag{3.5}$$

In order to obtain layer matrix which relates all components at one interface to another one we write down:

$$L_i \Psi_i = \Psi_i K_i \tag{3.6}$$

It is easy to see that layer matrix can be expressed as

$$L_i = \Psi_i K_i \Psi_i^{-1} \tag{3.7}$$

If we have a multilayer structure, one needs to project components from n to $n+m$ layer by doing simple multiplication between each layer matrices $L_n L_{n+1} ... L_{n+m}$. The resultant matrix, which project components from ambient interface to substrate interface, looks as follows

$$L = \prod_{i=1}^{n} L_i = \prod_{i=1}^{n} \Psi_i K_i \Psi_i^{-1} \tag{3.8}$$

The layer matrix for a bilayer structure can be obtained as shown below. In the previous chapter on bulk structures in Equation (2.23) we showed boundary conditions for an ambient-substrate interface.

$$L = L_1 L_2 = \Psi_2 K_2 \Psi_2^{-1} \Psi_1 K_1 \Psi_1^{-1} = \begin{pmatrix} l_{11} & l_{12} & l_{13} & l_{14} \\ l_{21} & l_{22} & l_{23} & l_{24} \\ l_{31} & l_{32} & l_{33} & l_{34} \\ l_{41} & l_{42} & l_{43} & l_{44} \end{pmatrix} \tag{3.9}$$

After adding layer matrix and modifying Equation (2.23) for bilayer structure with isotropic substrate we obtain:

$$
\begin{pmatrix} E_{tp}\cos\theta_s \\ N_s E_{tp} \\ E_{ts} \\ N_s E_{ts}\cos\theta_s \end{pmatrix} = \begin{pmatrix} l_{11} & l_{12} & l_{13} & l_{14} \\ l_{21} & l_{22} & l_{23} & l_{24} \\ l_{31} & l_{32} & l_{33} & l_{34} \\ l_{41} & l_{42} & l_{43} & l_{44} \end{pmatrix} \begin{pmatrix} (E_{ip}-E_{rp})\cos\theta_0 \\ N_0(E_{ip}+E_{rp}) \\ E_{is}+E_{rs} \\ N_0(E_{is}-E_{rs})\cos\theta_0 \end{pmatrix}
\tag{3.10}
$$

The system ratios $\dfrac{E_{rp}}{E_{ip}}, \dfrac{E_{tp}}{E_{ip}}, \dfrac{E_{rs}}{E_{is}}, \dfrac{E_{ts}}{E_{is}}$ can be easily found, which give reflection and transmission coefficients for media, or more explicitly:

$$
r = \begin{pmatrix} r_{pp} & r_{ps} \\ r_{sp} & r_{ss} \end{pmatrix} = \frac{1}{a_{rs}b_{rp}-a_{rp}b_{rs}} \begin{pmatrix} a_{ip}b_{rs}-a_{rs}b_{ip} & a_{is}b_{rs}-a_{rs}b_{is} \\ a_{rp}b_{ip}-a_{ip}b_{rp} & a_{rp}b_{is}-a_{is}b_{rp} \end{pmatrix}
\tag{3.11}
$$

with $a_{ip}, a_{rp}, a_{is}, a_{rs}, b_{ip}, b_{rp}, b_{is}, b_{rs}$ are given by

$$
\begin{aligned}
a_{ip} &= \cos\theta_0(l_{11}N_2 - l_{21}\cos\theta_2) + N_0(l_{12}N_2 - l_{22}\cos\theta_2) \\
a_{rp} &= -\cos\theta_0(l_{11}N_2 - l_{21}\cos\theta_2) + N_0(l_{12}N_2 - l_{22}\cos\theta_2) \\
a_{is} &= N_0\cos\theta_0(l_{14}N_2 - l_{24}\cos\theta_2) + (l_{13}N_2 - l_{23}\cos\theta_2) \\
a_{rs} &= -N_0\cos\theta_0(l_{14}N_2 - l_{24}\cos\theta_2) + (l_{13}N_2 - l_{23}\cos\theta_2) \\
b_{ip} &= \cos\theta_0(l_{31}N_2\cos\theta_2 - l_{41}) + N_0(l_{32}N_2\cos\theta_2 - l_{42}) \\
b_{rp} &= -\cos(\theta_0)(l_{31}N_2\cos(\theta_2) - l_{41}) + N_0(l_{32}N_2\cos(\theta_2) - l_{42}) \\
b_{is} &= N_0\cos(\theta_0)(l_{34}N_2\cos(\theta_2) - l_{44}) + (l_{33}N_2\cos(\theta_2) - l_{43}) \\
b_{rs} &= -N_0\cos(\theta_0)(l_{34}N_2\cos(\theta_2) - l_{44}) + (l_{33}N_2\cos(\theta_2) - l_{43})
\end{aligned}
\tag{3.12}
$$

Fresnel's coefficients for transmission can be found the same way, which gives

$$
t = \begin{pmatrix} t_{pp} & t_{ps} \\ t_{sp} & t_{ss} \end{pmatrix}
\tag{3.13}
$$

$$t_{pp} = \frac{1}{N_2}(l_{21}cos\theta_0 + l_{22}N_0 + r_{pp}(-l_{21}\cos\theta_0 + l_{22}N_0) + r_{sp}(l_{23} - l_{24}N_0\cos\theta_0))$$

$$t_{ps} = \frac{1}{N_2}(l_{23} + l_{24}N_0\cos\theta_0 + r_{ps}(-l_{21}\cos\theta_0 + l_{22}N_0) + r_{ss}(l_{23} - l_{24}N_0\cos\theta_0)) \qquad (3.14)$$

$$t_{sp} = l_{31}\cos\theta_0 + l_{32}N_0 + r_{pp}(-l_{31}\cos\theta_0 + l_{32}N_0) + r_{sp}(l_{33} - l_{34}N_0\cos\theta_0)$$

$$t_{ss} = l_{33} + l_{34}N_0\cos\theta_0 + r_{ps}(-l_{31}\cos\theta_0 + l_{32}N_0) + r_{ss}(l_{33} - l_{34}N_0\cos\theta_0)$$

Finally, we can obtain analytical expressions for Fresnel's coefficients:

$$t_{pp} = \frac{-4e^{ih_1 q_{zp1}} k_{z0} N_0 N_2 q_{zp1} q_{zp2} \varepsilon_{xx1} \varepsilon_{xx2}}{e^{2ih_1 q_{zp1}} \mathbb{N}_{p,0-}(q_{zp2}\mathbb{N}_{p,2-}\varepsilon_{xx2}\cos(h_2 q_{zp2}) + i\mathbb{N}_{p-}\sin(h_2 q_{zp2})) + \mathbb{N}_{p,0+}(-q_{zp2}\mathbb{N}_{p,2+}\varepsilon_{xx2}\cos(h_2 q_{zp2}) + i\mathbb{N}_{p+}\sin(h_2 q_{zp2}))}$$

$$t_{ss} = \frac{-4e^{ih_1 q_{zs1}} k_{z0} q_{zs1} q_{zs2} \mu_{xx1} \mu_{xx2}}{e^{2ih_1 q_{zs1}} \mathbb{N}_{s,0-}(q_{zs2}\mathbb{N}_{s,2-}\mu_{xx2}\cos(h_2 q_{zs2}) + i\mathbb{N}_{s-}\sin(h_2 q_{zs2})) + \mathbb{N}_{s,0+}(-q_{zs2}\mathbb{N}_{s,2+}\mu_{xx2}\cos(h_2 q_{zs2}) + i\mathbb{N}_{s+}\sin(h_2 q_{zs2}))}$$

$$r_{pp} = \frac{e^{2ih_1 q_{zp1}} \mathbb{N}_{p,0+}(-iq_{zp2}\mathbb{N}_{p,2-}\varepsilon_{xx2}\cos(h_2 q_{zp2}) + \mathbb{N}_{p-}\sin(h_2 q_{zp2})) + \mathbb{N}_{p,0-}(iq_{zp2}\mathbb{N}_{p,2+}\varepsilon_{xx2}\cos(h_2 q_{zs2}) + \mathbb{N}_{p+}\sin(h_2 q_{zp2}))}{e^{2ih_1 q_{zp1}} \mathbb{N}_{p,0-}(iq_{zp2}\mathbb{N}_{p,2-}\varepsilon_{xx2}\cos(h_2 q_{zp2}) - \mathbb{N}_{p-}\sin(h_2 q_{zp2})) + \mathbb{N}_{p,0+}(-iq_{zp2}\mathbb{N}_{p,2+}\varepsilon_{xx2}\cos(h_2 q_{zs2}) - \mathbb{N}_{p+}\sin(h_2 q_{zp2}))}$$

$$r_{ss} = \frac{e^{2ih_1 q_{zs1}} \mathbb{N}_{s,0+}(iq_{zs2}\mathbb{N}_{s,2-}\mu_{xx2}\cos(h_2 q_{zs2}) + \mathbb{N}_{s-}\sin(h_2 q_{zs2})) + \mathbb{N}_{s,0+}(-iq_{zs2}\mathbb{N}_{s,2+}\mu_{xx2}\cos(h_2 q_{zs2}) - \mathbb{N}_{s+}\sin(h_2 q_{zs2}))}{e^{2ih_1 q_{zs1}} \mathbb{N}_{s,0-}(-iq_{zs2}\mathbb{N}_{s,2-}\mu_{xx2}\cos(h_2 q_{zs2}) + \mathbb{N}_{s-}\sin(h_2 q_{zs2})) + \mathbb{N}_{s,0-}(iq_{zs2}\mathbb{N}_{s,2+}\mu_{xx2}\cos(h_2 q_{zs2}) - \mathbb{N}_{s+}\sin(h_2 q_{zs2}))}$$

$$(3.15)$$

With coefficients

$$\mathbb{N}_{p,0\pm} = N_0^2 q_{zp1} \pm k_{z0}\varepsilon_{xx1}$$

$$\mathbb{N}_{p,2\pm} = N_2^2 q_{zp1} \pm k_{z2}\varepsilon_{xx1}$$

$$\mathbb{N}_{p\pm} = N_2^2 q_{zp2}^2 \varepsilon_{xx1} \pm k_{z2} q_{zp1}\varepsilon_{xx2}^2 \qquad (3.16)$$

$$\mathbb{N}_{s,0\pm} = q_{zs1} \pm k_{z0}\mu_{xx1}$$

$$\mathbb{N}_{s,2\pm} = q_{zs1} \pm k_{z2}\mu_{xx1}$$

$$\mathbb{N}_{s\pm} = q_{zs2}^2 \mu_{xx1} \pm k_{z2} q_{zs1}\mu_{xx2}^2$$

Next we show some optical response simulations obtained with the help of the derived formulas. Parameters for simulation are given in the table below.

Table 3.1 Parameters of the Lorentz Model for the Optical Properties of the Bilayer Structure. The Layer Thickness h1=10 μm and h2=90 μm is in cm

		Layer 1 h1 = 0.001		Layer 2 h2 = 0.009	
AOI 60°		$\varepsilon_\infty = 15$	$\mu_\infty = 1$	$\varepsilon_\infty = 15$	$\mu_\infty = 1$
		el	m	el	m
ω		100	50	75	130
γ		1.5	1.5	1.5	1.5
S_x		0.1	0.02	0	0.01
S_y		0.1	0.04	0.3	0.01
S_z		0.1	0.01	0.1	0.01
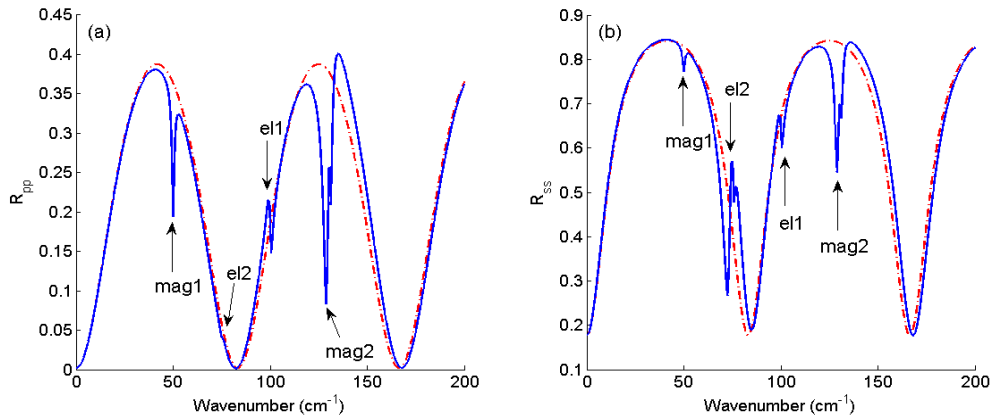
Figure 3.5 Simulation of (a) R_{pp} and (b) R_{ss} for bi-layer structure with anisotropic $\hat{\varepsilon}(\omega), \hat{\mu}(\omega)$ and isotropic substrate. Red line is a reference calculation with zero oscillator strengths. Blue line is the calculated response with parameters from Table 3.1.
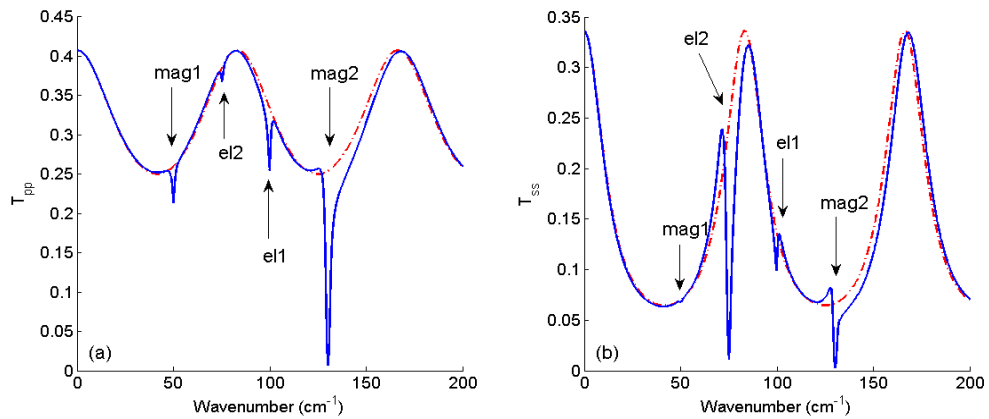
Figure 3.6 Simulation of (a) T_{pp} and (b) T_{ss} for bi-layer structure with anisotropic $\hat{\varepsilon}(\omega), \hat{\mu}(\omega)$ and isotropic substrate. Red line is a reference calculation with zero oscillator strengths. Blue line is the calculated response with parameters from Table 3.1

3.3 Transfer Matrix Technique and Analytical Solutions for General Multilayer Bi-Anisotropic Structures

In this section, we use transfer matrix formalism for obtaining the most general form of solutions for arbitrary symmetry systems on anisotropic substrate. At the end of this Section we will compare the layer matrix and transfer matrix techniques.

Information about $\psi(z)$ knowing $\psi(0)$ is provided in Equation (3.2). In other words, we start from projections of incident and reflected light on ambient interface and moving through layers till we get to the last substrate interface. There is a more convenient way to obtain solutions. Let's assume that our final matrix equation should be in the form

$$\begin{pmatrix} E_{is} \\ E_{rs} \\ E_{ip} \\ E_{rp} \end{pmatrix} = T \begin{pmatrix} E_{ts} \\ 0 \\ E_{tp} \\ 0 \end{pmatrix} = \begin{pmatrix} T_{11} & T_{12} & T_{13} & T_{14} \\ T_{21} & T_{22} & T_{23} & T_{24} \\ T_{31} & T_{32} & T_{33} & T_{34} \\ T_{41} & T_{42} & T_{43} & T_{44} \end{pmatrix} \begin{pmatrix} E_{ts} \\ 0 \\ E_{tp} \\ 0 \end{pmatrix} \tag{3.17}$$

where T is the so called transfer matrix, which will be constructed below. It is a better choice (no need to construct projection matrix from the *xy*-components at substrate interface to transmitted waves, which contains inverse eigenvectors components of the substrate's $\tilde{\Delta}$ matrix as in Equation (2.25) from the previous chapter) to start from transmitted modes E_{ts} and E_{tp}, and move to the incident and reflected ones in ambient. For this purpose, we rewrite Equation (3.2) in the following form:

$$\psi(0) = e^{-i\frac{\omega}{c}\tilde{\Delta}z} \psi(z) \tag{3.18}$$

Now we can start from using $\psi(z)$ and move back to $\psi(0)$. In Equation (3.18) matrix exponent is nothing else but matrix which relates components at different interfaces. We call it a partial transfer matrix T_p. Instead of calculating layer matrix, which has a relatively complicated structure, we need to get an expression for matrix exponent, which is basically infinite series.
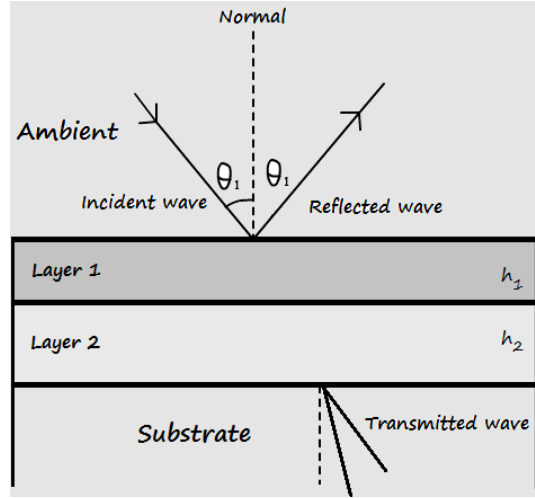
Figure 3.7 Ray propagation shematics in bilayer system.

In this situation, the Cayley-Hamilton theorem is very useful. In short, the theorem states that every square matrix satisfies its own characteristic equation. Wohler *et al.* [25] applied this theorem to partial transfer matrix and showed that matrix exponent can be written as a polynomial of the order of *r*-1, where *r* is the rank of the matrix, with coefficients solely depended on eigenvalues. Analytical expression is the following:

$$T_p = e^{-i\frac{\omega}{c}\tilde{\Delta}z} = \beta_0 I + \beta_1\tilde{\Delta} + \beta_2\tilde{\Delta}^2 + \beta_3\tilde{\Delta}^3 \tag{3.19}$$

with coefficients defined as

$$\beta_0 = -\sum_{j=1}^{4} q_k q_l q_m \frac{e^{-i\frac{\omega}{c}q_j z}}{(q_j - q_k)(q_j - q_l)(q_j - q_m)}$$

$$\beta_1 = \sum_{j=1}^{4} (q_k q_l + q_k q_m + q_l q_m) \frac{e^{-i\frac{\omega}{c}q_j z}}{(q_j - q_k)(q_j - q_l)(q_j - q_m)}$$

$$\beta_2 = -\sum_{j=1}^{4} (q_k + q_l + q_m) \frac{e^{-i\frac{\omega}{c}q_j z}}{(q_j - q_k)(q_j - q_l)(q_j - q_m)}$$

$$\beta_3 = \sum_{j=1}^{4} \frac{e^{-i\frac{\omega}{c}q_j z}}{(q_j - q_k)(q_j - q_l)(q_j - q_m)}$$

(3.20)

and q_j are eigenvalues of $\tilde{\Delta}$ matrix. For obtaining expressions for eigenvalues the

following equation should be solved

$$\begin{pmatrix} \Delta_{11} & \Delta_{12} & \Delta_{13} & \Delta_{14} \\ \Delta_{21} & \Delta_{22} & \Delta_{23} & \Delta_{24} \\ \Delta_{31} & \Delta_{32} & \Delta_{33} & \Delta_{34} \\ \Delta_{41} & \Delta_{42} & \Delta_{43} & \Delta_{44} \end{pmatrix} \begin{pmatrix} E_x \\ E_y \\ H_x \\ H_y \end{pmatrix} = q_z \begin{pmatrix} E_x \\ E_y \\ H_x \\ H_y \end{pmatrix}$$

(3.21)

as a result we get fourth order polynomial with complex coefficients. If we reduce high

order coefficient we obtain the following equation:

$$q_z^4 + C_1 q_z^3 + C_2 q_z^2 + C_3 q_z + C_4 = 0$$

(3.22)

"The Handbook of Functions" by Abramowits and Stegun [26] provides solutions of

Equation (3.22). That means there are no difficulties to construct analytical expression for

partial transfer matrix. If we have multilayer structure, total propagating matrix is given as

a product of partial transfer matrices of each layer $T_{p,1}...T_{p,i-1}T_{p,i}$. In the previous chapter,

we defined L_{in} in Equation (2.22) and L_{out} in Equation (2.50). In order to get solutions in

the form of Equation (2.15) we can write:

$$
\begin{pmatrix} E_{is} \\ E_{rs} \\ E_{ip} \\ E_{rp} \end{pmatrix} = T \begin{pmatrix} E_{ts} \\ 0 \\ E_{tp} \\ 0 \end{pmatrix} = L_{in} \prod_{i=1}^{N} T_{p,i} L_{out} \begin{pmatrix} E_{ts} \\ 0 \\ E_{tp} \\ 0 \end{pmatrix} = L_{in} \prod_{i=1}^{N} (\beta_{0i} I + \beta_{1i} \tilde{\Delta}_i + \beta_{2i} \tilde{\Delta}_i^2 + \beta_{3i} \tilde{\Delta}_i^3) L_{out} \begin{pmatrix} E_{ts} \\ 0 \\ E_{tp} \\ 0 \end{pmatrix} \quad (3.23)
$$

After plugging in Equation (3.23) the expressions for L_{in} and L_{out}, we obtain the final form:

$$
\begin{pmatrix} E_{is} \\ E_{rs} \\ E_{ip} \\ E_{rp} \end{pmatrix} = \frac{1}{2} \begin{pmatrix} 0 & 1 & -\dfrac{1}{N_0 \cos\theta_i} & 0 \\ 0 & 1 & \dfrac{1}{N_0 \cos\theta_i} & 0 \\ \dfrac{1}{\cos\theta_i} & 0 & 0 & \dfrac{1}{N_0} \\ -\dfrac{1}{\cos\theta_i} & 0 & 0 & \dfrac{1}{N_0} \end{pmatrix} \prod_{i=1}^{N} (\beta_{0i} I + \beta_{1i} \tilde{\Delta}_i + \beta_{2i} \tilde{\Delta}_i^2 + \beta_{3i} \tilde{\Delta}_i^3) \begin{pmatrix} \psi_{11}^{sub} & 0 & \psi_{12}^{sub} & 0 \\ \psi_{21}^{sub} & 0 & \psi_{22}^{sub} & 0 \\ \psi_{31}^{sub} & 0 & \psi_{32}^{sub} & 0 \\ \psi_{41}^{sub} & 0 & \psi_{42}^{sub} & 0 \end{pmatrix} \begin{pmatrix} E_{ts} \\ 0 \\ E_{tp} \\ 0 \end{pmatrix}
$$

$$(3.24)$$

Transfer matrix is defined as

$$
T = \frac{1}{2} \begin{pmatrix} 0 & 1 & -\dfrac{1}{N_0 \cos\theta_i} & 0 \\ 0 & 1 & \dfrac{1}{N_0 \cos\theta_i} & 0 \\ \dfrac{1}{\cos\theta_i} & 0 & 0 & \dfrac{1}{N_0} \\ -\dfrac{1}{\cos\theta_i} & 0 & 0 & \dfrac{1}{N_0} \end{pmatrix} \prod_{i=1}^{N} (\beta_{0i} I + \beta_{1i} \tilde{\Delta}_i + \beta_{2i} \tilde{\Delta}_i^2 + \beta_{3i} \tilde{\Delta}_i^3) \begin{pmatrix} \psi_{11}^{sub} & 0 & \psi_{12}^{sub} & 0 \\ \psi_{21}^{sub} & 0 & \psi_{22}^{sub} & 0 \\ \psi_{31}^{sub} & 0 & \psi_{32}^{sub} & 0 \\ \psi_{41}^{sub} & 0 & \psi_{42}^{sub} & 0 \end{pmatrix}
$$

$$(3.25)$$

As we discuss earlier, for biaxial substrates Equation (2.50) could be used, then

$$
T = \frac{1}{2} \begin{pmatrix} 0 & 1 & -\dfrac{1}{N_0 \cos\theta_i} & 0 \\ 0 & 1 & \dfrac{1}{N_0 \cos\theta_i} & 0 \\ \dfrac{1}{\cos\theta_i} & 0 & 0 & \dfrac{1}{N_0} \\ -\dfrac{1}{\cos\theta_i} & 0 & 0 & \dfrac{1}{N_0} \end{pmatrix} \prod_{i=1}^{N} (\beta_{0i} I + \beta_{1i} \tilde{\Delta}_i + \beta_{2i} \tilde{\Delta}_i^2 + \beta_{3i} \tilde{\Delta}_i^3) \begin{pmatrix} 0 & 0 & \dfrac{q_{zp}}{\sqrt{q_x^2 + q_{zp}^2}} & 0 \\ 1 & 0 & 0 & 0 \\ \dfrac{q_{zs}}{\Delta_{23}} & 0 & 0 & 0 \\ 0 & 0 & \dfrac{1}{\Delta_{14}} \dfrac{q_{zp}^2}{\sqrt{q_x^2 + q_{zp}^2}} & 0 \end{pmatrix} \quad (3.26)
$$

where right RHS matrix corresponds to substrate. Now it is easy to show solutions for Fresnel's coefficients:

$$r_{pp} = \frac{T_{11}T_{43} - T_{13}T_{41}}{T_{11}T_{33} - T_{13}T_{31}} \qquad t_{pp} = \frac{T_{11}}{T_{11}T_{33} - T_{13}T_{31}}$$

$$r_{sp} = \frac{T_{11}T_{23} - T_{13}T_{21}}{T_{11}T_{33} - T_{13}T_{31}} \qquad t_{sp} = -\frac{T_{13}}{T_{11}T_{33} - T_{13}T_{31}}$$

$$r_{ss} = \frac{T_{21}T_{33} - T_{23}T_{31}}{T_{11}T_{33} - T_{13}T_{31}} \qquad t_{ss} = \frac{T_{33}}{T_{11}T_{33} - T_{13}T_{31}}$$

$$r_{ps} = \frac{T_{33}T_{41} - T_{31}T_{43}}{T_{11}T_{33} - T_{13}T_{31}} \qquad t_{ps} = -\frac{T_{31}}{T_{11}T_{33} - T_{13}T_{31}}$$

(3.27)

To conclude, we compare layer matrix and transfer matrix techniques. When we use the layer matrix we start from ambient, project waves on the interface and then move through the layers by means of propagation matrix and arrive to the substrate. Then we project transmitted modes on the interface and, finally, obtain a solution. It was pointed out earlier that projecting transmitted modes on the interface involves matrix inverse operation which is not desirable for obtaining analytical solutions. Expression quickly becomes too bulky. The layer matrix gives some advantages though. We calculate eigenmodes for each layer and thus we know dynamics inside layers (Poynting vectors can be obtained fairly quickly). Energy conservation arguments are easier to justify knowing such information.

In the transfer matrix formalism we start from the substrate and represent substrate's fields projection in terms of transmitted waves (opposite to what we do using layer matrix L). Then we move from the last layer to ambient using partial transfer matrix. At the ambient interface we use L_{in} matrix to obtain p and s components of incident and reflected waves in terms of fields' projections. Then we get the solutions. Partial transfer matrix does not contain any eigenmodes information and solely defined by the eigenvalues

54

and by the elements of $\tilde{\Delta}$ matrix. We miss some information about waves propagation inside layers but get instead a faster method to obtain solutions and, as a result, more compact formulas. Both methods give the same results and both methods have their advantages and disadvantages.

Let's discuss the limitations for the applicability of our theoretical results, which cover only the linear optical effects and homogeneous layers without thickness gradient. We do not intend to cover the non-linear effects and inhomogeneous structures, which are outside of the scope of our work. For a non-linear media, certain approximations should be done to establish the relationship among the field vectors and to allow treating the material by means of the matrix formalism. For inhomogeneous media, the sample should be divided into regions where optical matrix does not depend on z, after that procedure described above can be applied for further analysis.

It should be mentioned that developed formalism is also applicable for metamaterials investigation.

In the following sections, we consider some particular systems which are bi-anisotropic single layer thin film on biaxial substrate, bi-anisotropic bilayer structure on biaxial substrate and superlattice on biaxial substrate. Discussion of formulae are in the beginning of the section and analytical versus numerical solutions and related simulation of MM matrices and Reflectance towards the end.

3.4 Single Layer Bi-anisotropic Thin Film on Anisotropic Substrate
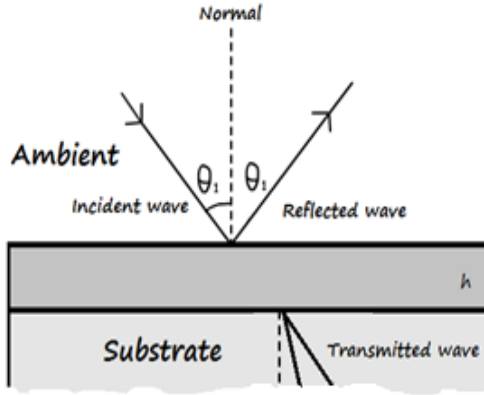
Figure 3.8 Bi-anisotropic thin film on a substrate.

Table 3.2 Layer and Substrate Parameters for Bi-anisotropic Thin Film and Substrate

Layer parameters			
Layer thickness		$5\,\mu m$	
Oscillators	$\varepsilon(\omega)$	$\mu(\omega)$	$\alpha(\omega)$
Infinity value	$\varepsilon_\infty = 10$	$\mu_\infty = 1$	$\alpha_\infty = 0$
Resonant frequency	---	---	$\omega_{0,\alpha} = 300$
Strength	---	---	$S_\alpha = 0.01$
Broadening	---	---	$\gamma_\alpha = 2$
Substrate parameters			
Permittivity ε	$\varepsilon_{xx} = 16$	$\varepsilon_{yy} = 9$	$\varepsilon_{zz} = 4$
Permeability μ	$\mu_{xx} = 1$	$\mu_{yy} = 1$	$\mu_{zz} = 1$
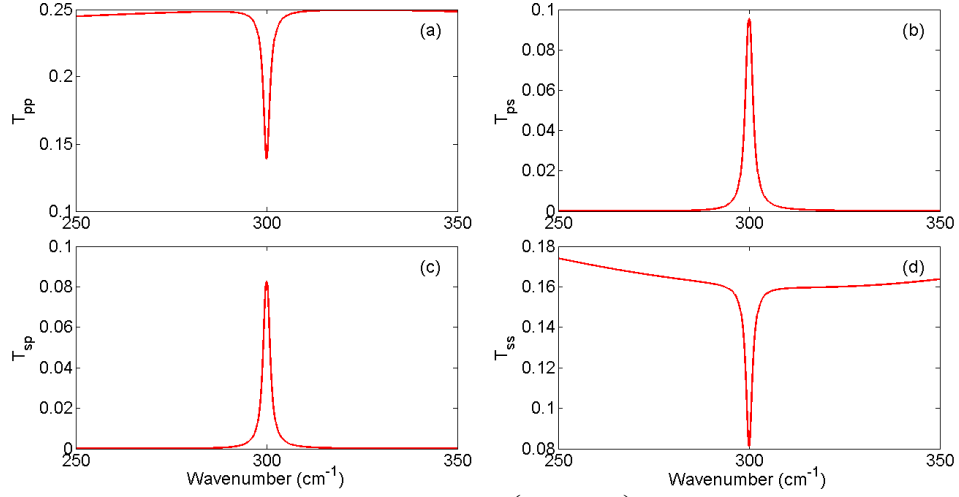
Figure 3.9 Transmittance components for $\begin{pmatrix} \alpha_{xx} & 0 & 0 \\ 0 & 0 & 0 \\ 0 & 0 & 0 \end{pmatrix}$ ME tensor symmetry. Model contains one oscillator with $S_{\alpha,xx} = 0.01$; $\omega_0 = 300$ cm^{-1}; $\gamma = 2$; dielectric constant $\varepsilon_{xx} = 16, \varepsilon_{yy} = 9, \varepsilon_{zz} = 4$; ; magnetic permeability $\mu_{xx} = \mu_{yy} = \mu_{zz} = 1$; $AOI = 0°$.
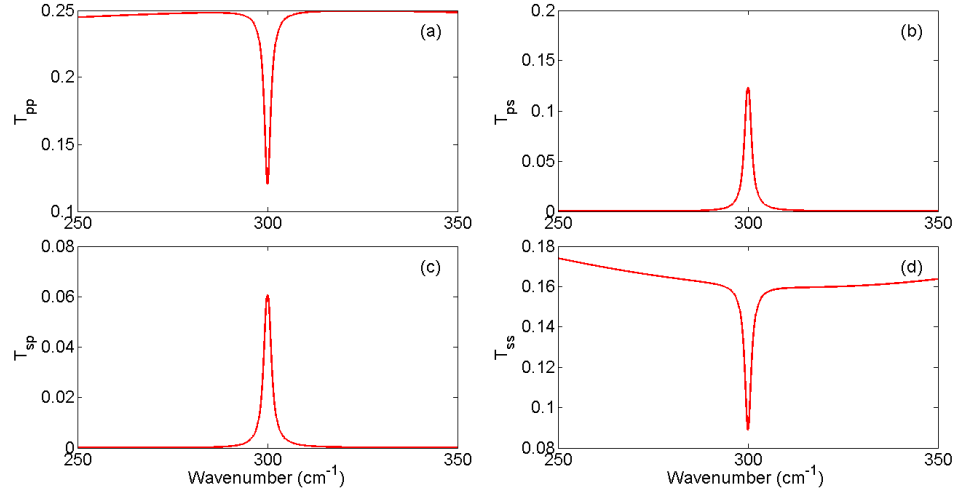
Figure 3.10 Transmittance components for $\begin{pmatrix} 0 & 0 & 0 \\ 0 & \alpha_{yy} & 0 \\ 0 & 0 & 0 \end{pmatrix}$ ME tensor symmetry. Model contains one oscillator with $S_{\alpha,xx} = 0.01$; $\omega_0 = 300$ cm^{-1}; $\gamma = 2$; dielectric constant $\varepsilon_{xx} = 16, \varepsilon_{yy} = 9, \varepsilon_{zz} = 4$; magnetic permeability $\mu_{xx} = \mu_{yy} = \mu_{zz} = 1$; $AOI = 0°$.
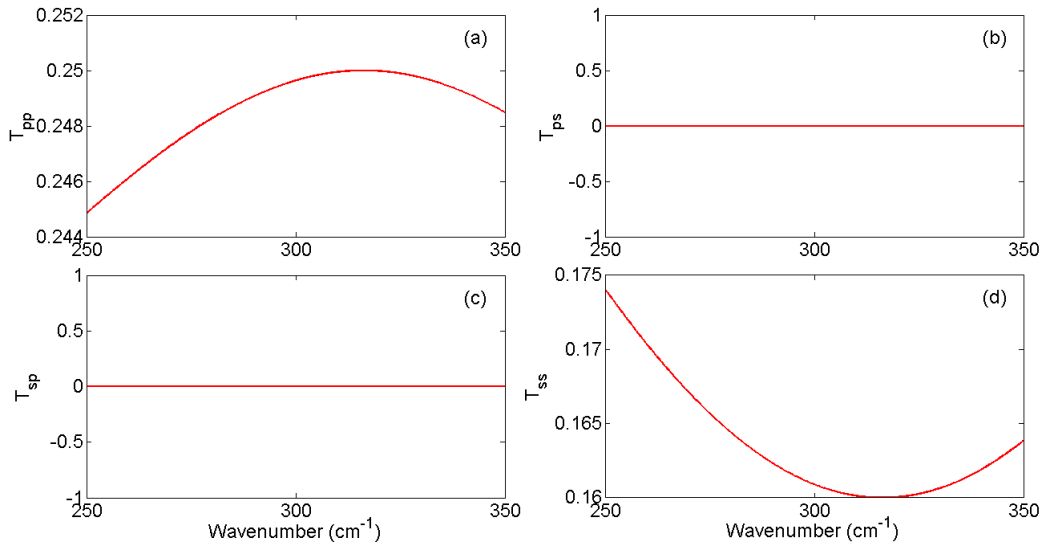
Figure 3.11 Transmittance components for $\begin{pmatrix} 0 & 0 & 0 \\ 0 & 0 & 0 \\ 0 & 0 & \alpha_{zz} \end{pmatrix}$ ME tensor symmetry. Model

contains one oscillator with $S_{\alpha,xx} = 0.01$; $\omega_0 = 300$ cm^{-1}; $\gamma = 2$; dielectric constant $\varepsilon_{xx} = 16, \varepsilon_{yy} = 9, \varepsilon_{zz} = 4$; ; magnetic permeability $\mu_{xx} = \mu_{yy} = \mu_{zz} = 1$; $AOI = 0°$.
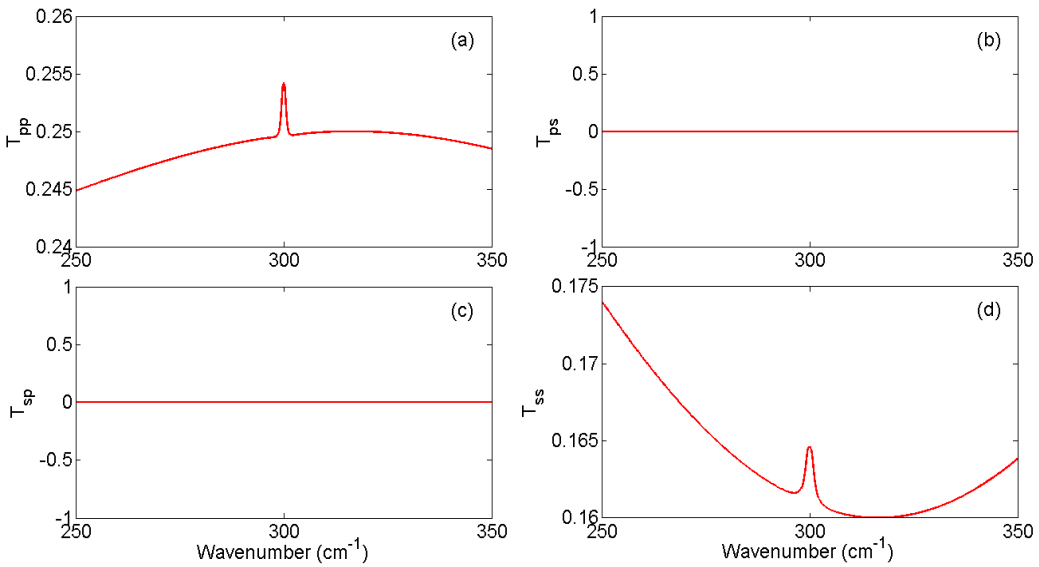
Figure 3.12 Transmittance components for $\begin{pmatrix} 0 & 0 & \alpha_{xz} \\ 0 & 0 & 0 \\ -\alpha_{xz} & 0 & 0 \end{pmatrix}$ ME tensor symmetry.

Model contains one oscillator with $S_{\alpha,xx} = 0.01$; $\omega_0 = 300$ cm^{-1}; $\gamma = 2$; dielectric constant $\varepsilon_{xx} = 16, \varepsilon_{yy} = 9, \varepsilon_{zz} = 4$; ; magnetic permeability $\mu_{xx} = \mu_{yy} = \mu_{zz} = 1$; $AOI = 0°$.
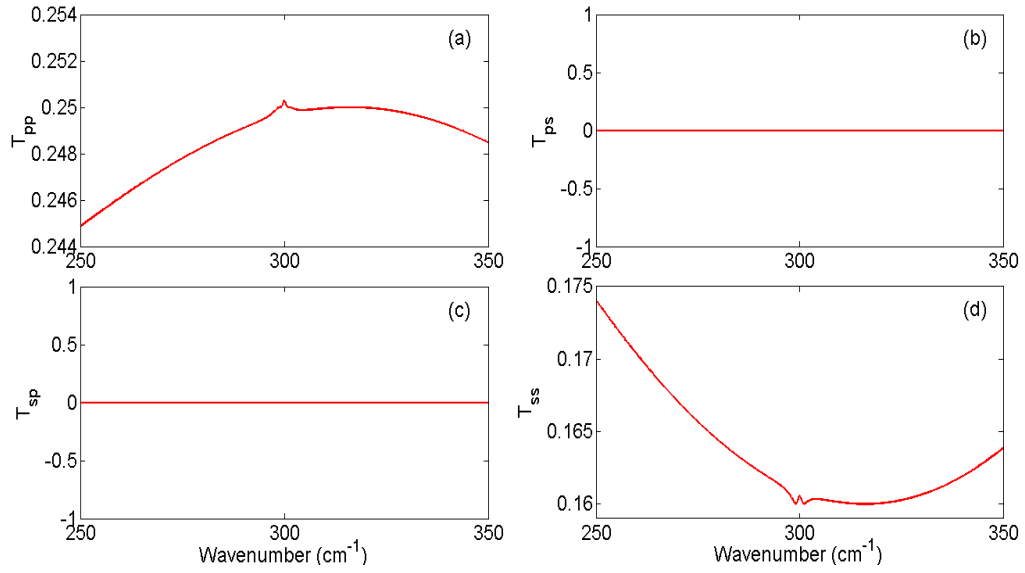
Figure 3.13 Transmittance components for $\begin{pmatrix} 0 & 0 & 0 \\ 0 & 0 & \alpha_{yz} \\ 0 & -\alpha_{yz} & 0 \end{pmatrix}$ ME tensor symmetry.

Model contains one oscillator with $S_{\alpha,xx} = 0.01$; $\omega_0 = 300$ cm^{-1}; $\gamma = 2$; dielectric constant $\varepsilon_{xx} = 16, \varepsilon_{yy} = 9, \varepsilon_{zz} = 4$; ; magnetic permeability $\mu_{xx} = \mu_{yy} = \mu_{zz} = 1$; $AOI = 0°$.

3.5 Bilayer Bi-anisotropic Structure on Anisotropic Substrate

Table 3.3 Layer and Substrate Parameters for Bilayer Bi-anisotropic Thin Film and Substrate

Layer 1 parameters			
Layer thickness		$5\mu m$	
Oscillators	$\varepsilon(\omega)$	$\mu(\omega)$	$\alpha(\omega)$
Infinity value	$\varepsilon_\infty = 10$	$\mu_\infty = 1$	$\alpha_\infty = 0$
Resonant frequency	---	---	$\omega_{0,\alpha} = 280$
Strength	---	---	$S_{\alpha,xx} = 0.01$
Broadening	---	---	$\gamma_\alpha = 2$

Layer 2 parameters			
Layer thickness		$3\mu m$	
Oscillators	$\varepsilon(\omega)$	$\mu(\omega)$	$\alpha(\omega)$
Infinity value	$\varepsilon_\infty = 8$	$\mu_\infty = 1$	$\alpha_\infty = 0$
Resonant frequency	---	---	$\omega_{0,\alpha} = 320$
Strength	---	---	$S_{\alpha,xx} = 0.01$
Broadening	---	---	$\gamma_\alpha = 2$

Substrate parameters			
Permittivity ε	$\varepsilon_{xx} = 16$	$\varepsilon_{yy} = 9$	$\varepsilon_{zz} = 4$
Permeability μ	$\mu_{xx} = 1$	$\mu_{yy} = 1$	$\mu_{zz} = 1$

Figure 3.14 Transmittance components for $\begin{pmatrix} \alpha_{xx} & 0 & 0 \\ 0 & 0 & 0 \\ 0 & 0 & 0 \end{pmatrix}$ ME tensor symmetry. Model

contains one oscillator with $S_{\alpha,xx} = 0.01$; $\gamma = 2$; $\omega_{0,1} = 280$, $\omega_{0,2} = 320$ cm^{-1}; $AOI = 0°$.
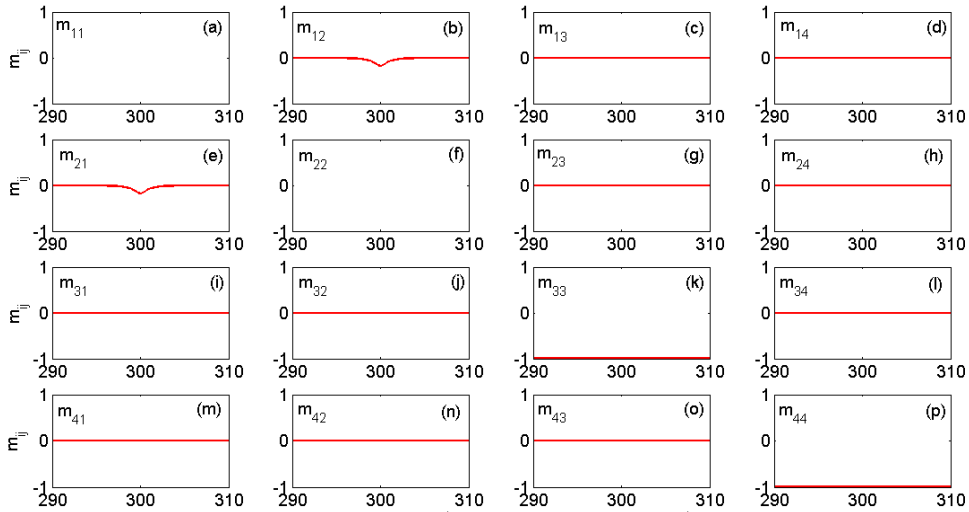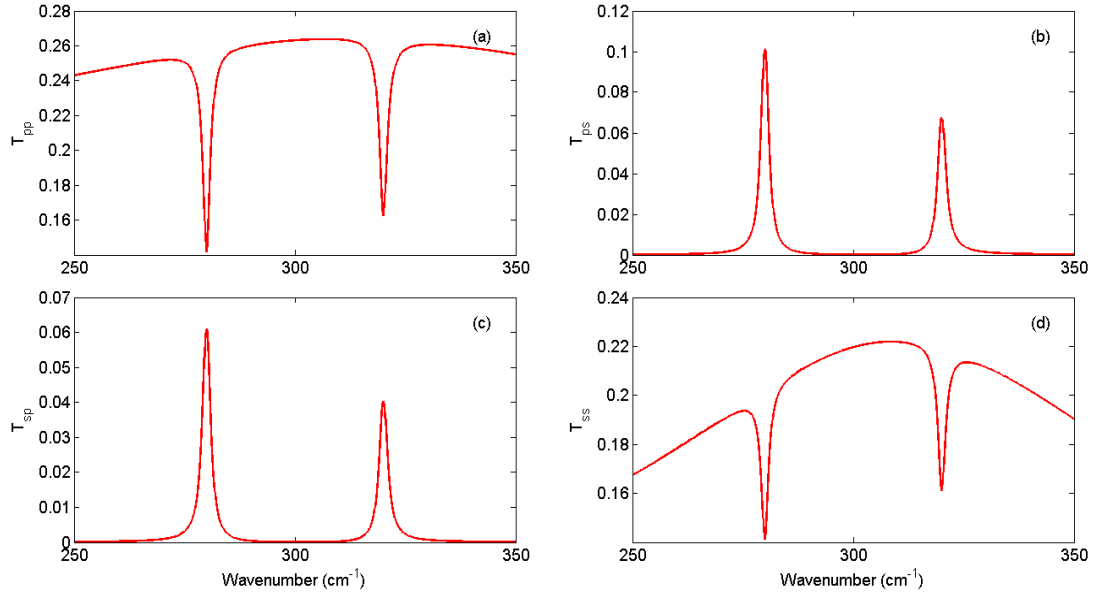
Figure 3.15 Normalized Mueller matrix components for $\begin{pmatrix} 0 & 0 & 0 \\ 0 & \alpha_{yy} & 0 \\ 0 & 0 & 0 \end{pmatrix}$ ME tensor symmetry.

Model contains one oscillator with $S_{\alpha,yy} = 0.01$; $\gamma = 2$; $\omega_{0,1} = 280$, $\omega_{0,2} = 320$ cm^{-1}; $AOI = 0°$.
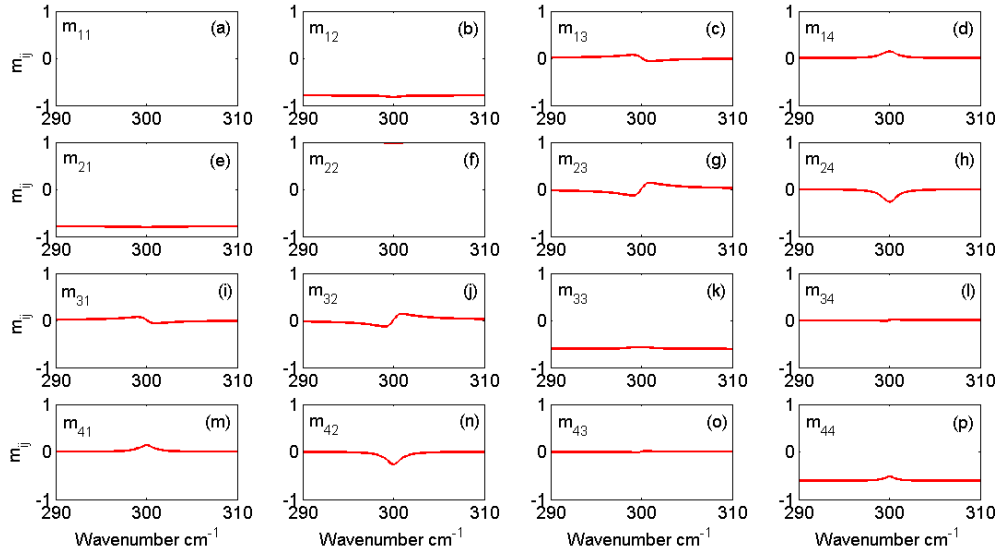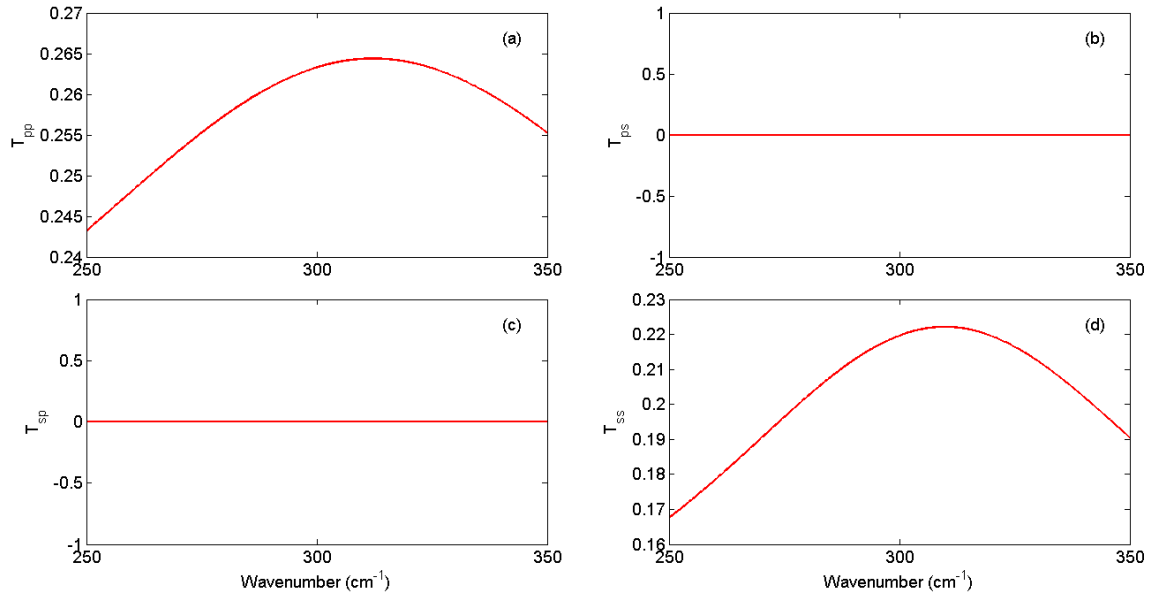

Figure 3.16 Normalized Mueller matrix components for $\begin{pmatrix} 0 & 0 & 0 \\ 0 & 0 & 0 \\ 0 & 0 & \alpha_{zz} \end{pmatrix}$ ME tensor symmetry.

Model contains one oscillator with $S_{\alpha,zz} = 0.01$; $\gamma = 2$; $\omega_{0,1} = 280$, $\omega_{0,2} = 320$ cm^{-1}; $AOI = 0°$.
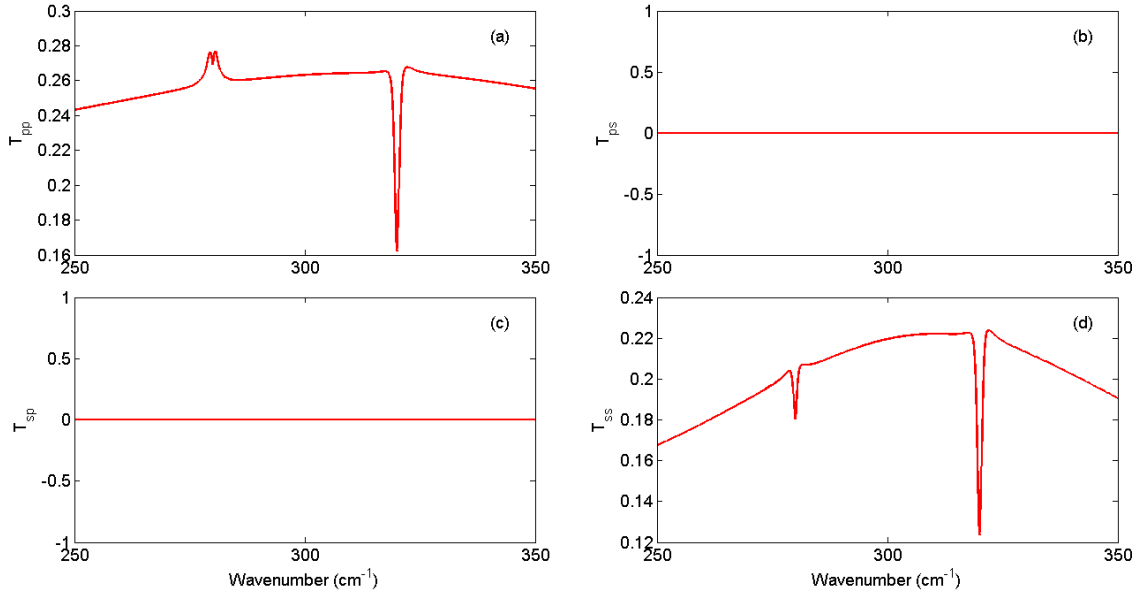
Figure 3.17 Normalized Mueller matrix components for $\begin{pmatrix} 0 & \alpha_{xy} & 0 \\ -\alpha_{xy} & 0 & 0 \\ 0 & 0 & 0 \end{pmatrix}$ ME tensor symmetry.

Model contains one oscillator with $S_{\alpha,xy} = 0.01; \gamma = 2;$ $\omega_{0,1} = 280$, $\omega_{0,2} = 320$ cm^{-1}; $AOI = 0°$.
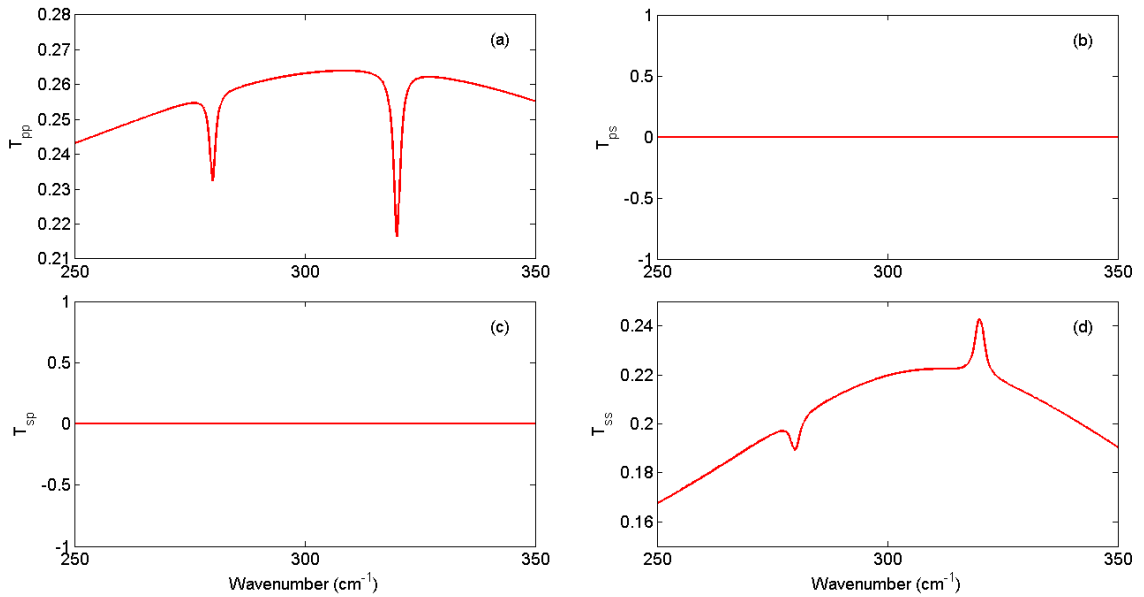
Figure 3.18 Normalized Mueller matrix components for $\begin{pmatrix} 0 & 0 & 0 \\ 0 & 0 & \alpha_{yz} \\ 0 & -\alpha_{yz} & 0 \end{pmatrix}$ ME tensor symmetry.

Model contains one oscillator with $S_{\alpha,yz} = 0.01; \gamma = 2;$ $\omega_{0,1} = 280$, $\omega_{0,2} = 320$ cm^{-1}; $AOI = 0°$.
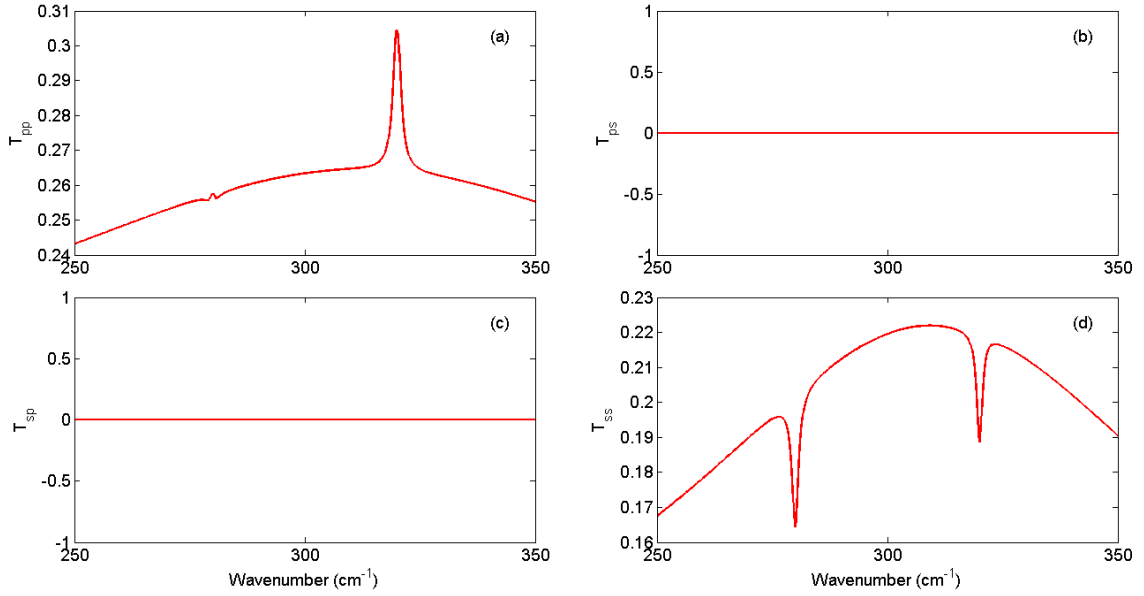
Figure 3.19 Normalized Mueller matrix components for $\begin{pmatrix} 0 & 0 & \alpha_{xz} \\ 0 & 0 & 0 \\ -\alpha_{xz} & 0 & 0 \end{pmatrix}$ ME tensor symmetry.

Model contains one oscillator with $S_{\alpha,xz} = 0.01$; $\gamma = 2$; $\omega_{0,1} = 280$, $\omega_{0,2} = 320$ cm^{-1}; $AOI = 0°$.

3.6 Bi-anisotropic Superlattice on Anisotropic Substrate
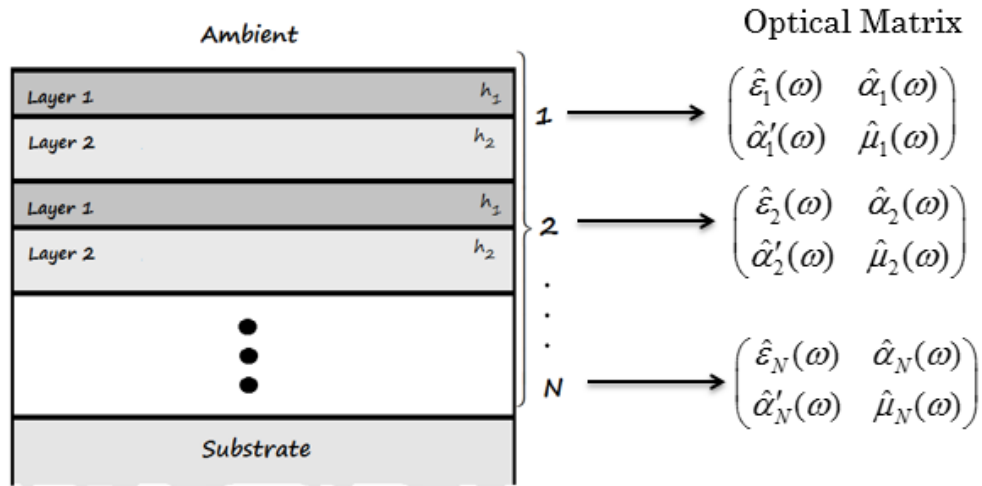
Figure 3.20 Superlattice on anisotropic substrate schematics.

Table 3.4 Superlattice on an Anisotropic Substrate Parameters

Layer 1 parameters			
Layer thickness	$3\mu m$		
Oscillators	$\varepsilon(\omega)$	$\mu(\omega)$	$\alpha(\omega)$
Infinity value	$\varepsilon_\infty = 16$	$\mu_\infty = 1$	$\alpha_\infty = 0$
Resonant frequency	---	---	$\omega_{0,\alpha} = 280$
Strength	---	---	$S_{\alpha,xx} = 0.01$
Broadening	---	---	$\gamma_\alpha = 2$

Layer 2 parameters			
Layer thickness	$1\mu m$		
Oscillators	$\varepsilon(\omega)$	$\mu(\omega)$	$\alpha(\omega)$
Infinity value	$\varepsilon_\infty = 12$	$\mu_\infty = 1$	$\alpha_\infty = 0$
Resonant frequency	---	---	$\omega_{0,\alpha} = 320$
Strength	---	---	$S_{\alpha,xx} = 0.01$
Broadening	---	---	$\gamma_\alpha = 2$

Substrate parameters			
Permittivity ε	$\varepsilon_{xx} = 16$	$\varepsilon_{yy} = 9$	$\varepsilon_{zz} = 4$
Permeability μ	$\mu_{xx} = 1$ $\mu_{yy} = 1$	$\mu_{zz} = 1$	

Figure. 3.21 Transmittance components for $\begin{pmatrix} \alpha_{xx} & 0 & 0 \\ 0 & 0 & 0 \\ 0 & 0 & 0 \end{pmatrix}$ ME tensor symmetry. Model

contains one oscillator in the first layer with $S_{\alpha,xx} = 0.01$; $\gamma = 2$; $\omega_{0,1} = 280$,and one oscillator in the second layer with $S_{\alpha,xx} = 0.01$; $\gamma = 2$; $\omega_{0,2} = 320$ cm^{-1}; $AOI = 0°$ .Number of double layers equals to ten.
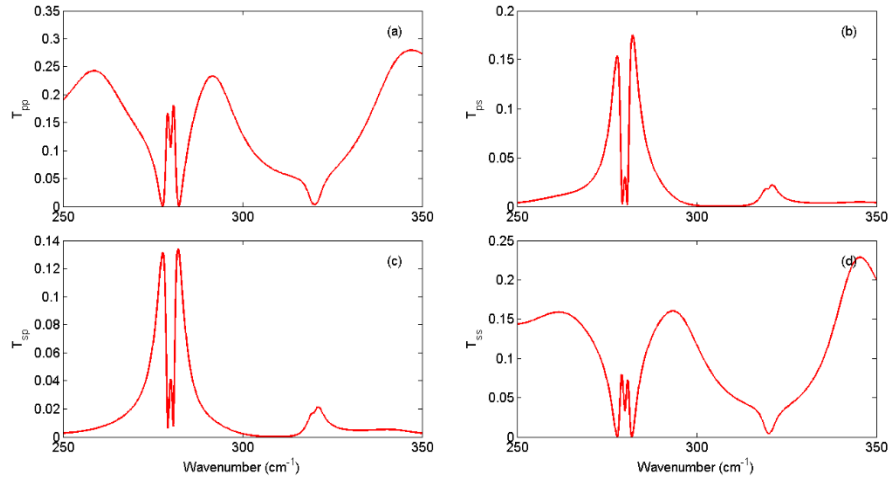
Figure. 3.22 Transmittance components for $\begin{pmatrix} 0 & 0 & 0 \\ 0 & \alpha_{yy} & 0 \\ 0 & 0 & 0 \end{pmatrix}$ ME tensor symmetry. Model

contains one oscillator in the first layer with $S_{\alpha,yy} = 0.01$; $\gamma = 2$; $\omega_{0,1} = 280$,and one oscillator in the second layer with $S_{\alpha,yy} = 0.01$; $\gamma = 2$; $\omega_{0,2} = 320$ cm^{-1}; $AOI = 0°$ .Number of double layers equals to ten.
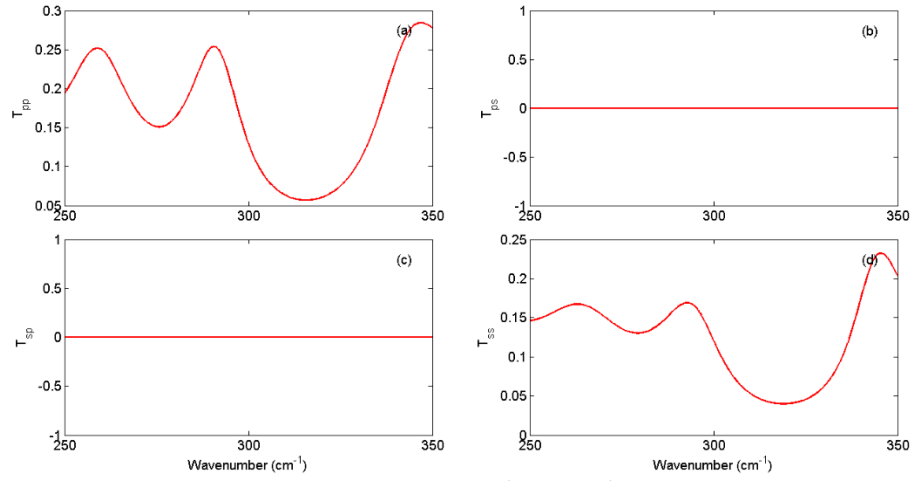
Figure. 3.23 Transmittance components for $\begin{pmatrix} 0 & 0 & 0 \\ 0 & 0 & 0 \\ 0 & 0 & \alpha_{zz} \end{pmatrix}$ ME tensor symmetry. Model contains one oscillator in the first layer with $S_{\alpha,zz} = 0.01$; $\gamma = 2$; $\omega_{0,1} = 280$, and one oscillator in the second layer with $S_{\alpha,zz} = 0.01$; $\gamma = 2$; $\omega_{0,2} = 320$ cm^{-1}; $AOI = 0°$. Number of double layers equals to ten.
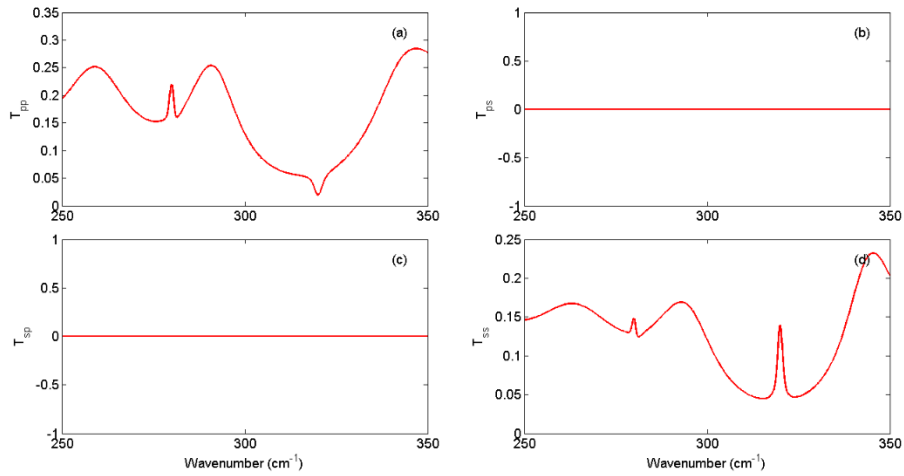
Figure. 3.24 Transmittance components for $\begin{pmatrix} 0 & 0 & \alpha_{xz} \\ 0 & 0 & 0 \\ -\alpha_{xz} & 0 \end{pmatrix}$ ME tensor symmetry. Model contains one oscillator in the first layer with $S_{\alpha,xz} = 0.01$; $\gamma = 2$; $\omega_{0,1} = 280$, and one oscillator in the second layer with $S_{\alpha,xz} = 0.01$; $\gamma = 2$; $\omega_{0,2} = 320$ cm^{-1}; $AOI = 0°$. Number of double layers equals to ten.
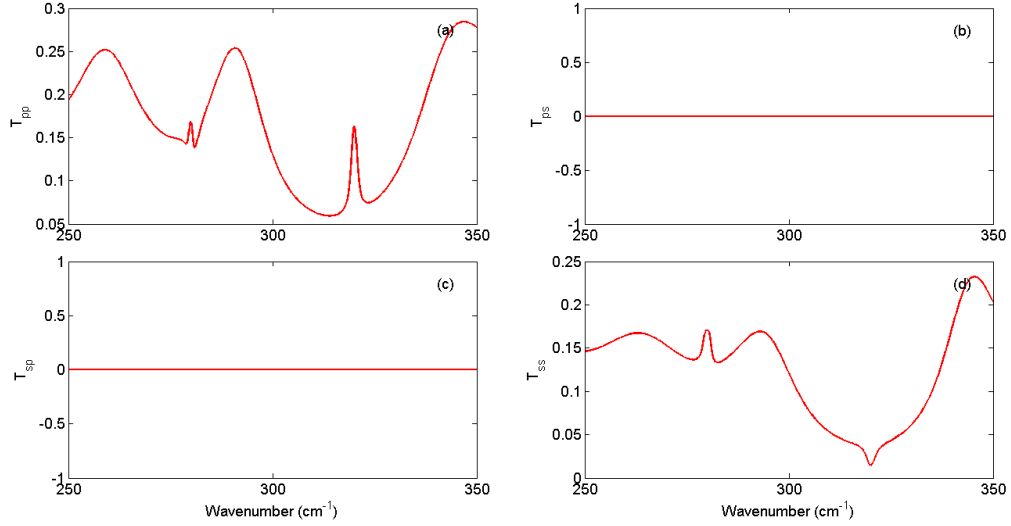
Figure. 3.25 Transmittance components for $\begin{pmatrix} 0 & 0 & 0 \\ 0 & 0 & \alpha_{yz} \\ 0 & -\alpha_{yz} & 0 \end{pmatrix}$ ME tensor symmetry Model contains one oscillator in the first layer with $S_{\alpha,yz} = 0.01; \gamma = 2; \quad \omega_{0,1} = 280$, and one oscillator in the second layer with $S_{\alpha,yz} = 0.01; \gamma = 2; \omega_{0,2} = 320$ cm^{-1}; $AOI = 0°$. Number of double layers equals to ten.
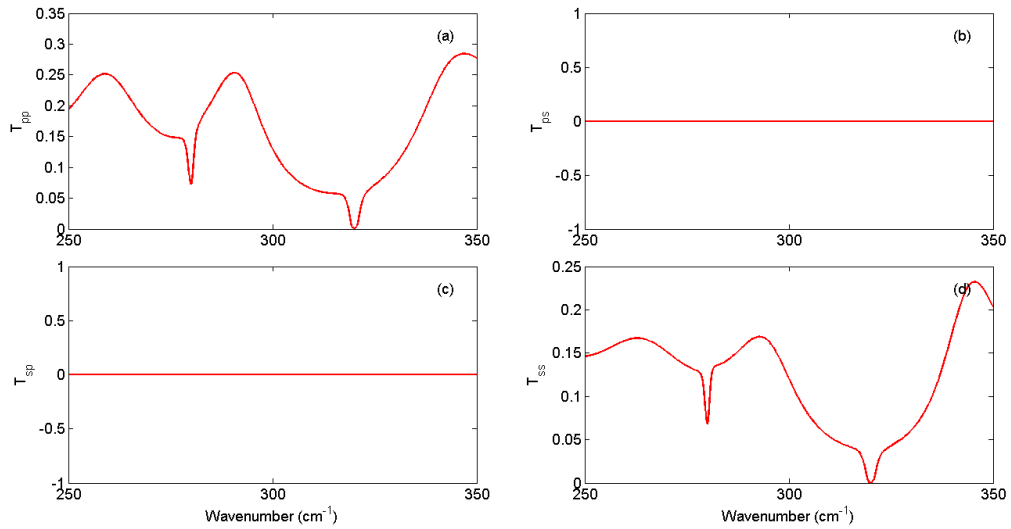
Figure. 3.26 Transmittance components for $\begin{pmatrix} 0 & \alpha_{xy} & 0 \\ -\alpha_{xy} & 0 & 0 \\ 0 & 0 & 0 \end{pmatrix}$ ME tensor symmetry Model contains one oscillator in the first layer with $S_{\alpha,xy} = 0.01; \gamma = 2; \quad \omega_{0,1} = 280$, and one oscillator in the second layer with $S_{\alpha,xy} = 0.01; \gamma = 2; \omega_{0,2} = 320$ cm^{-1}; $AOI = 0°$. Number of double layers equals to ten.

Simulations of the optical transmission functions are interesting and may be useful from the experimental point of view. Contributions from oscillators located in different layers give certain spectra features, such as minima or maxima, that can become their "fingerprints" in analysis of the optical response. Experimental and model spectra of the Mueller matrix components, reflectance, and transmittance may help to identify the location of the magneto-electric excitations in the particular layers of the multilayer structure.

As expected for ME oscillators polarized along the z-axis in α_{zz} (Figures 3.11, 3.17, 3.24), there is no corresponding optical response under normal light incidence. In contrast, for ME tensor with non-zero α_{xy} component there is a non-zero contribution of the oscillators under normal incidence. This effect occurs only in samples with anisotropic substrates. In the case of isotropic substrate, the ME response is not visible as demonstrated in MM components in Figure 2.8. For ME tensor with non-zero α_{xz} (Figures 3.19, 3.24), the peaks for p-polarized and s-polarized light for oscillator with higher frequency in each layer appear with the opposite amplitudes and, thus, those peaks can be distinguished from each other. For non-zero α_{yz} (Figures 3.18, 3.25), the behavior is similar: for both the bilayer and superlattice structures response is different and oscillators from different layers can be distinguished from each other. For non-zero diagonal α_{xx}, α_{yy} components of ME tensor, the contributions from oscillators in different layers are similar in sign, but the corresponding contribution in the transmittance coefficients is stronger for oscillators with higher frequency. In this measurement configuration it would be impossible to distinguish oscillators from different layers.

CHAPTER 4

MUELLER MATRIX ELLIPSOMETRY

The most general representation of the transformation of the state of polarization of light upon reflection or scattering by an object or sample is described by

$$\vec{S}'_{out} = \hat{M} \cdot \vec{S}_{in}$$

(4.1)

where $\vec{S}'_{out}$ and $\vec{S}_{in}$ are the Stokes vectors of the scattered and incident light correspondingly which is defined in equations below. $\hat{M}$ is the real 4x4 Mueller matrix (MM) that characterize elastic interaction light with a sample.

$$S_0 = I_x + I_y$$
$$S_1 = I_x - I_y$$
$$S_2 = I_{+45^0} - I_{-45^0}$$
$$S_3 = I_R - I_L$$

(4.2)

Here, S_0 represents the total light intensity and S_1 shows the light intensity determined by subtracting the light intensity of linear polarization in the y direction (I_y) from that in the x direction (I_x). On the other hand, S_2 represents the light intensity obtained by subtracting the light intensity of linear polarization at -45^0 from that at $+45^0$. With respect to the parameter S_3, the light intensity of left-circular polarization I_L is subtracted from that of right-circular polarization I_R. Thus, the parameters S_{1-3} represent the relative difference in light intensity between each state of polarization. When $S_1 > 0$, for example,

the light is polarized toward the *x* direction, while polarization of light is oriented in the *y*

direction when $S_1 < 0$. The Stokes parameters shown in Equation (4.2) can also be

expressed by using electric fields as described below. The Stokes parameters described by

electric fields are quite important for the interpretation of measured values in ellipsometry.

$$S_0 = I_x + I_y = E_{x0}^2 + E_{y0}^2 = E_x E_x^* + E_y E_y^*$$
$$S_1 = I_x - I_y = E_{x0}^2 - E_{y0}^2 = E_x E_x^* - E_y E_y^*$$
$$S_2 = E_{+45^0} E_{+45^0}^* - E_{-45^0} E_{-45^0}^* = E_x E_y^* - E_x^* E_y$$
$$S_3 = E_R E_R^* - E_L E_L^* = i(E_x E_y^* - E_x^* E_y)$$

(4.3)

In the most general case, Mueller matrix is given as

$$M = \begin{pmatrix} \frac{1}{2}(|r_{pp}|^2 + |r_{ss}|^2 + |r_{sp}|^2 + |r_{ps}|^2) & \frac{1}{2}(|r_{pp}|^2 - |r_{ss}|^2 - |r_{sp}|^2 + |r_{ps}|^2) & \mathrm{Re}(r_{pr}r_{sp}^* + r_{ss}^* r_{ps}) & \mathrm{Im}(r_{pr}r_{sp}^* + r_{ss}^* r_{ps}) \\ \frac{1}{2}(|r_{pp}|^2 - |r_{ss}|^2 + |r_{sp}|^2 - |r_{ps}|^2) & \frac{1}{2}(|r_{pp}|^2 + |r_{ss}|^2 - |r_{sp}|^2 - |r_{ps}|^2) & \mathrm{Re}(r_{pr}r_{sp}^* - r_{ss}^* r_{ps}) & \mathrm{Im}(r_{pr}r_{sp}^* - r_{ss}^* r_{ps}) \\ \mathrm{Re}(r_{pr}r_{ps}^* + r_{ss}^* r_{sp}) & \mathrm{Re}(r_{pr}r_{ps}^* - r_{ss}^* r_{sp}) & \mathrm{Re}(r_{pp}r_{ss}^* + r_{ps}^* r_{sp}) & \mathrm{Im}(r_{pp}r_{ss}^* - r_{ps}^* r_{sp}) \\ -\mathrm{Im}(r_{pr}r_{ps}^* + r_{ss}^* r_{sp}) & \mathrm{Im}(r_{pr}r_{ps}^* - r_{ss}^* r_{sp}) & -\mathrm{Im}(r_{pp}r_{ss}^* + r_{ps}^* r_{sp}) & \mathrm{Re}(r_{pp}r_{ss}^* - r_{ps}^* r_{sp}) \end{pmatrix}$$

(4.4)

where $r_{pp}, r_{ss}, r_{sp}, r_{ps}$ parameters determined from the experiment. Mueller matrix is the

connection point between theory and experiment. From MM-SE measurement we define

Mueller matrix and along with optical model we can give analysis to different phenomena.

In the following chapters, we would like to demonstrate versatility of MM-SE.

4.1 Far-IR Optics of Multiferroic Materials

Optical spectra of multiferroic crystals are in the focus of modern experimental and

theoretical studies [21,22,23,24,27,28,29,30,31,32,33]. These complex materials can

reveal a so-called bi-anisotropic optical behavior [34] in a form of the fascinating effects,

such as colossal nonreciprocal light propagation [35,36,37], and a negative index of refraction [1,4]. These optical phenomena are expected to occur in resonance with electric and magnetic dipoles, for example in the far-IR part of the optical spectrum, which is dominated by elementary excitations, such as optical phonons, magnons, electromagnons, and crystal field transitions. The common feature of all bi-anisotropic materials, and ME materials in particular, is that their optical properties cannot be correctly described with a dielectric susceptibility tensor $\hat{\varepsilon}(\omega)$ only. The magnetic permeability $\hat{\mu}(\omega)$ and ME tensors $\hat{\alpha}(\omega)$ and $\hat{\alpha}'(\omega)$ should be also included in consideration. As a result, a single transmission or reflection spectrum cannot properly describe the entangled contribution of $\hat{\varepsilon}(\omega)$, $\hat{\mu}(\omega)$, $\hat{\alpha}'(\omega)$, and $\hat{\alpha}(\omega)$ to, for example, the colossal nonreciprocal light propagation. Instead of the conventional transmission or reflection approaches, a combination of a more advanced spectroscopic technique together with an adequate theoretical description is required. Analysis of dynamic ME effects in multiferroics can be done using Mueller Matrix Spectroscopic Ellipsometry (MM-SE), which is one of the most versatile optical techniques. In the following discussion the MMs will be used for representation and analysis of experimental optical spectra, which will be calculated and fitted using the 4×4 Berreman's matrix formalism. In the following we will show that the off-diagonal components of the MM spectra are proportional to $\hat{\alpha}(\omega)$ and $\hat{\alpha}'(\omega)$, while the contributions of $\hat{\varepsilon}(\omega)$ and $\hat{\mu}(\omega)$ have opposite sign in the diagonal MM components, thus providing a direct experimental method of separation $\hat{\varepsilon}(\omega)$, $\hat{\mu}(\omega)$, $\hat{\alpha}(\omega)$, and $\hat{\alpha}'(\omega)$. Even more, the off-diagonal elements of the measured MM are sensitive to the magnetic point symmetry of the crystals.

4.2 Combination of MM-SE and 4×4 Berreman's Simulation Approach

In all publications known to us on the far-IR spectra in multiferroics, the polarization analysis of magnons, electromagnons, and phonons has been always restricted by the experimental geometry with the near-to-normal angle of incidence (AOI) and by the use of linear polarizers only. Using 4×4 Berreman's matrix propagation approach, one can easily show that the normal incidence geometry is not always sensitive to the dynamic ME effects described by the $\hat{\alpha}$ and $\hat{\alpha}'$ tensors. A simultaneous presence of the s- and p-polarizations is required to have complete information about the optical properties of a ME material. At AOI = 0, the s- and p-polarizations are obviously degenerate. Thus, the traditional approach to analysis of dynamic polarization in ME media at AOI = 0 is incomplete. For example, the limitations of the AOI = 0 geometry recently revealed themselves by failing to explain the experimentally-observed suppression of electromagnons in reflectivity measurements of GdMnO$_3$. As an alternative, we propose here a more advanced method, which is a combination of new experimental and computational techniques using AOI $\neq$ 0.

4.3 Basics of the Muller matrix Spectroscopic Ellipsometry (MMSE)

Spectroscopic ellipsometry analyses changes of the light polarization upon reflection from a sample in a wide frequency range [38,39,40,41,42,43,44,45,46,47,48,49,50,51]. MM-SE
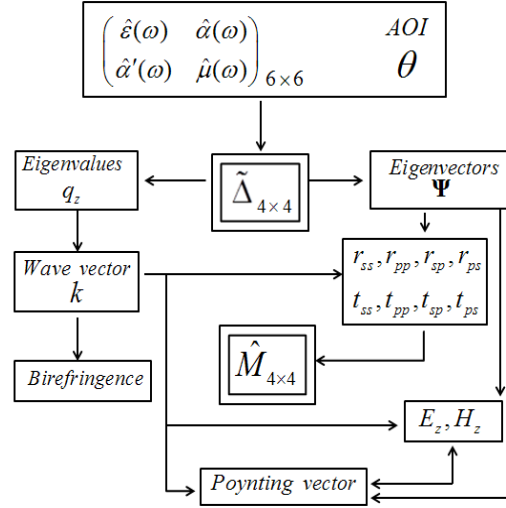
Figure 4.1 Flowchart for the calculation steps for MM in Berreman's 4×4 matrix formalism.

tools exist for mid-IR–VIS parts of the spectrum in many fields, from telecom and quantum cryptography to biology and, finally, condensed matter physics [42]. In spite of the power of the MMSE technique, no commercial MMSE are available for the far-IR/THz range. The first instrument was built in 2010 at U4IR beamline at NSLS-BNL by A. Sirenko et al. The main challenge was the lack of the optical components, such as optical retarders, for the far-IR spectral range. This issue has been successfully solved by using plastic, KRS5, and Si retarders to produce a broadband circularly polarized light in THz and far-IR [52].

In the Stokes representation, the polarization vectors for liner and circularly polarized light are $S_1 = (1, \pm 1, 0, 0)$, $S_2 = (1, 0, \pm 1, 0)$, and $S_3 = (1, 0, 0, \pm 1)$. The 16 components of $\hat{M}$ in (5.4) are real functions of the complex Fresnel coefficients and the

conversion between complex 2×2 Jones and real 4×4 MM's, $r_{s,p,sp,ps} \Rightarrow M_{ij}$ is straightforward as described in Reference [53]. To compensate for both, the spectral variation of the incoming radiation and for the spectral response of the experimental setup, the MM components $M_{ij}(\omega)$ are usually replaced by the normalized ones $m_{ij}(\omega)$, where $m_{ij} = M_{ij} / M_{11}$ and M_{11} is the total reflectivity. Thus, MM-SE can generate 15 normalized components of the MM spectra $\hat{m}(\omega)$ which contain significantly more information about anisotropic, magnetic, and ME samples compared to that for transmission/reflection experiments at AOI = 0. The theory of operations for MM-SE, which we implement at U4-IR setup, is published in our paper [54]: First, polarization measurements of the MM components $m_{ij}(\omega,\theta)$ at several AOIs in the range between 70° and 80° and correction for the systematic errors of experiment, such as non-ideal polarizers, retarders, windows, *etc*. Second, sample modeling using, a parametric description for the dielectric $\hat{\varepsilon}(\omega)$, magnetic $\hat{\mu}(\omega)$, and ME $\hat{\alpha}(\omega)$ and $\hat{\alpha}'(\omega)$ tensors and application of the 4×4 Berreman's matrix propagation approach to calculate the MM spectra $m_{ij}(\omega,\theta)$, or solving a "direct problem": $\left\{ \hat{\varepsilon}(\omega), \hat{\mu}(\omega), \hat{\alpha}(\omega), \hat{\alpha}'(\omega), \theta \right\} \Rightarrow m_{ij}(\omega,\theta)^{[4\times4]}$.

Third, solving the "inverse problem" to determine the model input parameters, such as the oscillator frequencies ω_0, broadening γ, and strength of electric, magnetic, and ME dipoles $S_{e,m,ME}$, that provide the best match between experimental and modeled spectra: $m_{ij}(\omega,\theta)^{[4\times4]} \Rightarrow \sum \omega_0, S_{e,m,ME}, \gamma, ...$ The fitting Program for MM spectra has been developed in our Group and is available to all Users of the MM-SE at U4IR beamline NSLS-BNL. The primary spectral range of our MM-SE at U4-IR beamline is between ~20

and 4,000 cm^{-1}. The low-frequency cut off is determined by diffraction and, correspondingly, can be shifted down to ~10 cm^{-1} for big crystals larger than 25 mm^2 or shifted up to ~30 cm^{-1} for small samples with the size of a few mm^2. Thus, we can cover the spectral range for almost all known magnetic excitations (magnons, electromagnons) and IR-active optical phonons in magnetic oxides.

4.4 Far-IR Ellipsometer at U4-IR, NSLS-BNL (Multiuser Facility)

This section provides a brief review of the MM ellipsometer installed at the U4-IR beamline of the National Synchrotron Light Source, Brookhaven National Laboratory The parameters of the setup and operational instructions are published in References [54,55].

Ellipsometer at U4IR beamline is shown in Figure 4.2. The spectral range for measurements is between 10 cm^{-1} and 4000 cm^{-1}, which is determined by the U4IR beamline parameters that are summarized in Table 4.1 [56]. Synchrotron radiation passes through the Bruker 66v FTIR spectrometer, which has a full complement of interchangeable beamsplitters for different spectral ranges from far-IR to visible. Then the radiation enters the Ellipsometer, which consists of three major sections:

1. Polarization State Generation (PSG) section.

2. Sample Stage with a cryostat, $\theta - \chi$ rotation, and X-Y-Z translation capability.

3. Polarization State Analyzer (PSA) section.

Optical schematic of ellipsometer is shown in Figure 4.3(a). To obtain ellipsometric data, synchrotron radiation passes Interferometer, after that is enters PSG section and the desired state of polarization is created with the help of rotating linear polarizers and a retarder. Then, polarized radiation reflects from the sample inside Sample Stage. Later on, the modified light polarization is analyzed inside PSA section with the help of rotating

retarder and linear polarizer. Finally, the radiation is focused on the bolometer with the help of a 90 degrees parabolic mirror. A single off-axis parabolic mirror in a combination with two other flat mirrors is used for the light focusing on the sample (see Figure 4.3(a)). This beam is "slowly" focused on the sample within the angle of less than 4 deg. The latter requirement is needed to (i) minimize depolarization on the linear polarizer and retarder surfaces and (ii) minimize the uncertainty in the value of the angle of incidence (AOI). Measurements of small samples with cross section dimension of ~ 1 mm^2 are possible with a microscope attachment for polarimetry measurements in transmission configuration. Two 15$\times$ objectives can be placed before and after the sample to bring the size of the focused beam to sub-mm scale. The gold-mirror objectives practically do not affect the light polarization.

To create and analyze the Stokes vectors for the light polarization *(S$_{IN}$* and *S$_{OUT}$)* in both, PSA and PSG, we are using a combination of the rotating linear polarizers and retarders (see Figure 4.3(b)). Retarders and polarizers are symmetrically positioned with respect to the sample. To cover the broad spectral range between 10 and 4000 cm^{-1} with linearly polarized light, we are using the following set of polarizers. For the frequency range from zero and up to 200 cm^{-1}, several free-standing wire-grid linear polarizer from SPECAC. There extinction ratio is between 1:2000 and 1:600, which is achieved by using "tandems" of linear polarizers in both PSA and PSG stages. The high frequency limit is
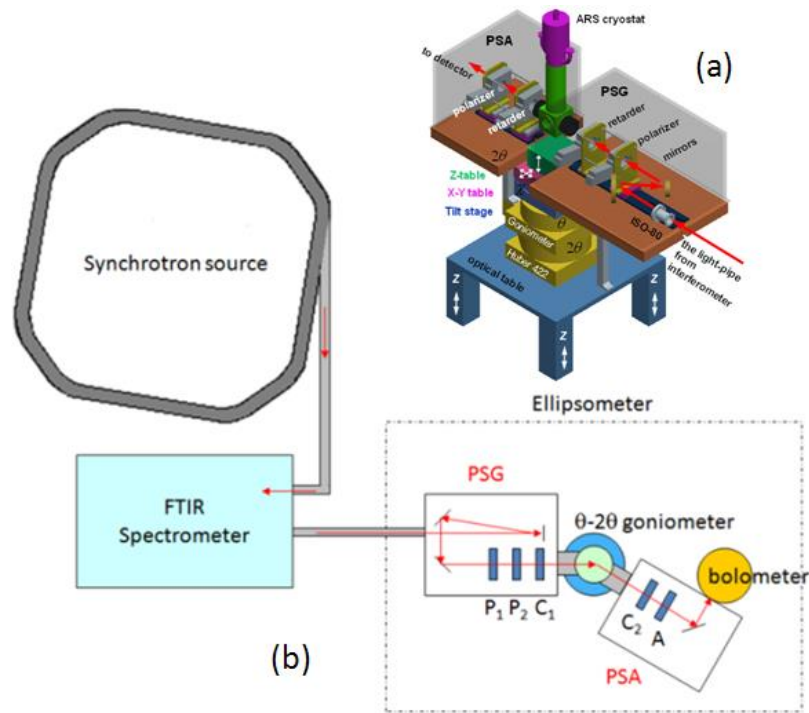
Figure 4.2 (a) 3D CAD schematics of the far-IR Ellipsometer in the standard configuration, which consists of PSG and PSA sections, sample stage (ARS or OXFORD optical cryostat and HUBER positioning system) The optical cryostat is mounted on the θ- table of the goniometer. The PSA section and bolometer are mounted on the 2θ-arm of the goniometer. The PSG optical section of the Ellipsometer shares the raw vacuum with the interferometer. (b) Schematics of the light propagation between the synchrotron source, Spectrometer, PSG, and PSA sections of the Ellipsometer. PSG section consists of a retarder C$_1$, two linear polarizer, P$_1$ and P$_2$, and three mirrors: an off-axis parabola with effective focus length of 1 m and two flat ones. PSA section consists of a compensator C$_2$, linear polarizer (analyzer) A, and a parabolic mirror for light focusing on a bolometer or a CuGe detector.

due to diffraction. Wire-grid polarizers on polyethylene substrate for frequency range between 30 and 700 cm^{-1}. Their extinction ratio is 1:1000 and no tandems are needed. The low-frequency limit is due to absorption in polyethylene substrate. Wire-grid linear polarizers on KRS5 substrates from SPECAC for the range between 400 and 4,000 cm^{-1}. The extinction ratio is better than 1:600. We are also using tandems in both PSG and PSA stages.

Broadband rotating retarders for the THz and far-IR spectral ranges are not commercially available. We developed several types of rotating retarders based on triangular prisms or double Fresnel rhombs. Preliminary results of this development effort were published in Reference [52]. Multiple conditions have been met in this design, such as (i) a reasonably high transmission in the operating frequency range and (ii) minimal displacement of the beam caused by the 360º retarder rotation around its optical axis.

Two schematics for the Si prism and KRS5 double Fresnel rhomb retarders are shown in Figure 4.4. The Si retarder is based on a single 45º prism with 15×15 mm^2 acceptance area and three 15×15 mm^2 gold mirrors. The maximum retardation of such retarder, which occurs inside Si due to total internal reflection, is about $\Delta \approx 95°$, which is different from the ideal theoretical value of $\Delta = \pi/4$ for a single 42º Si prism. Three gold mirrors practically do not change the polarization and intensity of radiation and allow to keep the light beam direction the same before and after the retarder. Rotation of the retarder around its optical axis by 45º allows to change the retardation between Δ=0 for linearly polarized light and $\Delta \approx 90°$ for nearly circular polarized light. The intensity attenuation factor for Si retarder is about 3 due to reflection and absorption in Si. The brightness of the synchrotron radiation is high enough to compensate these losses.

To cover the spectral window between 450 and 1400 cm^{-1}, we implemented the retarder based on two KRS5 Fresnel's rhombs (see Figure 4.4(b)). The split design allows for the independent alignment of two rhombs that is crucial for keeping the direction of the transmitted beam unchanged upon rotation of the retarder around its optical axis. KRS5 retarders pass more than 50% of light. Among disadvantages of the KRS5 retarder is a strong dispersion of $\Delta(\omega)$ above 900 cm^{-1}. In the nearest future we consider replacing KRS5 retarders with ZnSe or Ge rhombs that should be free from internal defects that cause a strong dispersion of $\Delta(\omega)$ in KRS5.
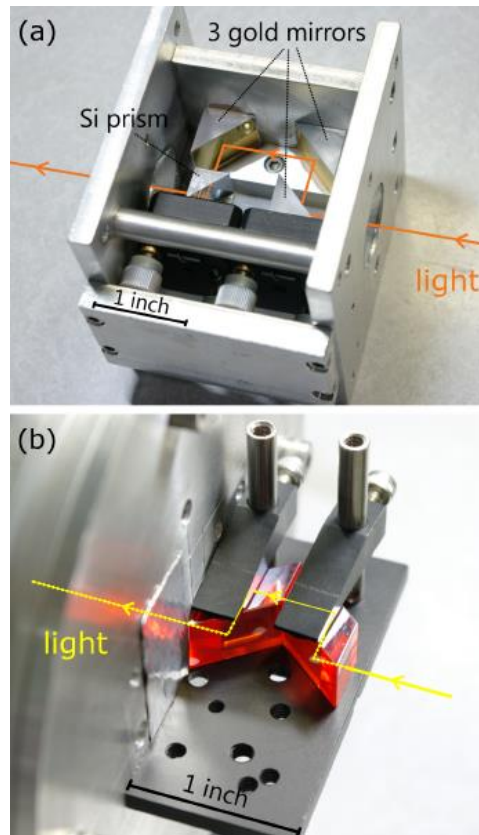
Figure 4.3 (a) rotating retarder based on a single Silicon prism and three gold mirrors (four bounces). (b) rotating retarder based on two adjacent KRS5 Fresnels rhombs (four internal bounces). Direction of the light propagation is shown with arrows.

CHAPTER 5

EXPERIMENTAL RESULTS FOR SPECTROSCOPIC ELLIPSOMETRY

In this chapter, the experimental results and their analysis are presented. Original data are published in Reference [61].

5.1 Experimental Data for Dy-IG ($DyFe_5O_{12}$)

Mueller Matrix analysis allows relatively easy to separate contributions from different origin such as magnons, electromagnons, chiral excitations, electric excitation, etc. We are going to demonstrate power of MM ellipsometry using experimental data for Dy-iron garnet (IG) and $TbMnO_3$ samples. Previously dysprosium iron garnet was studied in the spectral range between 12 and 700 cm^{-1} and in a wide temperature range between 5 K and 300 K using transmission spectroscopy and rotating analyzer ellipsometry.

Dy-IG, as well as the other related rare earth iron garnets (R-IG), is a ferrimagnetic material with a huge magnetostriction, which is related to the combination of a strong anisotropy of a crystal field of the R^{3+} ions and to a strong and anisotropic superexchange interaction between R^{3+} and iron [27,28,29]. At room temperature $DyFe_5O_{12}$ crystals form a cubic garnet structure. There are several nonequivalent Dy^{3+} ions in each unit cell with the same surrounding field, but their axes are inclined to each other. This has the overall effect of producing an average cubic symmetry. Below the transition temperature of $T_N =$ 550 K, the iron spins are ordered in a ferrimagnetic structure along the [111] direction. Among six possible exchange interactions between spins in three different magnetic subsystems only two dominate. The main magnetic superexchange interaction is between Fe in two different sites (a and c): spins of Fe in the tetrahedral site are parallel to those of

the octahedral site. Another important interaction is between Dy and Fe in the tetrahedral site resulting in the Dy spins to be antiparallel to Fe moments in tetrahedral sites and, hence, antiparallel to the net magnetic moment of Fe. Below 100 K, a rhombohedral distortion of the cubic cell causes the canting of Dy spins. Below 50 K, the iron sublattice magnetization does not change appreciably with temperature. However, the Dy sublattice magnetization increases rapidly with temperature decrease. Dy iron garnet has the most complex spectrum of the far-IR excitations among all other studied R-IGs. Based on the analysis of transmission in polycrystalline materials, it was shown that below 80 cm^{-1} the optical spectra of R-IGs are dominated by both R^{3+} single-ion electronic transitions and KK modes. Note, that in earlier studies of the far-IR excitations in R-IGs it was assumed that the optical transition inside $4f$ shell are magnetic dipoles, as expected for a free R^{3+} or for an R^{3+} at the center of inversion. At low temperatures the local electric polarization removes Dy^{3+} ions from the position of the center of inversion. This result is important for interpretation for the selection rules for the optical transition between $4f$ electrons levels of Dy^{3+}. In the non-centrosymmetric environment, the so-called 'forced electric dipole' optical transitions are allowed in addition to the conventional magnetic-dipole transitions. In Dy-IG was found stronger connection between the static dielectric constant and spectra of the optical phonons. Also hybridization between electric- and magnetic-dipole activity for the ligand field excitations was observed as well.
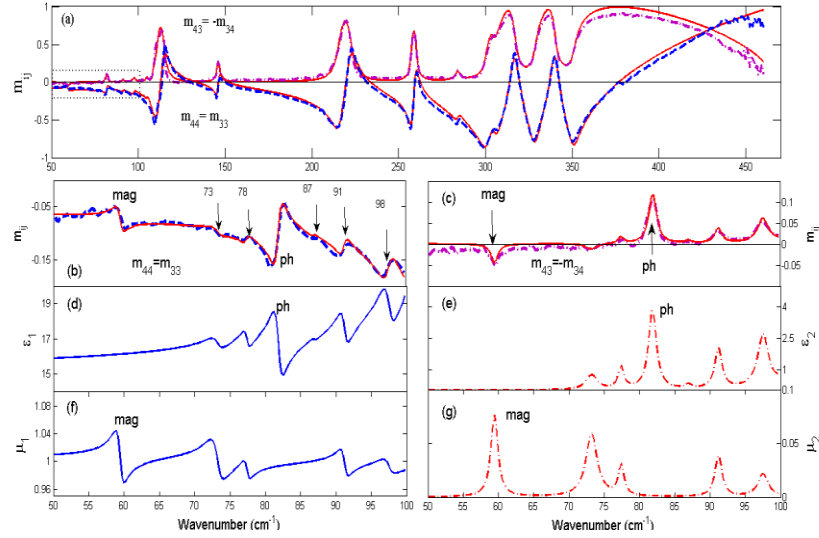
Figure 5.1 (a) Experimental spectra of the normalized MM components (magenta dot-dashed curve) and (blue dash curve) for Dy-IG measured at 5 K. The strong peaks above 80 cm^{-1} correspond to the optical phonons. Solid red curves show the fit results. (b-c) The low frequency part of the same spectra measured with a LHe-pumped 1.6 K bolometer. The corresponding range is shown in (a) with a black dotted rectangle. (d-g) and functions as extracted from the fit of MM spectra. The pure magnetic dipole excitation is observed at 59.5 cm^{-1} and the pure electric dipole excitation (phonon) is observed at 81cm^{-1}. The magnon amplitude in the spectra in (c) has an opposite sign compared to that for the optical phonon. A number of hybrid modes that contribute to both and in (d-g) correspond to the weak crystal field transitions and are marked in (b) with vertical arrows.

Normalized Mueller Matrix spectra, $m_{34} = -m_{43}$ and $m_{33}(\omega) = m_{44}(\omega)$ for the Dy-IR measured using rotating Si retarders and stationary linear polarizers in the frequency range between 50 cm^{-1} and 460 cm^{-1} is shown in Figure 5.1 (a). To simulate and fit MM spectra, results of the preceding chapters were used. The simultaneous fit to the normalized MM spectra are shown in Figure 5.1 (a) with solid red curves. The magnified view of the low frequency part of the normalized MM spectra measured with the same optical components and a LHe-pumped (1.6 K) bolometer is shown in Figure 5.1 (b,c). Functions $\varepsilon_{1,2}(\omega)$ and $\mu_{1,2}(\omega)$ extracted from the fit of MM spectra are depicted in Figure 5.1 (d-g). The pure magnetic diploe excitation (magnon) appears at 59.5 cm^{-1}, which is exactly the same frequency as previously determined. Pure electric dipole excitation at 81 cm^{-1}

corresponds to the optical phonon. Our measurement demonstrates that the sign of the magnon contribution in $m_{34} = -m_{43}$ is negative, that is the opposite to that for the electric dipoles, such as a phonon at 81 cm^{-1}. The spectra in Figure 5.1 (b,c) also shows several weak ligand-field excitations at 73, 78, 87, 91 and 98 cm^{-1}, which originate from 4f electronic levels in Dy^{3+} ions. From Figure 5.1 (d-g), one can see that these modes contribute to both $\varepsilon(\omega)$ and $\mu(\omega)$ and thus are hybrid. As expected from the material symmetry of Dy-IG, the measured off-diagonal components of the MM are equal to 0: $m_{13,31} = m_{14,41} = m_{23,32} = m_{24,42} \cong 0$ within the accuracy of our experiments. We did not detect any changes in the off-diagonal MM components if measured at temperatures below and above the antiferroelectric transition at $T = 100$ K.

5.2 Experimental Data for TbMnO₃

Another interesting case illustrates the experimental situation when the $\alpha(\omega)$ tensor is not equal to zero. TbMnO₃ is an ME material possesses simultaneously electric polarization and magnetic order at low temperature. We expect to find non-zero magneto-electric tensor elements (at least some of them) in the optical part of the spectrum. Due to the thermodynamical requirement of $\hat{\alpha}'(\omega) \cdot \hat{\alpha}(\omega) \le \hat{\mu}(\omega) \cdot \hat{\varepsilon}(\omega)$, we expect the strongest contribution in ME tensor at the frequencies where $\varepsilon(\omega)$ and $\mu(\omega)$ have poles, *i.e.* close to the resonance with phonons, magnons and electromagnons. The requirement that $\alpha(\omega) \ne 0$ infers a simultaneous absence of both center of inversion and the time-reverse invariance. In symmetry terms, the total number of magnetic point groups that allow ME effect is 58. The simulation analysis for the contributions of the $\hat{\varepsilon}, \hat{\mu}, \hat{\alpha}, \hat{\alpha}'$ tensor

components to the MM spectra shows that that $\hat{\varepsilon}, \hat{\mu}$ should reveal themselves in the close-to-diagonal $m_{ij}(\omega)$, such as $m_{12}, m_{21}, m_{33}, m_{44}, m_{34}, m_{43}$. In contrast, the appearance of non-zero $\hat{\alpha}(\omega)$ and $\hat{\alpha}'(\omega)$ tensors is equivalent to optical bi-anisotropy and should give some contribution to the some of the off-diagonal MM components.
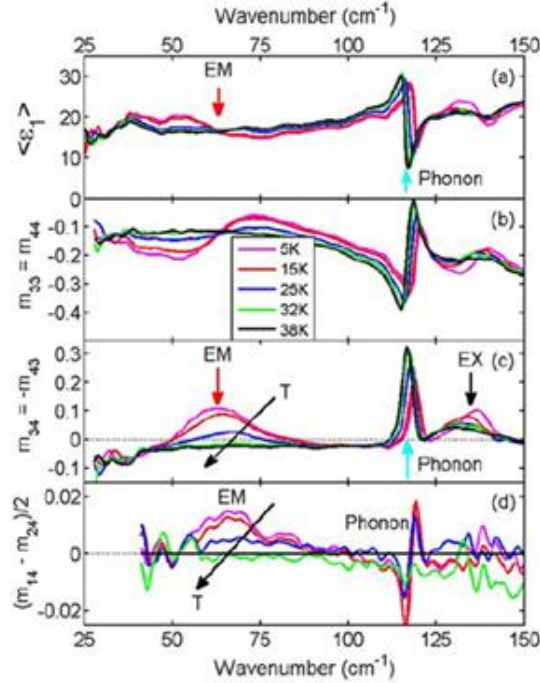
Figure 5.2 Experimental optical spectra of TbMnO$_3$ with crystallographic orientation of x‖a, y‖c, and z‖b measured in the temperature range between 5K and 40 K. Phonon peak at ~118.5 cm^{-1}, electromagnon (EM) peak at 62 cm^{-1}, and peak of excitation at 135 cm^{-1} (EX) are marked with arrows. (a) Real part of the pseudo-dielectric function. The normalized MM components are shown in (b) m34(ω)=−m43(ω) and (c) m33(ω) = m44(ω). (d) The difference between the off-diagonal MM components m14(ω) and m24(ω). Vertical arrows in (c) indicate the contribution of εxx(ω), μyy(ω), and αxy(ω) to m34(ω)=−m43(ω) components of the MM spectra.

Spectra of TbMnO$_3$ ware extensively studied prevoiously using transmittance and reflectance techniques [57,58,59]. It was shown that the electric component of light along the *a*-axis apart from excitation of optical phonons with frequencies above 100 cm^{-1}, can excite both electromagnons at 19 and 62 cm^{-1}, and another excitation at 135 cm^{-1}. The latter

excitation has controversial interpretation in the literature and was assigned to two-magnon process, one-phonon + one-magnon process or transition between crystal field levels of Tb^{3+} ground multiplet. The low-frequency part of the RAE and MM spectra measured at AOI = 75 degrees is shown in Figure 5.2. All measurements in Figure 5.2 were taken when the crystallographic directions of $TbMnO_3$ are oriented with respect to the ellipsometric axes $x - y - z$ as follows: $x \parallel a, y \parallel c$ and $z \parallel b$. The cross section to the available for us sample was only 5x5 mm^2, which resulted in low frequency cut off at ~ 25 cm^{-1} thus preventing the measurement of the lowest frequency electromagnon mode at 19 cm^{-1}. The pseudo-dielectric function in Figure. 5.2 (a), which was obtained from rotating analyser ellipsometry (RAE) spectra measured at different temperatures between 5 K and 38 K, shows a clear redistribution of the spectral weight from the optical phonon at 118.5 cm^{-1} towards electromagnons at 62 cm^{-1} and excitation at 135 cm^{-1} which is labeled as EX. The exchange of the spectral weigh occurs below the transition temperature of T_c = 28 K. The shape of the electromagnon peak in RAE measurements is different from that of the phonons and cannot be easily described with simple harmonic oscillator model indicating the limitations of pseudo-dielectric function approach to the optical spectra of magneto-electric materials. The normalized MM components of the same sample are shown in Figure 5.2 (b-c). The same peaks that correspond to the electromagnon, single phonon and EX are clearly seen in $m_{33} = m_{44}$ and $m_{34} = -m_{43}$ spectra at 62, 118.5 and 135 cm^{-1}. Note that the sign of the electromagnon excitation to the $m_{34} = -m_{43}$ spectra is the same as that for the phonon, thus providing unambiguously a well-known fact that the electromagnon is indeed a predominantly electric diploe polarized along the a-axis of $TbMnO_3$. The difference between the normalized off-diagonal components of the MM, which are

proportional to the electromagnon's contribution to the ME tensor is shown in Figure 5.2 (d). The symmetry consideration for the cycloidal spin structure in TbMnO$_3$ predicts that only $\alpha_{xz}(\omega) \neq 0$. It is this component of ME tensor that provides the coupling between the dynamic polarization of the lattice along the a-axis and magnetization caused by an external magnetic field applied along b-axis [12]. For $\alpha_{xz}(\omega) \neq 0$, the electromagnon's contribution in m_{24} and m_{14} spectra has opposite sign. To exclude small offsets caused by the polarizer/retarder calibration errors, we plot the difference $(m_{24} - m_{14})/2$, which shows a pure contribution from the electromagnon to the off-diagonal components of the MM. The low temperature amplitude of the electromagnon peak in $(m_{24} - m_{13})/2$ is about 0.015, which is smaller than the contribution of the same electromagnon to $m_{34} = -m_{43}$ at $T = 5$ K: $\omega_0 = 62 \pm 2$ cm^{-1}, $\gamma_0 = 20 \pm 2$ cm^{-1}, $S_{e,xx} = 1.7 \pm 0.2$ and $S_{EM,xz} = 0.2 \pm 0.05$. The spectral variation of $\alpha_{xz}(\omega)$ was calculated with these parameters using SHO model:

$$\alpha_{xz}(\omega) = \sum_{n=1}^{N} \frac{S_{n,EM}\,\omega_{n,EM0}^2}{\omega_{n,EM0}^2 - \omega^2 - i\gamma_{n,EM}\,\omega} \tag{5.1}$$

The oscillator strength of electromagnon $S_{e,xx}$ and $S_{EM,xz}$ determined from the MM measurements are important parameters that are related to the electric polarization of the lattice due to the spin structure, anisotropy and exchange fields [60]. The calculated maximum value of the ME function is $|\alpha_{xz}| \leq 0.5$, which is ~10 times smaller than the theoretical limit of $\alpha(\omega)^{max} = \sqrt{\varepsilon(\omega) \cdot \mu(\omega)} \approx 5$.

5.3 Ellipsometry of Infrared-Active Optical Phonons in Hexagonal Manganites RMnO₃

This section presents the original experimental results published in Physical Review B paper [61].

5.3.1 Structural and Magnetic Properties of Hexagonal RMnO₃

Multiferroic rare-earth (R) manganites RMnO₃ ($R=$ Ho, ...Lu, and Sc, Y) is one of the most investigated systems inside a broader class of hexagonal (h) materials [62,63,64,65,66,67,68,69,70]. One of the striking peculiarities of h-RMnO₃ is the ferroelectric (FE) order with a large remnant polarization and high FE transition temperature T_C in the range between 600 K and 1000 K.[71,72] The RMnO₃ hexagonal structure consists of close-packed layers of MnO₅ bipyramids, which share corners in the a-b planes. Along the hexagonal c-axis, the layers of MnO₅ are well separated by the R^{3+} ions. A cooperative tilting of the bipyramidal sites below T_C displaces the R^{3+} ions along the c-axis into two non-equivalent sites (Wyckoff positions 2a and 4b within the $P6_3cm$ space group). Two of the R^{3+} ions within the unit cell move up (down), and one – down (up), producing a ferroelectric state. The oxygen ions are also displaced in the a-b plane. Both displacements of R^{3+} ions and oxygen contribute to the FE polarization [73]. Schematics of the h-RMnO₃ crystal structure in the ferroelectric phase is shown in Figure 5.3. More detailed discussion of the ionic displacements in the FE phase can be found in References [64,74].
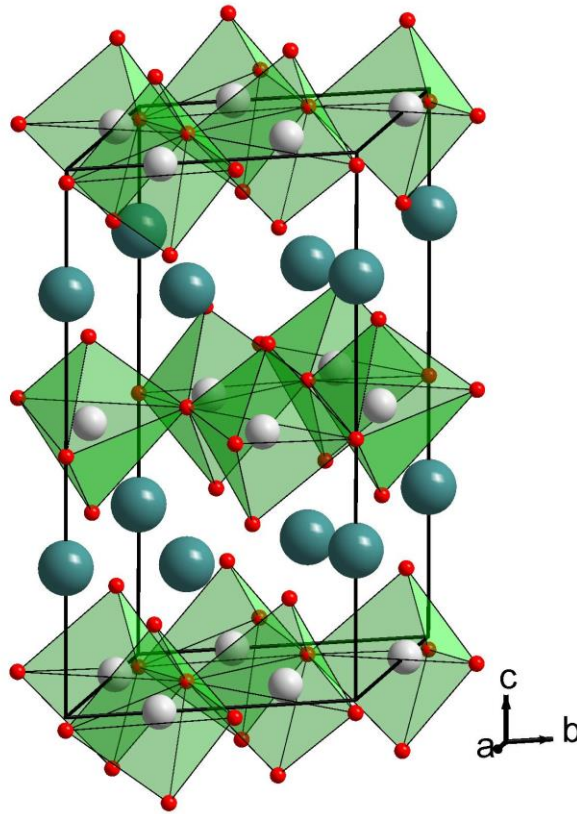
Figure 5.3 Crystal structure of hexagonal rare earth manganites RMnO$_3$ in the ferroelectric phase. View along (110) showing two layers of MnO$_5$ trigonal bipyramids and two layers of R^{3+} ions. Calculated lattice parameters for HoMnO$_3$ including the bipiramide tilts and displacements of R^{3+} ions along the c-axis have been used.

Phonon excitations in h-RMnO$_3$ (R=Y, Ho, Er, Yb, Lu) have been studied earlier using Raman scattering [64,75, 76, 77, 78, 79, 80, 81, 82, 83, 84, 85, 86, 87, 88], IR reflectance [75, 84, 89, 90], IR absorption [64, 90], THz time-domain [72] and femtosecond pump-probe [91] spectroscopic techniques. Lattice dynamics of RMnO$_3$ compounds was also analyzed theoretically using shell model calculations [64,75,80], Heisenberg and the transverse Ising model [92, 93] and first principles calculations [94, 95]. For the unit cell with 6 formula units (30 ions), the theory predicts 90 zone-center phonon modes. Three of

them are acoustic ($A_1 + E_1$), 67 are Raman active ($9A_1 + 14E_1 + 15E_2$), 37 are IR active (

$9A_1 + 14E_1$). The remaining modes are silent ($A_2, B_1,$ and B_2). Temperature dependence of

some phonon modes was shown to exhibit anomalies near the temperature of AFM

magnetic ordering of Mn^{3+} ions T_N , thus reflecting either atomic displacements [74] or

spin-lattice interaction [67, 70, 71, 72, 73, 74, 75, 79, 80, 81] below T_N. Dependence of

phonon spectra on rare-earth ion were studied in bulk crystals [69] and thin films [77].

The optical phonon spectra and their temperature dependencies cannot be

understood without taking into account the magnetic structure and its changes with

temperature. The magnetic structure of the h-REMnO$_3$ have been studied in a number of

publications [65,96,97,98,99]. However, the most intriguing part about the magnetic

interaction between Mn^{3+} and R^{3+} spins at low temperatures and high magnetic fields is

still under debate [30,100]. The commonly accepted view on the magnetic structure and

the corresponding magnetic phase transitions is the following. An antiferromagnetic

(AFM) order of the Mn^{3+} spins occurs at much lower temperatures compared to the FE

transition. The AFM transition temperature T_N for Mn^{3+} spins is in the range between 70

K and 87 K for R= Y, Ho, Er, Tm, Yb, and Lu. The neighboring Heisenberg spins of the

close-packed Mn^{3+} ions are AFM-coupled via the oxygen ions by superexchange

interaction, which gives rise to frustration effects of an ideal 120° angle structure with the

space group $P6'_3 c'm$. The Mn^{3+} spins are ordered perpendicular to the c-axis: $\vec{S}_{Mn} \perp c$,

while at low temperatures spins of R^{3+} ions (R=Ho, Er, Tm, Yb) are oriented along the c

axis: $\vec{S}_R \parallel c$. R^{3+} ion spins S_R can interact among themselves and with the Mn^{3+} spins.

These interactions result in a complex phase diagram in the temperature-magnetic field

parameter space $T - H$ [13,91]. Among all hexagonal RMnO$_3$ compounds with $S_{RE} \neq 0$, HoMnO$_3$ is the most studied material. Its magnetic structure is particularly interesting since it shows two additional phase transitions below T_N: Mn^{3+} spin reorientation occurs at $T_{SR} \approx 40$ K and AFM ordering of Ho^{3+} spins takes place at $T_{RE} \approx 5$ K, as observed in neutron scattering [101,102] and second-harmonic generation optical experiments [103,104,105,106]. The spin reorientation is believed to be related to the S_{Mn} rotation in the a-b plane by 90°, changing the magnetic symmetry from $P6'_3 c'm$ to $P6'_3 cm'$. At much lower temperatures $T < T_{RE}$, another modification of the Mn spin structure occurs restoring the $P6_3 cm$ symmetry. Both low-temperature transitions at T_{SR} and T_{RE} are also accompanied by a complete or partial ordering of the Ho^{3+} spins, which structure is not resolved yet. As mentioned in Reference [107], two possibilities are discussed in literature for the spins of two non-equivalent Ho^{3+} sites: (*i*) Ho spins on the 4*b* site develop AFM order below T_{SR} while Ho spins on the 2*a* site remain PM, and (*ii*) all Ho spins develop AFM order below T_{SR}. In any case, there is an agreement that the Ho sublattice exhibits long-range AFM order along the c-axis below $T_{RE} \approx 5$ K [107]. Magnetization of the *R* spins at low temperatures in other hexagonal manganites with *R*= Er, Tm, Yb has been also studied in References.[108, 109, 110] where Dzyaloshinskii–Moriya (DM) interaction [11,111] has been proposed as one of the mechanisms for coupling between *R* spins with the partial AFM order along the c-axis and Mn spins that are ordered in the a-b plane.

5.3.2 Motivation for Studies of the Optical Phonons in h-RMnO$_3$

In spite of a significant amount of the recent experimental and theoretical efforts, the IR phonon spectra in h-RMnO$_3$ still remain not fully understood. Some papers have exhausting information about one or two particular h-RMnO$_3$ compounds but they do not provide a broader view on the whole family of h-RMnO$_3$. Further, in the majority of available experimental papers the number of observed phonons is significantly smaller than the group theory prediction, (9 modes with A_1 symmetry polarized along the c-axis and 14 doubly-degenerate E_1 modes polarized in the a-b plane, as mentioned above). One of the possible reasons is that the sensitivity of conventional optical techniques, such as reflectivity and transmittivity, is not always sufficient for analysis of materials with closely spaced phonon modes which have drastically different oscillator strengths. Most of the previous phonon studies were carried out in the temperature range above the R^{3+} spin ordering transition that occurs below 5 K, thus leaving unanswered the question about the possible effect of magnetic ordering of R^{3+} ions on phonon excitations.

In this work, we present our systematic experimental studies of the IR-active phonons in the complete set of h-RMnO$_3$ (R= Ho, …Lu) by means of one of the most sensitive optical technique: spectroscopic ellipsometry. We complimented our ellipsometry studies with transmission measurements of the same samples in magnetic field. These experiments provided us with additional information about weak phonon modes and answered the question about possible field-induced modifications in external magnetic field. The low-frequency phonon spectra for YbMnO$_3$ have been measured for the temperatures above and below the AFM ordering of Yb spins $T_{RE} = 3.3$ K. This paper is a natural continuation of our recent studies of the AFM resonances and crystal-field

transitions in the far-IR spectra of the same family of h-RMnO$_3$ ($R=$ Ho, …Lu) compounds [112].

5.3.3 Sample Growth

The high-temperature flux growth technique was utilized to produce bulk crystals of RMnO$_3$ for $R=$Er, Tm, Yb, and Lu. Single crystal platelets with pristine, or as-grown, surfaces and hexagonal c-axis being perpendicular to the surface were used for both, ellipsometry and transmission measurements. The a-b plane surface area of the flux-grown samples was about 4×4 mm^2 and their thickness was about 0.1 mm. The opposite sides of the samples were not wedged, resulting in relatively strong thickness interference fringes in the measured optical spectra below the optical phonon frequencies. The natural platelet shape of the Er, Tm, Yb, and Lu samples did not allow for optical measurements from the a-c or b-c planes. In contrast, the HoMnO$_3$ sample was grown using the floating zone technique. The sample dimensions were about 4×4×4 mm^3, which allowed for the ellipsometry studies of both, c-axis and a-b plane optical properties of HoMnO$_3$.

5.3.4 Ellipsometry Technique

The rotating analyzer ellipsometry (RAE) and Mueller matrix ellipsometry (MME) measurement were carried out at U4IR beamline of the National Synchrotron Light Source, Brookhaven National Laboratory (NSLS-BNL). The ellipsometry setup, which is described in details in References [52,54], allowed us to measure the optical phonon spectra in the temperature range between 7 and 300 K in the spectral range between 100 and 2000 cm^{-1} using the spectral resolution of 0.7 cm^{-1}. This setup consists of a Bruker v66i spectrometer, several LHe-pumped (~1.6 K) and LHE 4 K bolometers, and LHe-cooled

CuGe detector. In our previous studies of the AFM resonances in the same set of hexagonal RMnO$_3$ samples, we had focused on the spectra of the AFM resonances in far-IR spectral range below 100 cm^{-1}.[102]. In this work, our main interest is in the optical phonon spectral range above 100 cm^{-1}. The main advantage of RAE in comparison with conventional reflectivity is the possibility to measure both, real and imaginary parts of the dielectric function. MME is even more powerful due to the simultaneous measurement of several components of the 4×4 Mueller matrix, that connect the Stokes polarization vectors for incoming $\vec{S}_{IN}$ and outgoing (reflected) light $\vec{S}_{OUT}$. For each frequency of the measured spectra, a Mueller matrix $\hat{M}(\omega)$ is defined as $\vec{S}_{OUT}(\omega) = \hat{M}(\omega) \cdot \vec{S}_{IN}(\omega)$. In the following discussion, the experimental data will be presented in terms of the normalized Mueller matrix components $m_{ij}(\omega) = M_{ij}(\omega) / M_{11}(\omega)$ that are more robust against systematic errors due to self-normalization by the total reflected intensity that is given by the $M_{11}(\omega)$ spectrum. The measured experimental spectra of $m_{ij}(\omega)$, which vary from −1 to +1, contain all information about optical phonons that can be polarized along or perpendicular to the c-axis of hexagonal manganites. The angle of incidence (AOI) for the light on the sample in all ellipsometric measurements was set to 75° that is close to the Brewster angle for the low-frequency spectral range of h-RMnO$_3$. In the following we use a standard ellipsometry convention for the Cartesian x, y, z coordinate system: z is perpendicular to the reflecting surface of the sample, x is parallel and y is, correspondingly, perpendicular to the reflection plane.

5.3.5 Transmission Experiments

Transmission experiments were carried out at the same U4IR beamline of NSLS-BNL. The main goal of these complementary experiments was to obtain additional information about the weak spectra of the low-frequency phonons between 100 and 200 cm^{-1} and high-frequency phonons above 500 cm^{-1}. In addition, a possible modification of the optical phonon spectra in external magnetic field was investigated. The experimental configuration for transmission experiments is the same as previously described in Ref. [102]. An optical Oxford magnet was used for the sample cooling and for application of external magnetic field up to 9 T along the *c*-axis of the samples, *i.e.* perpendicular to the sample surface. Correspondingly, the electric and magnetic fields of light were always in the hexagonal plane perpendicular to the *c*-axis. The spectral range for transmission experiments in magnetic field was between 20 and 210 cm^{-1} with a spectral resolution of 0.7 cm^{-1}. The low frequency cutoff was determined by diffraction, while the high frequencies were limited by the light absorption in the cryostat windows. The higher frequency transmission spectra above 500 cm^{-1} were measured in the same cold-finger cryostat as used for the ellipsometry measurements. For each sample, the raw data of transmitted intensity were normalized to transmission through an empty aperture with the size equal to that of the sample. Polarization of the transmitted light was not analyzed due to the expected optical isotropy in the *a−b* plane of the measured hexagonal samples.

5.3.6 Shell Model Lattice Dynamics Calculations

Lattice vibrations of h-RMnO$_3$ were calculated by means of the shell model,[113] which is proven to reasonably describe the properties of ionic materials, in particular, manganese oxides.[114,115] In the shell model, each ion is considered as a point core with charge Y surrounded by a massless shell with charge Q. The free ion polarizability $\alpha = Y^2/k$, where k is a force constant. The short range potentials $V(r)$ are chosen in the Born-Mayer-Buckingham from $V(r) = a \cdot e^{-b \cdot r} - c/r^6$, where r is the interatomic distance, a, b, and c are the potential parameters. The cation-anion short range interactions contain no attractive part and $c=0$ in the expression for $V(r)$. The Coulomb energy calculations are based on a real space summation involving a spherical cut-off boundary, which is defined by the cut-off radius and set to 10 Å, making the sum of all charges within the spherical cut-off region equal to zero. The parameters of the model used for a series of h-RMnO$_3$ compounds, are listed in Table 5.1. Note that they are somewhat different from those used earlier in Reference [84] due to a different set of R and Mn ionic charges and polarizabilities.

Table 5.1 Shell Model Parameters for h-RMnO$_3$

Ion	Z (|e|)	Y (|e|)	α (Å^3)	Ionic pair	a (eV)	b (Å^{-1})	c (eV·Å^6)
R	2.85	3.10	2.33	R–O	1738	3.04	0
Mn	2.85	3.15	2.71	Mn–O	2020	3.26	0
O	− 1.90	1.10	2.00	O–O	22764	6.71	20.37

5.3.7 Phonon Spectra
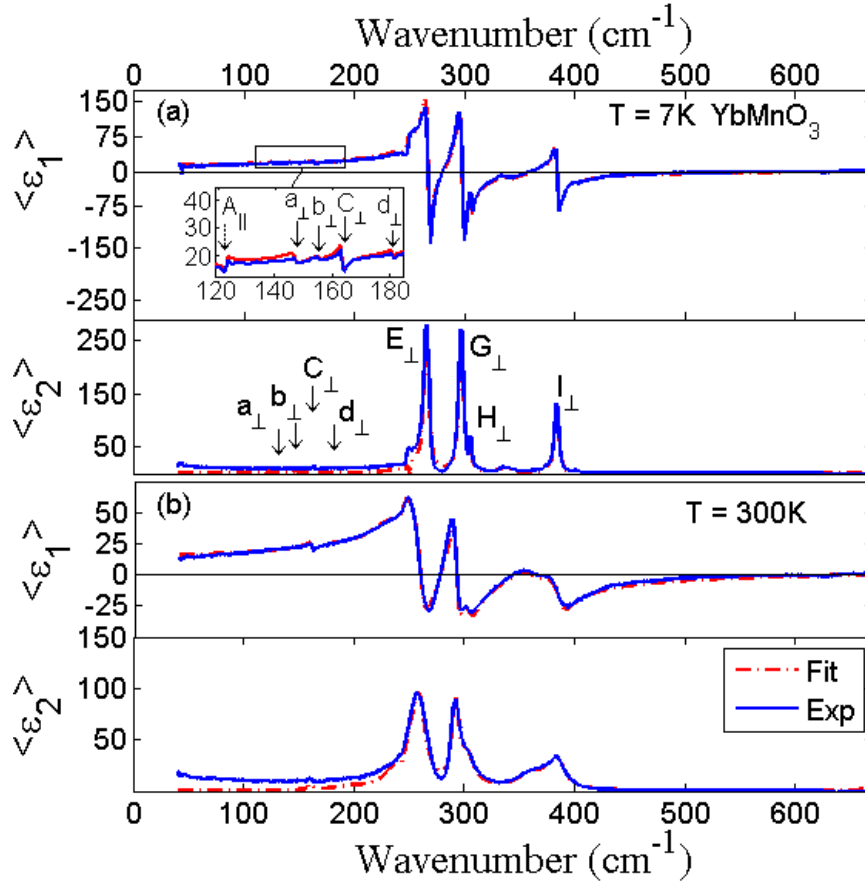
Figure. 5.4 Spectra of the real (a) and imaginary (b) components of the pseudo dielectric function $\langle \varepsilon_{1,2}(\omega) \rangle$ measured at T=7 K for YbMnO₃. Strong phonons are marked with arrows. Dashed curves correspond to the fit using Equation 5.2 for the parametric description model of the dielectric function.

Experimental data for the real $\langle \varepsilon_1(\omega) \rangle$ and imaginary $\langle \varepsilon_2(\omega) \rangle$ parts of the pseudo-dielectric functions for YbMnO₃ measured at *T*=7 K obtained using RAE at AOI=75° are shown Figure 5.4 (a,b). The optical spectra of $\langle \varepsilon_{1,2}(\omega) \rangle$ are dominated by multiple strong IR phonons that are marked in Figure 5.4 (a,b) with vertical arrows and labels that correspond to their frequencies in cm^{-1}. Due to hexagonal symmetry, the dielectric function tensor is diagonal in the laboratory x, y, z coordinate system ($c \parallel z$) with only three non-

zero components $\varepsilon_{xx}(\omega) = \varepsilon_{yy}(\omega) = \varepsilon_{\perp}(\omega)$ and $\varepsilon_{zz}(\omega) = \varepsilon_{\parallel}(\omega)$. At each frequency, the

measured $\langle \varepsilon_{1,2}(\omega) \rangle$ is a function of $\varepsilon_{\perp}(\omega)$, $\varepsilon_{\parallel}(\omega)$, and AOI=0 [116]:

$$\langle \varepsilon \rangle = \sin^2(\phi) \cdot \left[1 + \sin^2(\phi) \cdot \left(\frac{\varepsilon_{\perp} \sqrt{\varepsilon_{\perp} - \sin^2(\phi)} - \sqrt{\varepsilon_{\perp}(\varepsilon_{\parallel} - \sin^2(\phi))/\varepsilon_{\parallel}}}{\varepsilon_{\perp} \cos^2(\phi) - \sqrt{\varepsilon_{\perp} - \sin^2(\phi)} \cdot \sqrt{\varepsilon_{\perp}(\varepsilon_{\parallel} - \sin^2(\phi))/\varepsilon_{\parallel}}} \right)^2 \right]. \quad (5.2)$$

Note, however, that at AOI=75°, the main contribution to the measured pseudo dielectric

function originates from $\varepsilon_{\perp}(\omega)$, while only several strong poles and zeroes of $\varepsilon_{\parallel}(\omega)$ appear

in the spectra shown in Figure 5.4 (a,b), like for example the peak at 125 cm^{-1}, which

corresponds to lowest frequency LO phonon polarized along the c-axis. The measured

spectra were fitted using anisotropic model function consisting of two sets of Lorentz

oscillators polarized along and perpendicular to the c-axis

$$\varepsilon(\omega)_{\parallel} = \varepsilon_{\infty,\parallel} + \sum_{n=1}^{N} \frac{S_n \cdot \omega_{n,0}^2}{\omega^2 - \omega_{n,0}^2 - i\gamma_n \omega},$$

$$\varepsilon(\omega)_{\perp} = \varepsilon_{\infty,\perp} + \sum_{m=1}^{M} \frac{S_m \cdot \omega_{m,0}^2}{\omega^2 - \omega_{m,0}^2 - i\gamma_m \omega}, \quad (5.3)$$

where $\omega_{n(m),0}$ is the phonon frequency, $S_{n(m)}$ is the oscillator strength, $\gamma_{n(m)}$ stands for the

phonon broadening, and $\varepsilon_{\infty,\parallel(\perp)}$ represents the dielectric constant at frequencies above the

optical phonons. Due to the hexagonal symmetry, two sets of the phonon parameters $\omega_{n(m),0}$

$S_{n(m)}$, and $\gamma_{n(m)}$ are, of course, different for $\varepsilon_{\parallel}(\omega)$ and $\varepsilon_{\perp}(\omega)$. To describe the optical

Table 5.2. TO Phonon Frequencies with the E_1 Symmetry Polarized in the *ab*-plane for h-RMnO$_3$ in cm^{-1}, T=7 K. Strong and Weak Modes Are Marked with Small and Capital Letters, Respectively. Frequencies of the Magnetic Excitation and Crystal Field (CF) Transition are Listed at the Bottom

Number m	Letter symbol	HoMnO$_3$	ErMnO$_3$	TmMnO$_3$	YbMnO$_3$	LuMnO$_3$
1	a	---	147.9	146.0	147.4	147.1
2	b	151.5	154	---	155.3	155.5
3	C	165.5	164.6	163.7	163.5	162.1
4	d	---	184.5	179.8	181.4	182.4
5	E	245	254.5	257.5	265.4	270.5
6	f	266.5	270.5	---	267.5	273.5
7	G	292.5	294.6	295	297.2	303.3
8	h	308	311	301	305.5	313
9	I	368	371	372	383.5	368
10	j	---	408	---	---	415
11	K	420	421	422	---	428
12	l	---	522	526	526	528
13	m	591	594	---	---	600
Mag				180	190	191
				193		210
CF			366			

phonon spectra, we used N=6 for phonons polarized along the *c*-axis and M=13 for phonons polarized in the $a-b$ plane. A home-made program based on the 4×4 Berreman's model for anisotropic magneto-electric medium was used for all fits presented in this paper [117] The results of the fit are shown in Figure 5.4 (a,b) with red curves. The discrepancy between the fit and experimental data for the low-frequency part of $\langle \varepsilon_2(\omega) \rangle$ for $\omega < 100$ cm^{-1} is due to a systematic error of RAE. This error is caused by a well-known limitation of the RAE technique in the transparency region, where the phase of the reflected light changes upon reflection by the angle of ~ 180°, thus making RAE insensitive to the optical losses. In fact, $\langle \varepsilon_2(\omega) \rangle$ should be close to zero in this spectral range, as it appears in the model for the fit and as we also confirmed with our transmission measurements of the same

samples in reference[102]. The experimental values for the optical phonon parameters for all measured hexagonal manganites at $T= 7$ K are summarized in Table 5.2. Strong phonons are labeled with capital letters C, E, …, while weak phonons are differentiated from them by using small letters a, b, d,… in the alphabetic order for their frequency increase. The polarization of the phonon along or perpendicular to the c-axis is marked with the corresponding symbol $\parallel$ or $\perp$.

To obtain a better sensitivity to the optical phonons polarized along the c-axis of hexagonal compounds, we measured a bulk HoMnO$_3$ sample with the c-axis in the reflection plane ($c \parallel x$). We also utilized the MME technique, which is free from the aforementioned systematic errors of RAE for transparent samples. Another advantage of MME is the capability to measure several independent Mueller matrix components $m_{ij}(\omega)$
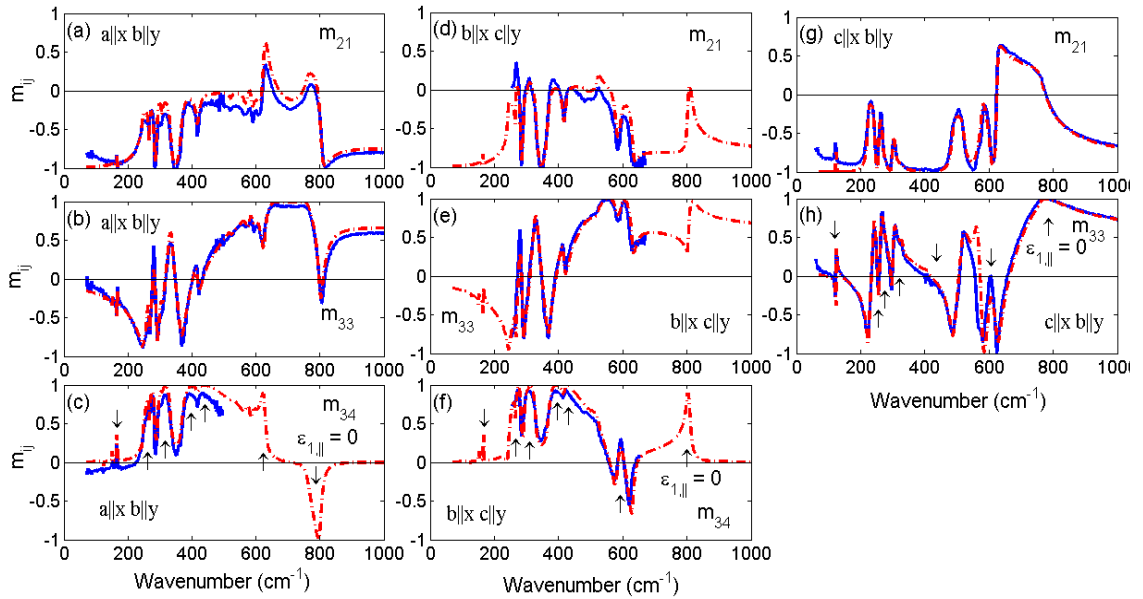
Figure. 5.5 Spectra of the normalized Mueller matrix components $m_{12}(\omega)$, $m_{33}(\omega)$, and $m_{34}(\omega)$ (blue curves) for the same HoMnO$_3$ sample at $T=7$ K in three experimental configurations (a,b,c) $c \parallel z$, (d,e,f) $c \parallel y$, and (g,h) $c \parallel x$. The results of the fit are shown with dashed red curves.

that are more reliable in the case of strong sample anisotropy. Spectra of $m_{12}(\omega)$, $m_{33}(\omega)$

$m_{34}(\omega)$, and $c \parallel z$ for the HoMnO$_3$ sample in all three possible configurations: $c \parallel x$, $c \parallel x$

and $c \parallel z$ are shown in Figure 5.5. Experimental data for all three configurations were fitted

using the same self-consistent anisotropic model for the phonon parameters $\omega_{n(m),0}$

$S_{n(m)}$, and $\gamma_{n(m)}$. The results of the fit for both components of the anisotropic

dielectric function, $\varepsilon_{\perp}(\omega)$ and $\varepsilon_{\parallel}(\omega)$, are shown in Figure 5.6 (a,b).
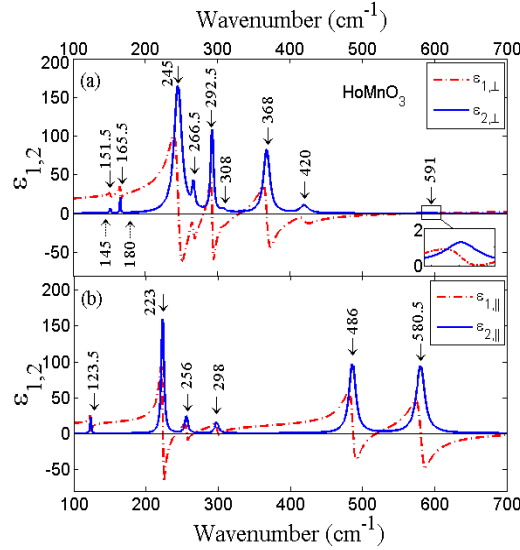
Figure. 5.6 Anisotropic dielectric function model for HoMnO$_3$ sample at T=7 K. (a) $\varepsilon_{\perp}(\omega)$ and (b) $\varepsilon_{\parallel}(\omega)$. Real part is shown with red and imaginary parts are shown with blue curves. The strongest optical phonons are marked with arrows.

Several low-frequency modes polarized in the *a-b* plane at about 145, 155, and 185 cm^{-1} were not clearly resolved, especially at high temperatures above 200 K. The corresponding peaks shown in Figure 5.7 (a) for YbMnO$_3$ have an electric dipole shape, as expected for phonons, but their strength decreased significantly in the paramagnetic phase for $T>T_N$, thus opening a room for other interpretations, such as modes of magnetic origin or crystal field transitions. To clarify the situation, we used a complementary transmission technique that for the given sample thickness turns out to be more sensitive to the weak

excitations. The corresponding spectra are shown in Figure 5.7(b) for YbMnO$_3$. The absorption peaks appeared in the transmission spectra at the same frequencies as in the ellipsometry spectra. And these peaks were observed in the temperature range much higher than the AFM-paramagnetic phase transition T_N=84 K for YbMnO$_3$. Figure 5.7(c) and Figure 5.8 (a,b) show a number of transmission maps for YbMnO$_3$, LuMnO$_3$, and TmMnO$_3$ in the frequency-temperature space, where the most of the weak phonon peaks at 145, 155, and 185 cm^{-1} are clearly visible up to ~200 K, that unambiguously confirms their phonon origin. An additional confirmation that those peaks are not R^{3+} crystal field transitions came from the measurements of LuMnO$_3$, where the 4f-shell of R^{3+} is complete and no crystal field transitions are expected (see Figure 5.8 (a)). Thus, observation of the low-frequency modes, such as the ones at 144, 155, 165, and 180 cm^{-1} can be significantly improved in transmission configuration when the thickness of the sample can compensate for the weak absorption by the modes. Note that this approach works well only if the sample is nearly transparent in the frequency range of interest. In other words, the background values of the dielectric function should be $\varepsilon_1(\omega) \gg 1$ and $\varepsilon_2(\omega) \approx 0$. These conditions have been naturally realized in the low-frequency range of h-RMnO$_3$ below the strong phonon absorption.
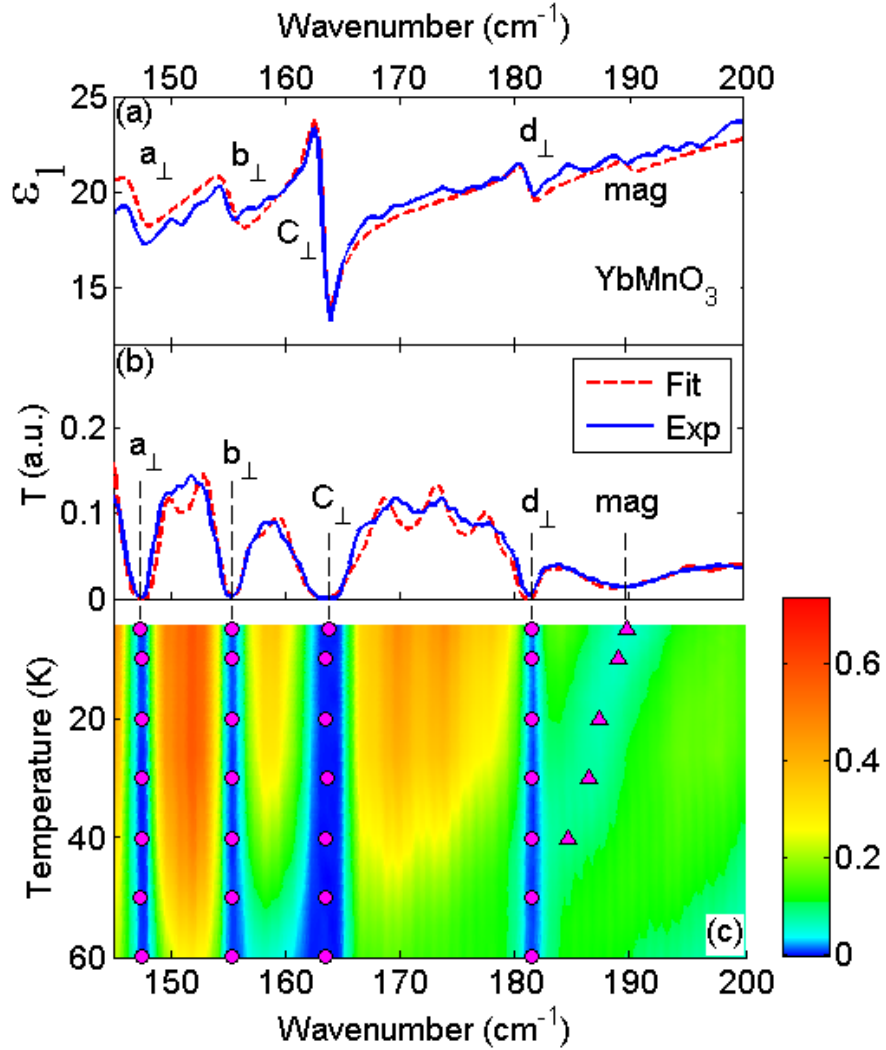
Figure. 5.7 (a) Experimental RAE data (blue curve) for the real part of the pseudo dielectric function $\langle \varepsilon_1(\omega) \rangle$ measured at T=7 K for YbMnO₃. The phonon peaks are marked with arrows. The fit results are shown with red curve. (b) Transmittivity spectra for the same YbMnO₃ sample for at T=7 K. (c) Transmittivity $\omega - T$ map for the same YbMnO₃ sample. The results of the fit for the phonon frequency are shown with circles. The magnetic mode at 190 cm^{-1} that is visible only at T < 50 K is marked with triangles.
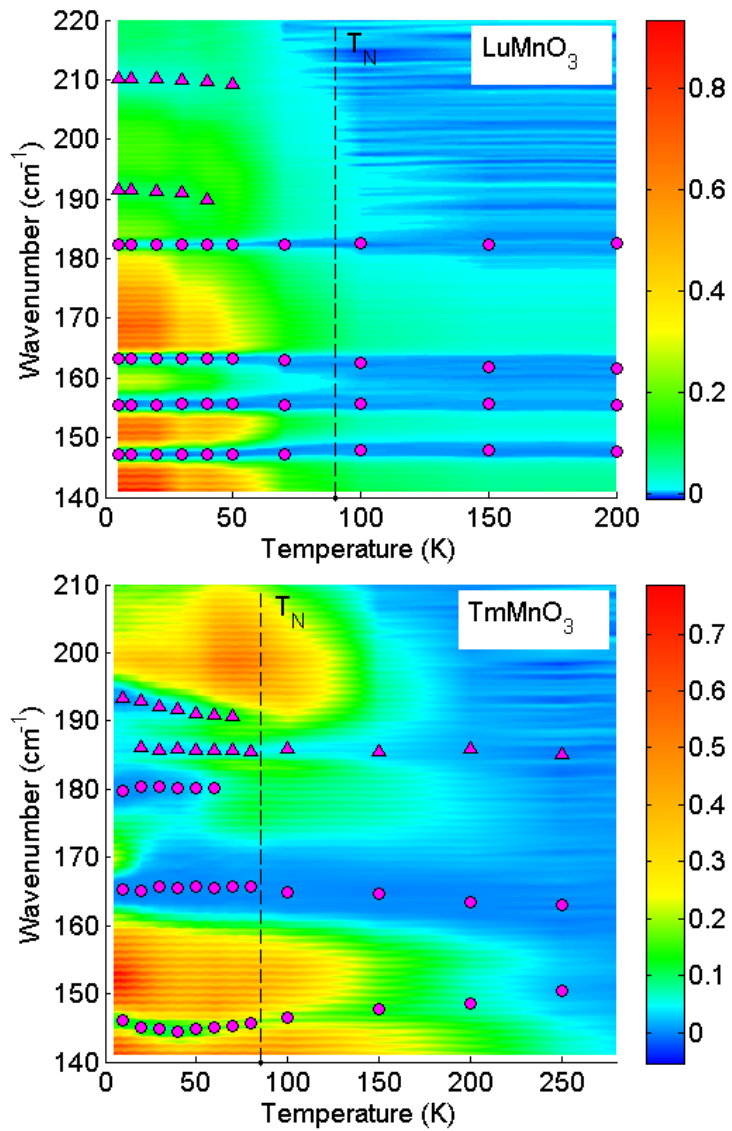
Figure. 5.8 Transmittivity $\omega-T$ maps for the LuMnO₃ (a) and TmMnO₃ (b). The results of the fit for the phonon frequency are shown with circles. Note that the weak optical phonons at ~148, 154, and 185 cm^{-1} are visible in the temperature range well above $T_N =$ 84 K shown with dashed vertical line.
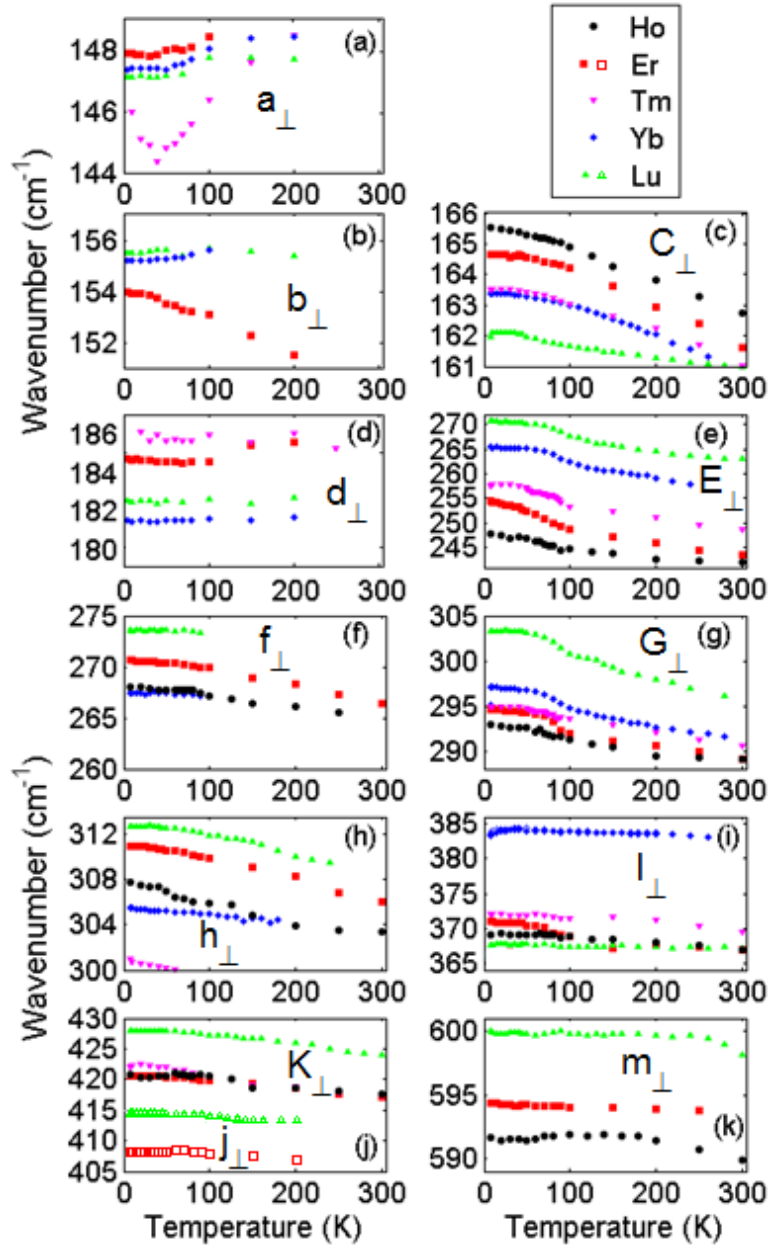
Figure 5.9 Temperature dependence of the frequency for the optical phonons polarized in the *a-b* plane for *R*MnO₃, *R*=Ho (black circles), Er (red squares, Tm (pink down triangles), Yb (blue diamonds, and Lu (green up triangles). Weak phonon modes are shown with open symbols; strong modes are shown with solid symbols. Letters correspond to the phonon notation in Table I.

5.3.8 Temperature Dependence of the Phonon Frequencies

Temperature dependencies of all optical phonon frequencies is shown in Figure 5.9 (a-k) for the phonons polarized in the $a-b$ plane. Data for all five measured hexagonal compounds with R=Ho, Er, Tm, Yb, and Lu are presented together for comparison. Each panel of Figure 5.9 corresponds to the same mode of the hexagonal structure. As one can see in both Figure 5.9 (c,d) and Table 5.2, several strong low-frequency phonons reveal systematic trend of their frequencies. Thus, the strong $C_\perp$ mode at ~163 cm^{-1}, which is predominantly determined by displacements of the heavy R^{3+} ions reveals a systematic decrease of the frequency for R^{3+} ions between Ho^{3+} and Lu^{3+}. (see Figure 5.9 (c)). This "classical" trend is illustrated in Figure 5.10 using a linear fit between the square root of the inverted mass $M_{R^{3+}}$ of the R^{3+} ions and the phonon frequency. Another two strong $E_\perp$ and $G_\perp$ phonons at 260 and 300 cm^{-1} also show a systematic variation of their frequency, but with an opposite trend (see Figure 5.11 (a,b)). A well-known decrease of the ionic
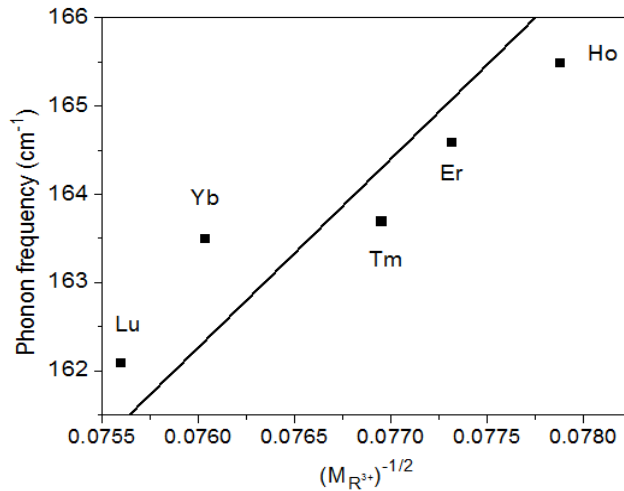
Figure 5.10 A quasi-linear increase of the optical phonon frequency for RMnO$_3$ compounds. Experimental data points were measured at T= 7 K. The solid line is a linear fit using $\omega_0 = c / \sqrt{M_{R^{3+}}}$.

radius for R^{3+} ions between Ho^{3+} and Lu^{3+} in the RMnO$_3$ compounds seems to be a dominant factor for the qualitative explanation of the systematic changes of these two mid-frequency phonons. The high-frequency (>350 cm^{-1}) phonons, which are associated with vibrations of the lighter ions (oxygen and manganese), are less sensitive to the properties of the R^{3+} ions and their frequencies vary rather randomly between different RMnO$_3$ compounds.

Most of the phonons have weak frequency dependence at $T < 95$ K and a typical decrease of their frequency with the quasi-linear slope for $T > 120$ K. This natural softening of the optical modes with the temperature increase is known to be caused by the thermal expansion of the lattice and anharmonic phonon–phonon interactions, which become more important as the temperature increases due to the statistical increase of the number phonons. We calculated the temperature dependence of several phonons using the following equation [118]

$$\omega_0(T) = \omega_{0|T=0} \times \exp\left[-3\gamma_G \int_0^T \alpha(T')dT' \right],$$

(5.4)

where γ_G is a Grüneisen parameter, $\alpha(T)$ is the linear expansion coefficient obtained from reference [92], and $\omega_{0|T=0}$ is the phonon frequency at zero temperature. The results of the calculation using $\gamma_G = 0.7 \pm 0.2$ are shown in Figure 5.11 (a,b) with solid curves. While most of the phonons can be well described by Equation (5.4) for their $\omega_0(T)$ in the whole temperature range between 7 and 300 K, several phonons show strong anomalies at T_N for AFM ordering of Mn^{3+} spins. The corresponding dependencies are shown in Figure 5.11

(a,b) for the $E_\perp$ and $G_\perp$ modes at ~260 and ~300 cm^{-1}. Below T_N their frequencies

increase by $\Delta\omega(T)$, which is equal to several wavenumbers (3 cm^{-1} for the phonon at 300
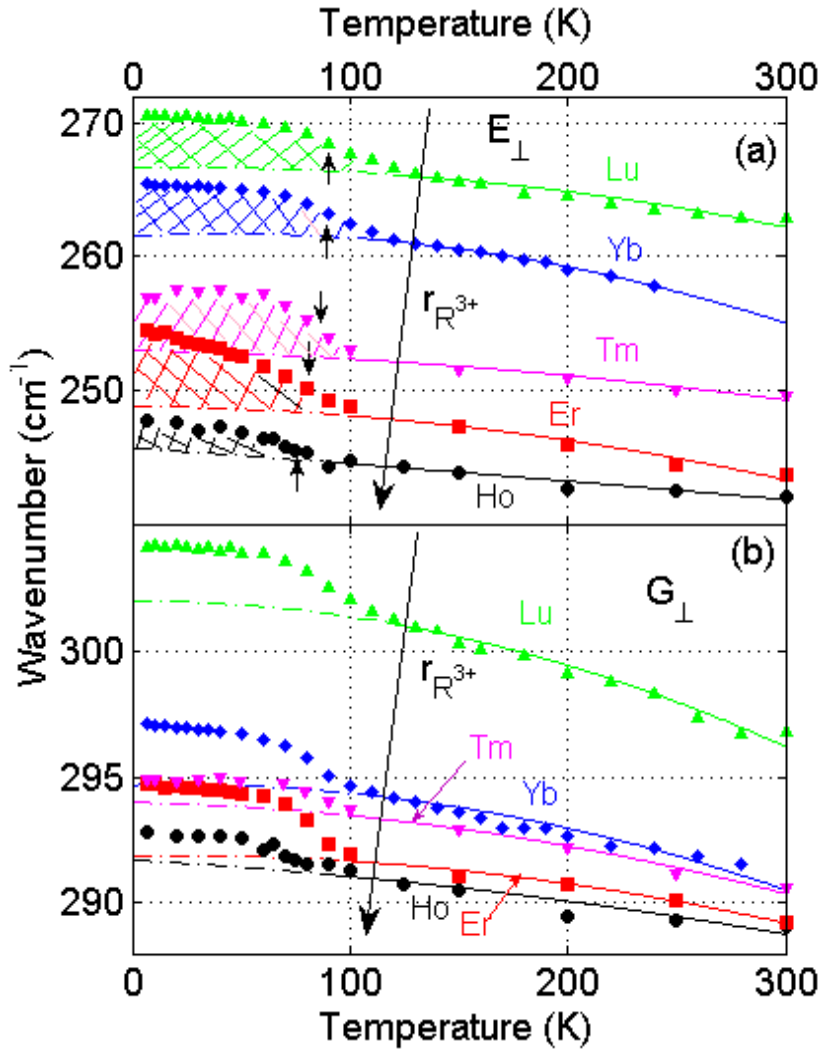
Figure 5.11 Temperature dependence of the frequency for two *ab*-plane E$_1$-symmetry optical phonons with the strongest spin-phonon interaction for RMnO$_3$, R=Ho (black circles), Er (red squares, Tm (pink down triangles), Yb (blue diamonds, and Lu (green up triangles). (a) $E_\perp$ and (b) $G_\perp$ phonons. The AFM ordering temperature for Mn^{3+} spins is shown in (b) with small vertical arrows. The long arrows in both (a) and (b) show schematically an increase of the R^{3+} ionic radius r_{R3+} from Lu to Ho. Solid curves are fits using Equation (5.4) for the high-temperature part of the $\omega_0(T)$ dependence. Dashed curves correspond to extrapolation of Equation (5.4) to low temperatures. The discrepancy between experimental data points and dashed curves is due to spin-phonon interaction.

cm^{-1} and 5 cm^{-1} for the phonon at 260 cm^{-1}) above the level predicted by the Grüneisen

formula. This difference is highlighted by the dashed regions in Figure 5.11 (a,b). This

non-Grüneisen behavior can be attributed to the strong spin-phonon interaction that

emerged in the low temperature AFM phase. It is natural that this effect is expected to be

the most pronounced for those phonon modes, where atomic displacements effectively

modulate Mn-Mn exchange interaction (see, e.g. Reference [119] and references therein).
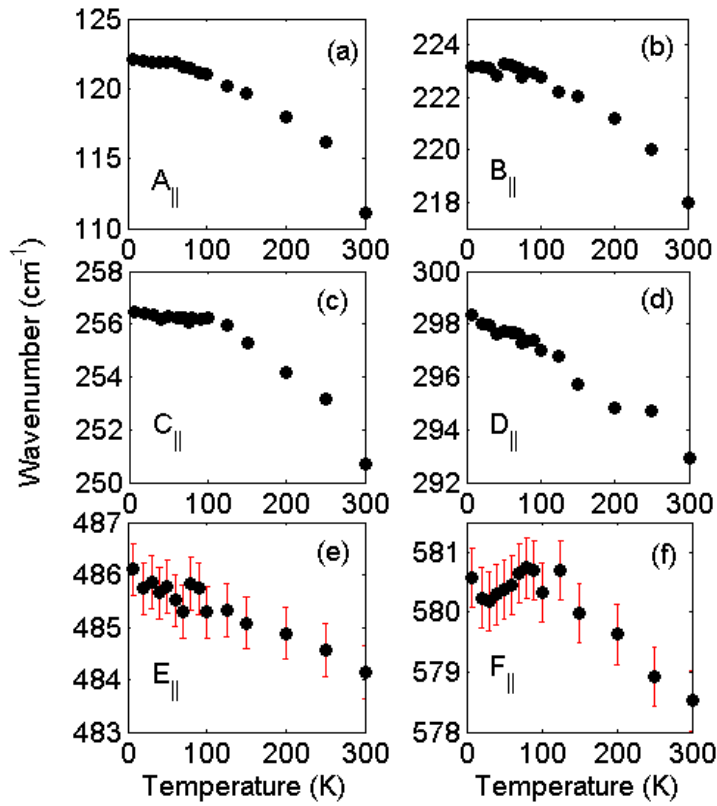
Figure 5.12 Temperature dependence of the frequency for the *c*-axil polarized optical phonons in HoMnO$_3$. The error bars in (e) and (f) show the fit accuracy for relatively broad high-frequency modes. The low-frequency phonons are much sharper and, hence, the accuracy of the fit is comparable with the symbol size that is about 0.3 cm^{-1}. The anomaly in the temperature dependence for $F_{||}$ mode in (f) is close to the AFM ordering temperature for Mn^{3+} spins T_N=75 K.

The weakest effect in terms of the $\Delta\omega(T)$ values at low temperature has been observed in HoMnO$_3$ $\Delta\omega(7K) \approx 1.5$ cm^{-1}, while in other compounds with R=Er, Tm, Yb, and Lu $\Delta\omega(7K)$ turns out to be close to 5 cm^{-1} for the mode at 300 cm^{-1}. Similar trends for the temperature dependence of the phonon frequencies at ~260 and ~300 cm^{-1} have been previously observed in the Raman spectra and reflectivity experiments in References [72,75].

Temperature dependence of the optical phonons in HoMnO$_3$ polarized along c-axis is shown in Figure 5.12. The total number of the measured modes is 6 that is less than that for the a-b plane phonons. Our measurement did not reveal any significant spin-phonon interaction anomalies for this phonon polarization except a small decrease of the $F_{\parallel}$ mode frequency for temperatures below $T_N = 75$ K for Mn^{3+} spins. This decrease of ~ 1 cm^{-1} exceeds slightly the error bars for the measured phonon frequencies.

5.3.9 Transmission Spectra in Magnetic Field

Transmittivity $\omega - H$ maps measured in YbMnO$_3$ at T= 1.5 and 5 K are shown in Figure 13 (a,b). The position of the phonon peaks at 144, 155, 165, and 180 cm^{-1} does not show any measurable changes with the strong magnetic field directed along the c-axis. In addition to the phonons, one can see a broader peak at 190 cm^{-1}. This peak is only observed for temperatures below T_N=84 K (see Figure 5.13 (c)). Note that the broadening of the magnetic peaks exceeds significantly that of the phonons in the same frequency range. The magnetic-field induced softening measured at T=5 K indicates a magnetic origin of these excitations. In addition to YbMnO$_3$, a similar broad peak at 190 cm^{-1} were also observed in TmMnO$_3$ and LuMnO$_3$ indicating Mn^{3+} spin system to be the origin of this particular

excitation and excluding crystal field transition-related interpretation. The peak frequencies are summarized in Table 5.1. The commonly accepted model for a 120° spin structure for Mn^{3+} ions in h-RMnO$_3$ does not include any single-particle excitations at the center of the Brillouin zone $\vec{k} = 0$ and polarized in the *a-b* plane other than the doubly-degenerate AFM resonance peak, which frequency is between 40 and 50 cm^{-1} depending on the R^{3+} ion [120]. This prediction has been confirmed by both IR transmission [102] and
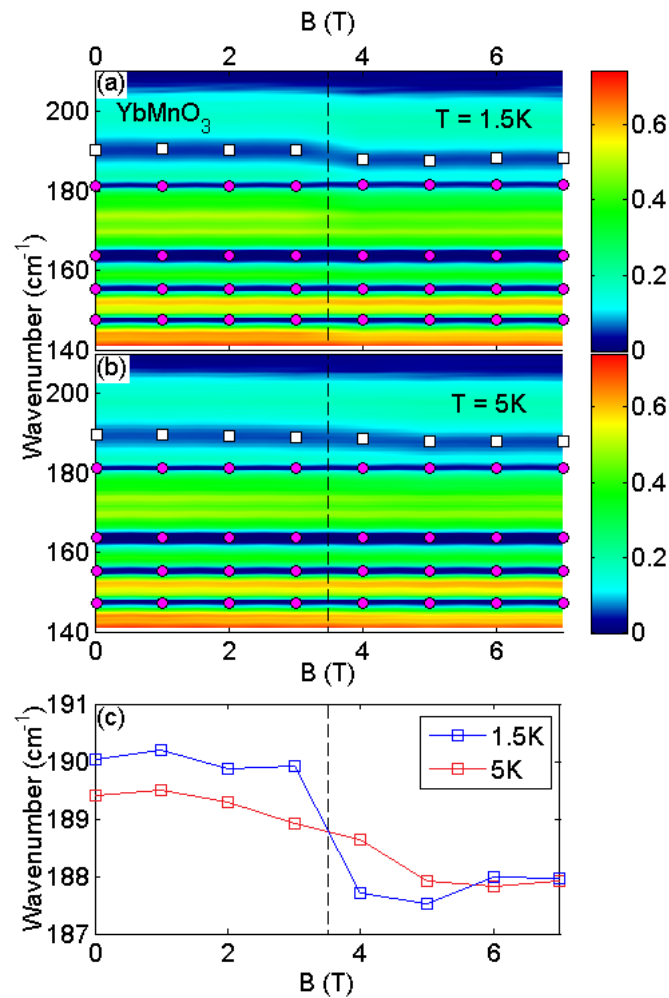
Figure 5.13 Magnetic field dependence of the transmittivity $\omega - H$ map measured in YbMnO$_3$. (a) T= 5 K and (b) T=1.5 K. The optical phonon peaks are marked with diamonds. The magnetic peaks at ∼ 190 cm^{-1} are marked with open squares.

recent neutron scattering experiments [121]. Thus, the most plausible interpretation of the observed magnetic peak at 190 cm^{-1} is related to two-magnon absorption. According to Reference [122] the maximum of the two-magnon density of states in h-RMnO$_3$ is close to 200 cm^{-1}, which is consistent with the observed position of our peak at 190 cm^{-1}.

For the temperature below the rare-earth spin ordering T_{Yb3+} = 3.3 K, [102] the magnetic field dependence of the peak at 190 cm^{-1} changes. One can see a step-like behavior at the field of about 3.5 T in Figure 5.13 (c). The position of this peak decreases by about 2 cm^{-1} when the magnetic field exceeds ~3.5 T. A qualitatively similar, i.e. step-like, behavior we observed recently for the AFM resonance peak at 53 cm^{-1} in the same YbMnO$_3$ crystal measured for T< T_{Yb3+} [102]. Several papers report critical endpoint behavior of magnetic spin system in h-RMnO$_3$ at magnetic fields close to 3 T and temperatures below the spin orientation for R^{3+} ions T< T_{R3+} [122]. In a simplified quantitative picture such steps in magnetic-field dependencies are usually attributed to the internal fields associated with orientation of Yb^{3+} spins to the direction of magnetic field (the c-axis) and simultaneous in-plane reorientation of Mn^{3+} spins.

In TmMnO$_3$ the magnetic peak has been observed at 193 cm^{-1}. The frequency of this peak softens under increase of both, the magnetic field and temperature. This peak disappears above T_N =82 K for Mn^{3+} ions. The softening of the magnetic peak under application of external magnetic field results in its down-shift to ~190 cm^{-1} and disappearance in the fields above 4 T. No step-like behavior was observed at low temperatures down to 1.5 K, probably due to even lower T_{Tm3+} temperature.

5.3.10 Transmission Spectra and Multi-phonon Absorption

For the high-frequency range, the transmission configuration is not that useful as it appears for the spectra below 200 cm^{-1}. For example, all phonons, which are above 400 cm^{-1} and are polarized in the *a-b* plane, fall into the bremsstrahlung band $370 - 580$ cm^{-1} with $\varepsilon_1(\omega) \ll 0$. As a result, reflectivity of the sample is close to 1 in that frequency range and the remaining transmitted intensity is close to zero regardless of the sample thickness. Nevertheless, the phonons that are close to 420, 530, and 590 cm^{-1} have been confirmed in
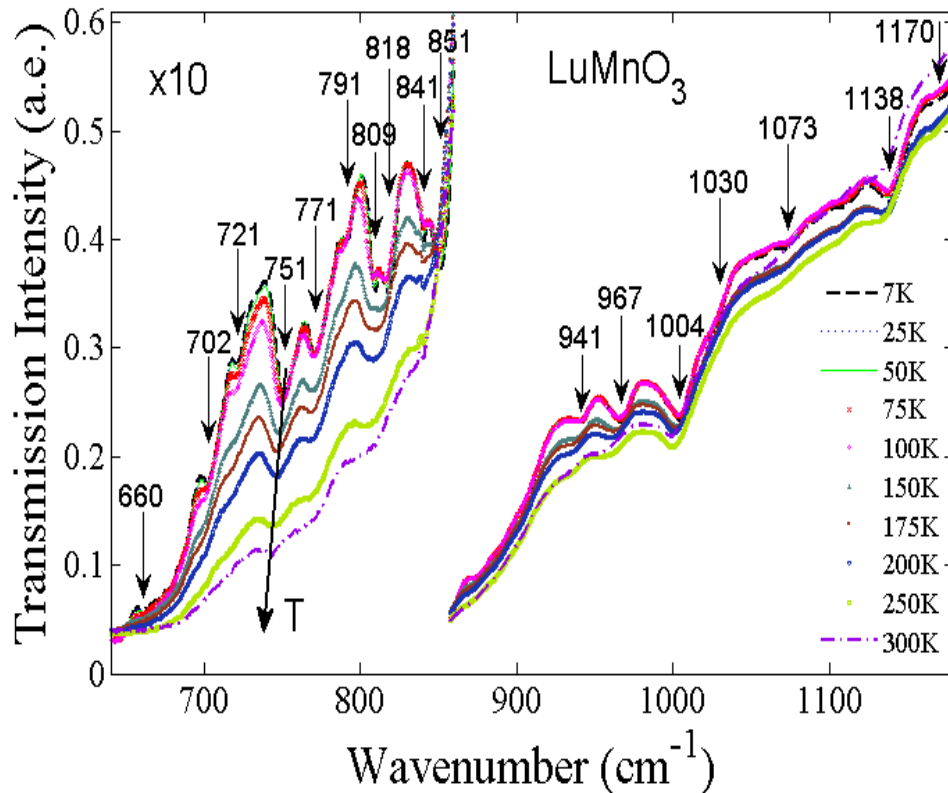
Figure 5.14 Transmittivity spectra dominated by absorption peaks due to the two- and three-phonon density of states. The minimum of transmitted intensity below 650 cm^{-1} is due to the bremsstrahlung band. The phonon-related absorption features are marked with vertical arrows. Note the broadening and the softening of the phonon absorption features with the temperature increase.

the transmission experiments, but the accuracy of our ellipsometry data for these weak modes is superior compared to the transmission approach.

Above the spectral region dominated by the first-order phonon excitations (< 600 cm^{-1}), transmission spectra demonstrated a number of peaks that can be attributed to two-phonon and three-phonon absorption. Figure 5.14 shown transmission spectra obtained at different temperatures in LuMnO$_3$. While other compounds show similar spectra, LuMnO$_3$ has been chosen for illustration due to the absence of the $4f$ $^{3+}$ transitions in R^{3+} ions. A number of absorption peaks between 650 and 850 correspond to the phonon density of states for two-phonon excitations, while the weaker absorption peaks in the range between 900 and 1150 are due to three-phonon absorption. The two-phonon frequencies at $T = 7$ K are the following: 660, 702, 721, 751, 771, 791, 809, 818, 841, and 851 cm^{-1}. The three-phonon peaks are 941, 967, 1004, 1030, 1073, 1138 cm^{-1}. Note that the peaks are much sharper at low temperatures and their frequency decrease for the temperature increase. This trend is expected for the phonon-related absorption and is also illustrated in Figure 5.14 for the peak at 751 cm^{-1}.

Table 5.3 Calculated and Experimental Parameters of TO Phonons with the E_1 Symmetry for h-HoMnO$_3$ Polarized in the *ab*-plane for T=7 K

Number m	Calculation $\omega_{0,m}$	S_m	Letter symbol	Experiment $\omega_{0,m}$	γ_m	S_m
1	125	0.1	a	–	–	–
2	166	0.001	b	151.5	1.6	0.07
3	196	0.001	C	165.5	1.0	0.12
			d	–		
4	276	0.01	E	245	12.0	8.0
			f	266.5	4.1	0.4
5	286	0.14	G	292.5	4.1	1.5
			h	308	7.1	0.08
6	370	2.89	I	368	10.1	2.2
7	398	0.02	j	–	–	–
8	415	0.04				
9	429	0.18	K	420	13.7	0.3
10	561	0.35	l	–	–	–
11	570	1.55				
12	571	0.001	m	591	14.8	0.03
13	609	0.001				
14	667	0.02				

$$\varepsilon_{\infty,\perp} = 4.75$$

Table 5.4 Calculated and Experimental Parameters of TO Phonons with the A_1 Symmetry for h-HoMnO$_3$ Polarized along the *c*-axis for T=7 K

Number	Calculation $\omega_{0,n}$	S_n	Letter symbol	Experiment $\omega_{0,n}$	γ_n	S_n
1	102	0.08	A	123.5	1.4	0.26
2	199	1.33	B	223.0	4.0	2.8
3	235	0.34	C	256.0	4.9	0.4
4	361	0.045	D	298.1	5.8	0.3
5	393	0.018				
6	427	0.066				
7	486	0.133	E	486.1	10.7	2.1
8	620	0.001				
9	654	3.25	F	580.5	13.5	2.2

$$\varepsilon_{\infty,\parallel} = 4.88$$

Table 5.5 Calculated Frequencies and Oscillator Strengths for TO Phonons with the E_1 Symmetry

Number	HoMnO$_3$ $\omega_{0,m}$	S_m	ErMnO$_3$ $\omega_{0,m}$	S_m	YbMnO$_3$ $\omega_{0,m}$	S_m
1	125	0.1	121	0.102	117	0.112
2	166	0.001	167	0.001	166	0.0001
3	196	0.001	198	0.001	197	0.001
4	276	0.01	277	0.001	277	0.001
5	286	0.14	288	0.14	288	0.134
6	370	2.89	377	2.78	382	2.7
7	398	0.02	400	0.001	407	0.046
8	415	0.04	423	0.033	429	0.031
9	429	0.18	435	0.223	441	0.26
10	561	0.35	579	0.61	590	0.81
11	570	1.55	589	1.3	600	1.14
12	571	0.001	581	0.013	601	0.001
13	609	0.001	617	0.001	623	0.0014
14	667	0.02	673	0.001	683	0.001

Table 5.6 Calculated Frequencies and Oscillator Strengths for TO Phonons with the A_1 Symmetry Transition

Number	HoMnO$_3$ $\omega_{0,n}$	S_n	ErMnO$_3$ $\omega_{0,n}$	S_n	YbMnO$_3$ $\omega_{0,n}$	S_n
1	102	0.081	107	0.08	109	0.08
2	199	1.33	205	1.25	208	1.2
3	235	0.34	245	0.45	250	0.48
4	361	0.045	363	0.046	364	0.046
5	393	0.018	397	0.008	400	0.004
6	427	0.066	434	0.063	438	0.063
7	486	0.133	490	0.148	493	0.146
8	620	0.001	625	0.001	629	0.0002
9	654	3.25	661	3.24	671	3.24

5.3.11 Discussion and Conclusion

First, we have to mention that only 6 out of expected 9 c-axis polarized phonons and 13 out of 14 phonons polarized in the a-b plane, are observed experimentally. This fact could be understood from the analysis of vibration–induced dipole momenta: for both A_1 and E_1 symmetries there are several modes whose oscillator strength $S_{n(m)}$ is expected to be rather small (less than 0.05, see Tables 5.5 and 5.6). Such weak oscillator strength, especially if combined with a significant broadening $\gamma_{n(m)}$ of more than 5 cm^{-1}, can indeed result in an experimental situation in which the mode falls below the observation limit, especially if it occurs in proximity with other strong phonons of the same polarization. Further, there is a reasonable agreement between the experimental and calculated mode frequencies, as shown in Tables 5.3 and 5.4 for HoMnO$_3$. For example, the model reproduces qualitatively the general trend of phonon frequency change upon variation of R^{3+}-ion (Tables 5.5 and 5.6). As far as calculated oscillator strengths are concerned, the agreement with experiment deteriorates, which could point towards deficiency of a simplified shell model. These facts confirm the importance of a proper accounting for a balance between electronic, magnetic, and lattice degrees of freedom and highlight the importance of systematic experimental information on optical properties and vibrational spectra of this class of materials.

In conclusion of this chapter, we have measured the optical phonons in five h-RMnO$_3$ compounds. The majority of the optical phonons have been identified for the a-b plane. Six strongest phonons that are polarized along the c-axis have been observed in HoMnO$_3$. The lowest frequency phonons with the E_1 symmetry show a systematic variation with the mass of the corresponding R^{3+} ions. Two of the mid-frequency phonons with the E_1 symmetry also show a systematic variation, which is determined by the systematic

change of the R^{3+} ionic radius. The spin-phonon interaction has been observed in all h-RMnO$_3$ compounds in a form of the frequency increase for the phonons associated with displacement of the Mn^{3+} ions. The weakest effect was observed in HoMnO$_3$, while other four h-RMnO$_3$ compounds have more pronounced spin-phonon interaction effects. The Grüneisen parameter $\gamma_G = 0.7 \pm 0.2$ has been determined for the strong phonons with the E_1 symmetry in all measured h-RMnO$_3$ compounds. Magnetic excitations at ~ 190 cm^{-1} have been found in three of the h-RMnO$_3$ compounds at the temperature range below the AFM phase. These excitations have been explained as due to the two-magnon density of states. A possible relationship of this magnetic excitation to the crystal field transitions has been ruled out by both the close proximity of the frequencies in three h-RMnO$_3$ compounds and by observation of such excitation in LuMnO$_3$ where the $4f$ shell of the R^{3+} ion is fully occupied. The experimental and theoretical data presented here will be useful for future studies of the phonon spectra in a broad class of hexagonal magnetic compounds, and in new materials, such as h-InMnO$_3$ in particular.

CHAPTER 6

MMFIT FITTING PROGRAM MANUAL

In this chapter, description of the developed MMFit program is given. There are three version of this software. One is for arbitrary bulk materials, second is for thin film layer on an anisotropic substrate, third is for a double layer superlattice on an anisotropic substrate. Both thin film layers and bulk layer can contain any combinations of electric, magnetic, magneto-electric and chiral oscillations. SHO model and Berreman formalism were utilized to get representation of pseudo-dielectric $<\varepsilon>$ function, ellipsometric Ψ, Δ, reflectance, transmittance and Mueller matrices. Maximum number of oscillators in this version is 36 which can be increased if needed. Levenberg-Marquardt algorithm was used for fitting, where number of iterations changing is available for user.
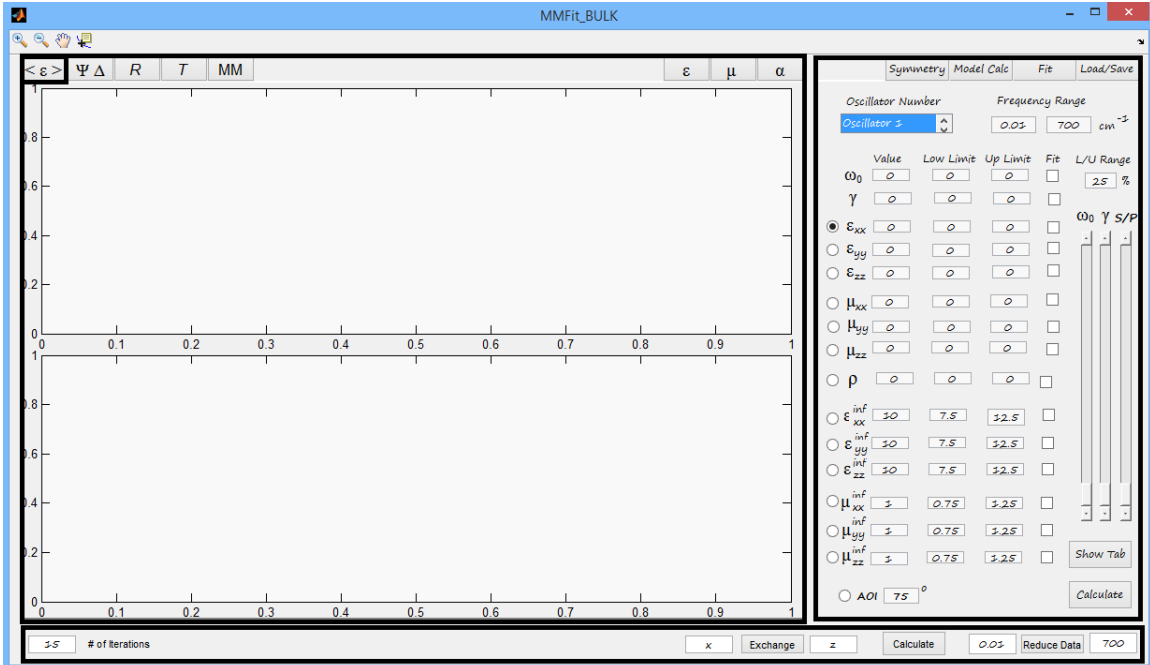
Figure 6.1 Start window of MMFit program. By default data panel (left) is for pseudo-dielectric function and model panel (right) is for model creation ("Model Calc").

Program consists of three main panels. Left one, consisting of eight subpanels, is for data and models representation, right one, consisting from four to five subpanels in different versions, is for loading, saving data and models, adjusting fitting parameters, creation of models, choosing tensor symmetry. Low panel allows to adjust data (reduce to desirable range), choose number of iterations for fitting, calculate current model and exchange columns in current model (analog to Euler rotation by 90 degrees in any direction).

6.1 Working with Data

In order to load or save data and models, one should click on "Load/Save" button in right panel.
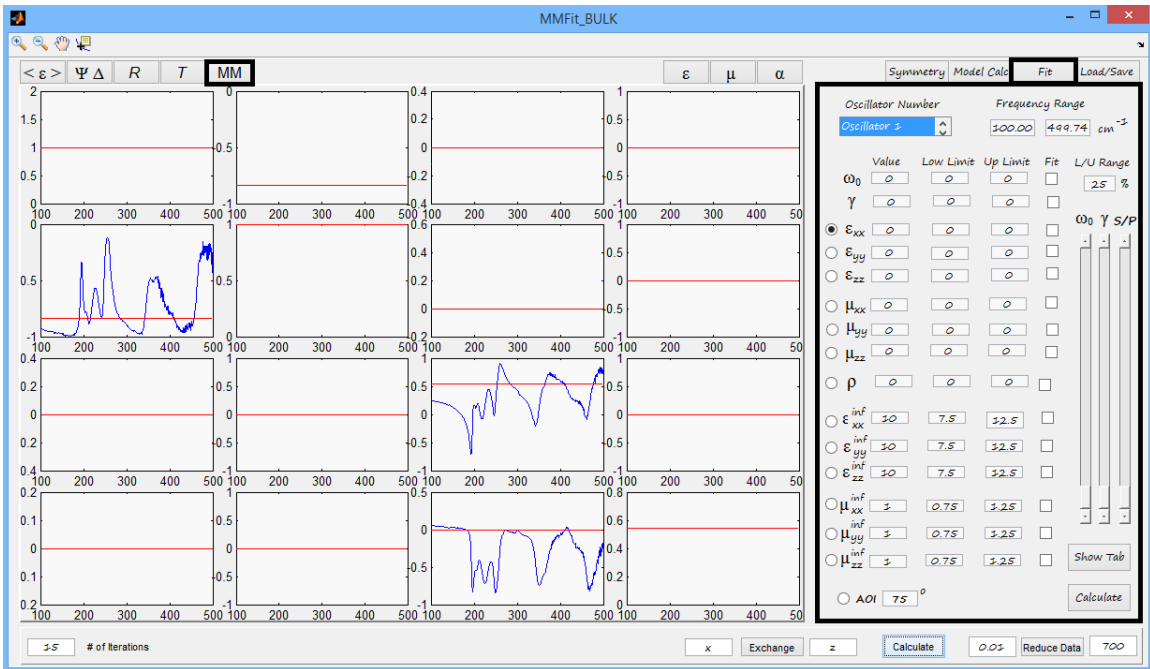
Figure 6.2 Load/Save panel in MMFit program after loading mmd format file and clicking on "MM Panel" button, containing three Mueller matrix components (m_{21}, m_{33}, m_{34}). Blue line – data. Red line – model.

There are 17 buttons on "Load/Save" panel. "Load *.mmd Data" allows user to load Mueller matrices data in mmd format. There are 16 non-normalized columns in mmd data file. MMFit normalize all MM components to the first MM component (first column).

```
* Start time : Wed 06/11/2014, 15:48:09
* Finish time : Wed 06/11/2014, 18:08:59
* OPUS data folder : \\Ellipse\Test data\2014 June\04 June TbFeO3
CxBy\opus
* The 1st OPUS data file : aaa.436
* The Last OPUS data file :  aaa.491
* OPUS XPM file : \\Ellipse\Test data\2014 June\GeMy_700_1cm_512
_x8_100kHz.XPM
* Schedule file : \\Ellipse\Test data\2014 June\09 June TbFeO3
BxCy AOI 70 80\TBFEO3 BXCY MUELLER T DEP.sch
* Operator : Taras and Andrei
* Comments : DyFeO3
theta       2.680e+01
2theta      060
chi   014
X     000
Y     9.400e+00
Z     -4.000e-01
SetT 7.500e+00
T1    7.436e+00
T2    7.357e+00
B     000
#Mueller:
0.00000E+00     0.001767   0.000839   -0.000481  -0.000141
        0.001092   0.000531   -0.000869  -0.000234  0.000026
        -0.000142  -0.001300  -0.000232  0.000113   0.000160
        0.000114   -0.000733
4.82116E-01     0.000859   0.000685   -0.000355  -0.000220
        0.000970   0.000312   -0.000749  -0.000272  -0.000112
        0.000138   -0.001097  0.000117   -0.000024  0.000147
        0.000192   -0.000831
9.64233E-01     0.000684   -0.000092  0.000110   -0.000114
        0.000329   -0.000090  0.000199   -0.000115  -0.000041
```

Figure 6.3 MMD data file structure.

"Load *.epd Data" button allows user to load data in epd format, containing real part of pseudo-dielectric function (column six), imaginary part of pseudo-dielectric function (column seven), Ψ function (column two) , Δ function (column three) . Mmd and epd data formats are shown in Figures 6.3,6.4 correspondingly.

```
   mAB2PD   2013-01-23 14:04:41   E:\EllipsometerData\January 2013
\01152013\SAMP TEST2 AOI 75 ALPHA2=(20 T=300+-20 T=300+25 T=300
+-25 T=300+30 T=300+-30 T=300+40 T=300+-40 T=300+45 T=300+-45 T=
300).big   "STO"
Phi=75.00deg   Po=(-2.83 ± 0.013)deg  Ao=(2.81 ± 0.02)deg
corr.coef.=-0.23   Pflip=30.00deg  E-calib(80, 650)1/cm
Comments:
wn[cm-1], Psi[deg]  , Delta[deg], dPsi[deg] ,dDelta[deg],
Epsilon1 ,  Epsilon2 , dEpsilon1 , dEpsilon2
70    12.110909 -0.51889921    12.110909 -0.51889921
      12.110909 -0.51889921
70.5 11.636195 -1.0725924 11.636195  -1.0725924 11.636195
      -1.0725924
71    12.684736 -2.1213488 12.684736  -2.1213488 12.684736
      -2.1213488
71.5 14.393121 -3.3437035 14.393121  -3.3437035 14.393121
      -3.3437035
72    15.600339 -4.2315141 15.600339  -4.2315141 15.600339
      -4.2315141
72.5 16.198761 -4.5870295 16.198761  -4.5870295 16.198761
      -4.5870295
73    16.713629 -4.4454636 16.713629  -4.4454636 16.713629
      -4.4454636
73.5 17.215107 -3.9070955 17.215107  -3.9070955 17.215107
      -3.9070955
74    17.574487 -3.2138467 17.574487  -3.2138467 17.574487
      -3.2138467
74.5 17.847448 -2.669105  17.847448  -2.669105   17.847448
      -2.669105
75    17.739289 -2.372324  17.739289  -2.372324   17.739289
      -2.372324
75.5 16.820506 -2.1473462 16.820506  -2.1473462 16.820506
      -2.1473462
```

Figure 6.4 EPD data file structure.

Following twelve buttons allow user to load separately pseudo-dielectric function data, Ψ function data, Δ function data, reflection data, transmission data. Data files must contain two columns only without any headers. First column should be frequency in inverse centimeters, second column is intensity data. If one loads pseudo-dielectric function data using "Load *.epd Data" and then load another pseudo-dielectric function data using "Load <Eps1> Data" and/or "Load <Eps2> Data", corresponding data will be rewritten to the newest one. This works for Ψ and Δ functions data as well.

"Reduce Data" button on the lower panel allows to cut data in the defined by user range". To restore original data, original data file should be loaded and reduced data will be rewritten to the new one.

"Load Project" button allows to load project previously saved by "Save Project" button. "Save Project" button gives overall saving option: all available data, models and parameters will be recorded.

"Save FitData" button saves all models and all data to separate files, consisting of two columns: first one is frequency, second one is intensity. If there were no loaded data previously, MMFit programs provides file with zero data. The same is valid for models. Total number of files saved after "Save FitData" button clicked is 25.

6.2 Working with Models

For creation and modifying model function user should click on "Model Calc" button in the right panel.
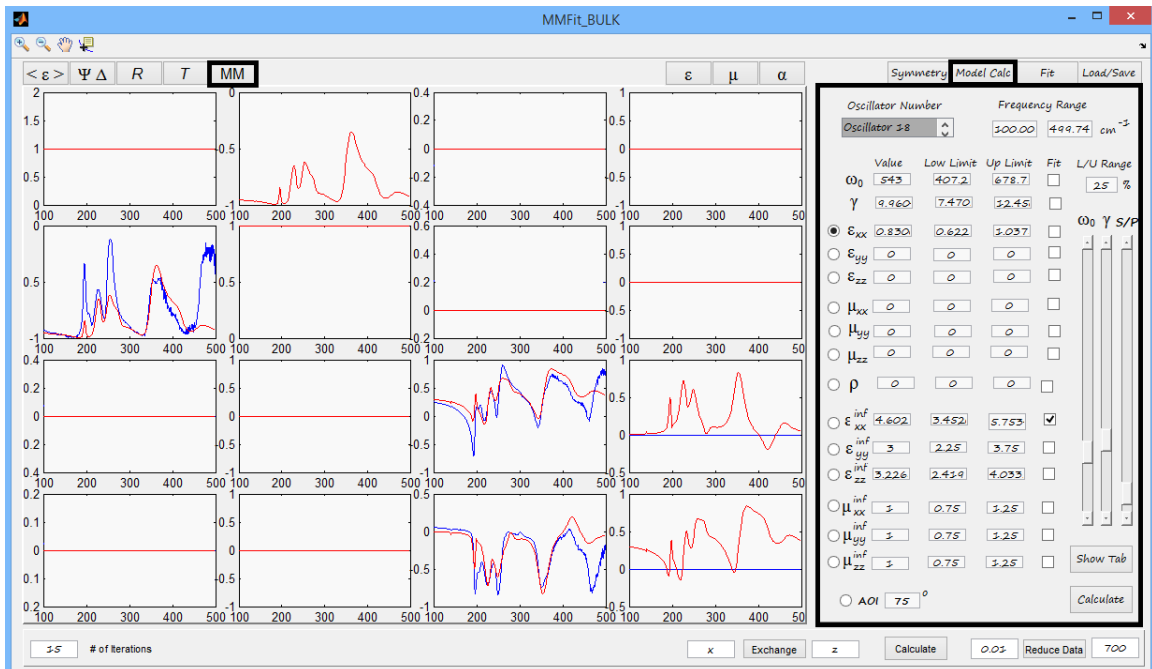
Figure 6.5 "Model Calc" panel with "MM" data panel after creating rough starting model for fitting. Blue line – data. Red line – model.

There are three sliders available for adjusting different values. First slider (from the left to the right) always changes oscillation frequency value. Second slider always changes Gamma (broadening coefficient) value. Third slider changes value chosen by radiobuttons. When one changes values with sliders current models are redrawn dynamically. Main purpose of this visualization is to find starting fitting point maximally close to the original data.

"Show Tab" button draws additional panel which gives overall picture of the

	Om...	L	U	F	Ga...	L	U	F	Sexx	L	U	F	Seyy	L	U	F	Sezz	L	U	F	Smxx	L	U	F	Smyy	L	U	F	Smzz
Osc1	175	131...	218...	☐	1.96...	1.47...	2.45...	☐	0	0	0	☐	0.01...	0.00...	0.01...	☐	0	0	0	☐	0	0	0	☐	0	0	0	☐	0
Osc2	262	196...	327...	☐	19.5...	14.6...	24.4...	☐	0	0	0	☐	0.07...	0.05...	0.09...	☐	0	0	0	☐	0	0	0	☐	0	0	0	☐	0
Osc3	140	105	175	☐	0.97...	0.72...	1.21...	☐	0	0	0	☐	0.04...	0.03...	0.05...	☐	0	0	0	☐	0	0	0	☐	0	0	0	☐	0
Osc4	241	180...	301...	☐	45.8...	34.3...	57.3...	☐	0	0	0	☐	1.03...	0.77...	1.29...	☐	0	0	0	☐	0	0	0	☐	0	0	0	☐	0
Osc5	343	257...	428...	☐	8.89...	6.67...	11.1...	☐	0	0	0	☐	0.00...	0.00...	0.00...	☐	0	0	0	☐	0	0	0	☐	0	0	0	☐	0
Osc6	481	360...	601...	☐	77	57.7...	96.2...	☐	0	0	0	☐	0.29...	0.22...	0.37...	☐	0	0	0	☐	0	0	0	☐	0	0	0	☐	0
Osc7	574	430...	717...	☐	5.98...	4.48...	7.47...	☐	0	0	0	☐	0.20...	0.15...	0.25...	☐	0	0	0	☐	0	0	0	☐	0	0	0	☐	0
Osc8	644	483	805	☑	7.17...	5.37...	8.96...	☐	0	0	0	☐	0	0	0	☐	0	0	0	☐	0	0	0	☐	0	0	0	☐	0
Osc9	0	0	0	☐	0	0	0	☐	0	0	0	☐	0	0	0	☐	0	0	0	☐	0	0	0	☐	0	0	0	☐	0
Osc10	0	0	0	☐	0	0	0	☐	0	0	0	☐	0	0	0	☐	0	0	0	☐	0	0	0	☐	0	0	0	☐	0
Osc11	0	0	0	☐	0	0	0	☐	0	0	0	☐	0	0	0	☐	0	0	0	☐	0	0	0	☐	0	0	0	☐	0
Osc12	0	0	0	☐	0	0	0	☐	0	0	0	☐	0	0	0	☐	0	0	0	☐	0	0	0	☐	0	0	0	☐	0
Osc13	194...	145...	242...	☐	6.16...	4.62...	7.70...	☐	0.35...	0.26...	0.43...	☐	0	0	0	☐	0	0	0	☐	0	0	0	☐	0	0	0	☐	0
Osc14	221...	166...	276...	☐	13.8...	10.3...	17.2...	☐	0.82...	0.61...	1.02...	☐	0	0	0	☐	0	0	0	☐	0	0	0	☐	0	0	0	☐	0
Osc15	246...	184...	307...	☐	15.1...	11.3...	18.9...	☐	0.30...	0.22...	0.37...	☐	0	0	0	☐	0	0	0	☐	0	0	0	☐	0	0	0	☐	0
Osc16	347...	260...	434...	☐	20.6...	15.4...	25.8...	☐	0.68...	0.51...	0.85...	☐	0	0	0	☐	0	0	0	☐	0	0	0	☐	0	0	0	☐	0
Osc17	458...	343...	572...	☐	36.7...	27.5...	45.9...	☐	0.13...	0.10...	0.17...	☐	0	0	0	☐	0	0	0	☐	0	0	0	☐	0	0	0	☐	0
Osc18	543	407...	678...	☐	9.96...	7.47...	12.4...	☐	0.83...	0.62...	1.03...	☐	0	0	0	☐	0	0	0	☐	0	0	0	☐	0	0	0	☐	0
Osc19	0	0	0	☐	0	0	0	☐	0	0	0	☐	0	0	0	☐	0	0	0	☐	0	0	0	☐	0	0	0	☐	0
Osc20	0	0	0	☐	0	0	0	☐	0	0	0	☐	0	0	0	☐	0	0	0	☐	0	0	0	☐	0	0	0	☐	0
Osc21	0	0	0	☐	0	0	0	☐	0	0	0	☐	0	0	0	☐	0	0	0	☐	0	0	0	☐	0	0	0	☐	0
Osc22	0	0	0	☐	0	0	0	☐	0	0	0	☐	0	0	0	☐	0	0	0	☐	0	0	0	☐	0	0	0	☐	0
Osc23	0	0	0	☐	0	0	0	☐	0	0	0	☐	0	0	0	☐	0	0	0	☐	0	0	0	☐	0	0	0	☐	0
Osc24	189	141...	236...	☐	3.80...	2.85...	4.75...	☐	0	0	0	☐	0	0	0	☐	0.90...	0.67...	1.12...	☐	0	0	0	☐	0	0	0	☐	0
Osc25	229	171...	286...	☐	3.71...	2.78...	4.63...	☐	0	0	0	☐	0	0	0	☐	0.40...	0.30...	0.50...	☐	0	0	0	☐	0	0	0	☐	0
Osc26	259	194...	323...	☐	15.4...	11.5...	19.2...	☐	0	0	0	☐	0	0	0	☐	0.70...	0.52...	0.87...	☐	0	0	0	☐	0	0	0	☐	0
Osc27	374	280...	467...	☐	31.5...	23.6...	39.3...	☐	0	0	0	☐	0	0	0	☐	1.17...	0.87...	1.46...	☐	0	0	0	☐	0	0	0	☐	0
Osc28	499	374...	623...	☐	33.8...	25.3...	42.2...	☐	0	0	0	☐	0	0	0	☐	0.60...	0.45...	0.75...	☐	0	0	0	☐	0	0	0	☐	0
Osc29	630	472...	787...	☐	0.53...	0.39...	0.66...	☐	0	0	0	☐	0	0	0	☐	0.17...	0.12...	0.21...	☐	0	0	0	☐	0	0	0	☐	0
Osc30	0	0	0	☐	0	0	0	☐	0	0	0	☐	0	0	0	☐	0	0	0	☐	0	0	0	☐	0	0	0	☐	0
Osc31	0	0	0	☐	0	0	0	☐	0	0	0	☐	0	0	0	☐	0	0	0	☐	0	0	0	☐	0	0	0	☐	0
Osc32	0	0	0	☐	0	0	0	☐	0	0	0	☐	0	0	0	☐	0	0	0	☐	0	0	0	☐	0	0	0	☐	0
Osc33	0	0	0	☐	0	0	0	☐	0	0	0	☐	0	0	0	☐	0	0	0	☐	0	0	0	☐	0	0	0	☐	0
Osc34	0	0	0	☐	0	0	0	☐	0	0	0	☐	0	0	0	☐	0	0	0	☐	0	0	0	☐	0	0	0	☐	0
Osc35	0	0	0	☐	0	0	0	☐	0	0	0	☐	0	0	0	☐	0	0	0	☐	0	0	0	☐	0	0	0	☐	0
Osc36	0	0	0	☐	0	0	0	☐	0	0	0	☐	0	0	0	☐	0	0	0	☐	0	0	0	☐	0	0	0	☐	0

Figure 6.6 "Show Tab" panel view with model parameters.

current model. User has option to change available values from this panel as well. After adjusting all values additional click on free space should be made and current window should be closed. "L" stands for low fitting boundary. "U" stands for high fitting boundary. "F" stands for fit. If some value is supposed to be fitted, one should mark corresponding checkbox. When checkbox is chosen, "L" and "U" values are updated automatically by ± value from "L/U Range" edit field percent from the initial value of current parameter.

"Fitting Range" allows to choose appropriate range in inverse centimeters for fitting.

In order to choose ME tensor symmetry or add off diagonal components of electric permittivity tensor user should click on "Symmetry" button in the right panel.
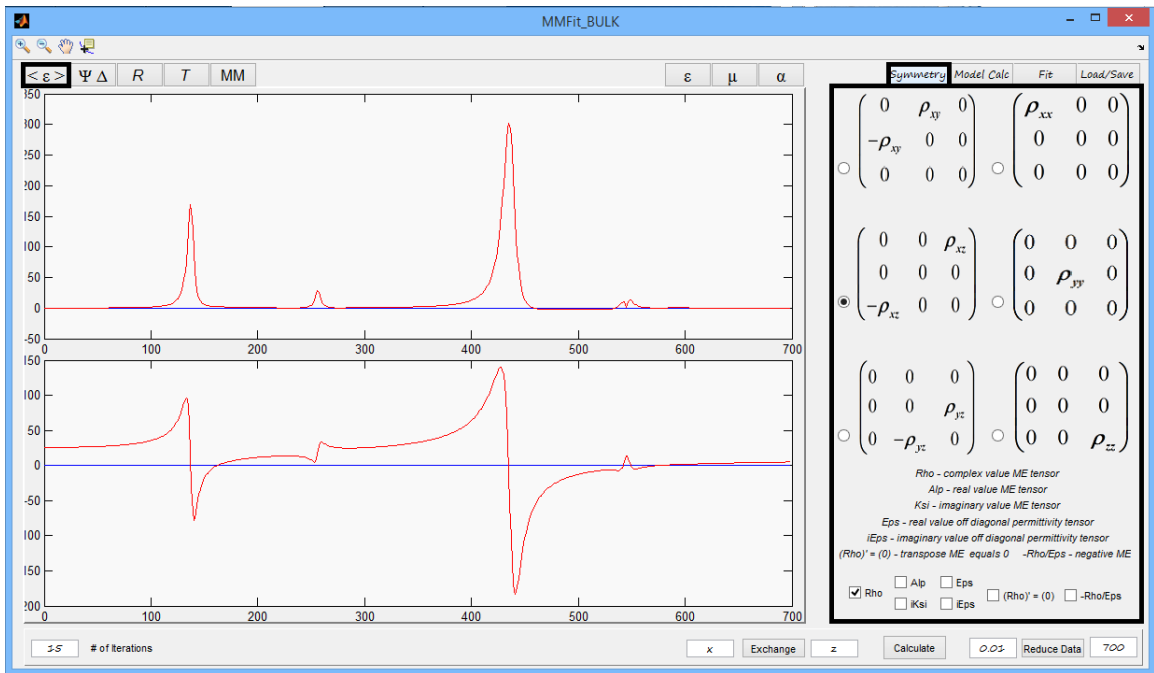
Figure 6.7 "Symmetry" panel view and pseudo-dielectric function data panel with model containing ME oscillator at 545 cm^{-1}.

There are six available options to construct ME tensor which are shown in Figure 6.7. Checkboxes in the low part of the panel allows to choose different options for ME tensor. "Rho" checkbox makes component of ME tensor complex , "Alp" checkbox makes them real, "Ksi" checkbox makes them purely imaginary, "Eps" makes ME tensor 0 and add corresponding real components to electric permittivity tensor. It should be noted that for this choice only off diagonal components available."iEps" does the same as "Eps" but makes components purely imaginary."Rho' = 0" make transpose ME tensor 0 and "-

125

Rho/Eps" makes negative ME tensor or if "Eps", "iEps" options are chosen makes negative off diagonal terms of permittivity tensor.

After model is constructed, clicking on "Calculate " button plots model in the left panel for all functions. There is "Calculate " button on the lower panel and on the "Model Calc" panel as well.

6.3 Working with Fitting

In this section fitting options are explained.
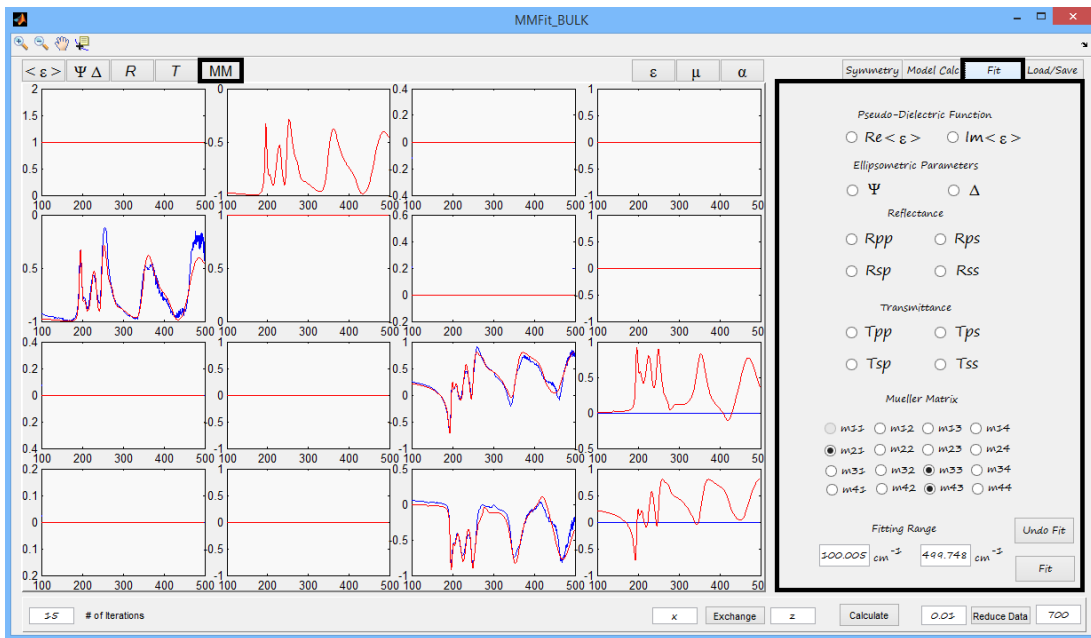
Figure 6.8 "Fitting" panel view with "MM" data panel after fitting three Mueller matrix components. Blue line – data. Red line – model.

"Fit" panel allows to choose different set of data for simultaneous fitting. Desired data for fit should be marked by means of radio buttons. After choosing appropriate sets of data fitting frequency, boundaries could be adjusted in "Fitting range Field"."Fit" button starts fitting procedure. After fit is finished, fitted values are renewed. Left edit box in the low panel allows to adjust number of fitting iterations.

CHAPTER 7

SUMMARY

In this Thesis, we accomplished the following research objectives:

- Analysis of numerical and analytical methods for electromagnetic wave propagation in bi-anisotropic media has been done.

- Analytical expressions for Fresnel's coefficients has been derived for bi-anisotropic bulk and multilayer materials.

- Based on obtained theoretical results the original data fitting and simulation software has been developed.

- IR spectra of Dy-IG and TbMnO$_3$ multiferroics have been analyzed and their parameters such as frequencies and oscillator strengths have been determined.

- Infrared active optical phonons in hexagonal rare earth manganites have been studied. A systematic variation of the photon frequencies vs. the rare earth ion mass and rare earth ion radius has been observed in RMnO$_3$ compounds.

A logical continuation of the current research should be focused on the experimental observation of the optical properties for new materials with predicted magneto-electric interaction. Interesting behavior of such samples is expected under application of external magnetic and electric field. Correspondingly, the developed theoretical formalism should be extended for cases with applied external fields. For thin films structures, which are suitable for different applications in industry and technology interlayer interaction of ME oscillations is under considerable interest and should be studied in more details using Mueller matrix ellipsometry.

APPENDIX A

$\tilde{\Delta}$ MATRIX EIGENVALUES EXPLICIT FORMULAS

In this appendix general formulas are given for eigenvalues of arbitrary structure $\tilde{\Delta}$ matrix which is in the form

$$\tilde{\Delta} = \begin{pmatrix} \Delta_{11} & \Delta_{12} & \Delta_{13} & \Delta_{14} \\ \Delta_{21} & \Delta_{22} & \Delta_{23} & \Delta_{24} \\ \Delta_{31} & \Delta_{32} & \Delta_{33} & \Delta_{34} \\ \Delta_{41} & \Delta_{42} & \Delta_{43} & \Delta_{44} \end{pmatrix} \qquad (5.5)$$

For the most general case when the symmetry of ME tensor is the lowest, optical matrix and $\tilde{\Delta}$ matrix have the following forms:

$$M = \begin{pmatrix} \varepsilon_{xx} & 0 & 0 & \alpha_{xx} & \alpha_{xy} & \alpha_{xz} \\ 0 & \varepsilon_{yy} & 0 & \alpha_{yx} & \alpha_{yy} & \alpha_{yz} \\ 0 & 0 & \varepsilon_{zz} & \alpha_{zx} & \alpha_{zy} & \alpha_{zz} \\ \alpha'_{xx} & \alpha'_{yx} & \alpha'_{zx} & \mu_{xx} & 0 & 0 \\ \alpha'_{xy} & \alpha'_{yy} & \alpha'_{zy} & 0 & \mu_{yy} & 0 \\ \alpha'_{xz} & \alpha'_{yz} & \alpha'_{zz} & 0 & 0 & \mu_{zz} \end{pmatrix} \qquad (5.6)$$

$$\tilde{\Delta} = \begin{pmatrix} \alpha'_{xy} + \dfrac{\alpha_{zz}\alpha'_{xz}(\alpha'_{zy}+q_x)}{\varepsilon_{zz}\mu_{zz}-\alpha_{zz}\alpha'_{zz}} & \alpha'_{yy} + \dfrac{\alpha_{zz}(\alpha'_{yz}-q_x)(\alpha'_{zy}+q_x)}{\varepsilon_{zz}\mu_{zz}-\alpha_{zz}\alpha'_{zz}} & -\dfrac{\mu_{zz}\alpha_{zx}(\alpha'_{zy}+q_x)}{\varepsilon_{zz}\mu_{zz}-\alpha_{zz}\alpha'_{zz}} & \mu_{yy} - \dfrac{\mu_{zz}(\alpha_{zy}+q_x)(\alpha'_{zy}+q_x)}{\varepsilon_{zz}\mu_{zz}-\alpha_{zz}\alpha'_{zz}} \\ -\alpha'_{xx} - \dfrac{(\alpha_{zz}\alpha'_{xz}\alpha'_{zx})}{\varepsilon_{zz}\mu_{zz}-\alpha_{zz}\alpha'_{zz}} & -\alpha'_{yx} - \dfrac{\alpha_{zz}\alpha'_{zx}(\alpha'_{yz}-q_x)}{\varepsilon_{zz}\mu_{zz}-\alpha_{zz}\alpha'_{zz}} & \dfrac{\mu_{zz}\alpha_{zx}\alpha'_{zx}}{\varepsilon_{zz}\mu_{zz}-\alpha_{zz}\alpha'_{zz}} - \mu_{xx} & -\dfrac{\mu_{zz}(\alpha_{zy}+q_x)\alpha'_{zx}}{\varepsilon_{zz}\mu_{zz}-\alpha_{zz}\alpha'_{zz}} \\ \dfrac{\varepsilon_{zz}\alpha'_{xz}(\alpha_{yz}-q_x)}{\varepsilon_{zz}\mu_{zz}-\alpha_{zz}\alpha'_{zz}} & \dfrac{\varepsilon_{zz}(\alpha'_{yz}-q_x)(\alpha_{yz}-q_x)}{\varepsilon_{zz}\mu_{zz}-\alpha_{zz}\alpha'_{zz}} - \varepsilon_{yy} & -\alpha_{yx} - \dfrac{\alpha'_{zz}\alpha_{zx}(\alpha_{yz}-q_x)}{\varepsilon_{zz}\mu_{zz}-\alpha_{zz}\alpha'_{zz}} & -\alpha_{yy} - \dfrac{\alpha'_{zz}(\alpha_{zy}-q_x)(\alpha_{zy}+q_x)}{\varepsilon_{zz}\mu_{zz}-\alpha_{zz}\alpha'_{zz}} \\ \varepsilon_{xx} - \dfrac{\varepsilon_{zz}\alpha_{xz}\alpha'_{xz}}{\varepsilon_{zz}\mu_{zz}-\alpha_{zz}\alpha'_{zz}} & -\dfrac{\varepsilon_{zz}\alpha_{xz}(\alpha'_{yz}-q_x)}{\varepsilon_{zz}\mu_{zz}-\alpha_{zz}\alpha'_{zz}} & \alpha_{xx} + \dfrac{\alpha'_{zz}\alpha_{zx}\alpha_{xz}}{\varepsilon_{zz}\mu_{zz}-\alpha_{zz}\alpha'_{zz}} & -\alpha_{xy} - \dfrac{\alpha'_{zz}\alpha_{xz}(\alpha_{zy}+q_x)}{\varepsilon_{zz}\mu_{zz}-\alpha_{zz}\alpha'_{zz}} \end{pmatrix}$$

$$(5.7)$$

Components of $\tilde{\Delta}$ matrix can be extracted from Equation (5.7). Earlier we pointed out that in order to resolve eigenvalue problem we need to extract solutions of fourth order

polynomial in the form Equation (3.22), where C_1, C_2, C_3, C_4 can be found from the

condition

$$\det\begin{pmatrix} \Delta_{11} - q_{z,i} & \Delta_{12} & \Delta_{13} & \Delta_{14} \\ \Delta_{21} & \Delta_{22} - q_{z,i} & \Delta_{23} & \Delta_{24} \\ \Delta_{31} & \Delta_{32} & \Delta_{33} - q_{z,i} & \Delta_{34} \\ \Delta_{41} & \Delta_{42} & \Delta_{43} & \Delta_{44} - q_{z,i} \end{pmatrix} = 0,$$

with solutions:

$$C_1 = -\Delta_{11} - \Delta_{22} - \Delta_{33} - \Delta_{44}$$

$$C_2 = -\Delta_{12}\Delta_{21} + \Delta_{11}\Delta_{22} - \Delta_{13}\Delta_{31} - \Delta_{23}\Delta_{32} + \Delta_{11}\Delta_{33} + \Delta_{22}\Delta_{33} - \Delta_{14}\Delta_{41} - \Delta_{24}\Delta_{42} - \Delta_{34}\Delta_{43} + \Delta_{11}\Delta_{44} + \Delta_{22}\Delta_{44} + \Delta_{33}\Delta_{44}$$

$$C_3 = \Delta_{13}\Delta_{22}\Delta_{31} - \Delta_{12}\Delta_{23}\Delta_{31} - \Delta_{13}\Delta_{21}\Delta_{32} + \Delta_{11}\Delta_{23}\Delta_{32} + \Delta_{12}\Delta_{21}\Delta_{33} - \Delta_{11}\Delta_{22}\Delta_{33} + \Delta_{14}\Delta_{22}\Delta_{41} - \Delta_{12}\Delta_{24}\Delta_{41} + \Delta_{14}\Delta_{33}\Delta_{41} - \Delta_{13}\Delta_{34}\Delta_{41} - \Delta_{14}\Delta_{21}\Delta_{42} + \Delta_{11}\Delta_{24}\Delta_{42} + \Delta_{24}\Delta_{33}\Delta_{42} - \Delta_{23}\Delta_{34}\Delta_{42} - \Delta_{14}\Delta_{31}\Delta_{43} - \Delta_{24}\Delta_{32}\Delta_{43} + \Delta_{11}\Delta_{34}\Delta_{43} + \Delta_{22}\Delta_{34}\Delta_{43} + \Delta_{12}\Delta_{21}\Delta_{44} - \Delta_{11}\Delta_{22}\Delta_{44} + \Delta_{13}\Delta_{31}\Delta_{44} + \Delta_{23}\Delta_{32}\Delta_{44} - \Delta_{11}\Delta_{33}\Delta_{44} - \Delta_{22}\Delta_{33}\Delta_{44}$$

$$C_4 = \Delta_{14}\Delta_{23}\Delta_{32}\Delta_{41} - \Delta_{13}\Delta_{24}\Delta_{32}\Delta_{41} - \Delta_{14}\Delta_{22}\Delta_{33}\Delta_{41} + \Delta_{12}\Delta_{24}\Delta_{33}\Delta_{41} + \Delta_{13}\Delta_{22}\Delta_{34}\Delta_{41} - \Delta_{12}\Delta_{23}\Delta_{34}\Delta_{41} - \Delta_{14}\Delta_{23}\Delta_{31}\Delta_{42} + \Delta_{13}\Delta_{24}\Delta_{31}\Delta_{42} + \Delta_{14}\Delta_{21}\Delta_{33}\Delta_{42} - \Delta_{11}\Delta_{24}\Delta_{33}\Delta_{42} - \Delta_{13}\Delta_{21}\Delta_{34}\Delta_{42} + \Delta_{11}\Delta_{23}\Delta_{34}\Delta_{42} + \Delta_{14}\Delta_{22}\Delta_{31}\Delta_{43} - \Delta_{14}\Delta_{21}\Delta_{32}\Delta_{43} + \Delta_{11}\Delta_{24}\Delta_{32}\Delta_{43} - \Delta_{11}\Delta_{22}\Delta_{34}\Delta_{43} - \Delta_{12}\left(\Delta_{24}\Delta_{31} - \Delta_{21}\Delta_{34}\right)\Delta_{43}$$

and $q_{z,i}$ is one of the four eigenvalues of $\tilde{\Delta}$ matrix. Eigenvalues formulas are given below

(discussion of universal method for solving quartic equation and analytical solutions are

given in [123]):

$$q_{z,1} =$$

$$-\frac{c_1}{4} -$$

$$\frac{1}{2}\sqrt{\left(\frac{c_1^2}{4} - \frac{2c_2}{3} + \frac{2^{1/3}\left(c_2^2 - 3c_1c_3 + 12c_4\right)}{3\left(2c_2^3 - 9c_1c_2c_3 + 27c_3^2 + 27c_1^2c_4 - 72c_2c_4 + \sqrt{-4\left(c_2^2 - 3c_1c_3 + 12c_4\right)^3 + \left(2c_2^3 - 9c_1c_2c_3 + 27c_3^2 + 27c_1^2c_4 - 72c_2c_4\right)^2}\right)^{1/3}} + \right.}$$

$$\left. \frac{\left(2c_2^3 - 9c_1c_2c_3 + 27c_3^2 + 27c_1^2c_4 - 72c_2c_4 + \sqrt{-4\left(c_2^2 - 3c_1c_3 + 12c_4\right)^3 + \left(2c_2^3 - 9c_1c_2c_3 + 27c_3^2 + 27c_1^2c_4 - 72c_2c_4\right)^2}\right)^{1/3}}{3 \times 2^{1/3}}\right) -$$

$$\frac{1}{2}\sqrt{\left(\frac{c_1^2}{2} - \frac{4c_2}{3} - \frac{2^{1/3}\left(c_2^2 - 3c_1c_3 + 12c_4\right)}{3\left(2c_2^3 - 9c_1c_2c_3 + 27c_3^2 + 27c_1^2c_4 - 72c_2c_4 + \sqrt{-4\left(c_2^2 - 3c_1c_3 + 12c_4\right)^3 + \left(2c_2^3 - 9c_1c_2c_3 + 27c_3^2 + 27c_1^2c_4 - 72c_2c_4\right)^2}\right)^{1/3}} - \right.}$$

$$\left. \frac{\left(2c_2^3 - 9c_1c_2c_3 + 27c_3^2 + 27c_1^2c_4 - 72c_2c_4 + \sqrt{-4\left(c_2^2 - 3c_1c_3 + 12c_4\right)^3 + \left(2c_2^3 - 9c_1c_2c_3 + 27c_3^2 + 27c_1^2c_4 - 72c_2c_4\right)^2}\right)^{1/3}}{3 \times 2^{1/3}} - \right.$$

$$\left(-c_1^3 + 4c_1c_2 - 8c_3\right) \Bigg/$$

$$\left(4\sqrt{\left(\frac{c_1^2}{4} - \frac{2c_2}{3} + \frac{2^{1/3}\left(c_2^2 - 3c_1c_3 + 12c_4\right)}{3\left(2c_2^3 - 9c_1c_2c_3 + 27c_3^2 + 27c_1^2c_4 - 72c_2c_4 + \sqrt{-4\left(c_2^2 - 3c_1c_3 + 12c_4\right)^3 + \left(2c_2^3 - 9c_1c_2c_3 + 27c_3^2 + 27c_1^2c_4 - 72c_2c_4\right)^2}\right)^{1/3}} + \right.}\right.$$

$$\left.\left. \frac{\left(2c_2^3 - 9c_1c_2c_3 + 27c_3^2 + 27c_1^2c_4 - 72c_2c_4 + \sqrt{-4\left(c_2^2 - 3c_1c_3 + 12c_4\right)^3 + \left(2c_2^3 - 9c_1c_2c_3 + 27c_3^2 + 27c_1^2c_4 - 72c_2c_4\right)^2}\right)^{1/3}}{3 \times 2^{1/3}}\right)\right)\right),$$

$$q_{z,2} =$$

$$-\frac{c_1}{4} - \frac{1}{2}\sqrt{\left(\frac{c_1^2}{4} - \frac{2c_2}{3} + \frac{2^{1/3}\left(c_2^2 - 3c_1c_3 + 12c_4\right)}{3\left(2c_2^3 - 9c_1c_2c_3 + 27c_3^2 + 27c_1^2c_4 - 72c_2c_4 + \sqrt{-4\left(c_2^2 - 3c_1c_3 + 12c_4\right)^3 + \left(2c_2^3 - 9c_1c_2c_3 + 27c_3^2 + 27c_1^2c_4 - 72c_2c_4\right)^2}\right)^{1/3}} + \right.}$$

$$\left. \frac{\left(2c_2^3 - 9c_1c_2c_3 + 27c_3^2 + 27c_1^2c_4 - 72c_2c_4 + \sqrt{-4\left(c_2^2 - 3c_1c_3 + 12c_4\right)^3 + \left(2c_2^3 - 9c_1c_2c_3 + 27c_3^2 + 27c_1^2c_4 - 72c_2c_4\right)^2}\right)^{1/3}}{3 \times 2^{1/3}}\right) +$$

$$\frac{1}{2}\sqrt{\left(\frac{c_1^2}{2} - \frac{4c_2}{3} - \frac{2^{1/3}\left(c_2^2 - 3c_1c_3 + 12c_4\right)}{3\left(2c_2^3 - 9c_1c_2c_3 + 27c_3^2 + 27c_1^2c_4 - 72c_2c_4 + \sqrt{-4\left(c_2^2 - 3c_1c_3 + 12c_4\right)^3 + \left(2c_2^3 - 9c_1c_2c_3 + 27c_3^2 + 27c_1^2c_4 - 72c_2c_4\right)^2}\right)^{1/3}} - \right.}$$

$$\left. \frac{\left(2c_2^3 - 9c_1c_2c_3 + 27c_3^2 + 27c_1^2c_4 - 72c_2c_4 + \sqrt{-4\left(c_2^2 - 3c_1c_3 + 12c_4\right)^3 + \left(2c_2^3 - 9c_1c_2c_3 + 27c_3^2 + 27c_1^2c_4 - 72c_2c_4\right)^2}\right)^{1/3}}{3 \times 2^{1/3}} - \right.$$

$$\left(-c_1^3 + 4c_1c_2 - 8c_3\right) \Bigg/$$

$$\left(4\sqrt{\left(\frac{c_1^2}{4} - \frac{2c_2}{3} + \frac{2^{1/3}\left(c_2^2 - 3c_1c_3 + 12c_4\right)}{3\left(2c_2^3 - 9c_1c_2c_3 + 27c_3^2 + 27c_1^2c_4 - 72c_2c_4 + \sqrt{-4\left(c_2^2 - 3c_1c_3 + 12c_4\right)^3 + \left(2c_2^3 - 9c_1c_2c_3 + 27c_3^2 + 27c_1^2c_4 - 72c_2c_4\right)^2}\right)^{1/3}} + \right.}\right.$$

$$\left.\left. \frac{\left(2c_2^3 - 9c_1c_2c_3 + 27c_3^2 + 27c_1^2c_4 - 72c_2c_4 + \sqrt{-4\left(c_2^2 - 3c_1c_3 + 12c_4\right)^3 + \left(2c_2^3 - 9c_1c_2c_3 + 27c_3^2 + 27c_1^2c_4 - 72c_2c_4\right)^2}\right)^{1/3}}{3 \times 2^{1/3}}\right)\right)\right),$$

$$q_{z,3} =$$

$$-\frac{C_1}{4} + \frac{1}{2}\sqrt{\left(\frac{C_1^2}{4} - \frac{2C_2}{3} + \frac{2^{1/3}\left(C_2^2 - 3C_1C_3 + 12C_4\right)}{3\left(2C_2^3 - 9C_1C_2C_3 + 27C_3^2 + 27C_1^2C_4 - 72C_2C_4 + \sqrt{-4\left(C_2^2 - 3C_1C_3 + 12C_4\right)^3 + \left(2C_2^3 - 9C_1C_2C_3 + 27C_3^2 + 27C_1^2C_4 - 72C_2C_4\right)^2}\right)^{1/3}} + \frac{\left(2C_2^3 - 9C_1C_2C_3 + 27C_3^2 + 27C_1^2C_4 - 72C_2C_4 + \sqrt{-4\left(C_2^2 - 3C_1C_3 + 12C_4\right)^3 + \left(2C_2^3 - 9C_1C_2C_3 + 27C_3^2 + 27C_1^2C_4 - 72C_2C_4\right)^2}\right)^{1/3}}{3\times 2^{1/3}}\right)}$$

$$-\frac{1}{2}\sqrt{\left(\frac{C_1^2}{2} - \frac{4C_2}{3} - \frac{2^{1/3}\left(C_2^2 - 3C_1C_3 + 12C_4\right)}{3\left(2C_2^3 - 9C_1C_2C_3 + 27C_3^2 + 27C_1^2C_4 - 72C_2C_4 + \sqrt{-4\left(C_2^2 - 3C_1C_3 + 12C_4\right)^3 + \left(2C_2^3 - 9C_1C_2C_3 + 27C_3^2 + 27C_1^2C_4 - 72C_2C_4\right)^2}\right)^{1/3}} - \frac{\left(2C_2^3 - 9C_1C_2C_3 + 27C_3^2 + 27C_1^2C_4 - 72C_2C_4 + \sqrt{-4\left(C_2^2 - 3C_1C_3 + 12C_4\right)^3 + \left(2C_2^3 - 9C_1C_2C_3 + 27C_3^2 + 27C_1^2C_4 - 72C_2C_4\right)^2}\right)^{1/3}}{3\times 2^{1/3}}\right.}$$

$$\left. + \left(-C_1^3 + 4C_1C_2 - 8C_3\right)\bigg/ \left(4\sqrt{\left(\frac{C_1^2}{4} - \frac{2C_2}{3} + \frac{2^{1/3}\left(C_2^2 - 3C_1C_3 + 12C_4\right)}{3\left(2C_2^3 - 9C_1C_2C_3 + 27C_3^2 + 27C_1^2C_4 - 72C_2C_4 + \sqrt{-4\left(C_2^2 - 3C_1C_3 + 12C_4\right)^3 + \left(2C_2^3 - 9C_1C_2C_3 + 27C_3^2 + 27C_1^2C_4 - 72C_2C_4\right)^2}\right)^{1/3}} + \frac{\left(2C_2^3 - 9C_1C_2C_3 + 27C_3^2 + 27C_1^2C_4 - 72C_2C_4 + \sqrt{-4\left(C_2^2 - 3C_1C_3 + 12C_4\right)^3 + \left(2C_2^3 - 9C_1C_2C_3 + 27C_3^2 + 27C_1^2C_4 - 72C_2C_4\right)^2}\right)^{1/3}}{3\times 2^{1/3}}\right)}\right)},$$

$$q_{z,4} =$$

$$-\frac{C_1}{4} + \frac{1}{2}\sqrt{\left(\frac{C_1^2}{4} - \frac{2C_2}{3} + \frac{2^{1/3}\left(C_2^2 - 3C_1C_3 + 12C_4\right)}{3\left(2C_2^3 - 9C_1C_2C_3 + 27C_3^2 + 27C_1^2C_4 - 72C_2C_4 + \sqrt{-4\left(C_2^2 - 3C_1C_3 + 12C_4\right)^3 + \left(2C_2^3 - 9C_1C_2C_3 + 27C_3^2 + 27C_1^2C_4 - 72C_2C_4\right)^2}\right)^{1/3}} + \frac{\left(2C_2^3 - 9C_1C_2C_3 + 27C_3^2 + 27C_1^2C_4 - 72C_2C_4 + \sqrt{-4\left(C_2^2 - 3C_1C_3 + 12C_4\right)^3 + \left(2C_2^3 - 9C_1C_2C_3 + 27C_3^2 + 27C_1^2C_4 - 72C_2C_4\right)^2}\right)^{1/3}}{3\times 2^{1/3}}\right)}$$

$$+\frac{1}{2}\sqrt{\left(\frac{C_1^2}{2} - \frac{4C_2}{3} - \frac{2^{1/3}\left(C_2^2 - 3C_1C_3 + 12C_4\right)}{3\left(2C_2^3 - 9C_1C_2C_3 + 27C_3^2 + 27C_1^2C_4 - 72C_2C_4 + \sqrt{-4\left(C_2^2 - 3C_1C_3 + 12C_4\right)^3 + \left(2C_2^3 - 9C_1C_2C_3 + 27C_3^2 + 27C_1^2C_4 - 72C_2C_4\right)^2}\right)^{1/3}} - \frac{\left(2C_2^3 - 9C_1C_2C_3 + 27C_3^2 + 27C_1^2C_4 - 72C_2C_4 + \sqrt{-4\left(C_2^2 - 3C_1C_3 + 12C_4\right)^3 + \left(2C_2^3 - 9C_1C_2C_3 + 27C_3^2 + 27C_1^2C_4 - 72C_2C_4\right)^2}\right)^{1/3}}{3\times 2^{1/3}}\right.}$$

$$\left. + \left(-C_1^3 + 4C_1C_2 - 8C_3\right)\bigg/ \left(4\sqrt{\left(\frac{C_1^2}{4} - \frac{2C_2}{3} + \frac{2^{1/3}\left(C_2^2 - 3C_1C_3 + 12C_4\right)}{3\left(2C_2^3 - 9C_1C_2C_3 + 27C_3^2 + 27C_1^2C_4 - 72C_2C_4 + \sqrt{-4\left(C_2^2 - 3C_1C_3 + 12C_4\right)^3 + \left(2C_2^3 - 9C_1C_2C_3 + 27C_3^2 + 27C_1^2C_4 - 72C_2C_4\right)^2}\right)^{1/3}} + \frac{\left(2C_2^3 - 9C_1C_2C_3 + 27C_3^2 + 27C_1^2C_4 - 72C_2C_4 + \sqrt{-4\left(C_2^2 - 3C_1C_3 + 12C_4\right)^3 + \left(2C_2^3 - 9C_1C_2C_3 + 27C_3^2 + 27C_1^2C_4 - 72C_2C_4\right)^2}\right)^{1/3}}{3\times 2^{1/3}}\right)}\right)}.$$

Thus we found solutions for eigenvalues in terms of $\widetilde{\Delta}$ matrix components.

APPENDIX B

$\tilde{\Delta}$ MATRIX EIGENVECTORS EXPLICIT FORMULAS

In this appendix we find eigenvectors representation of $\tilde{\Delta}$ matrix. In order to get solutions we need to consider the following equation:

$$
\begin{pmatrix}
\Delta_{11} - q_{z,i} & \Delta_{12} & \Delta_{13} & \Delta_{14} \\
\Delta_{21} & \Delta_{22} - q_{z,i} & \Delta_{23} & \Delta_{24} \\
\Delta_{31} & \Delta_{32} & \Delta_{33} - q_{z,i} & \Delta_{34} \\
\Delta_{41} & \Delta_{42} & \Delta_{43} & \Delta_{44} - q_{z,i}
\end{pmatrix}
\begin{pmatrix}
E_x \\
E_y \\
H_x \\
H_y
\end{pmatrix} = 0
\tag{5.8}
$$

where $q_{z,i}$ is one of the four eigenvalues of $\tilde{\Delta}$ matrix and their analytical solutions are given in Appendix A. Let's rewrite Equation (5.8) in the following form:

$$
\begin{cases}
(\Delta_{11} - q_{z,i})E_x + \Delta_{12}E_y + \Delta_{13}H_x + \Delta_{14}H_y = 0 \\
\Delta_{21}E_x + (\Delta_{22} - q_{z,i})E_y + \Delta_{23}H_x + \Delta_{24}H_y = 0 \\
\Delta_{31}E_x + \Delta_{32}E_y + (\Delta_{33} - q_{z,i})H_x + \Delta_{34}H_y = 0 \\
\Delta_{41}E_x + \Delta_{42}E_y + \Delta_{43}H_x + (\Delta_{44} - q_{z,i})H_y = 0.
\end{cases}
\tag{5.9}
$$

Equation (5.9) is a linear system with respect to the tangential field components. It's not hard to show that general solution for each out of four possible eigenvectors has the structure shown below:

$$
\begin{pmatrix}
\psi_{1,i} \\
\psi_{2,i} \\
\psi_{3,i} \\
\psi_{4,i}
\end{pmatrix} =
\begin{pmatrix}
E_x \\
E_y \\
H_x \\
H_y
\end{pmatrix}_{eigen,q_{z,i}} =
\begin{pmatrix}
\dfrac{\Delta_{12}\left(-\Delta_{23}\Delta_{34} + \Delta_{24}\left(\Delta_{33} - q_{z,i}\right)\right) - \Delta_{13}\left(\Delta_{24}\Delta_{32} + \Delta_{34}\left(-\Delta_{22} + q_{z,i}\right)\right) + \Delta_{14}\left(\Delta_{23}\Delta_{32} + \left(\Delta_{22} - q_{z,i}\right)\left(-\Delta_{33} + q_{z,i}\right)\right)}{\left(-\Delta_{23}\Delta_{32} + \left(\Delta_{22} - q_{z,i}\right)\left(\Delta_{33} - q_{z,i}\right)\right)\left(\Delta_{11} - q_{z,i}\right) + \Delta_{13}\left(\Delta_{21}\Delta_{32} + \Delta_{31}\left(-\Delta_{22} + q_{z,i}\right)\right) + \Delta_{12}\left(\Delta_{23}\Delta_{31} + \Delta_{21}\left(-\Delta_{33} + q_{z,i}\right)\right)} \\[6pt]
\dfrac{\Delta_{13}\left(-\Delta_{24}\Delta_{31} + \Delta_{21}\Delta_{34}\right) + \Delta_{14}\left(\Delta_{23}\Delta_{31} + \Delta_{21}\left(-\Delta_{33} + q_{z,i}\right)\right) - \left(\Delta_{11} - q_{z,i}\right)\left(\Delta_{23}\Delta_{34} + \Delta_{24}\left(-\Delta_{33} + q_{z,i}\right)\right)}{\left(-\Delta_{23}\Delta_{32} + \left(\Delta_{22} - q_{z,i}\right)\left(\Delta_{33} - q_{z,i}\right)\right)\left(\Delta_{11} - q_{z,i}\right) + \Delta_{13}\left(\Delta_{21}\Delta_{32} + \Delta_{31}\left(-\Delta_{22} + q_{z,i}\right)\right) + \Delta_{12}\left(\Delta_{23}\Delta_{31} + \Delta_{21}\left(-\Delta_{33} + q_{z,i}\right)\right)} \\[6pt]
\dfrac{\Delta_{12}\left(-\Delta_{24}\Delta_{31} + \Delta_{21}\Delta_{34}\right) + \Delta_{14}\left(-\Delta_{21}\Delta_{32} + \Delta_{31}\left(\Delta_{22} - q_{z,i}\right)\right) + \left(\Delta_{11} - q_{z,i}\right)\left(\Delta_{24}\Delta_{32} + \Delta_{34}\left(-\Delta_{22} + q_{z,i}\right)\right)}{\left(-\Delta_{23}\Delta_{32} + \left(\Delta_{22} - q_{z,i}\right)\left(\Delta_{33} - q_{z,i}\right)\right)\left(\Delta_{11} - q_{z,i}\right) + \Delta_{13}\left(\Delta_{21}\Delta_{32} + \Delta_{31}\left(-\Delta_{22} + q_{z,i}\right)\right) + \Delta_{12}\left(\Delta_{23}\Delta_{31} + \Delta_{21}\left(-\Delta_{33} + q_{z,i}\right)\right)} \\[6pt]
1
\end{pmatrix}
\tag{5.10}
$$

In Equation (5.10) eigenvector components are normalized by H_y. In previous appendix A we showed explicit solutions for eigenvalues. That means eigenvectors problem is solved completely. Due to a very bulky structure of formulas in terms of optical parameters such as $\varepsilon, \mu, \alpha, AOI$, etc., we don't show final results here, though they are available in MatLab m-functions.

APPENDIX C

DOUBLE LAYER STRUCTURE PARTIAL
TRANSFER MATRIX REPRESENTATION

In Chapter 3 on electromagnetic waves propagation in multilayer structures we showed that

partial transfer matrix can be written in the form of Equation (3.19) with β coefficients in

the form of Equation (3.20). We present transfer matrix formulas for bilayer structure below:

$$T_{11} =$$

$$\big(\beta_{a,0} + \beta_{a,1}\,\triangle_{a,11} + \beta_{a,2}\,(\triangle^2_{a,11} + \triangle_{a,12}\,\triangle_{a,21} + \triangle_{a,13}\,\triangle_{a,31} + \triangle_{a,14}\,\triangle_{a,41}) + \beta_{a,3}\,(\triangle_{a,11}\,(\triangle^2_{a,11} + \triangle_{a,12}\,\triangle_{a,21} + \triangle_{a,13}\,\triangle_{a,31} + \triangle_{a,14}\,\triangle_{a,41}) +$$
$$\triangle_{a,21}\,(\triangle_{a,11}\,\triangle_{a,12} + \triangle_{a,12}\,\triangle_{a,22} + \triangle_{a,13}\,\triangle_{a,32} + \triangle_{a,14}\,\triangle_{a,42}) + \triangle_{a,31}\,(\triangle_{a,11}\,\triangle_{a,13} + \triangle_{a,12}\,\triangle_{a,23} + \triangle_{a,13}\,\triangle_{a,33} + \triangle_{a,14}\,\triangle_{a,43}) + \triangle_{a,41}\,(\triangle_{a,11}\,\triangle_{a,14} + \triangle_{a,12}\,\triangle_{a,24} + \triangle_{a,13}\,\triangle_{a,34} + \triangle_{a,14}\,\triangle_{a,44})))$$
$$\big(\beta_{b,0} + \beta_{b,1}\,\triangle_{b,11} + \beta_{b,2}\,(\triangle^2_{b,11} + \triangle_{b,12}\,\triangle_{b,21} + \triangle_{b,13}\,\triangle_{b,31} + \triangle_{b,14}\,\triangle_{b,41}) + \beta_{b,3}\,(\triangle_{b,11}\,(\triangle^2_{b,11} + \triangle_{b,12}\,\triangle_{b,21} + \triangle_{b,13}\,\triangle_{b,31} + \triangle_{b,14}\,\triangle_{b,41}) + \triangle_{b,21}\,(\triangle_{b,11}\,\triangle_{b,12} + \triangle_{b,12}\,\triangle_{b,22} + \triangle_{b,13}\,\triangle_{b,32} + \triangle_{b,14}\,\triangle_{b,42}) +$$
$$\triangle_{b,31}\,(\triangle_{b,11}\,\triangle_{b,13} + \triangle_{b,12}\,\triangle_{b,23} + \triangle_{b,13}\,\triangle_{b,33} + \triangle_{b,14}\,\triangle_{b,43}) + \triangle_{b,41}\,(\triangle_{b,11}\,\triangle_{b,14} + \triangle_{b,12}\,\triangle_{b,24} + \triangle_{b,13}\,\triangle_{b,34} + \triangle_{b,14}\,\triangle_{b,44}))) +$$
$$\big(\beta_{a,0} + \beta_{a,1}\,\triangle_{a,12} + \beta_{a,2}\,(\triangle_{a,11}\,\triangle_{a,12} + \triangle_{a,12}\,\triangle_{a,22} + \triangle_{a,13}\,\triangle_{a,32} + \triangle_{a,14}\,\triangle_{a,42}) + \beta_{a,3}\,(\triangle_{a,12}\,(\triangle^2_{a,11} + \triangle_{a,12}\,\triangle_{a,21} + \triangle_{a,13}\,\triangle_{a,31} + \triangle_{a,14}\,\triangle_{a,41}) + \triangle_{a,22}\,(\triangle_{a,11}\,\triangle_{a,12} + \triangle_{a,12}\,\triangle_{a,22} + \triangle_{a,13}\,\triangle_{a,32} + \triangle_{a,14}\,\triangle_{a,42}) +$$
$$\triangle_{a,32}\,(\triangle_{a,11}\,\triangle_{a,13} + \triangle_{a,12}\,\triangle_{a,23} + \triangle_{a,13}\,\triangle_{a,33} + \triangle_{a,14}\,\triangle_{a,43}) + \triangle_{a,42}\,(\triangle_{a,11}\,\triangle_{a,14} + \triangle_{a,12}\,\triangle_{a,24} + \triangle_{a,13}\,\triangle_{a,34} + \triangle_{a,14}\,\triangle_{a,44})))$$
$$\big(\beta_{b,0} + \beta_{b,1}\,\triangle_{b,21} + \beta_{b,2}\,(\triangle_{b,11}\,\triangle_{b,21} + \triangle_{b,21}\,\triangle_{b,22} + \triangle_{b,23}\,\triangle_{b,31} + \triangle_{b,24}\,\triangle_{b,41}) + \beta_{b,3}\,(\triangle_{b,11}\,(\triangle_{b,11}\,\triangle_{b,21} + \triangle_{b,21}\,\triangle_{b,22} + \triangle_{b,23}\,\triangle_{b,31} + \triangle_{b,24}\,\triangle_{b,41}) +$$
$$\triangle_{b,21}\,(\triangle_{b,12}\,\triangle_{b,21} + \triangle^2_{b,22} + \triangle_{b,23}\,\triangle_{b,32} + \triangle_{b,24}\,\triangle_{b,42}) + \triangle_{b,31}\,(\triangle_{b,13}\,\triangle_{b,21} + \triangle_{b,22}\,\triangle_{b,23} + \triangle_{b,23}\,\triangle_{b,33} + \triangle_{b,24}\,\triangle_{b,43}) + \triangle_{b,41}\,(\triangle_{b,14}\,\triangle_{b,21} + \triangle_{b,22}\,\triangle_{b,24} + \triangle_{b,23}\,\triangle_{b,34} + \triangle_{b,24}\,\triangle_{b,44}))) +$$
$$\big(\beta_{a,0} + \beta_{a,1}\,\triangle_{a,13} + \beta_{a,2}\,(\triangle_{a,11}\,\triangle_{a,13} + \triangle_{a,12}\,\triangle_{a,23} + \triangle_{a,13}\,\triangle_{a,33} + \triangle_{a,14}\,\triangle_{a,43}) + \beta_{a,3}\,(\triangle_{a,13}\,(\triangle^2_{a,11} + \triangle_{a,12}\,\triangle_{a,21} + \triangle_{a,13}\,\triangle_{a,31} + \triangle_{a,14}\,\triangle_{a,41}) + \triangle_{a,23}\,(\triangle_{a,11}\,\triangle_{a,12} + \triangle_{a,12}\,\triangle_{a,22} + \triangle_{a,13}\,\triangle_{a,32} + \triangle_{a,14}\,\triangle_{a,42}) +$$
$$\triangle_{a,33}\,(\triangle_{a,11}\,\triangle_{a,13} + \triangle_{a,12}\,\triangle_{a,23} + \triangle_{a,13}\,\triangle_{a,33} + \triangle_{a,14}\,\triangle_{a,43}) + \triangle_{a,43}\,(\triangle_{a,11}\,\triangle_{a,14} + \triangle_{a,12}\,\triangle_{a,24} + \triangle_{a,13}\,\triangle_{a,34} + \triangle_{a,14}\,\triangle_{a,44})))$$
$$\big(\beta_{b,0} + \beta_{b,1}\,\triangle_{b,31} + \beta_{b,2}\,(\triangle_{b,11}\,\triangle_{b,31} + \triangle_{b,21}\,\triangle_{b,32} + \triangle_{b,31}\,\triangle_{b,33} + \triangle_{b,34}\,\triangle_{b,41}) + \beta_{b,3}\,(\triangle_{b,11}\,(\triangle_{b,11}\,\triangle_{b,31} + \triangle_{b,21}\,\triangle_{b,32} + \triangle_{b,31}\,\triangle_{b,33} + \triangle_{b,34}\,\triangle_{b,41}) +$$
$$\triangle_{b,21}\,(\triangle_{b,12}\,\triangle_{b,31} + \triangle_{b,22}\,\triangle_{b,32} + \triangle_{b,32}\,\triangle_{b,33} + \triangle_{b,34}\,\triangle_{b,42}) + \triangle_{b,31}\,(\triangle_{b,13}\,\triangle_{b,31} + \triangle_{b,23}\,\triangle_{b,32} + \triangle^2_{b,33} + \triangle_{b,34}\,\triangle_{b,43}) + \triangle_{b,41}\,(\triangle_{b,14}\,\triangle_{b,31} + \triangle_{b,24}\,\triangle_{b,32} + \triangle_{b,33}\,\triangle_{b,34} + \triangle_{b,34}\,\triangle_{b,44}))) +$$
$$\big(\beta_{a,0} + \beta_{a,1}\,\triangle_{a,14} + \beta_{a,2}\,(\triangle_{a,11}\,\triangle_{a,14} + \triangle_{a,12}\,\triangle_{a,24} + \triangle_{a,13}\,\triangle_{a,34} + \triangle_{a,14}\,\triangle_{a,44}) + \beta_{a,3}\,(\triangle_{a,14}\,(\triangle^2_{a,11} + \triangle_{a,12}\,\triangle_{a,21} + \triangle_{a,13}\,\triangle_{a,31} + \triangle_{a,14}\,\triangle_{a,41}) + \triangle_{a,24}\,(\triangle_{a,11}\,\triangle_{a,12} + \triangle_{a,12}\,\triangle_{a,22} + \triangle_{a,13}\,\triangle_{a,32} + \triangle_{a,14}\,\triangle_{a,42}) +$$
$$\triangle_{a,34}\,(\triangle_{a,11}\,\triangle_{a,13} + \triangle_{a,12}\,\triangle_{a,23} + \triangle_{a,13}\,\triangle_{a,33} + \triangle_{a,14}\,\triangle_{a,43}) + \triangle_{a,44}\,(\triangle_{a,11}\,\triangle_{a,14} + \triangle_{a,12}\,\triangle_{a,24} + \triangle_{a,13}\,\triangle_{a,34} + \triangle_{a,14}\,\triangle_{a,44})))$$
$$\big(\beta_{b,0} + \beta_{b,1}\,\triangle_{b,41} + \beta_{b,2}\,(\triangle_{b,11}\,\triangle_{b,41} + \triangle_{b,21}\,\triangle_{b,42} + \triangle_{b,31}\,\triangle_{b,43} + \triangle_{b,41}\,\triangle_{b,44}) + \beta_{b,3}\,(\triangle_{b,11}\,(\triangle_{b,11}\,\triangle_{b,41} + \triangle_{b,21}\,\triangle_{b,42} + \triangle_{b,31}\,\triangle_{b,43} + \triangle_{b,41}\,\triangle_{b,44}) +$$
$$\triangle_{b,21}\,(\triangle_{b,12}\,\triangle_{b,41} + \triangle_{b,22}\,\triangle_{b,42} + \triangle_{b,32}\,\triangle_{b,43} + \triangle_{b,42}\,\triangle_{b,44}) + \triangle_{b,31}\,(\triangle_{b,13}\,\triangle_{b,41} + \triangle_{b,23}\,\triangle_{b,42} + \triangle_{b,33}\,\triangle_{b,43} + \triangle_{b,43}\,\triangle_{b,44}) + \triangle_{b,41}\,(\triangle_{b,14}\,\triangle_{b,41} + \triangle_{b,24}\,\triangle_{b,42} + \triangle_{b,34}\,\triangle_{b,43} + \triangle^2_{b,44})))$$

$$T_{12} =$$

$$\big(\beta_{a,0} + \beta_{a,1}\,\triangle_{a,11} + \beta_{a,2}\,(\triangle^2_{a,11} + \triangle_{a,12}\,\triangle_{a,21} + \triangle_{a,13}\,\triangle_{a,31} + \triangle_{a,14}\,\triangle_{a,41}) + \beta_{a,3}\,(\triangle_{a,11}\,(\triangle^2_{a,11} + \triangle_{a,12}\,\triangle_{a,21} + \triangle_{a,13}\,\triangle_{a,31} + \triangle_{a,14}\,\triangle_{a,41}) +$$
$$\triangle_{a,21}\,(\triangle_{a,11}\,\triangle_{a,12} + \triangle_{a,12}\,\triangle_{a,22} + \triangle_{a,13}\,\triangle_{a,32} + \triangle_{a,14}\,\triangle_{a,42}) + \triangle_{a,31}\,(\triangle_{a,11}\,\triangle_{a,13} + \triangle_{a,12}\,\triangle_{a,23} + \triangle_{a,13}\,\triangle_{a,33} + \triangle_{a,14}\,\triangle_{a,43}) + \triangle_{a,41}\,(\triangle_{a,11}\,\triangle_{a,14} + \triangle_{a,12}\,\triangle_{a,24} + \triangle_{a,13}\,\triangle_{a,34} + \triangle_{a,14}\,\triangle_{a,44})))$$
$$\big(\beta_{b,0} + \beta_{b,1}\,\triangle_{b,12} + \beta_{b,2}\,(\triangle_{b,11}\,\triangle_{b,12} + \triangle_{b,12}\,\triangle_{b,22} + \triangle_{b,13}\,\triangle_{b,32} + \triangle_{b,14}\,\triangle_{b,42}) + \beta_{b,3}\,(\triangle_{b,12}\,(\triangle^2_{b,11} + \triangle_{b,12}\,\triangle_{b,21} + \triangle_{b,13}\,\triangle_{b,31} + \triangle_{b,14}\,\triangle_{b,41}) + \triangle_{b,22}\,(\triangle_{b,11}\,\triangle_{b,12} + \triangle_{b,12}\,\triangle_{b,22} + \triangle_{b,13}\,\triangle_{b,32} + \triangle_{b,14}\,\triangle_{b,42}) +$$
$$\triangle_{b,32}\,(\triangle_{b,11}\,\triangle_{b,13} + \triangle_{b,12}\,\triangle_{b,23} + \triangle_{b,13}\,\triangle_{b,33} + \triangle_{b,14}\,\triangle_{b,43}) + \triangle_{b,42}\,(\triangle_{b,11}\,\triangle_{b,14} + \triangle_{b,12}\,\triangle_{b,24} + \triangle_{b,13}\,\triangle_{b,34} + \triangle_{b,14}\,\triangle_{b,44}))) +$$
$$\big(\beta_{a,0} + \beta_{a,1}\,\triangle_{a,12} + \beta_{a,2}\,(\triangle_{a,11}\,\triangle_{a,12} + \triangle_{a,12}\,\triangle_{a,22} + \triangle_{a,13}\,\triangle_{a,32} + \triangle_{a,14}\,\triangle_{a,42}) + \beta_{a,3}\,(\triangle_{a,12}\,(\triangle^2_{a,11} + \triangle_{a,12}\,\triangle_{a,21} + \triangle_{a,13}\,\triangle_{a,31} + \triangle_{a,14}\,\triangle_{a,41}) + \triangle_{a,22}\,(\triangle_{a,11}\,\triangle_{a,12} + \triangle_{a,12}\,\triangle_{a,22} + \triangle_{a,13}\,\triangle_{a,32} + \triangle_{a,14}\,\triangle_{a,42}) +$$
$$\triangle_{a,32}\,(\triangle_{a,11}\,\triangle_{a,13} + \triangle_{a,12}\,\triangle_{a,23} + \triangle_{a,13}\,\triangle_{a,33} + \triangle_{a,14}\,\triangle_{a,43}) + \triangle_{a,42}\,(\triangle_{a,11}\,\triangle_{a,14} + \triangle_{a,12}\,\triangle_{a,24} + \triangle_{a,13}\,\triangle_{a,34} + \triangle_{a,14}\,\triangle_{a,44})))$$
$$\big(\beta_{b,0} + \beta_{b,1}\,\triangle_{b,22} + \beta_{b,2}\,(\triangle_{b,12}\,\triangle_{b,21} + \triangle^2_{b,22} + \triangle_{b,23}\,\triangle_{b,32} + \triangle_{b,24}\,\triangle_{b,42}) + \beta_{b,3}\,(\triangle_{b,12}\,(\triangle_{b,11}\,\triangle_{b,21} + \triangle_{b,21}\,\triangle_{b,22} + \triangle_{b,23}\,\triangle_{b,31} + \triangle_{b,24}\,\triangle_{b,41}) + \triangle_{b,22}\,(\triangle_{b,12}\,\triangle_{b,21} + \triangle^2_{b,22} + \triangle_{b,23}\,\triangle_{b,32} + \triangle_{b,24}\,\triangle_{b,42}) +$$
$$\triangle_{b,32}\,(\triangle_{b,13}\,\triangle_{b,21} + \triangle_{b,22}\,\triangle_{b,23} + \triangle_{b,23}\,\triangle_{b,33} + \triangle_{b,24}\,\triangle_{b,43}) + \triangle_{b,42}\,(\triangle_{b,14}\,\triangle_{b,21} + \triangle_{b,22}\,\triangle_{b,24} + \triangle_{b,23}\,\triangle_{b,34} + \triangle_{b,24}\,\triangle_{b,44}))) +$$
$$\big(\beta_{a,0} + \beta_{a,1}\,\triangle_{a,13} + \beta_{a,2}\,(\triangle_{a,11}\,\triangle_{a,13} + \triangle_{a,12}\,\triangle_{a,23} + \triangle_{a,13}\,\triangle_{a,33} + \triangle_{a,14}\,\triangle_{a,43}) + \beta_{a,3}\,(\triangle_{a,13}\,(\triangle^2_{a,11} + \triangle_{a,12}\,\triangle_{a,21} + \triangle_{a,13}\,\triangle_{a,31} + \triangle_{a,14}\,\triangle_{a,41}) + \triangle_{a,23}\,(\triangle_{a,11}\,\triangle_{a,12} + \triangle_{a,12}\,\triangle_{a,22} + \triangle_{a,13}\,\triangle_{a,32} + \triangle_{a,14}\,\triangle_{a,42}) +$$
$$\triangle_{a,33}\,(\triangle_{a,11}\,\triangle_{a,13} + \triangle_{a,12}\,\triangle_{a,23} + \triangle_{a,13}\,\triangle_{a,33} + \triangle_{a,14}\,\triangle_{a,43}) + \triangle_{a,43}\,(\triangle_{a,11}\,\triangle_{a,14} + \triangle_{a,12}\,\triangle_{a,24} + \triangle_{a,13}\,\triangle_{a,34} + \triangle_{a,14}\,\triangle_{a,44})))$$
$$\big(\beta_{b,0} + \beta_{b,1}\,\triangle_{b,32} + \beta_{b,2}\,(\triangle_{b,12}\,\triangle_{b,31} + \triangle_{b,22}\,\triangle_{b,32} + \triangle_{b,32}\,\triangle_{b,33} + \triangle_{b,34}\,\triangle_{b,42}) + \beta_{b,3}\,(\triangle_{b,12}\,(\triangle_{b,11}\,\triangle_{b,31} + \triangle_{b,21}\,\triangle_{b,32} + \triangle_{b,31}\,\triangle_{b,33} + \triangle_{b,34}\,\triangle_{b,41}) +$$
$$\triangle_{b,22}\,(\triangle_{b,12}\,\triangle_{b,31} + \triangle_{b,22}\,\triangle_{b,32} + \triangle_{b,32}\,\triangle_{b,33} + \triangle_{b,34}\,\triangle_{b,42}) + \triangle_{b,32}\,(\triangle_{b,13}\,\triangle_{b,31} + \triangle_{b,23}\,\triangle_{b,32} + \triangle^2_{b,33} + \triangle_{b,34}\,\triangle_{b,43}) + \triangle_{b,42}\,(\triangle_{b,14}\,\triangle_{b,31} + \triangle_{b,24}\,\triangle_{b,32} + \triangle_{b,33}\,\triangle_{b,34} + \triangle_{b,34}\,\triangle_{b,44}))) +$$
$$\big(\beta_{a,0} + \beta_{a,1}\,\triangle_{a,14} + \beta_{a,2}\,(\triangle_{a,11}\,\triangle_{a,14} + \triangle_{a,12}\,\triangle_{a,24} + \triangle_{a,13}\,\triangle_{a,34} + \triangle_{a,14}\,\triangle_{a,44}) + \beta_{a,3}\,(\triangle_{a,14}\,(\triangle^2_{a,11} + \triangle_{a,12}\,\triangle_{a,21} + \triangle_{a,13}\,\triangle_{a,31} + \triangle_{a,14}\,\triangle_{a,41}) + \triangle_{a,24}\,(\triangle_{a,11}\,\triangle_{a,12} + \triangle_{a,12}\,\triangle_{a,22} + \triangle_{a,13}\,\triangle_{a,32} + \triangle_{a,14}\,\triangle_{a,42}) +$$
$$\triangle_{a,34}\,(\triangle_{a,11}\,\triangle_{a,13} + \triangle_{a,12}\,\triangle_{a,23} + \triangle_{a,13}\,\triangle_{a,33} + \triangle_{a,14}\,\triangle_{a,43}) + \triangle_{a,44}\,(\triangle_{a,11}\,\triangle_{a,14} + \triangle_{a,12}\,\triangle_{a,24} + \triangle_{a,13}\,\triangle_{a,34} + \triangle_{a,14}\,\triangle_{a,44})))$$
$$\big(\beta_{b,0} + \beta_{b,1}\,\triangle_{b,42} + \beta_{b,2}\,(\triangle_{b,12}\,\triangle_{b,41} + \triangle_{b,22}\,\triangle_{b,42} + \triangle_{b,32}\,\triangle_{b,43} + \triangle_{b,42}\,\triangle_{b,44}) + \beta_{b,3}\,(\triangle_{b,12}\,(\triangle_{b,11}\,\triangle_{b,41} + \triangle_{b,21}\,\triangle_{b,42} + \triangle_{b,31}\,\triangle_{b,43} + \triangle_{b,41}\,\triangle_{b,44}) +$$
$$\triangle_{b,22}\,(\triangle_{b,12}\,\triangle_{b,41} + \triangle_{b,22}\,\triangle_{b,42} + \triangle_{b,32}\,\triangle_{b,43} + \triangle_{b,42}\,\triangle_{b,44}) + \triangle_{b,32}\,(\triangle_{b,13}\,\triangle_{b,41} + \triangle_{b,23}\,\triangle_{b,42} + \triangle_{b,33}\,\triangle_{b,43} + \triangle_{b,43}\,\triangle_{b,44}) + \triangle_{b,42}\,(\triangle_{b,14}\,\triangle_{b,41} + \triangle_{b,24}\,\triangle_{b,42} + \triangle_{b,34}\,\triangle_{b,43} + \triangle^2_{b,44})))$$

$T_{13} =$

$$\left(\beta_{a,0} + \beta_{a,1}\,\Delta_{a,11} + \beta_{a,2}\left(\Delta_{a,11}^2 + \Delta_{a,12}\,\Delta_{a,21} + \Delta_{a,13}\,\Delta_{a,31} + \Delta_{a,14}\,\Delta_{a,41}\right) + \beta_{a,3}\left(\Delta_{a,11}\left(\Delta_{a,11}^2 + \Delta_{a,12}\,\Delta_{a,21} + \Delta_{a,13}\,\Delta_{a,31} + \Delta_{a,14}\,\Delta_{a,41}\right) + \right.\right.$$
$$\left.\Delta_{a,21}\left(\Delta_{a,11}\,\Delta_{a,12} + \Delta_{a,12}\,\Delta_{a,22} + \Delta_{a,13}\,\Delta_{a,32} + \Delta_{a,14}\,\Delta_{a,42}\right) + \Delta_{a,31}\left(\Delta_{a,11}\,\Delta_{a,13} + \Delta_{a,12}\,\Delta_{a,23} + \Delta_{a,13}\,\Delta_{a,33} + \Delta_{a,14}\,\Delta_{a,43}\right) + \Delta_{a,41}\left(\Delta_{a,11}\,\Delta_{a,14} + \Delta_{a,12}\,\Delta_{a,24} + \Delta_{a,13}\,\Delta_{a,34} + \Delta_{a,14}\,\Delta_{a,44}\right)\right)\right)$$
$$\left(\beta_{b,0} + \beta_{b,1}\,\Delta_{b,13} + \beta_{b,2}\left(\Delta_{b,11}\,\Delta_{b,13} + \Delta_{b,12}\,\Delta_{b,23} + \Delta_{b,13}\,\Delta_{b,33} + \Delta_{b,14}\,\Delta_{b,43}\right) + \beta_{b,3}\left(\Delta_{b,13}\left(\Delta_{b,11}^2 + \Delta_{b,12}\,\Delta_{b,21} + \Delta_{b,13}\,\Delta_{b,31} + \Delta_{b,14}\,\Delta_{b,41}\right) + \Delta_{b,23}\left(\Delta_{b,11}\,\Delta_{b,12} + \Delta_{b,12}\,\Delta_{b,22} + \Delta_{b,13}\,\Delta_{b,32} + \Delta_{b,14}\,\Delta_{b,42}\right) + \right.\right.$$
$$\left.\left.\Delta_{b,33}\left(\Delta_{b,11}\,\Delta_{b,13} + \Delta_{b,12}\,\Delta_{b,23} + \Delta_{b,13}\,\Delta_{b,33} + \Delta_{b,14}\,\Delta_{b,43}\right) + \Delta_{b,43}\left(\Delta_{b,11}\,\Delta_{b,14} + \Delta_{b,12}\,\Delta_{b,24} + \Delta_{b,13}\,\Delta_{b,34} + \Delta_{b,14}\,\Delta_{b,44}\right)\right)\right) +$$
$$\left(\beta_{a,0} + \beta_{a,1}\,\Delta_{a,12} + \beta_{a,2}\left(\Delta_{a,11}\,\Delta_{a,12} + \Delta_{a,12}\,\Delta_{a,22} + \Delta_{a,13}\,\Delta_{a,32} + \Delta_{a,14}\,\Delta_{a,42}\right) + \beta_{a,3}\left(\Delta_{a,12}\left(\Delta_{a,11}^2 + \Delta_{a,12}\,\Delta_{a,21} + \Delta_{a,13}\,\Delta_{a,31} + \Delta_{a,14}\,\Delta_{a,41}\right) + \Delta_{a,22}\left(\Delta_{a,11}\,\Delta_{a,12} + \Delta_{a,12}\,\Delta_{a,22} + \Delta_{a,13}\,\Delta_{a,32} + \Delta_{a,14}\,\Delta_{a,42}\right) + \right.\right.$$
$$\left.\left.\Delta_{a,32}\left(\Delta_{a,11}\,\Delta_{a,13} + \Delta_{a,12}\,\Delta_{a,23} + \Delta_{a,13}\,\Delta_{a,33} + \Delta_{a,14}\,\Delta_{a,43}\right) + \Delta_{a,42}\left(\Delta_{a,11}\,\Delta_{a,14} + \Delta_{a,12}\,\Delta_{a,24} + \Delta_{a,13}\,\Delta_{a,34} + \Delta_{a,14}\,\Delta_{a,44}\right)\right)\right)$$
$$\left(\beta_{b,0} + \beta_{b,1}\,\Delta_{b,23} + \beta_{b,2}\left(\Delta_{b,13}\,\Delta_{b,21} + \Delta_{b,22}\,\Delta_{b,23} + \Delta_{b,23}\,\Delta_{b,33} + \Delta_{b,24}\,\Delta_{b,43}\right) + \beta_{b,3}\left(\Delta_{b,13}\left(\Delta_{b,11}\,\Delta_{b,21} + \Delta_{b,21}\,\Delta_{b,22} + \Delta_{b,23}\,\Delta_{b,31} + \Delta_{b,24}\,\Delta_{b,41}\right) + \right.\right.$$
$$\left.\left.\Delta_{b,23}\left(\Delta_{b,12}\,\Delta_{b,21} + \Delta_{b,22}^2 + \Delta_{b,23}\,\Delta_{b,32} + \Delta_{b,24}\,\Delta_{b,42}\right) + \Delta_{b,33}\left(\Delta_{b,13}\,\Delta_{b,21} + \Delta_{b,22}\,\Delta_{b,23} + \Delta_{b,23}\,\Delta_{b,33} + \Delta_{b,24}\,\Delta_{b,43}\right) + \Delta_{b,43}\left(\Delta_{b,14}\,\Delta_{b,21} + \Delta_{b,22}\,\Delta_{b,24} + \Delta_{b,23}\,\Delta_{b,34} + \Delta_{b,24}\,\Delta_{b,44}\right)\right)\right) +$$
$$\left(\beta_{a,0} + \beta_{a,1}\,\Delta_{a,13} + \beta_{a,2}\left(\Delta_{a,11}\,\Delta_{a,13} + \Delta_{a,12}\,\Delta_{a,23} + \Delta_{a,13}\,\Delta_{a,33} + \Delta_{a,14}\,\Delta_{a,43}\right) + \beta_{a,3}\left(\Delta_{a,13}\left(\Delta_{a,11}^2 + \Delta_{a,12}\,\Delta_{a,21} + \Delta_{a,13}\,\Delta_{a,31} + \Delta_{a,14}\,\Delta_{a,41}\right) + \Delta_{a,23}\left(\Delta_{a,11}\,\Delta_{a,12} + \Delta_{a,12}\,\Delta_{a,22} + \Delta_{a,13}\,\Delta_{a,32} + \Delta_{a,14}\,\Delta_{a,42}\right) + \right.\right.$$
$$\left.\left.\Delta_{a,33}\left(\Delta_{a,11}\,\Delta_{a,13} + \Delta_{a,12}\,\Delta_{a,23} + \Delta_{a,13}\,\Delta_{a,33} + \Delta_{a,14}\,\Delta_{a,43}\right) + \Delta_{a,43}\left(\Delta_{a,11}\,\Delta_{a,14} + \Delta_{a,12}\,\Delta_{a,24} + \Delta_{a,13}\,\Delta_{a,34} + \Delta_{a,14}\,\Delta_{a,44}\right)\right)\right)$$
$$\left(\beta_{b,0} + \beta_{b,1}\,\Delta_{b,33} + \beta_{b,2}\left(\Delta_{b,13}\,\Delta_{b,31} + \Delta_{b,23}\,\Delta_{b,32} + \Delta_{b,33}^2 + \Delta_{b,34}\,\Delta_{b,43}\right) + \beta_{b,3}\left(\Delta_{b,13}\left(\Delta_{b,11}\,\Delta_{b,31} + \Delta_{b,21}\,\Delta_{b,32} + \Delta_{b,31}\,\Delta_{b,33} + \Delta_{b,34}\,\Delta_{b,41}\right) + \Delta_{b,23}\left(\Delta_{b,12}\,\Delta_{b,31} + \Delta_{b,22}\,\Delta_{b,32} + \Delta_{b,32}\,\Delta_{b,33} + \Delta_{b,34}\,\Delta_{b,42}\right) + \right.\right.$$
$$\left.\left.\Delta_{b,33}\left(\Delta_{b,13}\,\Delta_{b,31} + \Delta_{b,23}\,\Delta_{b,32} + \Delta_{b,33}^2 + \Delta_{b,34}\,\Delta_{b,43}\right) + \Delta_{b,43}\left(\Delta_{b,14}\,\Delta_{b,31} + \Delta_{b,24}\,\Delta_{b,32} + \Delta_{b,33}\,\Delta_{b,34} + \Delta_{b,34}\,\Delta_{b,44}\right)\right)\right) +$$
$$\left(\beta_{a,0} + \beta_{a,1}\,\Delta_{a,14} + \beta_{a,2}\left(\Delta_{a,11}\,\Delta_{a,14} + \Delta_{a,12}\,\Delta_{a,24} + \Delta_{a,13}\,\Delta_{a,34} + \Delta_{a,14}\,\Delta_{a,44}\right) + \beta_{a,3}\left(\Delta_{a,14}\left(\Delta_{a,11}^2 + \Delta_{a,12}\,\Delta_{a,21} + \Delta_{a,13}\,\Delta_{a,31} + \Delta_{a,14}\,\Delta_{a,41}\right) + \Delta_{a,24}\left(\Delta_{a,11}\,\Delta_{a,12} + \Delta_{a,12}\,\Delta_{a,22} + \Delta_{a,13}\,\Delta_{a,32} + \Delta_{a,14}\,\Delta_{a,42}\right) + \right.\right.$$
$$\left.\left.\Delta_{a,34}\left(\Delta_{a,11}\,\Delta_{a,13} + \Delta_{a,12}\,\Delta_{a,23} + \Delta_{a,13}\,\Delta_{a,33} + \Delta_{a,14}\,\Delta_{a,43}\right) + \Delta_{a,44}\left(\Delta_{a,11}\,\Delta_{a,14} + \Delta_{a,12}\,\Delta_{a,24} + \Delta_{a,13}\,\Delta_{a,34} + \Delta_{a,14}\,\Delta_{a,44}\right)\right)\right)$$
$$\left(\beta_{b,0} + \beta_{b,1}\,\Delta_{b,43} + \beta_{b,2}\left(\Delta_{b,13}\,\Delta_{b,41} + \Delta_{b,23}\,\Delta_{b,42} + \Delta_{b,33}\,\Delta_{b,43} + \Delta_{b,43}\,\Delta_{b,44}\right) + \beta_{b,3}\left(\Delta_{b,13}\left(\Delta_{b,11}\,\Delta_{b,41} + \Delta_{b,21}\,\Delta_{b,42} + \Delta_{b,31}\,\Delta_{b,43} + \Delta_{b,41}\,\Delta_{b,44}\right) + \right.\right.$$
$$\left.\left.\Delta_{b,23}\left(\Delta_{b,12}\,\Delta_{b,41} + \Delta_{b,22}\,\Delta_{b,42} + \Delta_{b,32}\,\Delta_{b,43} + \Delta_{b,42}\,\Delta_{b,44}\right) + \Delta_{b,33}\left(\Delta_{b,13}\,\Delta_{b,41} + \Delta_{b,23}\,\Delta_{b,42} + \Delta_{b,33}\,\Delta_{b,43} + \Delta_{b,43}\,\Delta_{b,44}\right) + \Delta_{b,43}\left(\Delta_{b,14}\,\Delta_{b,41} + \Delta_{b,24}\,\Delta_{b,42} + \Delta_{b,34}\,\Delta_{b,43} + \Delta_{b,44}^2\right)\right)\right)$$

$T_{14} =$

$$\left(\beta_{a,0} + \beta_{a,1}\,\Delta_{a,11} + \beta_{a,2}\left(\Delta_{a,11}^2 + \Delta_{a,12}\,\Delta_{a,21} + \Delta_{a,13}\,\Delta_{a,31} + \Delta_{a,14}\,\Delta_{a,41}\right) + \beta_{a,3}\left(\Delta_{a,11}\left(\Delta_{a,11}^2 + \Delta_{a,12}\,\Delta_{a,21} + \Delta_{a,13}\,\Delta_{a,31} + \Delta_{a,14}\,\Delta_{a,41}\right) + \right.\right.$$
$$\left.\left.\Delta_{a,21}\left(\Delta_{a,11}\,\Delta_{a,12} + \Delta_{a,12}\,\Delta_{a,22} + \Delta_{a,13}\,\Delta_{a,32} + \Delta_{a,14}\,\Delta_{a,42}\right) + \Delta_{a,31}\left(\Delta_{a,11}\,\Delta_{a,13} + \Delta_{a,12}\,\Delta_{a,23} + \Delta_{a,13}\,\Delta_{a,33} + \Delta_{a,14}\,\Delta_{a,43}\right) + \Delta_{a,41}\left(\Delta_{a,11}\,\Delta_{a,14} + \Delta_{a,12}\,\Delta_{a,24} + \Delta_{a,13}\,\Delta_{a,34} + \Delta_{a,14}\,\Delta_{a,44}\right)\right)\right)$$
$$\left(\beta_{b,0} + \beta_{b,1}\,\Delta_{b,14} + \beta_{b,2}\left(\Delta_{b,11}\,\Delta_{b,14} + \Delta_{b,12}\,\Delta_{b,24} + \Delta_{b,13}\,\Delta_{b,34} + \Delta_{b,14}\,\Delta_{b,44}\right) + \beta_{b,3}\left(\Delta_{b,14}\left(\Delta_{b,11}^2 + \Delta_{b,12}\,\Delta_{b,21} + \Delta_{b,13}\,\Delta_{b,31} + \Delta_{b,14}\,\Delta_{b,41}\right) + \Delta_{b,24}\left(\Delta_{b,11}\,\Delta_{b,12} + \Delta_{b,12}\,\Delta_{b,22} + \Delta_{b,13}\,\Delta_{b,32} + \Delta_{b,14}\,\Delta_{b,42}\right) + \right.\right.$$
$$\left.\left.\Delta_{b,34}\left(\Delta_{b,11}\,\Delta_{b,13} + \Delta_{b,12}\,\Delta_{b,23} + \Delta_{b,13}\,\Delta_{b,33} + \Delta_{b,14}\,\Delta_{b,43}\right) + \Delta_{b,44}\left(\Delta_{b,11}\,\Delta_{b,14} + \Delta_{b,12}\,\Delta_{b,24} + \Delta_{b,13}\,\Delta_{b,34} + \Delta_{b,14}\,\Delta_{b,44}\right)\right)\right) +$$
$$\left(\beta_{a,0} + \beta_{a,1}\,\Delta_{a,12} + \beta_{a,2}\left(\Delta_{a,11}\,\Delta_{a,12} + \Delta_{a,12}\,\Delta_{a,22} + \Delta_{a,13}\,\Delta_{a,32} + \Delta_{a,14}\,\Delta_{a,42}\right) + \beta_{a,3}\left(\Delta_{a,12}\left(\Delta_{a,11}^2 + \Delta_{a,12}\,\Delta_{a,21} + \Delta_{a,13}\,\Delta_{a,31} + \Delta_{a,14}\,\Delta_{a,41}\right) + \Delta_{a,22}\left(\Delta_{a,11}\,\Delta_{a,12} + \Delta_{a,12}\,\Delta_{a,22} + \Delta_{a,13}\,\Delta_{a,32} + \Delta_{a,14}\,\Delta_{a,42}\right) + \right.\right.$$
$$\left.\left.\Delta_{a,32}\left(\Delta_{a,11}\,\Delta_{a,13} + \Delta_{a,12}\,\Delta_{a,23} + \Delta_{a,13}\,\Delta_{a,33} + \Delta_{a,14}\,\Delta_{a,43}\right) + \Delta_{a,42}\left(\Delta_{a,11}\,\Delta_{a,14} + \Delta_{a,12}\,\Delta_{a,24} + \Delta_{a,13}\,\Delta_{a,34} + \Delta_{a,14}\,\Delta_{a,44}\right)\right)\right)$$
$$\left(\beta_{b,0} + \beta_{b,1}\,\Delta_{b,24} + \beta_{b,2}\left(\Delta_{b,14}\,\Delta_{b,21} + \Delta_{b,22}\,\Delta_{b,24} + \Delta_{b,23}\,\Delta_{b,34} + \Delta_{b,24}\,\Delta_{b,44}\right) + \beta_{b,3}\left(\Delta_{b,14}\left(\Delta_{b,11}\,\Delta_{b,21} + \Delta_{b,21}\,\Delta_{b,22} + \Delta_{b,23}\,\Delta_{b,31} + \Delta_{b,24}\,\Delta_{b,41}\right) + \right.\right.$$
$$\left.\left.\Delta_{b,24}\left(\Delta_{b,12}\,\Delta_{b,21} + \Delta_{b,22}^2 + \Delta_{b,23}\,\Delta_{b,32} + \Delta_{b,24}\,\Delta_{b,42}\right) + \Delta_{b,34}\left(\Delta_{b,13}\,\Delta_{b,21} + \Delta_{b,22}\,\Delta_{b,23} + \Delta_{b,23}\,\Delta_{b,33} + \Delta_{b,24}\,\Delta_{b,43}\right) + \Delta_{b,44}\left(\Delta_{b,14}\,\Delta_{b,21} + \Delta_{b,22}\,\Delta_{b,24} + \Delta_{b,23}\,\Delta_{b,34} + \Delta_{b,24}\,\Delta_{b,44}\right)\right)\right) +$$
$$\left(\beta_{a,0} + \beta_{a,1}\,\Delta_{a,13} + \beta_{a,2}\left(\Delta_{a,11}\,\Delta_{a,13} + \Delta_{a,12}\,\Delta_{a,23} + \Delta_{a,13}\,\Delta_{a,33} + \Delta_{a,14}\,\Delta_{a,43}\right) + \beta_{a,3}\left(\Delta_{a,13}\left(\Delta_{a,11}^2 + \Delta_{a,12}\,\Delta_{a,21} + \Delta_{a,13}\,\Delta_{a,31} + \Delta_{a,14}\,\Delta_{a,41}\right) + \Delta_{a,23}\left(\Delta_{a,11}\,\Delta_{a,12} + \Delta_{a,12}\,\Delta_{a,22} + \Delta_{a,13}\,\Delta_{a,32} + \Delta_{a,14}\,\Delta_{a,42}\right) + \right.\right.$$
$$\left.\left.\Delta_{a,33}\left(\Delta_{a,11}\,\Delta_{a,13} + \Delta_{a,12}\,\Delta_{a,23} + \Delta_{a,13}\,\Delta_{a,33} + \Delta_{a,14}\,\Delta_{a,43}\right) + \Delta_{a,43}\left(\Delta_{a,11}\,\Delta_{a,14} + \Delta_{a,12}\,\Delta_{a,24} + \Delta_{a,13}\,\Delta_{a,34} + \Delta_{a,14}\,\Delta_{a,44}\right)\right)\right)$$
$$\left(\beta_{b,0} + \beta_{b,1}\,\Delta_{b,34} + \beta_{b,2}\left(\Delta_{b,14}\,\Delta_{b,31} + \Delta_{b,24}\,\Delta_{b,32} + \Delta_{b,33}\,\Delta_{b,34} + \Delta_{b,34}\,\Delta_{b,44}\right) + \beta_{b,3}\left(\Delta_{b,14}\left(\Delta_{b,11}\,\Delta_{b,31} + \Delta_{b,21}\,\Delta_{b,32} + \Delta_{b,31}\,\Delta_{b,33} + \Delta_{b,34}\,\Delta_{b,41}\right) + \right.\right.$$
$$\left.\left.\Delta_{b,24}\left(\Delta_{b,12}\,\Delta_{b,31} + \Delta_{b,22}\,\Delta_{b,32} + \Delta_{b,32}\,\Delta_{b,33} + \Delta_{b,34}\,\Delta_{b,42}\right) + \Delta_{b,34}\left(\Delta_{b,13}\,\Delta_{b,31} + \Delta_{b,23}\,\Delta_{b,32} + \Delta_{b,33}^2 + \Delta_{b,34}\,\Delta_{b,43}\right) + \Delta_{b,44}\left(\Delta_{b,14}\,\Delta_{b,31} + \Delta_{b,24}\,\Delta_{b,32} + \Delta_{b,33}\,\Delta_{b,34} + \Delta_{b,34}\,\Delta_{b,44}\right)\right)\right) +$$
$$\left(\beta_{a,0} + \beta_{a,1}\,\Delta_{a,14} + \beta_{a,2}\left(\Delta_{a,11}\,\Delta_{a,14} + \Delta_{a,12}\,\Delta_{a,24} + \Delta_{a,13}\,\Delta_{a,34} + \Delta_{a,14}\,\Delta_{a,44}\right) + \beta_{a,3}\left(\Delta_{a,14}\left(\Delta_{a,11}^2 + \Delta_{a,12}\,\Delta_{a,21} + \Delta_{a,13}\,\Delta_{a,31} + \Delta_{a,14}\,\Delta_{a,41}\right) + \Delta_{a,24}\left(\Delta_{a,11}\,\Delta_{a,12} + \Delta_{a,12}\,\Delta_{a,22} + \Delta_{a,13}\,\Delta_{a,32} + \Delta_{a,14}\,\Delta_{a,42}\right) + \right.\right.$$
$$\left.\left.\Delta_{a,34}\left(\Delta_{a,11}\,\Delta_{a,13} + \Delta_{a,12}\,\Delta_{a,23} + \Delta_{a,13}\,\Delta_{a,33} + \Delta_{a,14}\,\Delta_{a,43}\right) + \Delta_{a,44}\left(\Delta_{a,11}\,\Delta_{a,14} + \Delta_{a,12}\,\Delta_{a,24} + \Delta_{a,13}\,\Delta_{a,34} + \Delta_{a,14}\,\Delta_{a,44}\right)\right)\right)$$
$$\left(\beta_{b,0} + \beta_{b,1}\,\Delta_{b,44} + \beta_{b,2}\left(\Delta_{b,14}\,\Delta_{b,41} + \Delta_{b,24}\,\Delta_{b,42} + \Delta_{b,34}\,\Delta_{b,43} + \Delta_{b,44}^2\right) + \beta_{b,3}\left(\Delta_{b,14}\left(\Delta_{b,11}\,\Delta_{b,41} + \Delta_{b,21}\,\Delta_{b,42} + \Delta_{b,31}\,\Delta_{b,43} + \Delta_{b,41}\,\Delta_{b,44}\right) + \Delta_{b,24}\left(\Delta_{b,12}\,\Delta_{b,41} + \Delta_{b,22}\,\Delta_{b,42} + \Delta_{b,32}\,\Delta_{b,43} + \Delta_{b,42}\,\Delta_{b,44}\right) + \right.\right.$$
$$\left.\left.\Delta_{b,34}\left(\Delta_{b,13}\,\Delta_{b,41} + \Delta_{b,23}\,\Delta_{b,42} + \Delta_{b,33}\,\Delta_{b,43} + \Delta_{b,43}\,\Delta_{b,44}\right) + \Delta_{b,44}\left(\Delta_{b,14}\,\Delta_{b,41} + \Delta_{b,24}\,\Delta_{b,42} + \Delta_{b,34}\,\Delta_{b,43} + \Delta_{b,44}^2\right)\right)\right)$$

$$T_{21} =$$

$$\big(\beta_{a,0} + \beta_{a,1}\,\Delta_{a,21} + \beta_{a,2}\,(\Delta_{a,11}\,\Delta_{a,21} + \Delta_{a,21}\,\Delta_{a,22} + \Delta_{a,23}\,\Delta_{a,31} + \Delta_{a,24}\,\Delta_{a,41}) + \beta_{a,3}\,\big(\Delta_{a,11}\,(\Delta_{a,11}\,\Delta_{a,21} + \Delta_{a,21}\,\Delta_{a,22} + \Delta_{a,23}\,\Delta_{a,31} + \Delta_{a,24}\,\Delta_{a,41}) + \Delta_{a,21}\,(\Delta_{a,12}\,\Delta_{a,21} + \Delta_{a,22}^2 + \Delta_{a,23}\,\Delta_{a,32} + \Delta_{a,24}\,\Delta_{a,42}) + \Delta_{a,31}\,(\Delta_{a,13}\,\Delta_{a,21} + \Delta_{a,22}\,\Delta_{a,23} + \Delta_{a,23}\,\Delta_{a,33} + \Delta_{a,24}\,\Delta_{a,43}) + \Delta_{a,41}\,(\Delta_{a,14}\,\Delta_{a,21} + \Delta_{a,22}\,\Delta_{a,24} + \Delta_{a,23}\,\Delta_{a,34} + \Delta_{a,24}\,\Delta_{a,44})\big)\big)$$

$$\big(\beta_{b,0} + \beta_{b,1}\,\Delta_{b,11} + \beta_{b,2}\,(\Delta_{b,11}^2 + \Delta_{b,12}\,\Delta_{b,21} + \Delta_{b,13}\,\Delta_{b,31} + \Delta_{b,14}\,\Delta_{b,41}) + \beta_{b,3}\,\big(\Delta_{b,11}\,(\Delta_{b,11}^2 + \Delta_{b,12}\,\Delta_{b,21} + \Delta_{b,13}\,\Delta_{b,31} + \Delta_{b,14}\,\Delta_{b,41}) + \Delta_{b,21}\,(\Delta_{b,11}\,\Delta_{b,12} + \Delta_{b,12}\,\Delta_{b,22} + \Delta_{b,13}\,\Delta_{b,32} + \Delta_{b,14}\,\Delta_{b,42}) + \Delta_{b,31}\,(\Delta_{b,11}\,\Delta_{b,13} + \Delta_{b,12}\,\Delta_{b,23} + \Delta_{b,13}\,\Delta_{b,33} + \Delta_{b,14}\,\Delta_{b,43}) + \Delta_{b,41}\,(\Delta_{b,11}\,\Delta_{b,14} + \Delta_{b,12}\,\Delta_{b,24} + \Delta_{b,13}\,\Delta_{b,34} + \Delta_{b,14}\,\Delta_{b,44})\big)\big) +$$

$$\big(\beta_{a,0} + \beta_{a,1}\,\Delta_{a,22} + \beta_{a,2}\,(\Delta_{a,12}\,\Delta_{a,21} + \Delta_{a,22}^2 + \Delta_{a,23}\,\Delta_{a,32} + \Delta_{a,24}\,\Delta_{a,42}) + \beta_{a,3}\,\big(\Delta_{a,12}\,(\Delta_{a,11}\,\Delta_{a,21} + \Delta_{a,21}\,\Delta_{a,22} + \Delta_{a,23}\,\Delta_{a,31} + \Delta_{a,24}\,\Delta_{a,41}) + \Delta_{a,22}\,(\Delta_{a,12}\,\Delta_{a,21} + \Delta_{a,22}^2 + \Delta_{a,23}\,\Delta_{a,32} + \Delta_{a,24}\,\Delta_{a,42}) + \Delta_{a,32}\,(\Delta_{a,13}\,\Delta_{a,21} + \Delta_{a,22}\,\Delta_{a,23} + \Delta_{a,23}\,\Delta_{a,33} + \Delta_{a,24}\,\Delta_{a,43}) + \Delta_{a,42}\,(\Delta_{a,14}\,\Delta_{a,21} + \Delta_{a,22}\,\Delta_{a,24} + \Delta_{a,23}\,\Delta_{a,34} + \Delta_{a,24}\,\Delta_{a,44})\big)\big)$$

$$\big(\beta_{b,0} + \beta_{b,1}\,\Delta_{b,21} + \beta_{b,2}\,(\Delta_{b,11}\,\Delta_{b,21} + \Delta_{b,21}\,\Delta_{b,22} + \Delta_{b,23}\,\Delta_{b,31} + \Delta_{b,24}\,\Delta_{b,41}) + \beta_{b,3}\,\big(\Delta_{b,11}\,(\Delta_{b,11}\,\Delta_{b,21} + \Delta_{b,21}\,\Delta_{b,22} + \Delta_{b,23}\,\Delta_{b,31} + \Delta_{b,24}\,\Delta_{b,41}) + \Delta_{b,21}\,(\Delta_{b,12}\,\Delta_{b,21} + \Delta_{b,22}^2 + \Delta_{b,23}\,\Delta_{b,32} + \Delta_{b,24}\,\Delta_{b,42}) + \Delta_{b,31}\,(\Delta_{b,13}\,\Delta_{b,21} + \Delta_{b,22}\,\Delta_{b,23} + \Delta_{b,23}\,\Delta_{b,33} + \Delta_{b,24}\,\Delta_{b,43}) + \Delta_{b,41}\,(\Delta_{b,14}\,\Delta_{b,21} + \Delta_{b,22}\,\Delta_{b,24} + \Delta_{b,23}\,\Delta_{b,34} + \Delta_{b,24}\,\Delta_{b,44})\big)\big) +$$

$$\big(\beta_{a,0} + \beta_{a,1}\,\Delta_{a,23} + \beta_{a,2}\,(\Delta_{a,13}\,\Delta_{a,21} + \Delta_{a,22}\,\Delta_{a,23} + \Delta_{a,23}\,\Delta_{a,33} + \Delta_{a,24}\,\Delta_{a,43}) + \beta_{a,3}\,\big(\Delta_{a,13}\,(\Delta_{a,11}\,\Delta_{a,21} + \Delta_{a,21}\,\Delta_{a,22} + \Delta_{a,23}\,\Delta_{a,31} + \Delta_{a,24}\,\Delta_{a,41}) + \Delta_{a,23}\,(\Delta_{a,12}\,\Delta_{a,21} + \Delta_{a,22}^2 + \Delta_{a,23}\,\Delta_{a,32} + \Delta_{a,24}\,\Delta_{a,42}) + \Delta_{a,33}\,(\Delta_{a,13}\,\Delta_{a,21} + \Delta_{a,22}\,\Delta_{a,23} + \Delta_{a,23}\,\Delta_{a,33} + \Delta_{a,24}\,\Delta_{a,43}) + \Delta_{a,43}\,(\Delta_{a,14}\,\Delta_{a,21} + \Delta_{a,22}\,\Delta_{a,24} + \Delta_{a,23}\,\Delta_{a,34} + \Delta_{a,24}\,\Delta_{a,44})\big)\big)$$

$$\big(\beta_{b,0} + \beta_{b,1}\,\Delta_{b,31} + \beta_{b,2}\,(\Delta_{b,11}\,\Delta_{b,31} + \Delta_{b,21}\,\Delta_{b,32} + \Delta_{b,31}\,\Delta_{b,33} + \Delta_{b,34}\,\Delta_{b,41}) + \beta_{b,3}\,\big(\Delta_{b,11}\,(\Delta_{b,11}\,\Delta_{b,31} + \Delta_{b,21}\,\Delta_{b,32} + \Delta_{b,31}\,\Delta_{b,33} + \Delta_{b,34}\,\Delta_{b,41}) + \Delta_{b,21}\,(\Delta_{b,12}\,\Delta_{b,31} + \Delta_{b,22}\,\Delta_{b,32} + \Delta_{b,32}\,\Delta_{b,33} + \Delta_{b,34}\,\Delta_{b,42}) + \Delta_{b,31}\,(\Delta_{b,13}\,\Delta_{b,31} + \Delta_{b,23}\,\Delta_{b,32} + \Delta_{b,33}^2 + \Delta_{b,34}\,\Delta_{b,43}) + \Delta_{b,41}\,(\Delta_{b,14}\,\Delta_{b,31} + \Delta_{b,24}\,\Delta_{b,32} + \Delta_{b,33}\,\Delta_{b,34} + \Delta_{b,34}\,\Delta_{b,44})\big)\big) +$$

$$\big(\beta_{a,0} + \beta_{a,1}\,\Delta_{a,24} + \beta_{a,2}\,(\Delta_{a,14}\,\Delta_{a,21} + \Delta_{a,22}\,\Delta_{a,24} + \Delta_{a,23}\,\Delta_{a,34} + \Delta_{a,24}\,\Delta_{a,44}) + \beta_{a,3}\,\big(\Delta_{a,14}\,(\Delta_{a,11}\,\Delta_{a,21} + \Delta_{a,21}\,\Delta_{a,22} + \Delta_{a,23}\,\Delta_{a,31} + \Delta_{a,24}\,\Delta_{a,41}) + \Delta_{a,24}\,(\Delta_{a,12}\,\Delta_{a,21} + \Delta_{a,22}^2 + \Delta_{a,23}\,\Delta_{a,32} + \Delta_{a,24}\,\Delta_{a,42}) + \Delta_{a,34}\,(\Delta_{a,13}\,\Delta_{a,21} + \Delta_{a,22}\,\Delta_{a,23} + \Delta_{a,23}\,\Delta_{a,33} + \Delta_{a,24}\,\Delta_{a,43}) + \Delta_{a,44}\,(\Delta_{a,14}\,\Delta_{a,21} + \Delta_{a,22}\,\Delta_{a,24} + \Delta_{a,23}\,\Delta_{a,34} + \Delta_{a,24}\,\Delta_{a,44})\big)\big)$$

$$\big(\beta_{b,0} + \beta_{b,1}\,\Delta_{b,41} + \beta_{b,2}\,(\Delta_{b,11}\,\Delta_{b,41} + \Delta_{b,21}\,\Delta_{b,42} + \Delta_{b,31}\,\Delta_{b,43} + \Delta_{b,41}\,\Delta_{b,44}) + \beta_{b,3}\,\big(\Delta_{b,11}\,(\Delta_{b,11}\,\Delta_{b,41} + \Delta_{b,21}\,\Delta_{b,42} + \Delta_{b,31}\,\Delta_{b,43} + \Delta_{b,41}\,\Delta_{b,44}) + \Delta_{b,21}\,(\Delta_{b,12}\,\Delta_{b,41} + \Delta_{b,22}\,\Delta_{b,42} + \Delta_{b,32}\,\Delta_{b,43} + \Delta_{b,42}\,\Delta_{b,44}) + \Delta_{b,31}\,(\Delta_{b,13}\,\Delta_{b,41} + \Delta_{b,23}\,\Delta_{b,42} + \Delta_{b,33}\,\Delta_{b,43} + \Delta_{b,43}\,\Delta_{b,44}) + \Delta_{b,41}\,(\Delta_{b,14}\,\Delta_{b,41} + \Delta_{b,24}\,\Delta_{b,42} + \Delta_{b,34}\,\Delta_{b,43} + \Delta_{b,44}^2)\big)\big)$$

$$T_{22} =$$

$$\big(\beta_{a,0} + \beta_{a,1}\,\Delta_{a,21} + \beta_{a,2}\,(\Delta_{a,11}\,\Delta_{a,21} + \Delta_{a,21}\,\Delta_{a,22} + \Delta_{a,23}\,\Delta_{a,31} + \Delta_{a,24}\,\Delta_{a,41}) + \beta_{a,3}\,\big(\Delta_{a,11}\,(\Delta_{a,11}\,\Delta_{a,21} + \Delta_{a,21}\,\Delta_{a,22} + \Delta_{a,23}\,\Delta_{a,31} + \Delta_{a,24}\,\Delta_{a,41}) + \Delta_{a,21}\,(\Delta_{a,12}\,\Delta_{a,21} + \Delta_{a,22}^2 + \Delta_{a,23}\,\Delta_{a,32} + \Delta_{a,24}\,\Delta_{a,42}) + \Delta_{a,31}\,(\Delta_{a,13}\,\Delta_{a,21} + \Delta_{a,22}\,\Delta_{a,23} + \Delta_{a,23}\,\Delta_{a,33} + \Delta_{a,24}\,\Delta_{a,43}) + \Delta_{a,41}\,(\Delta_{a,14}\,\Delta_{a,21} + \Delta_{a,22}\,\Delta_{a,24} + \Delta_{a,23}\,\Delta_{a,34} + \Delta_{a,24}\,\Delta_{a,44})\big)\big)$$

$$\big(\beta_{b,0} + \beta_{b,1}\,\Delta_{b,12} + \beta_{b,2}\,(\Delta_{b,11}\,\Delta_{b,12} + \Delta_{b,12}\,\Delta_{b,22} + \Delta_{b,13}\,\Delta_{b,32} + \Delta_{b,14}\,\Delta_{b,42}) + \beta_{b,3}\,\big(\Delta_{b,12}\,(\Delta_{b,11}^2 + \Delta_{b,12}\,\Delta_{b,21} + \Delta_{b,13}\,\Delta_{b,31} + \Delta_{b,14}\,\Delta_{b,41}) + \Delta_{b,22}\,(\Delta_{b,11}\,\Delta_{b,12} + \Delta_{b,12}\,\Delta_{b,22} + \Delta_{b,13}\,\Delta_{b,32} + \Delta_{b,14}\,\Delta_{b,42}) + \Delta_{b,32}\,(\Delta_{b,11}\,\Delta_{b,13} + \Delta_{b,12}\,\Delta_{b,23} + \Delta_{b,13}\,\Delta_{b,33} + \Delta_{b,14}\,\Delta_{b,43}) + \Delta_{b,42}\,(\Delta_{b,11}\,\Delta_{b,14} + \Delta_{b,12}\,\Delta_{b,24} + \Delta_{b,13}\,\Delta_{b,34} + \Delta_{b,14}\,\Delta_{b,44})\big)\big) +$$

$$\big(\beta_{a,0} + \beta_{a,1}\,\Delta_{a,22} + \beta_{a,2}\,(\Delta_{a,12}\,\Delta_{a,21} + \Delta_{a,22}^2 + \Delta_{a,23}\,\Delta_{a,32} + \Delta_{a,24}\,\Delta_{a,42}) + \beta_{a,3}\,\big(\Delta_{a,12}\,(\Delta_{a,11}\,\Delta_{a,21} + \Delta_{a,21}\,\Delta_{a,22} + \Delta_{a,23}\,\Delta_{a,31} + \Delta_{a,24}\,\Delta_{a,41}) + \Delta_{a,22}\,(\Delta_{a,12}\,\Delta_{a,21} + \Delta_{a,22}^2 + \Delta_{a,23}\,\Delta_{a,32} + \Delta_{a,24}\,\Delta_{a,42}) + \Delta_{a,32}\,(\Delta_{a,13}\,\Delta_{a,21} + \Delta_{a,22}\,\Delta_{a,23} + \Delta_{a,23}\,\Delta_{a,33} + \Delta_{a,24}\,\Delta_{a,43}) + \Delta_{a,42}\,(\Delta_{a,14}\,\Delta_{a,21} + \Delta_{a,22}\,\Delta_{a,24} + \Delta_{a,23}\,\Delta_{a,34} + \Delta_{a,24}\,\Delta_{a,44})\big)\big)$$

$$\big(\beta_{b,0} + \beta_{b,1}\,\Delta_{b,22} + \beta_{b,2}\,(\Delta_{b,12}\,\Delta_{b,21} + \Delta_{b,22}^2 + \Delta_{b,23}\,\Delta_{b,32} + \Delta_{b,24}\,\Delta_{b,42}) + \beta_{b,3}\,\big(\Delta_{b,12}\,(\Delta_{b,11}\,\Delta_{b,21} + \Delta_{b,21}\,\Delta_{b,22} + \Delta_{b,23}\,\Delta_{b,31} + \Delta_{b,24}\,\Delta_{b,41}) + \Delta_{b,22}\,(\Delta_{b,12}\,\Delta_{b,21} + \Delta_{b,22}^2 + \Delta_{b,23}\,\Delta_{b,32} + \Delta_{b,24}\,\Delta_{b,42}) + \Delta_{b,32}\,(\Delta_{b,13}\,\Delta_{b,21} + \Delta_{b,22}\,\Delta_{b,23} + \Delta_{b,23}\,\Delta_{b,33} + \Delta_{b,24}\,\Delta_{b,43}) + \Delta_{b,42}\,(\Delta_{b,14}\,\Delta_{b,21} + \Delta_{b,22}\,\Delta_{b,24} + \Delta_{b,23}\,\Delta_{b,34} + \Delta_{b,24}\,\Delta_{b,44})\big)\big) +$$

$$\big(\beta_{a,0} + \beta_{a,1}\,\Delta_{a,23} + \beta_{a,2}\,(\Delta_{a,13}\,\Delta_{a,21} + \Delta_{a,22}\,\Delta_{a,23} + \Delta_{a,23}\,\Delta_{a,33} + \Delta_{a,24}\,\Delta_{a,43}) + \beta_{a,3}\,\big(\Delta_{a,13}\,(\Delta_{a,11}\,\Delta_{a,21} + \Delta_{a,21}\,\Delta_{a,22} + \Delta_{a,23}\,\Delta_{a,31} + \Delta_{a,24}\,\Delta_{a,41}) + \Delta_{a,23}\,(\Delta_{a,12}\,\Delta_{a,21} + \Delta_{a,22}^2 + \Delta_{a,23}\,\Delta_{a,32} + \Delta_{a,24}\,\Delta_{a,42}) + \Delta_{a,33}\,(\Delta_{a,13}\,\Delta_{a,21} + \Delta_{a,22}\,\Delta_{a,23} + \Delta_{a,23}\,\Delta_{a,33} + \Delta_{a,24}\,\Delta_{a,43}) + \Delta_{a,43}\,(\Delta_{a,14}\,\Delta_{a,21} + \Delta_{a,22}\,\Delta_{a,24} + \Delta_{a,23}\,\Delta_{a,34} + \Delta_{a,24}\,\Delta_{a,44})\big)\big)$$

$$\big(\beta_{b,0} + \beta_{b,1}\,\Delta_{b,32} + \beta_{b,2}\,(\Delta_{b,12}\,\Delta_{b,31} + \Delta_{b,22}\,\Delta_{b,32} + \Delta_{b,32}\,\Delta_{b,33} + \Delta_{b,34}\,\Delta_{b,42}) + \beta_{b,3}\,\big(\Delta_{b,12}\,(\Delta_{b,11}\,\Delta_{b,31} + \Delta_{b,21}\,\Delta_{b,32} + \Delta_{b,31}\,\Delta_{b,33} + \Delta_{b,34}\,\Delta_{b,41}) + \Delta_{b,22}\,(\Delta_{b,12}\,\Delta_{b,31} + \Delta_{b,22}\,\Delta_{b,32} + \Delta_{b,32}\,\Delta_{b,33} + \Delta_{b,34}\,\Delta_{b,42}) + \Delta_{b,32}\,(\Delta_{b,13}\,\Delta_{b,31} + \Delta_{b,23}\,\Delta_{b,32} + \Delta_{b,33}^2 + \Delta_{b,34}\,\Delta_{b,43}) + \Delta_{b,42}\,(\Delta_{b,14}\,\Delta_{b,31} + \Delta_{b,24}\,\Delta_{b,32} + \Delta_{b,33}\,\Delta_{b,34} + \Delta_{b,34}\,\Delta_{b,44})\big)\big) +$$

$$\big(\beta_{a,0} + \beta_{a,1}\,\Delta_{a,24} + \beta_{a,2}\,(\Delta_{a,14}\,\Delta_{a,21} + \Delta_{a,22}\,\Delta_{a,24} + \Delta_{a,23}\,\Delta_{a,34} + \Delta_{a,24}\,\Delta_{a,44}) + \beta_{a,3}\,\big(\Delta_{a,14}\,(\Delta_{a,11}\,\Delta_{a,21} + \Delta_{a,21}\,\Delta_{a,22} + \Delta_{a,23}\,\Delta_{a,31} + \Delta_{a,24}\,\Delta_{a,41}) + \Delta_{a,24}\,(\Delta_{a,12}\,\Delta_{a,21} + \Delta_{a,22}^2 + \Delta_{a,23}\,\Delta_{a,32} + \Delta_{a,24}\,\Delta_{a,42}) + \Delta_{a,34}\,(\Delta_{a,13}\,\Delta_{a,21} + \Delta_{a,22}\,\Delta_{a,23} + \Delta_{a,23}\,\Delta_{a,33} + \Delta_{a,24}\,\Delta_{a,43}) + \Delta_{a,44}\,(\Delta_{a,14}\,\Delta_{a,21} + \Delta_{a,22}\,\Delta_{a,24} + \Delta_{a,23}\,\Delta_{a,34} + \Delta_{a,24}\,\Delta_{a,44})\big)\big)$$

$$\big(\beta_{b,0} + \beta_{b,1}\,\Delta_{b,42} + \beta_{b,2}\,(\Delta_{b,12}\,\Delta_{b,41} + \Delta_{b,22}\,\Delta_{b,42} + \Delta_{b,32}\,\Delta_{b,43} + \Delta_{b,42}\,\Delta_{b,44}) + \beta_{b,3}\,\big(\Delta_{b,12}\,(\Delta_{b,11}\,\Delta_{b,41} + \Delta_{b,21}\,\Delta_{b,42} + \Delta_{b,31}\,\Delta_{b,43} + \Delta_{b,41}\,\Delta_{b,44}) + \Delta_{b,22}\,(\Delta_{b,12}\,\Delta_{b,41} + \Delta_{b,22}\,\Delta_{b,42} + \Delta_{b,32}\,\Delta_{b,43} + \Delta_{b,42}\,\Delta_{b,44}) + \Delta_{b,32}\,(\Delta_{b,13}\,\Delta_{b,41} + \Delta_{b,23}\,\Delta_{b,42} + \Delta_{b,33}\,\Delta_{b,43} + \Delta_{b,43}\,\Delta_{b,44}) + \Delta_{b,42}\,(\Delta_{b,14}\,\Delta_{b,41} + \Delta_{b,24}\,\Delta_{b,42} + \Delta_{b,34}\,\Delta_{b,43} + \Delta_{b,44}^2)\big)\big)$$

$$T_{23} =$$

$$\big(\beta_{a,0} + \beta_{a,1}\Delta_{a,21} + \beta_{a,2}(\Delta_{a,11}\Delta_{a,21} + \Delta_{a,21}\Delta_{a,22} + \Delta_{a,23}\Delta_{a,31} + \Delta_{a,24}\Delta_{a,41}) + \beta_{a,3}\big(\Delta_{a,11}(\Delta_{a,11}\Delta_{a,21} + \Delta_{a,21}\Delta_{a,22} + \Delta_{a,23}\Delta_{a,31} + \Delta_{a,24}\Delta_{a,41}) +$$
$$\Delta_{a,21}(\Delta_{a,12}\Delta_{a,21} + \Delta_{a,22}^2 + \Delta_{a,23}\Delta_{a,32} + \Delta_{a,24}\Delta_{a,42}) + \Delta_{a,31}(\Delta_{a,13}\Delta_{a,21} + \Delta_{a,22}\Delta_{a,23} + \Delta_{a,23}\Delta_{a,33} + \Delta_{a,24}\Delta_{a,43}) + \Delta_{a,41}(\Delta_{a,14}\Delta_{a,21} + \Delta_{a,22}\Delta_{a,24} + \Delta_{a,23}\Delta_{a,34} + \Delta_{a,24}\Delta_{a,44})\big)\big)$$
$$\big(\beta_{b,0} + \beta_{b,1}\Delta_{b,13} + \beta_{b,2}(\Delta_{b,11}\Delta_{b,13} + \Delta_{b,12}\Delta_{b,23} + \Delta_{b,13}\Delta_{b,33} + \Delta_{b,14}\Delta_{b,43}) + \beta_{b,3}\big(\Delta_{b,13}(\Delta_{b,11}^2 + \Delta_{b,12}\Delta_{b,21} + \Delta_{b,13}\Delta_{b,31} + \Delta_{b,14}\Delta_{b,41}) + \Delta_{b,23}(\Delta_{b,11}\Delta_{b,12} + \Delta_{b,12}\Delta_{b,22} + \Delta_{b,13}\Delta_{b,32} + \Delta_{b,14}\Delta_{b,42}) +$$
$$\Delta_{b,33}(\Delta_{b,11}\Delta_{b,13} + \Delta_{b,12}\Delta_{b,23} + \Delta_{b,13}\Delta_{b,33} + \Delta_{b,14}\Delta_{b,43}) + \Delta_{b,43}(\Delta_{b,11}\Delta_{b,14} + \Delta_{b,12}\Delta_{b,24} + \Delta_{b,13}\Delta_{b,34} + \Delta_{b,14}\Delta_{b,44})\big)\big) +$$
$$\big(\beta_{a,0} + \beta_{a,1}\Delta_{a,22} + \beta_{a,2}(\Delta_{a,12}\Delta_{a,21} + \Delta_{a,22}^2 + \Delta_{a,23}\Delta_{a,32} + \Delta_{a,24}\Delta_{a,42}) + \beta_{a,3}\big(\Delta_{a,12}(\Delta_{a,11}\Delta_{a,21} + \Delta_{a,21}\Delta_{a,22} + \Delta_{a,23}\Delta_{a,31} + \Delta_{a,24}\Delta_{a,41}) + \Delta_{a,22}(\Delta_{a,12}\Delta_{a,21} + \Delta_{a,22}^2 + \Delta_{a,23}\Delta_{a,32} + \Delta_{a,24}\Delta_{a,42}) +$$
$$\Delta_{a,32}(\Delta_{a,13}\Delta_{a,21} + \Delta_{a,22}\Delta_{a,23} + \Delta_{a,23}\Delta_{a,33} + \Delta_{a,24}\Delta_{a,43}) + \Delta_{a,42}(\Delta_{a,14}\Delta_{a,21} + \Delta_{a,22}\Delta_{a,24} + \Delta_{a,23}\Delta_{a,34} + \Delta_{a,24}\Delta_{a,44})\big)\big)$$
$$\big(\beta_{b,0} + \beta_{b,1}\Delta_{b,23} + \beta_{b,2}(\Delta_{b,13}\Delta_{b,21} + \Delta_{b,22}\Delta_{b,23} + \Delta_{b,23}\Delta_{b,33} + \Delta_{b,24}\Delta_{b,43}) + \beta_{b,3}\big(\Delta_{b,13}(\Delta_{b,11}\Delta_{b,21} + \Delta_{b,21}\Delta_{b,22} + \Delta_{b,23}\Delta_{b,31} + \Delta_{b,24}\Delta_{b,41}) +$$
$$\Delta_{b,23}(\Delta_{b,12}\Delta_{b,21} + \Delta_{b,22}^2 + \Delta_{b,23}\Delta_{b,32} + \Delta_{b,24}\Delta_{b,42}) + \Delta_{b,33}(\Delta_{b,13}\Delta_{b,21} + \Delta_{b,22}\Delta_{b,23} + \Delta_{b,23}\Delta_{b,33} + \Delta_{b,24}\Delta_{b,43}) + \Delta_{b,43}(\Delta_{b,14}\Delta_{b,21} + \Delta_{b,22}\Delta_{b,24} + \Delta_{b,23}\Delta_{b,34} + \Delta_{b,24}\Delta_{b,44})\big)\big) +$$
$$\big(\beta_{a,0} + \beta_{a,1}\Delta_{a,23} + \beta_{a,2}(\Delta_{a,13}\Delta_{a,21} + \Delta_{a,22}\Delta_{a,23} + \Delta_{a,23}\Delta_{a,33} + \Delta_{a,24}\Delta_{a,43}) + \beta_{a,3}\big(\Delta_{a,13}(\Delta_{a,11}\Delta_{a,21} + \Delta_{a,21}\Delta_{a,22} + \Delta_{a,23}\Delta_{a,31} + \Delta_{a,24}\Delta_{a,41}) +$$
$$\Delta_{a,23}(\Delta_{a,12}\Delta_{a,21} + \Delta_{a,22}^2 + \Delta_{a,23}\Delta_{a,32} + \Delta_{a,24}\Delta_{a,42}) + \Delta_{a,33}(\Delta_{a,13}\Delta_{a,21} + \Delta_{a,22}\Delta_{a,23} + \Delta_{a,23}\Delta_{a,33} + \Delta_{a,24}\Delta_{a,43}) + \Delta_{a,43}(\Delta_{a,14}\Delta_{a,21} + \Delta_{a,22}\Delta_{a,24} + \Delta_{a,23}\Delta_{a,34} + \Delta_{a,24}\Delta_{a,44})\big)\big)$$
$$\big(\beta_{b,0} + \beta_{b,1}\Delta_{b,33} + \beta_{b,2}(\Delta_{b,13}\Delta_{b,31} + \Delta_{b,23}\Delta_{b,32} + \Delta_{b,33}^2 + \Delta_{b,34}\Delta_{b,43}) + \beta_{b,3}\big(\Delta_{b,13}(\Delta_{b,11}\Delta_{b,31} + \Delta_{b,21}\Delta_{b,32} + \Delta_{b,31}\Delta_{b,33} + \Delta_{b,34}\Delta_{b,41}) + \Delta_{b,23}(\Delta_{b,12}\Delta_{b,31} + \Delta_{b,22}\Delta_{b,32} + \Delta_{b,32}\Delta_{b,33} + \Delta_{b,34}\Delta_{b,42}) +$$
$$\Delta_{b,33}(\Delta_{b,13}\Delta_{b,31} + \Delta_{b,23}\Delta_{b,32} + \Delta_{b,33}^2 + \Delta_{b,34}\Delta_{b,43}) + \Delta_{b,43}(\Delta_{b,14}\Delta_{b,31} + \Delta_{b,24}\Delta_{b,32} + \Delta_{b,33}\Delta_{b,34} + \Delta_{b,34}\Delta_{b,44})\big)\big) +$$
$$\big(\beta_{a,0} + \beta_{a,1}\Delta_{a,24} + \beta_{a,2}(\Delta_{a,14}\Delta_{a,21} + \Delta_{a,22}\Delta_{a,24} + \Delta_{a,23}\Delta_{a,34} + \Delta_{a,24}\Delta_{a,44}) + \beta_{a,3}\big(\Delta_{a,14}(\Delta_{a,11}\Delta_{a,21} + \Delta_{a,21}\Delta_{a,22} + \Delta_{a,23}\Delta_{a,31} + \Delta_{a,24}\Delta_{a,41}) +$$
$$\Delta_{a,24}(\Delta_{a,12}\Delta_{a,21} + \Delta_{a,22}^2 + \Delta_{a,23}\Delta_{a,32} + \Delta_{a,24}\Delta_{a,42}) + \Delta_{a,34}(\Delta_{a,13}\Delta_{a,21} + \Delta_{a,22}\Delta_{a,23} + \Delta_{a,23}\Delta_{a,33} + \Delta_{a,24}\Delta_{a,43}) + \Delta_{a,44}(\Delta_{a,14}\Delta_{a,21} + \Delta_{a,22}\Delta_{a,24} + \Delta_{a,23}\Delta_{a,34} + \Delta_{a,24}\Delta_{a,44})\big)\big)$$
$$\big(\beta_{b,0} + \beta_{b,1}\Delta_{b,43} + \beta_{b,2}(\Delta_{b,13}\Delta_{b,41} + \Delta_{b,23}\Delta_{b,42} + \Delta_{b,33}\Delta_{b,43} + \Delta_{b,43}\Delta_{b,44}) + \beta_{b,3}\big(\Delta_{b,13}(\Delta_{b,11}\Delta_{b,41} + \Delta_{b,21}\Delta_{b,42} + \Delta_{b,31}\Delta_{b,43} + \Delta_{b,41}\Delta_{b,44}) +$$
$$\Delta_{b,23}(\Delta_{b,12}\Delta_{b,41} + \Delta_{b,22}\Delta_{b,42} + \Delta_{b,32}\Delta_{b,43} + \Delta_{b,42}\Delta_{b,44}) + \Delta_{b,33}(\Delta_{b,13}\Delta_{b,41} + \Delta_{b,23}\Delta_{b,42} + \Delta_{b,33}\Delta_{b,43} + \Delta_{b,43}\Delta_{b,44}) + \Delta_{b,43}(\Delta_{b,14}\Delta_{b,41} + \Delta_{b,24}\Delta_{b,42} + \Delta_{b,34}\Delta_{b,43} + \Delta_{b,44}^2)\big)\big)$$

$$T_{24} =$$

$$\big(\beta_{a,0} + \beta_{a,1}\Delta_{a,21} + \beta_{a,2}(\Delta_{a,11}\Delta_{a,21} + \Delta_{a,21}\Delta_{a,22} + \Delta_{a,23}\Delta_{a,31} + \Delta_{a,24}\Delta_{a,41}) + \beta_{a,3}\big(\Delta_{a,11}(\Delta_{a,11}\Delta_{a,21} + \Delta_{a,21}\Delta_{a,22} + \Delta_{a,23}\Delta_{a,31} + \Delta_{a,24}\Delta_{a,41}) +$$
$$\Delta_{a,21}(\Delta_{a,12}\Delta_{a,21} + \Delta_{a,22}^2 + \Delta_{a,23}\Delta_{a,32} + \Delta_{a,24}\Delta_{a,42}) + \Delta_{a,31}(\Delta_{a,13}\Delta_{a,21} + \Delta_{a,22}\Delta_{a,23} + \Delta_{a,23}\Delta_{a,33} + \Delta_{a,24}\Delta_{a,43}) + \Delta_{a,41}(\Delta_{a,14}\Delta_{a,21} + \Delta_{a,22}\Delta_{a,24} + \Delta_{a,23}\Delta_{a,34} + \Delta_{a,24}\Delta_{a,44})\big)\big)$$
$$\big(\beta_{b,0} + \beta_{b,1}\Delta_{b,14} + \beta_{b,2}(\Delta_{b,11}\Delta_{b,14} + \Delta_{b,12}\Delta_{b,24} + \Delta_{b,13}\Delta_{b,34} + \Delta_{b,14}\Delta_{b,44}) + \beta_{b,3}\big(\Delta_{b,14}(\Delta_{b,11}^2 + \Delta_{b,12}\Delta_{b,21} + \Delta_{b,13}\Delta_{b,31} + \Delta_{b,14}\Delta_{b,41}) + \Delta_{b,24}(\Delta_{b,11}\Delta_{b,12} + \Delta_{b,12}\Delta_{b,22} + \Delta_{b,13}\Delta_{b,32} + \Delta_{b,14}\Delta_{b,42}) +$$
$$\Delta_{b,34}(\Delta_{b,11}\Delta_{b,13} + \Delta_{b,12}\Delta_{b,23} + \Delta_{b,13}\Delta_{b,33} + \Delta_{b,14}\Delta_{b,43}) + \Delta_{b,44}(\Delta_{b,11}\Delta_{b,14} + \Delta_{b,12}\Delta_{b,24} + \Delta_{b,13}\Delta_{b,34} + \Delta_{b,14}\Delta_{b,44})\big)\big) +$$
$$\big(\beta_{a,0} + \beta_{a,1}\Delta_{a,22} + \beta_{a,2}(\Delta_{a,12}\Delta_{a,21} + \Delta_{a,22}^2 + \Delta_{a,23}\Delta_{a,32} + \Delta_{a,24}\Delta_{a,42}) + \beta_{a,3}\big(\Delta_{a,12}(\Delta_{a,11}\Delta_{a,21} + \Delta_{a,21}\Delta_{a,22} + \Delta_{a,23}\Delta_{a,31} + \Delta_{a,24}\Delta_{a,41}) + \Delta_{a,22}(\Delta_{a,12}\Delta_{a,21} + \Delta_{a,22}^2 + \Delta_{a,23}\Delta_{a,32} + \Delta_{a,24}\Delta_{a,42}) +$$
$$\Delta_{a,32}(\Delta_{a,13}\Delta_{a,21} + \Delta_{a,22}\Delta_{a,23} + \Delta_{a,23}\Delta_{a,33} + \Delta_{a,24}\Delta_{a,43}) + \Delta_{a,42}(\Delta_{a,14}\Delta_{a,21} + \Delta_{a,22}\Delta_{a,24} + \Delta_{a,23}\Delta_{a,34} + \Delta_{a,24}\Delta_{a,44})\big)\big)$$
$$\big(\beta_{b,0} + \beta_{b,1}\Delta_{b,24} + \beta_{b,2}(\Delta_{b,14}\Delta_{b,21} + \Delta_{b,22}\Delta_{b,24} + \Delta_{b,23}\Delta_{b,34} + \Delta_{b,24}\Delta_{b,44}) + \beta_{b,3}\big(\Delta_{b,14}(\Delta_{b,11}\Delta_{b,21} + \Delta_{b,21}\Delta_{b,22} + \Delta_{b,23}\Delta_{b,31} + \Delta_{b,24}\Delta_{b,41}) +$$
$$\Delta_{b,24}(\Delta_{b,12}\Delta_{b,21} + \Delta_{b,22}^2 + \Delta_{b,23}\Delta_{b,32} + \Delta_{b,24}\Delta_{b,42}) + \Delta_{b,34}(\Delta_{b,13}\Delta_{b,21} + \Delta_{b,22}\Delta_{b,23} + \Delta_{b,23}\Delta_{b,33} + \Delta_{b,24}\Delta_{b,43}) + \Delta_{b,44}(\Delta_{b,14}\Delta_{b,21} + \Delta_{b,22}\Delta_{b,24} + \Delta_{b,23}\Delta_{b,34} + \Delta_{b,24}\Delta_{b,44})\big)\big) +$$
$$\big(\beta_{a,0} + \beta_{a,1}\Delta_{a,23} + \beta_{a,2}(\Delta_{a,13}\Delta_{a,21} + \Delta_{a,22}\Delta_{a,23} + \Delta_{a,23}\Delta_{a,33} + \Delta_{a,24}\Delta_{a,43}) + \beta_{a,3}\big(\Delta_{a,13}(\Delta_{a,11}\Delta_{a,21} + \Delta_{a,21}\Delta_{a,22} + \Delta_{a,23}\Delta_{a,31} + \Delta_{a,24}\Delta_{a,41}) +$$
$$\Delta_{a,23}(\Delta_{a,12}\Delta_{a,21} + \Delta_{a,22}^2 + \Delta_{a,23}\Delta_{a,32} + \Delta_{a,24}\Delta_{a,42}) + \Delta_{a,33}(\Delta_{a,13}\Delta_{a,21} + \Delta_{a,22}\Delta_{a,23} + \Delta_{a,23}\Delta_{a,33} + \Delta_{a,24}\Delta_{a,43}) + \Delta_{a,43}(\Delta_{a,14}\Delta_{a,21} + \Delta_{a,22}\Delta_{a,24} + \Delta_{a,23}\Delta_{a,34} + \Delta_{a,24}\Delta_{a,44})\big)\big)$$
$$\big(\beta_{b,0} + \beta_{b,1}\Delta_{b,34} + \beta_{b,2}(\Delta_{b,14}\Delta_{b,31} + \Delta_{b,24}\Delta_{b,32} + \Delta_{b,33}\Delta_{b,34} + \Delta_{b,34}\Delta_{b,44}) + \beta_{b,3}\big(\Delta_{b,14}(\Delta_{b,11}\Delta_{b,31} + \Delta_{b,21}\Delta_{b,32} + \Delta_{b,31}\Delta_{b,33} + \Delta_{b,34}\Delta_{b,41}) +$$
$$\Delta_{b,24}(\Delta_{b,12}\Delta_{b,31} + \Delta_{b,22}\Delta_{b,32} + \Delta_{b,32}\Delta_{b,33} + \Delta_{b,34}\Delta_{b,42}) + \Delta_{b,34}(\Delta_{b,13}\Delta_{b,31} + \Delta_{b,23}\Delta_{b,32} + \Delta_{b,33}^2 + \Delta_{b,34}\Delta_{b,43}) + \Delta_{b,44}(\Delta_{b,14}\Delta_{b,31} + \Delta_{b,24}\Delta_{b,32} + \Delta_{b,33}\Delta_{b,34} + \Delta_{b,34}\Delta_{b,44})\big)\big) +$$
$$\big(\beta_{a,0} + \beta_{a,1}\Delta_{a,24} + \beta_{a,2}(\Delta_{a,14}\Delta_{a,21} + \Delta_{a,22}\Delta_{a,24} + \Delta_{a,23}\Delta_{a,34} + \Delta_{a,24}\Delta_{a,44}) + \beta_{a,3}\big(\Delta_{a,14}(\Delta_{a,11}\Delta_{a,21} + \Delta_{a,21}\Delta_{a,22} + \Delta_{a,23}\Delta_{a,31} + \Delta_{a,24}\Delta_{a,41}) +$$
$$\Delta_{a,24}(\Delta_{a,12}\Delta_{a,21} + \Delta_{a,22}^2 + \Delta_{a,23}\Delta_{a,32} + \Delta_{a,24}\Delta_{a,42}) + \Delta_{a,34}(\Delta_{a,13}\Delta_{a,21} + \Delta_{a,22}\Delta_{a,23} + \Delta_{a,23}\Delta_{a,33} + \Delta_{a,24}\Delta_{a,43}) + \Delta_{a,44}(\Delta_{a,14}\Delta_{a,21} + \Delta_{a,22}\Delta_{a,24} + \Delta_{a,23}\Delta_{a,34} + \Delta_{a,24}\Delta_{a,44})\big)\big)$$
$$\big(\beta_{b,0} + \beta_{b,1}\Delta_{b,44} + \beta_{b,2}(\Delta_{b,14}\Delta_{b,41} + \Delta_{b,24}\Delta_{b,42} + \Delta_{b,34}\Delta_{b,43} + \Delta_{b,44}^2) + \beta_{b,3}\big(\Delta_{b,14}(\Delta_{b,11}\Delta_{b,41} + \Delta_{b,21}\Delta_{b,42} + \Delta_{b,31}\Delta_{b,43} + \Delta_{b,41}\Delta_{b,44}) + \Delta_{b,24}(\Delta_{b,12}\Delta_{b,41} + \Delta_{b,22}\Delta_{b,42} + \Delta_{b,32}\Delta_{b,43} + \Delta_{b,42}\Delta_{b,44}) +$$
$$\Delta_{b,34}(\Delta_{b,13}\Delta_{b,41} + \Delta_{b,23}\Delta_{b,42} + \Delta_{b,33}\Delta_{b,43} + \Delta_{b,43}\Delta_{b,44}) + \Delta_{b,44}(\Delta_{b,14}\Delta_{b,41} + \Delta_{b,24}\Delta_{b,42} + \Delta_{b,34}\Delta_{b,43} + \Delta_{b,44}^2)\big)\big)$$

$$T_{31} =$$

$$(\beta_{a,0} + \beta_{a,1}\Delta_{a,31} + \beta_{a,2}(\Delta_{a,11}\Delta_{a,31} + \Delta_{a,21}\Delta_{a,32} + \Delta_{a,31}\Delta_{a,33} + \Delta_{a,34}\Delta_{a,41}) + \beta_{a,3}(\Delta_{a,11}(\Delta_{a,11}\Delta_{a,31} + \Delta_{a,21}\Delta_{a,32} + \Delta_{a,31}\Delta_{a,33} + \Delta_{a,34}\Delta_{a,41}) +$$
$$\Delta_{a,21}(\Delta_{a,12}\Delta_{a,31} + \Delta_{a,22}\Delta_{a,32} + \Delta_{a,32}\Delta_{a,33} + \Delta_{a,34}\Delta_{a,42}) + \Delta_{a,31}(\Delta_{a,13}\Delta_{a,31} + \Delta_{a,23}\Delta_{a,32} + \Delta^2_{a,33} + \Delta_{a,34}\Delta_{a,43}) + \Delta_{a,41}(\Delta_{a,14}\Delta_{a,31} + \Delta_{a,24}\Delta_{a,32} + \Delta_{a,33}\Delta_{a,34} + \Delta_{a,34}\Delta_{a,44})))$$
$$(\beta_{b,0} + \beta_{b,1}\Delta_{b,11} + \beta_{b,2}(\Delta^2_{b,11} + \Delta_{b,12}\Delta_{b,21} + \Delta_{b,13}\Delta_{b,31} + \Delta_{b,14}\Delta_{b,41}) + \beta_{b,3}(\Delta_{b,11}(\Delta^2_{b,11} + \Delta_{b,12}\Delta_{b,21} + \Delta_{b,13}\Delta_{b,31} + \Delta_{b,14}\Delta_{b,41}) + \Delta_{b,21}(\Delta_{b,11}\Delta_{b,12} + \Delta_{b,12}\Delta_{b,22} + \Delta_{b,13}\Delta_{b,32} + \Delta_{b,14}\Delta_{b,42}) +$$
$$\Delta_{b,31}(\Delta_{b,11}\Delta_{b,13} + \Delta_{b,12}\Delta_{b,23} + \Delta_{b,13}\Delta_{b,33} + \Delta_{b,14}\Delta_{b,43}) + \Delta_{b,41}(\Delta_{b,11}\Delta_{b,14} + \Delta_{b,12}\Delta_{b,24} + \Delta_{b,13}\Delta_{b,34} + \Delta_{b,14}\Delta_{b,44}))) +$$

$$(\beta_{a,0} + \beta_{a,1}\Delta_{a,32} + \beta_{a,2}(\Delta_{a,12}\Delta_{a,31} + \Delta_{a,22}\Delta_{a,32} + \Delta_{a,32}\Delta_{a,33} + \Delta_{a,34}\Delta_{a,42}) + \beta_{a,3}(\Delta_{a,12}(\Delta_{a,11}\Delta_{a,31} + \Delta_{a,21}\Delta_{a,32} + \Delta_{a,31}\Delta_{a,33} + \Delta_{a,34}\Delta_{a,41}) +$$
$$\Delta_{a,22}(\Delta_{a,12}\Delta_{a,31} + \Delta_{a,22}\Delta_{a,32} + \Delta_{a,32}\Delta_{a,33} + \Delta_{a,34}\Delta_{a,42}) + \Delta_{a,32}(\Delta_{a,13}\Delta_{a,31} + \Delta_{a,23}\Delta_{a,32} + \Delta^2_{a,33} + \Delta_{a,34}\Delta_{a,43}) + \Delta_{a,42}(\Delta_{a,14}\Delta_{a,31} + \Delta_{a,24}\Delta_{a,32} + \Delta_{a,33}\Delta_{a,34} + \Delta_{a,34}\Delta_{a,44})))$$
$$(\beta_{b,0} + \beta_{b,1}\Delta_{b,21} + \beta_{b,2}(\Delta_{b,11}\Delta_{b,21} + \Delta_{b,21}\Delta_{b,22} + \Delta_{b,23}\Delta_{b,31} + \Delta_{b,24}\Delta_{b,41}) + \beta_{b,3}(\Delta_{b,11}(\Delta_{b,11}\Delta_{b,21} + \Delta_{b,21}\Delta_{b,22} + \Delta_{b,23}\Delta_{b,31} + \Delta_{b,24}\Delta_{b,41}) +$$
$$\Delta_{b,21}(\Delta_{b,12}\Delta_{b,21} + \Delta^2_{b,22} + \Delta_{b,23}\Delta_{b,32} + \Delta_{b,24}\Delta_{b,42}) + \Delta_{b,31}(\Delta_{b,13}\Delta_{b,21} + \Delta_{b,22}\Delta_{b,23} + \Delta_{b,23}\Delta_{b,33} + \Delta_{b,24}\Delta_{b,43}) + \Delta_{b,41}(\Delta_{b,14}\Delta_{b,21} + \Delta_{b,22}\Delta_{b,24} + \Delta_{b,23}\Delta_{b,34} + \Delta_{b,24}\Delta_{b,44}))) +$$

$$(\beta_{a,0} + \beta_{a,1}\Delta_{a,33} + \beta_{a,2}(\Delta_{a,13}\Delta_{a,31} + \Delta_{a,23}\Delta_{a,32} + \Delta^2_{a,33} + \Delta_{a,34}\Delta_{a,43}) + \beta_{a,3}(\Delta_{a,13}(\Delta_{a,11}\Delta_{a,31} + \Delta_{a,21}\Delta_{a,32} + \Delta_{a,31}\Delta_{a,33} + \Delta_{a,34}\Delta_{a,41}) + \Delta_{a,23}(\Delta_{a,12}\Delta_{a,31} + \Delta_{a,22}\Delta_{a,32} + \Delta_{a,32}\Delta_{a,33} + \Delta_{a,34}\Delta_{a,42}) +$$
$$\Delta_{a,33}(\Delta_{a,13}\Delta_{a,31} + \Delta_{a,23}\Delta_{a,32} + \Delta^2_{a,33} + \Delta_{a,34}\Delta_{a,43}) + \Delta_{a,43}(\Delta_{a,14}\Delta_{a,31} + \Delta_{a,24}\Delta_{a,32} + \Delta_{a,33}\Delta_{a,34} + \Delta_{a,34}\Delta_{a,44})))$$
$$(\beta_{b,0} + \beta_{b,1}\Delta_{b,31} + \beta_{b,2}(\Delta_{b,11}\Delta_{b,31} + \Delta_{b,21}\Delta_{b,32} + \Delta_{b,31}\Delta_{b,33} + \Delta_{b,34}\Delta_{b,41}) + \beta_{b,3}(\Delta_{b,11}(\Delta_{b,11}\Delta_{b,31} + \Delta_{b,21}\Delta_{b,32} + \Delta_{b,31}\Delta_{b,33} + \Delta_{b,34}\Delta_{b,41}) +$$
$$\Delta_{b,21}(\Delta_{b,12}\Delta_{b,31} + \Delta_{b,22}\Delta_{b,32} + \Delta_{b,32}\Delta_{b,33} + \Delta_{b,34}\Delta_{b,42}) + \Delta_{b,31}(\Delta_{b,13}\Delta_{b,31} + \Delta_{b,23}\Delta_{b,32} + \Delta^2_{b,33} + \Delta_{b,34}\Delta_{b,43}) + \Delta_{b,41}(\Delta_{b,14}\Delta_{b,31} + \Delta_{b,24}\Delta_{b,32} + \Delta_{b,33}\Delta_{b,34} + \Delta_{b,34}\Delta_{b,44}))) +$$

$$(\beta_{a,0} + \beta_{a,1}\Delta_{a,34} + \beta_{a,2}(\Delta_{a,14}\Delta_{a,31} + \Delta_{a,24}\Delta_{a,32} + \Delta_{a,33}\Delta_{a,34} + \Delta_{a,34}\Delta_{a,44}) + \beta_{a,3}(\Delta_{a,14}(\Delta_{a,11}\Delta_{a,31} + \Delta_{a,21}\Delta_{a,32} + \Delta_{a,31}\Delta_{a,33} + \Delta_{a,34}\Delta_{a,41}) +$$
$$\Delta_{a,24}(\Delta_{a,12}\Delta_{a,31} + \Delta_{a,22}\Delta_{a,32} + \Delta_{a,32}\Delta_{a,33} + \Delta_{a,34}\Delta_{a,42}) + \Delta_{a,34}(\Delta_{a,13}\Delta_{a,31} + \Delta_{a,23}\Delta_{a,32} + \Delta^2_{a,33} + \Delta_{a,34}\Delta_{a,43}) + \Delta_{a,44}(\Delta_{a,14}\Delta_{a,31} + \Delta_{a,24}\Delta_{a,32} + \Delta_{a,33}\Delta_{a,34} + \Delta_{a,34}\Delta_{a,44})))$$
$$(\beta_{b,0} + \beta_{b,1}\Delta_{b,41} + \beta_{b,2}(\Delta_{b,11}\Delta_{b,41} + \Delta_{b,21}\Delta_{b,42} + \Delta_{b,31}\Delta_{b,43} + \Delta_{b,41}\Delta_{b,44}) + \beta_{b,3}(\Delta_{b,11}(\Delta_{b,11}\Delta_{b,41} + \Delta_{b,21}\Delta_{b,42} + \Delta_{b,31}\Delta_{b,43} + \Delta_{b,41}\Delta_{b,44}) +$$
$$\Delta_{b,21}(\Delta_{b,12}\Delta_{b,41} + \Delta_{b,22}\Delta_{b,42} + \Delta_{b,32}\Delta_{b,43} + \Delta_{b,42}\Delta_{b,44}) + \Delta_{b,31}(\Delta_{b,13}\Delta_{b,41} + \Delta_{b,23}\Delta_{b,42} + \Delta_{b,33}\Delta_{b,43} + \Delta_{b,43}\Delta_{b,44}) + \Delta_{b,41}(\Delta_{b,14}\Delta_{b,41} + \Delta_{b,24}\Delta_{b,42} + \Delta_{b,34}\Delta_{b,43} + \Delta^2_{b,44})))$$

$$T_{32} =$$

$$(\beta_{a,0} + \beta_{a,1}\Delta_{a,31} + \beta_{a,2}(\Delta_{a,11}\Delta_{a,31} + \Delta_{a,21}\Delta_{a,32} + \Delta_{a,31}\Delta_{a,33} + \Delta_{a,34}\Delta_{a,41}) + \beta_{a,3}(\Delta_{a,11}(\Delta_{a,11}\Delta_{a,31} + \Delta_{a,21}\Delta_{a,32} + \Delta_{a,31}\Delta_{a,33} + \Delta_{a,34}\Delta_{a,41}) +$$
$$\Delta_{a,21}(\Delta_{a,12}\Delta_{a,31} + \Delta_{a,22}\Delta_{a,32} + \Delta_{a,32}\Delta_{a,33} + \Delta_{a,34}\Delta_{a,42}) + \Delta_{a,31}(\Delta_{a,13}\Delta_{a,31} + \Delta_{a,23}\Delta_{a,32} + \Delta^2_{a,33} + \Delta_{a,34}\Delta_{a,43}) + \Delta_{a,41}(\Delta_{a,14}\Delta_{a,31} + \Delta_{a,24}\Delta_{a,32} + \Delta_{a,33}\Delta_{a,34} + \Delta_{a,34}\Delta_{a,44})))$$
$$(\beta_{b,0} + \beta_{b,1}\Delta_{b,12} + \beta_{b,2}(\Delta_{b,11}\Delta_{b,12} + \Delta_{b,12}\Delta_{b,22} + \Delta_{b,13}\Delta_{b,32} + \Delta_{b,14}\Delta_{b,42}) + \beta_{b,3}(\Delta_{b,12}(\Delta^2_{b,11} + \Delta_{b,12}\Delta_{b,21} + \Delta_{b,13}\Delta_{b,31} + \Delta_{b,14}\Delta_{b,41}) + \Delta_{b,22}(\Delta_{b,11}\Delta_{b,12} + \Delta_{b,12}\Delta_{b,22} + \Delta_{b,13}\Delta_{b,32} + \Delta_{b,14}\Delta_{b,42}) +$$
$$\Delta_{b,32}(\Delta_{b,11}\Delta_{b,13} + \Delta_{b,12}\Delta_{b,23} + \Delta_{b,13}\Delta_{b,33} + \Delta_{b,14}\Delta_{b,43}) + \Delta_{b,42}(\Delta_{b,11}\Delta_{b,14} + \Delta_{b,12}\Delta_{b,24} + \Delta_{b,13}\Delta_{b,34} + \Delta_{b,14}\Delta_{b,44}))) +$$

$$(\beta_{a,0} + \beta_{a,1}\Delta_{a,32} + \beta_{a,2}(\Delta_{a,12}\Delta_{a,31} + \Delta_{a,22}\Delta_{a,32} + \Delta_{a,32}\Delta_{a,33} + \Delta_{a,34}\Delta_{a,42}) + \beta_{a,3}(\Delta_{a,12}(\Delta_{a,11}\Delta_{a,31} + \Delta_{a,21}\Delta_{a,32} + \Delta_{a,31}\Delta_{a,33} + \Delta_{a,34}\Delta_{a,41}) +$$
$$\Delta_{a,22}(\Delta_{a,12}\Delta_{a,31} + \Delta_{a,22}\Delta_{a,32} + \Delta_{a,32}\Delta_{a,33} + \Delta_{a,34}\Delta_{a,42}) + \Delta_{a,32}(\Delta_{a,13}\Delta_{a,31} + \Delta_{a,23}\Delta_{a,32} + \Delta^2_{a,33} + \Delta_{a,34}\Delta_{a,43}) + \Delta_{a,42}(\Delta_{a,14}\Delta_{a,31} + \Delta_{a,24}\Delta_{a,32} + \Delta_{a,33}\Delta_{a,34} + \Delta_{a,34}\Delta_{a,44})))$$
$$(\beta_{b,0} + \beta_{b,1}\Delta_{b,22} + \beta_{b,2}(\Delta_{b,12}\Delta_{b,21} + \Delta^2_{b,22} + \Delta_{b,23}\Delta_{b,32} + \Delta_{b,24}\Delta_{b,42}) + \beta_{b,3}(\Delta_{b,12}(\Delta_{b,11}\Delta_{b,21} + \Delta_{b,21}\Delta_{b,22} + \Delta_{b,23}\Delta_{b,31} + \Delta_{b,24}\Delta_{b,41}) + \Delta_{b,22}(\Delta_{b,12}\Delta_{b,21} + \Delta^2_{b,22} + \Delta_{b,23}\Delta_{b,32} + \Delta_{b,24}\Delta_{b,42}) +$$
$$\Delta_{b,32}(\Delta_{b,13}\Delta_{b,21} + \Delta_{b,22}\Delta_{b,23} + \Delta_{b,23}\Delta_{b,33} + \Delta_{b,24}\Delta_{b,43}) + \Delta_{b,42}(\Delta_{b,14}\Delta_{b,21} + \Delta_{b,22}\Delta_{b,24} + \Delta_{b,23}\Delta_{b,34} + \Delta_{b,24}\Delta_{b,44}))) +$$

$$(\beta_{a,0} + \beta_{a,1}\Delta_{a,33} + \beta_{a,2}(\Delta_{a,13}\Delta_{a,31} + \Delta_{a,23}\Delta_{a,32} + \Delta^2_{a,33} + \Delta_{a,34}\Delta_{a,43}) + \beta_{a,3}(\Delta_{a,13}(\Delta_{a,11}\Delta_{a,31} + \Delta_{a,21}\Delta_{a,32} + \Delta_{a,31}\Delta_{a,33} + \Delta_{a,34}\Delta_{a,41}) + \Delta_{a,23}(\Delta_{a,12}\Delta_{a,31} + \Delta_{a,22}\Delta_{a,32} + \Delta_{a,32}\Delta_{a,33} + \Delta_{a,34}\Delta_{a,42}) +$$
$$\Delta_{a,33}(\Delta_{a,13}\Delta_{a,31} + \Delta_{a,23}\Delta_{a,32} + \Delta^2_{a,33} + \Delta_{a,34}\Delta_{a,43}) + \Delta_{a,43}(\Delta_{a,14}\Delta_{a,31} + \Delta_{a,24}\Delta_{a,32} + \Delta_{a,33}\Delta_{a,34} + \Delta_{a,34}\Delta_{a,44})))$$
$$(\beta_{b,0} + \beta_{b,1}\Delta_{b,32} + \beta_{b,2}(\Delta_{b,12}\Delta_{b,31} + \Delta_{b,22}\Delta_{b,32} + \Delta_{b,32}\Delta_{b,33} + \Delta_{b,34}\Delta_{b,42}) + \beta_{b,3}(\Delta_{b,12}(\Delta_{b,11}\Delta_{b,31} + \Delta_{b,21}\Delta_{b,32} + \Delta_{b,31}\Delta_{b,33} + \Delta_{b,34}\Delta_{b,41}) +$$
$$\Delta_{b,22}(\Delta_{b,12}\Delta_{b,31} + \Delta_{b,22}\Delta_{b,32} + \Delta_{b,32}\Delta_{b,33} + \Delta_{b,34}\Delta_{b,42}) + \Delta_{b,32}(\Delta_{b,13}\Delta_{b,31} + \Delta_{b,23}\Delta_{b,32} + \Delta^2_{b,33} + \Delta_{b,34}\Delta_{b,43}) + \Delta_{b,42}(\Delta_{b,14}\Delta_{b,31} + \Delta_{b,24}\Delta_{b,32} + \Delta_{b,33}\Delta_{b,34} + \Delta_{b,34}\Delta_{b,44}))) +$$

$$(\beta_{a,0} + \beta_{a,1}\Delta_{a,34} + \beta_{a,2}(\Delta_{a,14}\Delta_{a,31} + \Delta_{a,24}\Delta_{a,32} + \Delta_{a,33}\Delta_{a,34} + \Delta_{a,34}\Delta_{a,44}) + \beta_{a,3}(\Delta_{a,14}(\Delta_{a,11}\Delta_{a,31} + \Delta_{a,21}\Delta_{a,32} + \Delta_{a,31}\Delta_{a,33} + \Delta_{a,34}\Delta_{a,41}) +$$
$$\Delta_{a,24}(\Delta_{a,12}\Delta_{a,31} + \Delta_{a,22}\Delta_{a,32} + \Delta_{a,32}\Delta_{a,33} + \Delta_{a,34}\Delta_{a,42}) + \Delta_{a,34}(\Delta_{a,13}\Delta_{a,31} + \Delta_{a,23}\Delta_{a,32} + \Delta^2_{a,33} + \Delta_{a,34}\Delta_{a,43}) + \Delta_{a,44}(\Delta_{a,14}\Delta_{a,31} + \Delta_{a,24}\Delta_{a,32} + \Delta_{a,33}\Delta_{a,34} + \Delta_{a,34}\Delta_{a,44})))$$
$$(\beta_{b,0} + \beta_{b,1}\Delta_{b,42} + \beta_{b,2}(\Delta_{b,12}\Delta_{b,41} + \Delta_{b,22}\Delta_{b,42} + \Delta_{b,32}\Delta_{b,43} + \Delta_{b,42}\Delta_{b,44}) + \beta_{b,3}(\Delta_{b,12}(\Delta_{b,11}\Delta_{b,41} + \Delta_{b,21}\Delta_{b,42} + \Delta_{b,31}\Delta_{b,43} + \Delta_{b,41}\Delta_{b,44}) +$$
$$\Delta_{b,22}(\Delta_{b,12}\Delta_{b,41} + \Delta_{b,22}\Delta_{b,42} + \Delta_{b,32}\Delta_{b,43} + \Delta_{b,42}\Delta_{b,44}) + \Delta_{b,32}(\Delta_{b,13}\Delta_{b,41} + \Delta_{b,23}\Delta_{b,42} + \Delta_{b,33}\Delta_{b,43} + \Delta_{b,43}\Delta_{b,44}) + \Delta_{b,42}(\Delta_{b,14}\Delta_{b,41} + \Delta_{b,24}\Delta_{b,42} + \Delta_{b,34}\Delta_{b,43} + \Delta^2_{b,44})))$$

$T_{33} =$

$(\beta_{a,0} + \beta_{a,1}\,\triangle_{a,31} + \beta_{a,2}\,(\triangle_{a,11}\,\triangle_{a,31} + \triangle_{a,21}\,\triangle_{a,32} + \triangle_{a,31}\,\triangle_{a,33} + \triangle_{a,34}\,\triangle_{a,41}) + \beta_{a,3}\,(\triangle_{a,11}\,(\triangle_{a,11}\,\triangle_{a,31} + \triangle_{a,21}\,\triangle_{a,32} + \triangle_{a,31}\,\triangle_{a,33} + \triangle_{a,34}\,\triangle_{a,41}) +$
$\quad \triangle_{a,21}\,(\triangle_{a,12}\,\triangle_{a,31} + \triangle_{a,22}\,\triangle_{a,32} + \triangle_{a,32}\,\triangle_{a,33} + \triangle_{a,34}\,\triangle_{a,42}) + \triangle_{a,31}\,(\triangle_{a,13}\,\triangle_{a,31} + \triangle_{a,23}\,\triangle_{a,32} + \triangle_{a,33}^2 + \triangle_{a,34}\,\triangle_{a,43}) + \triangle_{a,41}\,(\triangle_{a,14}\,\triangle_{a,31} + \triangle_{a,24}\,\triangle_{a,32} + \triangle_{a,33}\,\triangle_{a,34} + \triangle_{a,34}\,\triangle_{a,44})))$
$(\beta_{b,0} + \beta_{b,1}\,\triangle_{b,13} + \beta_{b,2}\,(\triangle_{b,11}\,\triangle_{b,13} + \triangle_{b,12}\,\triangle_{b,23} + \triangle_{b,13}\,\triangle_{b,33} + \triangle_{b,14}\,\triangle_{b,43}) + \beta_{b,3}\,(\triangle_{b,13}\,(\triangle_{b,11}^2 + \triangle_{b,12}\,\triangle_{b,21} + \triangle_{b,13}\,\triangle_{b,31} + \triangle_{b,14}\,\triangle_{b,41}) + \triangle_{b,23}\,(\triangle_{b,11}\,\triangle_{b,12} + \triangle_{b,12}\,\triangle_{b,22} + \triangle_{b,13}\,\triangle_{b,32} + \triangle_{b,14}\,\triangle_{b,42}) +$
$\quad \triangle_{b,33}\,(\triangle_{b,11}\,\triangle_{b,13} + \triangle_{b,12}\,\triangle_{b,23} + \triangle_{b,13}\,\triangle_{b,33} + \triangle_{b,14}\,\triangle_{b,43}) + \triangle_{b,43}\,(\triangle_{b,11}\,\triangle_{b,14} + \triangle_{b,12}\,\triangle_{b,24} + \triangle_{b,13}\,\triangle_{b,34} + \triangle_{b,14}\,\triangle_{b,44})))\ +$
$(\beta_{a,0} + \beta_{a,1}\,\triangle_{a,32} + \beta_{a,2}\,(\triangle_{a,12}\,\triangle_{a,31} + \triangle_{a,22}\,\triangle_{a,32} + \triangle_{a,32}\,\triangle_{a,33} + \triangle_{a,34}\,\triangle_{a,42}) + \beta_{a,3}\,(\triangle_{a,12}\,(\triangle_{a,11}\,\triangle_{a,31} + \triangle_{a,21}\,\triangle_{a,32} + \triangle_{a,31}\,\triangle_{a,33} + \triangle_{a,34}\,\triangle_{a,41}) +$
$\quad \triangle_{a,22}\,(\triangle_{a,12}\,\triangle_{a,31} + \triangle_{a,22}\,\triangle_{a,32} + \triangle_{a,32}\,\triangle_{a,33} + \triangle_{a,34}\,\triangle_{a,42}) + \triangle_{a,32}\,(\triangle_{a,13}\,\triangle_{a,31} + \triangle_{a,23}\,\triangle_{a,32} + \triangle_{a,33}^2 + \triangle_{a,34}\,\triangle_{a,43}) + \triangle_{a,42}\,(\triangle_{a,14}\,\triangle_{a,31} + \triangle_{a,24}\,\triangle_{a,32} + \triangle_{a,33}\,\triangle_{a,34} + \triangle_{a,34}\,\triangle_{a,44})))$
$(\beta_{b,0} + \beta_{b,1}\,\triangle_{b,23} + \beta_{b,2}\,(\triangle_{b,13}\,\triangle_{b,21} + \triangle_{b,22}\,\triangle_{b,23} + \triangle_{b,23}\,\triangle_{b,33} + \triangle_{b,24}\,\triangle_{b,43}) + \beta_{b,3}\,(\triangle_{b,13}\,(\triangle_{b,11}\,\triangle_{b,21} + \triangle_{b,21}\,\triangle_{b,22} + \triangle_{b,23}\,\triangle_{b,31} + \triangle_{b,24}\,\triangle_{b,41}) +$
$\quad \triangle_{b,23}\,(\triangle_{b,12}\,\triangle_{b,21} + \triangle_{b,22}^2 + \triangle_{b,23}\,\triangle_{b,32} + \triangle_{b,24}\,\triangle_{b,42}) + \triangle_{b,33}\,(\triangle_{b,13}\,\triangle_{b,21} + \triangle_{b,22}\,\triangle_{b,23} + \triangle_{b,23}\,\triangle_{b,33} + \triangle_{b,24}\,\triangle_{b,43}) + \triangle_{b,43}\,(\triangle_{b,14}\,\triangle_{b,21} + \triangle_{b,22}\,\triangle_{b,24} + \triangle_{b,23}\,\triangle_{b,34} + \triangle_{b,24}\,\triangle_{b,44})))\ +$
$(\beta_{a,0} + \beta_{a,1}\,\triangle_{a,33} + \beta_{a,2}\,(\triangle_{a,13}\,\triangle_{a,31} + \triangle_{a,23}\,\triangle_{a,32} + \triangle_{a,33}^2 + \triangle_{a,34}\,\triangle_{a,43}) + \beta_{a,3}\,(\triangle_{a,13}\,(\triangle_{a,11}\,\triangle_{a,31} + \triangle_{a,21}\,\triangle_{a,32} + \triangle_{a,31}\,\triangle_{a,33} + \triangle_{a,34}\,\triangle_{a,41}) + \triangle_{a,23}\,(\triangle_{a,12}\,\triangle_{a,31} + \triangle_{a,22}\,\triangle_{a,32} + \triangle_{a,32}\,\triangle_{a,33} + \triangle_{a,34}\,\triangle_{a,42}) +$
$\quad \triangle_{a,33}\,(\triangle_{a,13}\,\triangle_{a,31} + \triangle_{a,23}\,\triangle_{a,32} + \triangle_{a,33}^2 + \triangle_{a,34}\,\triangle_{a,43}) + \triangle_{a,43}\,(\triangle_{a,14}\,\triangle_{a,31} + \triangle_{a,24}\,\triangle_{a,32} + \triangle_{a,33}\,\triangle_{a,34} + \triangle_{a,34}\,\triangle_{a,44})))$
$(\beta_{b,0} + \beta_{b,1}\,\triangle_{b,33} + \beta_{b,2}\,(\triangle_{b,13}\,\triangle_{b,31} + \triangle_{b,23}\,\triangle_{b,32} + \triangle_{b,33}^2 + \triangle_{b,34}\,\triangle_{b,43}) + \beta_{b,3}\,(\triangle_{b,13}\,(\triangle_{b,11}\,\triangle_{b,31} + \triangle_{b,21}\,\triangle_{b,32} + \triangle_{b,31}\,\triangle_{b,33} + \triangle_{b,34}\,\triangle_{b,41}) + \triangle_{b,23}\,(\triangle_{b,12}\,\triangle_{b,31} + \triangle_{b,22}\,\triangle_{b,32} + \triangle_{b,32}\,\triangle_{b,33} + \triangle_{b,34}\,\triangle_{b,42}) +$
$\quad \triangle_{b,33}\,(\triangle_{b,13}\,\triangle_{b,31} + \triangle_{b,23}\,\triangle_{b,32} + \triangle_{b,33}^2 + \triangle_{b,34}\,\triangle_{b,43}) + \triangle_{b,43}\,(\triangle_{b,14}\,\triangle_{b,31} + \triangle_{b,24}\,\triangle_{b,32} + \triangle_{b,33}\,\triangle_{b,34} + \triangle_{b,34}\,\triangle_{b,44})))\ +$
$(\beta_{a,0} + \beta_{a,1}\,\triangle_{a,34} + \beta_{a,2}\,(\triangle_{a,14}\,\triangle_{a,31} + \triangle_{a,24}\,\triangle_{a,32} + \triangle_{a,33}\,\triangle_{a,34} + \triangle_{a,34}\,\triangle_{a,44}) + \beta_{a,3}\,(\triangle_{a,14}\,(\triangle_{a,11}\,\triangle_{a,31} + \triangle_{a,21}\,\triangle_{a,32} + \triangle_{a,31}\,\triangle_{a,33} + \triangle_{a,34}\,\triangle_{a,41}) +$
$\quad \triangle_{a,24}\,(\triangle_{a,12}\,\triangle_{a,31} + \triangle_{a,22}\,\triangle_{a,32} + \triangle_{a,32}\,\triangle_{a,33} + \triangle_{a,34}\,\triangle_{a,42}) + \triangle_{a,34}\,(\triangle_{a,13}\,\triangle_{a,31} + \triangle_{a,23}\,\triangle_{a,32} + \triangle_{a,33}^2 + \triangle_{a,34}\,\triangle_{a,43}) + \triangle_{a,44}\,(\triangle_{a,14}\,\triangle_{a,31} + \triangle_{a,24}\,\triangle_{a,32} + \triangle_{a,33}\,\triangle_{a,34} + \triangle_{a,34}\,\triangle_{a,44})))$
$(\beta_{b,0} + \beta_{b,1}\,\triangle_{b,43} + \beta_{b,2}\,(\triangle_{b,13}\,\triangle_{b,41} + \triangle_{b,23}\,\triangle_{b,42} + \triangle_{b,33}\,\triangle_{b,43} + \triangle_{b,43}\,\triangle_{b,44}) + \beta_{b,3}\,(\triangle_{b,13}\,(\triangle_{b,11}\,\triangle_{b,41} + \triangle_{b,21}\,\triangle_{b,42} + \triangle_{b,31}\,\triangle_{b,43} + \triangle_{b,41}\,\triangle_{b,44}) +$
$\quad \triangle_{b,23}\,(\triangle_{b,12}\,\triangle_{b,41} + \triangle_{b,22}\,\triangle_{b,42} + \triangle_{b,32}\,\triangle_{b,43} + \triangle_{b,42}\,\triangle_{b,44}) + \triangle_{b,33}\,(\triangle_{b,13}\,\triangle_{b,41} + \triangle_{b,23}\,\triangle_{b,42} + \triangle_{b,33}\,\triangle_{b,43} + \triangle_{b,43}\,\triangle_{b,44}) + \triangle_{b,43}\,(\triangle_{b,14}\,\triangle_{b,41} + \triangle_{b,24}\,\triangle_{b,42} + \triangle_{b,34}\,\triangle_{b,43} + \triangle_{b,44}^2)))$

$T_{34} =$

$(\beta_{a,0} + \beta_{a,1}\,\triangle_{a,31} + \beta_{a,2}\,(\triangle_{a,11}\,\triangle_{a,31} + \triangle_{a,21}\,\triangle_{a,32} + \triangle_{a,31}\,\triangle_{a,33} + \triangle_{a,34}\,\triangle_{a,41}) + \beta_{a,3}\,(\triangle_{a,11}\,(\triangle_{a,11}\,\triangle_{a,31} + \triangle_{a,21}\,\triangle_{a,32} + \triangle_{a,31}\,\triangle_{a,33} + \triangle_{a,34}\,\triangle_{a,41}) +$
$\quad \triangle_{a,21}\,(\triangle_{a,12}\,\triangle_{a,31} + \triangle_{a,22}\,\triangle_{a,32} + \triangle_{a,32}\,\triangle_{a,33} + \triangle_{a,34}\,\triangle_{a,42}) + \triangle_{a,31}\,(\triangle_{a,13}\,\triangle_{a,31} + \triangle_{a,23}\,\triangle_{a,32} + \triangle_{a,33}^2 + \triangle_{a,34}\,\triangle_{a,43}) + \triangle_{a,41}\,(\triangle_{a,14}\,\triangle_{a,31} + \triangle_{a,24}\,\triangle_{a,32} + \triangle_{a,33}\,\triangle_{a,34} + \triangle_{a,34}\,\triangle_{a,44})))$
$(\beta_{b,0} + \beta_{b,1}\,\triangle_{b,14} + \beta_{b,2}\,(\triangle_{b,11}\,\triangle_{b,14} + \triangle_{b,12}\,\triangle_{b,24} + \triangle_{b,13}\,\triangle_{b,34} + \triangle_{b,14}\,\triangle_{b,44}) + \beta_{b,3}\,(\triangle_{b,14}\,(\triangle_{b,11}^2 + \triangle_{b,12}\,\triangle_{b,21} + \triangle_{b,13}\,\triangle_{b,31} + \triangle_{b,14}\,\triangle_{b,41}) + \triangle_{b,24}\,(\triangle_{b,11}\,\triangle_{b,12} + \triangle_{b,12}\,\triangle_{b,22} + \triangle_{b,13}\,\triangle_{b,32} + \triangle_{b,14}\,\triangle_{b,42}) +$
$\quad \triangle_{b,34}\,(\triangle_{b,11}\,\triangle_{b,13} + \triangle_{b,12}\,\triangle_{b,23} + \triangle_{b,13}\,\triangle_{b,33} + \triangle_{b,14}\,\triangle_{b,43}) + \triangle_{b,44}\,(\triangle_{b,11}\,\triangle_{b,14} + \triangle_{b,12}\,\triangle_{b,24} + \triangle_{b,13}\,\triangle_{b,34} + \triangle_{b,14}\,\triangle_{b,44})))\ +$
$(\beta_{a,0} + \beta_{a,1}\,\triangle_{a,32} + \beta_{a,2}\,(\triangle_{a,12}\,\triangle_{a,31} + \triangle_{a,22}\,\triangle_{a,32} + \triangle_{a,32}\,\triangle_{a,33} + \triangle_{a,34}\,\triangle_{a,42}) + \beta_{a,3}\,(\triangle_{a,12}\,(\triangle_{a,11}\,\triangle_{a,31} + \triangle_{a,21}\,\triangle_{a,32} + \triangle_{a,31}\,\triangle_{a,33} + \triangle_{a,34}\,\triangle_{a,41}) +$
$\quad \triangle_{a,22}\,(\triangle_{a,12}\,\triangle_{a,31} + \triangle_{a,22}\,\triangle_{a,32} + \triangle_{a,32}\,\triangle_{a,33} + \triangle_{a,34}\,\triangle_{a,42}) + \triangle_{a,32}\,(\triangle_{a,13}\,\triangle_{a,31} + \triangle_{a,23}\,\triangle_{a,32} + \triangle_{a,33}^2 + \triangle_{a,34}\,\triangle_{a,43}) + \triangle_{a,42}\,(\triangle_{a,14}\,\triangle_{a,31} + \triangle_{a,24}\,\triangle_{a,32} + \triangle_{a,33}\,\triangle_{a,34} + \triangle_{a,34}\,\triangle_{a,44})))$
$(\beta_{b,0} + \beta_{b,1}\,\triangle_{b,24} + \beta_{b,2}\,(\triangle_{b,14}\,\triangle_{b,21} + \triangle_{b,22}\,\triangle_{b,24} + \triangle_{b,23}\,\triangle_{b,34} + \triangle_{b,24}\,\triangle_{b,44}) + \beta_{b,3}\,(\triangle_{b,14}\,(\triangle_{b,11}\,\triangle_{b,21} + \triangle_{b,21}\,\triangle_{b,22} + \triangle_{b,23}\,\triangle_{b,31} + \triangle_{b,24}\,\triangle_{b,41}) +$
$\quad \triangle_{b,24}\,(\triangle_{b,12}\,\triangle_{b,21} + \triangle_{b,22}^2 + \triangle_{b,23}\,\triangle_{b,32} + \triangle_{b,24}\,\triangle_{b,42}) + \triangle_{b,34}\,(\triangle_{b,13}\,\triangle_{b,21} + \triangle_{b,22}\,\triangle_{b,23} + \triangle_{b,23}\,\triangle_{b,33} + \triangle_{b,24}\,\triangle_{b,43}) + \triangle_{b,44}\,(\triangle_{b,14}\,\triangle_{b,21} + \triangle_{b,22}\,\triangle_{b,24} + \triangle_{b,23}\,\triangle_{b,34} + \triangle_{b,24}\,\triangle_{b,44})))\ +$
$(\beta_{a,0} + \beta_{a,1}\,\triangle_{a,33} + \beta_{a,2}\,(\triangle_{a,13}\,\triangle_{a,31} + \triangle_{a,23}\,\triangle_{a,32} + \triangle_{a,33}^2 + \triangle_{a,34}\,\triangle_{a,43}) + \beta_{a,3}\,(\triangle_{a,13}\,(\triangle_{a,11}\,\triangle_{a,31} + \triangle_{a,21}\,\triangle_{a,32} + \triangle_{a,31}\,\triangle_{a,33} + \triangle_{a,34}\,\triangle_{a,41}) + \triangle_{a,23}\,(\triangle_{a,12}\,\triangle_{a,31} + \triangle_{a,22}\,\triangle_{a,32} + \triangle_{a,32}\,\triangle_{a,33} + \triangle_{a,34}\,\triangle_{a,42}) +$
$\quad \triangle_{a,33}\,(\triangle_{a,13}\,\triangle_{a,31} + \triangle_{a,23}\,\triangle_{a,32} + \triangle_{a,33}^2 + \triangle_{a,34}\,\triangle_{a,43}) + \triangle_{a,43}\,(\triangle_{a,14}\,\triangle_{a,31} + \triangle_{a,24}\,\triangle_{a,32} + \triangle_{a,33}\,\triangle_{a,34} + \triangle_{a,34}\,\triangle_{a,44})))$
$(\beta_{b,0} + \beta_{b,1}\,\triangle_{b,34} + \beta_{b,2}\,(\triangle_{b,14}\,\triangle_{b,31} + \triangle_{b,24}\,\triangle_{b,32} + \triangle_{b,33}\,\triangle_{b,34} + \triangle_{b,34}\,\triangle_{b,44}) + \beta_{b,3}\,(\triangle_{b,14}\,(\triangle_{b,11}\,\triangle_{b,31} + \triangle_{b,21}\,\triangle_{b,32} + \triangle_{b,31}\,\triangle_{b,33} + \triangle_{b,34}\,\triangle_{b,41}) +$
$\quad \triangle_{b,24}\,(\triangle_{b,12}\,\triangle_{b,31} + \triangle_{b,22}\,\triangle_{b,32} + \triangle_{b,32}\,\triangle_{b,33} + \triangle_{b,34}\,\triangle_{b,42}) + \triangle_{b,34}\,(\triangle_{b,13}\,\triangle_{b,31} + \triangle_{b,23}\,\triangle_{b,32} + \triangle_{b,33}^2 + \triangle_{b,34}\,\triangle_{b,43}) + \triangle_{b,44}\,(\triangle_{b,14}\,\triangle_{b,31} + \triangle_{b,24}\,\triangle_{b,32} + \triangle_{b,33}\,\triangle_{b,34} + \triangle_{b,34}\,\triangle_{b,44})))\ +$
$(\beta_{a,0} + \beta_{a,1}\,\triangle_{a,34} + \beta_{a,2}\,(\triangle_{a,14}\,\triangle_{a,31} + \triangle_{a,24}\,\triangle_{a,32} + \triangle_{a,33}\,\triangle_{a,34} + \triangle_{a,34}\,\triangle_{a,44}) + \beta_{a,3}\,(\triangle_{a,14}\,(\triangle_{a,11}\,\triangle_{a,31} + \triangle_{a,21}\,\triangle_{a,32} + \triangle_{a,31}\,\triangle_{a,33} + \triangle_{a,34}\,\triangle_{a,41}) +$
$\quad \triangle_{a,24}\,(\triangle_{a,12}\,\triangle_{a,31} + \triangle_{a,22}\,\triangle_{a,32} + \triangle_{a,32}\,\triangle_{a,33} + \triangle_{a,34}\,\triangle_{a,42}) + \triangle_{a,34}\,(\triangle_{a,13}\,\triangle_{a,31} + \triangle_{a,23}\,\triangle_{a,32} + \triangle_{a,33}^2 + \triangle_{a,34}\,\triangle_{a,43}) + \triangle_{a,44}\,(\triangle_{a,14}\,\triangle_{a,31} + \triangle_{a,24}\,\triangle_{a,32} + \triangle_{a,33}\,\triangle_{a,34} + \triangle_{a,34}\,\triangle_{a,44})))$
$(\beta_{b,0} + \beta_{b,1}\,\triangle_{b,44} + \beta_{b,2}\,(\triangle_{b,14}\,\triangle_{b,41} + \triangle_{b,24}\,\triangle_{b,42} + \triangle_{b,34}\,\triangle_{b,43} + \triangle_{b,44}^2) + \beta_{b,3}\,(\triangle_{b,14}\,(\triangle_{b,11}\,\triangle_{b,41} + \triangle_{b,21}\,\triangle_{b,42} + \triangle_{b,31}\,\triangle_{b,43} + \triangle_{b,41}\,\triangle_{b,44}) + \triangle_{b,24}\,(\triangle_{b,12}\,\triangle_{b,41} + \triangle_{b,22}\,\triangle_{b,42} + \triangle_{b,32}\,\triangle_{b,43} + \triangle_{b,42}\,\triangle_{b,44}) +$
$\quad \triangle_{b,34}\,(\triangle_{b,13}\,\triangle_{b,41} + \triangle_{b,23}\,\triangle_{b,42} + \triangle_{b,33}\,\triangle_{b,43} + \triangle_{b,43}\,\triangle_{b,44}) + \triangle_{b,44}\,(\triangle_{b,14}\,\triangle_{b,41} + \triangle_{b,24}\,\triangle_{b,42} + \triangle_{b,34}\,\triangle_{b,43} + \triangle_{b,44}^2)))$

$$T_{41} =$$

$$\big(\beta_{a,0} + \beta_{a,1}\triangle_{a,41} + \beta_{a,2}\left(\triangle_{a,11}\triangle_{a,41} + \triangle_{a,21}\triangle_{a,42} + \triangle_{a,31}\triangle_{a,43} + \triangle_{a,41}\triangle_{a,44}\right) + \beta_{a,3}\big(\triangle_{a,11}\left(\triangle_{a,11}\triangle_{a,41} + \triangle_{a,21}\triangle_{a,42} + \triangle_{a,31}\triangle_{a,43} + \triangle_{a,41}\triangle_{a,44}\right) +$$
$$\triangle_{a,21}\left(\triangle_{a,12}\triangle_{a,41} + \triangle_{a,22}\triangle_{a,42} + \triangle_{a,32}\triangle_{a,43} + \triangle_{a,42}\triangle_{a,44}\right) + \triangle_{a,31}\left(\triangle_{a,13}\triangle_{a,41} + \triangle_{a,23}\triangle_{a,42} + \triangle_{a,33}\triangle_{a,43} + \triangle_{a,43}\triangle_{a,44}\right) + \triangle_{a,41}\left(\triangle_{a,14}\triangle_{a,41} + \triangle_{a,24}\triangle_{a,42} + \triangle_{a,34}\triangle_{a,43} + \triangle_{a,44}^2\right)\big)\big)$$
$$\big(\beta_{b,0} + \beta_{b,1}\triangle_{b,11} + \beta_{b,2}\left(\triangle_{b,11}^2 + \triangle_{b,12}\triangle_{b,21} + \triangle_{b,13}\triangle_{b,31} + \triangle_{b,14}\triangle_{b,41}\right) + \beta_{b,3}\big(\triangle_{b,11}\left(\triangle_{b,11}^2 + \triangle_{b,12}\triangle_{b,21} + \triangle_{b,13}\triangle_{b,31} + \triangle_{b,14}\triangle_{b,41}\right) + \triangle_{b,21}\left(\triangle_{b,11}\triangle_{b,12} + \triangle_{b,12}\triangle_{b,22} + \triangle_{b,13}\triangle_{b,32} + \triangle_{b,14}\triangle_{b,42}\right) +$$
$$\triangle_{b,31}\left(\triangle_{b,11}\triangle_{b,13} + \triangle_{b,12}\triangle_{b,23} + \triangle_{b,13}\triangle_{b,33} + \triangle_{b,14}\triangle_{b,43}\right) + \triangle_{b,41}\left(\triangle_{b,11}\triangle_{b,14} + \triangle_{b,12}\triangle_{b,24} + \triangle_{b,13}\triangle_{b,34} + \triangle_{b,14}\triangle_{b,44}\right)\big)\big) +$$
$$\big(\beta_{a,0} + \beta_{a,1}\triangle_{a,42} + \beta_{a,2}\left(\triangle_{a,12}\triangle_{a,41} + \triangle_{a,22}\triangle_{a,42} + \triangle_{a,32}\triangle_{a,43} + \triangle_{a,42}\triangle_{a,44}\right) + \beta_{a,3}\big(\triangle_{a,12}\left(\triangle_{a,11}\triangle_{a,41} + \triangle_{a,21}\triangle_{a,42} + \triangle_{a,31}\triangle_{a,43} + \triangle_{a,41}\triangle_{a,44}\right) +$$
$$\triangle_{a,22}\left(\triangle_{a,12}\triangle_{a,41} + \triangle_{a,22}\triangle_{a,42} + \triangle_{a,32}\triangle_{a,43} + \triangle_{a,42}\triangle_{a,44}\right) + \triangle_{a,32}\left(\triangle_{a,13}\triangle_{a,41} + \triangle_{a,23}\triangle_{a,42} + \triangle_{a,33}\triangle_{a,43} + \triangle_{a,43}\triangle_{a,44}\right) + \triangle_{a,42}\left(\triangle_{a,14}\triangle_{a,41} + \triangle_{a,24}\triangle_{a,42} + \triangle_{a,34}\triangle_{a,43} + \triangle_{a,44}^2\right)\big)\big)$$
$$\big(\beta_{b,0} + \beta_{b,1}\triangle_{b,21} + \beta_{b,2}\left(\triangle_{b,11}\triangle_{b,21} + \triangle_{b,21}\triangle_{b,22} + \triangle_{b,23}\triangle_{b,31} + \triangle_{b,24}\triangle_{b,41}\right) + \beta_{b,3}\big(\triangle_{b,11}\left(\triangle_{b,11}\triangle_{b,21} + \triangle_{b,21}\triangle_{b,22} + \triangle_{b,23}\triangle_{b,31} + \triangle_{b,24}\triangle_{b,41}\right) +$$
$$\triangle_{b,21}\left(\triangle_{b,12}\triangle_{b,21} + \triangle_{b,22}^2 + \triangle_{b,23}\triangle_{b,32} + \triangle_{b,24}\triangle_{b,42}\right) + \triangle_{b,31}\left(\triangle_{b,13}\triangle_{b,21} + \triangle_{b,22}\triangle_{b,23} + \triangle_{b,23}\triangle_{b,33} + \triangle_{b,24}\triangle_{b,43}\right) + \triangle_{b,41}\left(\triangle_{b,14}\triangle_{b,21} + \triangle_{b,22}\triangle_{b,24} + \triangle_{b,23}\triangle_{b,34} + \triangle_{b,24}\triangle_{b,44}\right)\big)\big) +$$
$$\big(\beta_{a,0} + \beta_{a,1}\triangle_{a,43} + \beta_{a,2}\left(\triangle_{a,13}\triangle_{a,41} + \triangle_{a,23}\triangle_{a,42} + \triangle_{a,33}\triangle_{a,43} + \triangle_{a,43}\triangle_{a,44}\right) + \beta_{a,3}\big(\triangle_{a,13}\left(\triangle_{a,11}\triangle_{a,41} + \triangle_{a,21}\triangle_{a,42} + \triangle_{a,31}\triangle_{a,43} + \triangle_{a,41}\triangle_{a,44}\right) +$$
$$\triangle_{a,23}\left(\triangle_{a,12}\triangle_{a,41} + \triangle_{a,22}\triangle_{a,42} + \triangle_{a,32}\triangle_{a,43} + \triangle_{a,42}\triangle_{a,44}\right) + \triangle_{a,33}\left(\triangle_{a,13}\triangle_{a,41} + \triangle_{a,23}\triangle_{a,42} + \triangle_{a,33}\triangle_{a,43} + \triangle_{a,43}\triangle_{a,44}\right) + \triangle_{a,43}\left(\triangle_{a,14}\triangle_{a,41} + \triangle_{a,24}\triangle_{a,42} + \triangle_{a,34}\triangle_{a,43} + \triangle_{a,44}^2\right)\big)\big)$$
$$\big(\beta_{b,0} + \beta_{b,1}\triangle_{b,31} + \beta_{b,2}\left(\triangle_{b,11}\triangle_{b,31} + \triangle_{b,21}\triangle_{b,32} + \triangle_{b,31}\triangle_{b,33} + \triangle_{b,34}\triangle_{b,41}\right) + \beta_{b,3}\big(\triangle_{b,11}\left(\triangle_{b,11}\triangle_{b,31} + \triangle_{b,21}\triangle_{b,32} + \triangle_{b,31}\triangle_{b,33} + \triangle_{b,34}\triangle_{b,41}\right) +$$
$$\triangle_{b,21}\left(\triangle_{b,12}\triangle_{b,31} + \triangle_{b,22}\triangle_{b,32} + \triangle_{b,32}\triangle_{b,33} + \triangle_{b,34}\triangle_{b,42}\right) + \triangle_{b,31}\left(\triangle_{b,13}\triangle_{b,31} + \triangle_{b,23}\triangle_{b,32} + \triangle_{b,33}^2 + \triangle_{b,34}\triangle_{b,43}\right) + \triangle_{b,41}\left(\triangle_{b,14}\triangle_{b,31} + \triangle_{b,24}\triangle_{b,32} + \triangle_{b,33}\triangle_{b,34} + \triangle_{b,34}\triangle_{b,44}\right)\big)\big) +$$
$$\big(\beta_{a,0} + \beta_{a,1}\triangle_{a,44} + \beta_{a,2}\left(\triangle_{a,14}\triangle_{a,41} + \triangle_{a,24}\triangle_{a,42} + \triangle_{a,34}\triangle_{a,43} + \triangle_{a,44}^2\right) + \beta_{a,3}\big(\triangle_{a,14}\left(\triangle_{a,11}\triangle_{a,41} + \triangle_{a,21}\triangle_{a,42} + \triangle_{a,31}\triangle_{a,43} + \triangle_{a,41}\triangle_{a,44}\right) + \triangle_{a,24}\left(\triangle_{a,12}\triangle_{a,41} + \triangle_{a,22}\triangle_{a,42} + \triangle_{a,32}\triangle_{a,43} + \triangle_{a,42}\triangle_{a,44}\right) +$$
$$\triangle_{a,34}\left(\triangle_{a,13}\triangle_{a,41} + \triangle_{a,23}\triangle_{a,42} + \triangle_{a,33}\triangle_{a,43} + \triangle_{a,43}\triangle_{a,44}\right) + \triangle_{a,44}\left(\triangle_{a,14}\triangle_{a,41} + \triangle_{a,24}\triangle_{a,42} + \triangle_{a,34}\triangle_{a,43} + \triangle_{a,44}^2\right)\big)\big)$$
$$\big(\beta_{b,0} + \beta_{b,1}\triangle_{b,41} + \beta_{b,2}\left(\triangle_{b,11}\triangle_{b,41} + \triangle_{b,21}\triangle_{b,42} + \triangle_{b,31}\triangle_{b,43} + \triangle_{b,41}\triangle_{b,44}\right) + \beta_{b,3}\big(\triangle_{b,11}\left(\triangle_{b,11}\triangle_{b,41} + \triangle_{b,21}\triangle_{b,42} + \triangle_{b,31}\triangle_{b,43} + \triangle_{b,41}\triangle_{b,44}\right) +$$
$$\triangle_{b,21}\left(\triangle_{b,12}\triangle_{b,41} + \triangle_{b,22}\triangle_{b,42} + \triangle_{b,32}\triangle_{b,43} + \triangle_{b,42}\triangle_{b,44}\right) + \triangle_{b,31}\left(\triangle_{b,13}\triangle_{b,41} + \triangle_{b,23}\triangle_{b,42} + \triangle_{b,33}\triangle_{b,43} + \triangle_{b,43}\triangle_{b,44}\right) + \triangle_{b,41}\left(\triangle_{b,14}\triangle_{b,41} + \triangle_{b,24}\triangle_{b,42} + \triangle_{b,34}\triangle_{b,43} + \triangle_{b,44}^2\right)\big)\big)$$

$$T_{42} =$$

$$\big(\beta_{a,0} + \beta_{a,1}\triangle_{a,41} + \beta_{a,2}\left(\triangle_{a,11}\triangle_{a,41} + \triangle_{a,21}\triangle_{a,42} + \triangle_{a,31}\triangle_{a,43} + \triangle_{a,41}\triangle_{a,44}\right) + \beta_{a,3}\big(\triangle_{a,11}\left(\triangle_{a,11}\triangle_{a,41} + \triangle_{a,21}\triangle_{a,42} + \triangle_{a,31}\triangle_{a,43} + \triangle_{a,41}\triangle_{a,44}\right) +$$
$$\triangle_{a,21}\left(\triangle_{a,12}\triangle_{a,41} + \triangle_{a,22}\triangle_{a,42} + \triangle_{a,32}\triangle_{a,43} + \triangle_{a,42}\triangle_{a,44}\right) + \triangle_{a,31}\left(\triangle_{a,13}\triangle_{a,41} + \triangle_{a,23}\triangle_{a,42} + \triangle_{a,33}\triangle_{a,43} + \triangle_{a,43}\triangle_{a,44}\right) + \triangle_{a,41}\left(\triangle_{a,14}\triangle_{a,41} + \triangle_{a,24}\triangle_{a,42} + \triangle_{a,34}\triangle_{a,43} + \triangle_{a,44}^2\right)\big)\big)$$
$$\big(\beta_{b,0} + \beta_{b,1}\triangle_{b,12} + \beta_{b,2}\left(\triangle_{b,11}\triangle_{b,12} + \triangle_{b,12}\triangle_{b,22} + \triangle_{b,13}\triangle_{b,32} + \triangle_{b,14}\triangle_{b,42}\right) + \beta_{b,3}\big(\triangle_{b,12}\left(\triangle_{b,11}^2 + \triangle_{b,12}\triangle_{b,21} + \triangle_{b,13}\triangle_{b,31} + \triangle_{b,14}\triangle_{b,41}\right) + \triangle_{b,22}\left(\triangle_{b,11}\triangle_{b,12} + \triangle_{b,12}\triangle_{b,22} + \triangle_{b,13}\triangle_{b,32} + \triangle_{b,14}\triangle_{b,42}\right) +$$
$$\triangle_{b,32}\left(\triangle_{b,11}\triangle_{b,13} + \triangle_{b,12}\triangle_{b,23} + \triangle_{b,13}\triangle_{b,33} + \triangle_{b,14}\triangle_{b,43}\right) + \triangle_{b,42}\left(\triangle_{b,11}\triangle_{b,14} + \triangle_{b,12}\triangle_{b,24} + \triangle_{b,13}\triangle_{b,34} + \triangle_{b,14}\triangle_{b,44}\right)\big)\big) +$$
$$\big(\beta_{a,0} + \beta_{a,1}\triangle_{a,42} + \beta_{a,2}\left(\triangle_{a,12}\triangle_{a,41} + \triangle_{a,22}\triangle_{a,42} + \triangle_{a,32}\triangle_{a,43} + \triangle_{a,42}\triangle_{a,44}\right) + \beta_{a,3}\big(\triangle_{a,12}\left(\triangle_{a,11}\triangle_{a,41} + \triangle_{a,21}\triangle_{a,42} + \triangle_{a,31}\triangle_{a,43} + \triangle_{a,41}\triangle_{a,44}\right) +$$
$$\triangle_{a,22}\left(\triangle_{a,12}\triangle_{a,41} + \triangle_{a,22}\triangle_{a,42} + \triangle_{a,32}\triangle_{a,43} + \triangle_{a,42}\triangle_{a,44}\right) + \triangle_{a,32}\left(\triangle_{a,13}\triangle_{a,41} + \triangle_{a,23}\triangle_{a,42} + \triangle_{a,33}\triangle_{a,43} + \triangle_{a,43}\triangle_{a,44}\right) + \triangle_{a,42}\left(\triangle_{a,14}\triangle_{a,41} + \triangle_{a,24}\triangle_{a,42} + \triangle_{a,34}\triangle_{a,43} + \triangle_{a,44}^2\right)\big)\big)$$
$$\big(\beta_{b,0} + \beta_{b,1}\triangle_{b,22} + \beta_{b,2}\left(\triangle_{b,12}\triangle_{b,21} + \triangle_{b,22}^2 + \triangle_{b,23}\triangle_{b,32} + \triangle_{b,24}\triangle_{b,42}\right) + \beta_{b,3}\big(\triangle_{b,12}\left(\triangle_{b,11}\triangle_{b,21} + \triangle_{b,21}\triangle_{b,22} + \triangle_{b,23}\triangle_{b,31} + \triangle_{b,24}\triangle_{b,41}\right) + \triangle_{b,22}\left(\triangle_{b,12}\triangle_{b,21} + \triangle_{b,22}^2 + \triangle_{b,23}\triangle_{b,32} + \triangle_{b,24}\triangle_{b,42}\right) +$$
$$\triangle_{b,32}\left(\triangle_{b,13}\triangle_{b,21} + \triangle_{b,22}\triangle_{b,23} + \triangle_{b,23}\triangle_{b,33} + \triangle_{b,24}\triangle_{b,43}\right) + \triangle_{b,42}\left(\triangle_{b,14}\triangle_{b,21} + \triangle_{b,22}\triangle_{b,24} + \triangle_{b,23}\triangle_{b,34} + \triangle_{b,24}\triangle_{b,44}\right)\big)\big) +$$
$$\big(\beta_{a,0} + \beta_{a,1}\triangle_{a,43} + \beta_{a,2}\left(\triangle_{a,13}\triangle_{a,41} + \triangle_{a,23}\triangle_{a,42} + \triangle_{a,33}\triangle_{a,43} + \triangle_{a,43}\triangle_{a,44}\right) + \beta_{a,3}\big(\triangle_{a,13}\left(\triangle_{a,11}\triangle_{a,41} + \triangle_{a,21}\triangle_{a,42} + \triangle_{a,31}\triangle_{a,43} + \triangle_{a,41}\triangle_{a,44}\right) +$$
$$\triangle_{a,23}\left(\triangle_{a,12}\triangle_{a,41} + \triangle_{a,22}\triangle_{a,42} + \triangle_{a,32}\triangle_{a,43} + \triangle_{a,42}\triangle_{a,44}\right) + \triangle_{a,33}\left(\triangle_{a,13}\triangle_{a,41} + \triangle_{a,23}\triangle_{a,42} + \triangle_{a,33}\triangle_{a,43} + \triangle_{a,43}\triangle_{a,44}\right) + \triangle_{a,43}\left(\triangle_{a,14}\triangle_{a,41} + \triangle_{a,24}\triangle_{a,42} + \triangle_{a,34}\triangle_{a,43} + \triangle_{a,44}^2\right)\big)\big)$$
$$\big(\beta_{b,0} + \beta_{b,1}\triangle_{b,32} + \beta_{b,2}\left(\triangle_{b,12}\triangle_{b,31} + \triangle_{b,22}\triangle_{b,32} + \triangle_{b,32}\triangle_{b,33} + \triangle_{b,34}\triangle_{b,42}\right) + \beta_{b,3}\big(\triangle_{b,12}\left(\triangle_{b,11}\triangle_{b,31} + \triangle_{b,21}\triangle_{b,32} + \triangle_{b,31}\triangle_{b,33} + \triangle_{b,34}\triangle_{b,41}\right) +$$
$$\triangle_{b,22}\left(\triangle_{b,12}\triangle_{b,31} + \triangle_{b,22}\triangle_{b,32} + \triangle_{b,32}\triangle_{b,33} + \triangle_{b,34}\triangle_{b,42}\right) + \triangle_{b,32}\left(\triangle_{b,13}\triangle_{b,31} + \triangle_{b,23}\triangle_{b,32} + \triangle_{b,33}^2 + \triangle_{b,34}\triangle_{b,43}\right) + \triangle_{b,42}\left(\triangle_{b,14}\triangle_{b,31} + \triangle_{b,24}\triangle_{b,32} + \triangle_{b,33}\triangle_{b,34} + \triangle_{b,34}\triangle_{b,44}\right)\big)\big) +$$
$$\big(\beta_{a,0} + \beta_{a,1}\triangle_{a,44} + \beta_{a,2}\left(\triangle_{a,14}\triangle_{a,41} + \triangle_{a,24}\triangle_{a,42} + \triangle_{a,34}\triangle_{a,43} + \triangle_{a,44}^2\right) + \beta_{a,3}\big(\triangle_{a,14}\left(\triangle_{a,11}\triangle_{a,41} + \triangle_{a,21}\triangle_{a,42} + \triangle_{a,31}\triangle_{a,43} + \triangle_{a,41}\triangle_{a,44}\right) + \triangle_{a,24}\left(\triangle_{a,12}\triangle_{a,41} + \triangle_{a,22}\triangle_{a,42} + \triangle_{a,32}\triangle_{a,43} + \triangle_{a,42}\triangle_{a,44}\right) +$$
$$\triangle_{a,34}\left(\triangle_{a,13}\triangle_{a,41} + \triangle_{a,23}\triangle_{a,42} + \triangle_{a,33}\triangle_{a,43} + \triangle_{a,43}\triangle_{a,44}\right) + \triangle_{a,44}\left(\triangle_{a,14}\triangle_{a,41} + \triangle_{a,24}\triangle_{a,42} + \triangle_{a,34}\triangle_{a,43} + \triangle_{a,44}^2\right)\big)\big)$$
$$\big(\beta_{b,0} + \beta_{b,1}\triangle_{b,42} + \beta_{b,2}\left(\triangle_{b,12}\triangle_{b,41} + \triangle_{b,22}\triangle_{b,42} + \triangle_{b,32}\triangle_{b,43} + \triangle_{b,42}\triangle_{b,44}\right) + \beta_{b,3}\big(\triangle_{b,12}\left(\triangle_{b,11}\triangle_{b,41} + \triangle_{b,21}\triangle_{b,42} + \triangle_{b,31}\triangle_{b,43} + \triangle_{b,41}\triangle_{b,44}\right) +$$
$$\triangle_{b,22}\left(\triangle_{b,12}\triangle_{b,41} + \triangle_{b,22}\triangle_{b,42} + \triangle_{b,32}\triangle_{b,43} + \triangle_{b,42}\triangle_{b,44}\right) + \triangle_{b,32}\left(\triangle_{b,13}\triangle_{b,41} + \triangle_{b,23}\triangle_{b,42} + \triangle_{b,33}\triangle_{b,43} + \triangle_{b,43}\triangle_{b,44}\right) + \triangle_{b,42}\left(\triangle_{b,14}\triangle_{b,41} + \triangle_{b,24}\triangle_{b,42} + \triangle_{b,34}\triangle_{b,43} + \triangle_{b,44}^2\right)\big)\big)$$

$$T_{43} =$$

$$\left(\beta_{a,0} + \beta_{a,1}\,\triangle_{a,41} + \beta_{a,2}\,(\triangle_{a,11}\,\triangle_{a,41} + \triangle_{a,21}\,\triangle_{a,42} + \triangle_{a,31}\,\triangle_{a,43} + \triangle_{a,41}\,\triangle_{a,44}) + \beta_{a,3}\,(\triangle_{a,11}\,(\triangle_{a,11}\,\triangle_{a,41} + \triangle_{a,21}\,\triangle_{a,42} + \triangle_{a,31}\,\triangle_{a,43} + \triangle_{a,41}\,\triangle_{a,44}) + \right.$$
$$\left. \triangle_{a,21}\,(\triangle_{a,12}\,\triangle_{a,41} + \triangle_{a,22}\,\triangle_{a,42} + \triangle_{a,32}\,\triangle_{a,43} + \triangle_{a,42}\,\triangle_{a,44}) + \triangle_{a,31}\,(\triangle_{a,13}\,\triangle_{a,41} + \triangle_{a,23}\,\triangle_{a,42} + \triangle_{a,33}\,\triangle_{a,43} + \triangle_{a,43}\,\triangle_{a,44}) + \triangle_{a,41}\,(\triangle_{a,14}\,\triangle_{a,41} + \triangle_{a,24}\,\triangle_{a,42} + \triangle_{a,34}\,\triangle_{a,43} + \triangle_{a,44}^{2}))\right)$$
$$\left(\beta_{b,0} + \beta_{b,1}\,\triangle_{b,13} + \beta_{b,2}\,(\triangle_{b,11}\,\triangle_{b,13} + \triangle_{b,12}\,\triangle_{b,23} + \triangle_{b,13}\,\triangle_{b,33} + \triangle_{b,14}\,\triangle_{b,43}) + \beta_{b,3}\,(\triangle_{b,13}\,(\triangle_{b,11}^{2} + \triangle_{b,12}\,\triangle_{b,21} + \triangle_{b,13}\,\triangle_{b,31} + \triangle_{b,14}\,\triangle_{b,41}) + \triangle_{b,23}\,(\triangle_{b,11}\,\triangle_{b,12} + \triangle_{b,12}\,\triangle_{b,22} + \triangle_{b,13}\,\triangle_{b,32} + \triangle_{b,14}\,\triangle_{b,42}) + \right.$$
$$\left. \triangle_{b,33}\,(\triangle_{b,11}\,\triangle_{b,13} + \triangle_{b,12}\,\triangle_{b,23} + \triangle_{b,13}\,\triangle_{b,33} + \triangle_{b,14}\,\triangle_{b,43}) + \triangle_{b,43}\,(\triangle_{b,11}\,\triangle_{b,14} + \triangle_{b,12}\,\triangle_{b,24} + \triangle_{b,13}\,\triangle_{b,34} + \triangle_{b,14}\,\triangle_{b,44}))\right) +$$
$$\left(\beta_{a,0} + \beta_{a,1}\,\triangle_{a,42} + \beta_{a,2}\,(\triangle_{a,12}\,\triangle_{a,41} + \triangle_{a,22}\,\triangle_{a,42} + \triangle_{a,32}\,\triangle_{a,43} + \triangle_{a,42}\,\triangle_{a,44}) + \beta_{a,3}\,(\triangle_{a,12}\,(\triangle_{a,11}\,\triangle_{a,41} + \triangle_{a,21}\,\triangle_{a,42} + \triangle_{a,31}\,\triangle_{a,43} + \triangle_{a,41}\,\triangle_{a,44}) + \right.$$
$$\left. \triangle_{a,22}\,(\triangle_{a,12}\,\triangle_{a,41} + \triangle_{a,22}\,\triangle_{a,42} + \triangle_{a,32}\,\triangle_{a,43} + \triangle_{a,42}\,\triangle_{a,44}) + \triangle_{a,32}\,(\triangle_{a,13}\,\triangle_{a,41} + \triangle_{a,23}\,\triangle_{a,42} + \triangle_{a,33}\,\triangle_{a,43} + \triangle_{a,43}\,\triangle_{a,44}) + \triangle_{a,42}\,(\triangle_{a,14}\,\triangle_{a,41} + \triangle_{a,24}\,\triangle_{a,42} + \triangle_{a,34}\,\triangle_{a,43} + \triangle_{a,44}^{2}))\right)$$
$$\left(\beta_{b,0} + \beta_{b,1}\,\triangle_{b,23} + \beta_{b,2}\,(\triangle_{b,13}\,\triangle_{b,21} + \triangle_{b,22}\,\triangle_{b,23} + \triangle_{b,23}\,\triangle_{b,33} + \triangle_{b,24}\,\triangle_{b,43}) + \beta_{b,3}\,(\triangle_{b,13}\,(\triangle_{b,11}\,\triangle_{b,21} + \triangle_{b,21}\,\triangle_{b,22} + \triangle_{b,23}\,\triangle_{b,31} + \triangle_{b,24}\,\triangle_{b,41}) + \right.$$
$$\left. \triangle_{b,23}\,(\triangle_{b,12}\,\triangle_{b,21} + \triangle_{b,22}^{2} + \triangle_{b,23}\,\triangle_{b,32} + \triangle_{b,24}\,\triangle_{b,42}) + \triangle_{b,33}\,(\triangle_{b,13}\,\triangle_{b,21} + \triangle_{b,22}\,\triangle_{b,23} + \triangle_{b,23}\,\triangle_{b,33} + \triangle_{b,24}\,\triangle_{b,43}) + \triangle_{b,43}\,(\triangle_{b,14}\,\triangle_{b,21} + \triangle_{b,22}\,\triangle_{b,24} + \triangle_{b,23}\,\triangle_{b,34} + \triangle_{b,24}\,\triangle_{b,44}))\right) +$$
$$\left(\beta_{a,0} + \beta_{a,1}\,\triangle_{a,43} + \beta_{a,2}\,(\triangle_{a,13}\,\triangle_{a,41} + \triangle_{a,23}\,\triangle_{a,42} + \triangle_{a,33}\,\triangle_{a,43} + \triangle_{a,43}\,\triangle_{a,44}) + \beta_{a,3}\,(\triangle_{a,13}\,(\triangle_{a,11}\,\triangle_{a,41} + \triangle_{a,21}\,\triangle_{a,42} + \triangle_{a,31}\,\triangle_{a,43} + \triangle_{a,41}\,\triangle_{a,44}) + \right.$$
$$\left. \triangle_{a,23}\,(\triangle_{a,12}\,\triangle_{a,41} + \triangle_{a,22}\,\triangle_{a,42} + \triangle_{a,32}\,\triangle_{a,43} + \triangle_{a,42}\,\triangle_{a,44}) + \triangle_{a,33}\,(\triangle_{a,13}\,\triangle_{a,41} + \triangle_{a,23}\,\triangle_{a,42} + \triangle_{a,33}\,\triangle_{a,43} + \triangle_{a,43}\,\triangle_{a,44}) + \triangle_{a,43}\,(\triangle_{a,14}\,\triangle_{a,41} + \triangle_{a,24}\,\triangle_{a,42} + \triangle_{a,34}\,\triangle_{a,43} + \triangle_{a,44}^{2}))\right)$$
$$\left(\beta_{b,0} + \beta_{b,1}\,\triangle_{b,33} + \beta_{b,2}\,(\triangle_{b,13}\,\triangle_{b,31} + \triangle_{b,23}\,\triangle_{b,32} + \triangle_{b,33}^{2} + \triangle_{b,34}\,\triangle_{b,43}) + \beta_{b,3}\,(\triangle_{b,13}\,(\triangle_{b,11}\,\triangle_{b,31} + \triangle_{b,21}\,\triangle_{b,32} + \triangle_{b,31}\,\triangle_{b,33} + \triangle_{b,34}\,\triangle_{b,41}) + \triangle_{b,23}\,(\triangle_{b,12}\,\triangle_{b,31} + \triangle_{b,22}\,\triangle_{b,32} + \triangle_{b,32}\,\triangle_{b,33} + \triangle_{b,34}\,\triangle_{b,42}) + \right.$$
$$\left. \triangle_{b,33}\,(\triangle_{b,13}\,\triangle_{b,31} + \triangle_{b,23}\,\triangle_{b,32} + \triangle_{b,33}^{2} + \triangle_{b,34}\,\triangle_{b,43}) + \triangle_{b,43}\,(\triangle_{b,14}\,\triangle_{b,31} + \triangle_{b,24}\,\triangle_{b,32} + \triangle_{b,33}\,\triangle_{b,34} + \triangle_{b,34}\,\triangle_{b,44}))\right) +$$
$$\left(\beta_{a,0} + \beta_{a,1}\,\triangle_{a,44} + \beta_{a,2}\,(\triangle_{a,14}\,\triangle_{a,41} + \triangle_{a,24}\,\triangle_{a,42} + \triangle_{a,34}\,\triangle_{a,43} + \triangle_{a,44}^{2}) + \beta_{a,3}\,(\triangle_{a,14}\,(\triangle_{a,11}\,\triangle_{a,41} + \triangle_{a,21}\,\triangle_{a,42} + \triangle_{a,31}\,\triangle_{a,43} + \triangle_{a,41}\,\triangle_{a,44}) + \triangle_{a,24}\,(\triangle_{a,12}\,\triangle_{a,41} + \triangle_{a,22}\,\triangle_{a,42} + \triangle_{a,32}\,\triangle_{a,43} + \triangle_{a,42}\,\triangle_{a,44}) + \right.$$
$$\left. \triangle_{a,34}\,(\triangle_{a,13}\,\triangle_{a,41} + \triangle_{a,23}\,\triangle_{a,42} + \triangle_{a,33}\,\triangle_{a,43} + \triangle_{a,43}\,\triangle_{a,44}) + \triangle_{a,44}\,(\triangle_{a,14}\,\triangle_{a,41} + \triangle_{a,24}\,\triangle_{a,42} + \triangle_{a,34}\,\triangle_{a,43} + \triangle_{a,44}^{2}))\right)$$
$$\left(\beta_{b,0} + \beta_{b,1}\,\triangle_{b,43} + \beta_{b,2}\,(\triangle_{b,13}\,\triangle_{b,41} + \triangle_{b,23}\,\triangle_{b,42} + \triangle_{b,33}\,\triangle_{b,43} + \triangle_{b,43}\,\triangle_{b,44}) + \beta_{b,3}\,(\triangle_{b,13}\,(\triangle_{b,11}\,\triangle_{b,41} + \triangle_{b,21}\,\triangle_{b,42} + \triangle_{b,31}\,\triangle_{b,43} + \triangle_{b,41}\,\triangle_{b,44}) + \right.$$
$$\left. \triangle_{b,23}\,(\triangle_{b,12}\,\triangle_{b,41} + \triangle_{b,22}\,\triangle_{b,42} + \triangle_{b,32}\,\triangle_{b,43} + \triangle_{b,42}\,\triangle_{b,44}) + \triangle_{b,33}\,(\triangle_{b,13}\,\triangle_{b,41} + \triangle_{b,23}\,\triangle_{b,42} + \triangle_{b,33}\,\triangle_{b,43} + \triangle_{b,43}\,\triangle_{b,44}) + \triangle_{b,43}\,(\triangle_{b,14}\,\triangle_{b,41} + \triangle_{b,24}\,\triangle_{b,42} + \triangle_{b,34}\,\triangle_{b,43} + \triangle_{b,44}^{2}))\right)$$

$$T_{44} =$$

$$\left(\beta_{a,0} + \beta_{a,1}\,\triangle_{a,41} + \beta_{a,2}\,(\triangle_{a,11}\,\triangle_{a,41} + \triangle_{a,21}\,\triangle_{a,42} + \triangle_{a,31}\,\triangle_{a,43} + \triangle_{a,41}\,\triangle_{a,44}) + \beta_{a,3}\,(\triangle_{a,11}\,(\triangle_{a,11}\,\triangle_{a,41} + \triangle_{a,21}\,\triangle_{a,42} + \triangle_{a,31}\,\triangle_{a,43} + \triangle_{a,41}\,\triangle_{a,44}) + \right.$$
$$\left. \triangle_{a,21}\,(\triangle_{a,12}\,\triangle_{a,41} + \triangle_{a,22}\,\triangle_{a,42} + \triangle_{a,32}\,\triangle_{a,43} + \triangle_{a,42}\,\triangle_{a,44}) + \triangle_{a,31}\,(\triangle_{a,13}\,\triangle_{a,41} + \triangle_{a,23}\,\triangle_{a,42} + \triangle_{a,33}\,\triangle_{a,43} + \triangle_{a,43}\,\triangle_{a,44}) + \triangle_{a,41}\,(\triangle_{a,14}\,\triangle_{a,41} + \triangle_{a,24}\,\triangle_{a,42} + \triangle_{a,34}\,\triangle_{a,43} + \triangle_{a,44}^{2}))\right)$$
$$\left(\beta_{b,0} + \beta_{b,1}\,\triangle_{b,14} + \beta_{b,2}\,(\triangle_{b,11}\,\triangle_{b,14} + \triangle_{b,12}\,\triangle_{b,24} + \triangle_{b,13}\,\triangle_{b,34} + \triangle_{b,14}\,\triangle_{b,44}) + \beta_{b,3}\,(\triangle_{b,14}\,(\triangle_{b,11}^{2} + \triangle_{b,12}\,\triangle_{b,21} + \triangle_{b,13}\,\triangle_{b,31} + \triangle_{b,14}\,\triangle_{b,41}) + \triangle_{b,24}\,(\triangle_{b,11}\,\triangle_{b,12} + \triangle_{b,12}\,\triangle_{b,22} + \triangle_{b,13}\,\triangle_{b,32} + \triangle_{b,14}\,\triangle_{b,42}) + \right.$$
$$\left. \triangle_{b,34}\,(\triangle_{b,11}\,\triangle_{b,13} + \triangle_{b,12}\,\triangle_{b,23} + \triangle_{b,13}\,\triangle_{b,33} + \triangle_{b,14}\,\triangle_{b,43}) + \triangle_{b,44}\,(\triangle_{b,11}\,\triangle_{b,14} + \triangle_{b,12}\,\triangle_{b,24} + \triangle_{b,13}\,\triangle_{b,34} + \triangle_{b,14}\,\triangle_{b,44}))\right) +$$
$$\left(\beta_{a,0} + \beta_{a,1}\,\triangle_{a,42} + \beta_{a,2}\,(\triangle_{a,12}\,\triangle_{a,41} + \triangle_{a,22}\,\triangle_{a,42} + \triangle_{a,32}\,\triangle_{a,43} + \triangle_{a,42}\,\triangle_{a,44}) + \beta_{a,3}\,(\triangle_{a,12}\,(\triangle_{a,11}\,\triangle_{a,41} + \triangle_{a,21}\,\triangle_{a,42} + \triangle_{a,31}\,\triangle_{a,43} + \triangle_{a,41}\,\triangle_{a,44}) + \right.$$
$$\left. \triangle_{a,22}\,(\triangle_{a,12}\,\triangle_{a,41} + \triangle_{a,22}\,\triangle_{a,42} + \triangle_{a,32}\,\triangle_{a,43} + \triangle_{a,42}\,\triangle_{a,44}) + \triangle_{a,32}\,(\triangle_{a,13}\,\triangle_{a,41} + \triangle_{a,23}\,\triangle_{a,42} + \triangle_{a,33}\,\triangle_{a,43} + \triangle_{a,43}\,\triangle_{a,44}) + \triangle_{a,42}\,(\triangle_{a,14}\,\triangle_{a,41} + \triangle_{a,24}\,\triangle_{a,42} + \triangle_{a,34}\,\triangle_{a,43} + \triangle_{a,44}^{2}))\right)$$
$$\left(\beta_{b,0} + \beta_{b,1}\,\triangle_{b,24} + \beta_{b,2}\,(\triangle_{b,14}\,\triangle_{b,21} + \triangle_{b,22}\,\triangle_{b,24} + \triangle_{b,23}\,\triangle_{b,34} + \triangle_{b,24}\,\triangle_{b,44}) + \beta_{b,3}\,(\triangle_{b,14}\,(\triangle_{b,11}\,\triangle_{b,21} + \triangle_{b,21}\,\triangle_{b,22} + \triangle_{b,23}\,\triangle_{b,31} + \triangle_{b,24}\,\triangle_{b,41}) + \right.$$
$$\left. \triangle_{b,24}\,(\triangle_{b,12}\,\triangle_{b,21} + \triangle_{b,22}^{2} + \triangle_{b,23}\,\triangle_{b,32} + \triangle_{b,24}\,\triangle_{b,42}) + \triangle_{b,34}\,(\triangle_{b,13}\,\triangle_{b,21} + \triangle_{b,22}\,\triangle_{b,23} + \triangle_{b,23}\,\triangle_{b,33} + \triangle_{b,24}\,\triangle_{b,43}) + \triangle_{b,44}\,(\triangle_{b,14}\,\triangle_{b,21} + \triangle_{b,22}\,\triangle_{b,24} + \triangle_{b,23}\,\triangle_{b,34} + \triangle_{b,24}\,\triangle_{b,44}))\right) +$$
$$\left(\beta_{a,0} + \beta_{a,1}\,\triangle_{a,43} + \beta_{a,2}\,(\triangle_{a,13}\,\triangle_{a,41} + \triangle_{a,23}\,\triangle_{a,42} + \triangle_{a,33}\,\triangle_{a,43} + \triangle_{a,43}\,\triangle_{a,44}) + \beta_{a,3}\,(\triangle_{a,13}\,(\triangle_{a,11}\,\triangle_{a,41} + \triangle_{a,21}\,\triangle_{a,42} + \triangle_{a,31}\,\triangle_{a,43} + \triangle_{a,41}\,\triangle_{a,44}) + \right.$$
$$\left. \triangle_{a,23}\,(\triangle_{a,12}\,\triangle_{a,41} + \triangle_{a,22}\,\triangle_{a,42} + \triangle_{a,32}\,\triangle_{a,43} + \triangle_{a,42}\,\triangle_{a,44}) + \triangle_{a,33}\,(\triangle_{a,13}\,\triangle_{a,41} + \triangle_{a,23}\,\triangle_{a,42} + \triangle_{a,33}\,\triangle_{a,43} + \triangle_{a,43}\,\triangle_{a,44}) + \triangle_{a,43}\,(\triangle_{a,14}\,\triangle_{a,41} + \triangle_{a,24}\,\triangle_{a,42} + \triangle_{a,34}\,\triangle_{a,43} + \triangle_{a,44}^{2}))\right)$$
$$\left(\beta_{b,0} + \beta_{b,1}\,\triangle_{b,34} + \beta_{b,2}\,(\triangle_{b,14}\,\triangle_{b,31} + \triangle_{b,24}\,\triangle_{b,32} + \triangle_{b,33}\,\triangle_{b,34} + \triangle_{b,34}\,\triangle_{b,44}) + \beta_{b,3}\,(\triangle_{b,14}\,(\triangle_{b,11}\,\triangle_{b,31} + \triangle_{b,21}\,\triangle_{b,32} + \triangle_{b,31}\,\triangle_{b,33} + \triangle_{b,34}\,\triangle_{b,41}) + \right.$$
$$\left. \triangle_{b,24}\,(\triangle_{b,12}\,\triangle_{b,31} + \triangle_{b,22}\,\triangle_{b,32} + \triangle_{b,32}\,\triangle_{b,33} + \triangle_{b,34}\,\triangle_{b,42}) + \triangle_{b,34}\,(\triangle_{b,13}\,\triangle_{b,31} + \triangle_{b,23}\,\triangle_{b,32} + \triangle_{b,33}^{2} + \triangle_{b,34}\,\triangle_{b,43}) + \triangle_{b,44}\,(\triangle_{b,14}\,\triangle_{b,31} + \triangle_{b,24}\,\triangle_{b,32} + \triangle_{b,33}\,\triangle_{b,34} + \triangle_{b,34}\,\triangle_{b,44}))\right) +$$
$$\left(\beta_{a,0} + \beta_{a,1}\,\triangle_{a,44} + \beta_{a,2}\,(\triangle_{a,14}\,\triangle_{a,41} + \triangle_{a,24}\,\triangle_{a,42} + \triangle_{a,34}\,\triangle_{a,43} + \triangle_{a,44}^{2}) + \beta_{a,3}\,(\triangle_{a,14}\,(\triangle_{a,11}\,\triangle_{a,41} + \triangle_{a,21}\,\triangle_{a,42} + \triangle_{a,31}\,\triangle_{a,43} + \triangle_{a,41}\,\triangle_{a,44}) + \triangle_{a,24}\,(\triangle_{a,12}\,\triangle_{a,41} + \triangle_{a,22}\,\triangle_{a,42} + \triangle_{a,32}\,\triangle_{a,43} + \triangle_{a,42}\,\triangle_{a,44}) + \right.$$
$$\left. \triangle_{a,34}\,(\triangle_{a,13}\,\triangle_{a,41} + \triangle_{a,23}\,\triangle_{a,42} + \triangle_{a,33}\,\triangle_{a,43} + \triangle_{a,43}\,\triangle_{a,44}) + \triangle_{a,44}\,(\triangle_{a,14}\,\triangle_{a,41} + \triangle_{a,24}\,\triangle_{a,42} + \triangle_{a,34}\,\triangle_{a,43} + \triangle_{a,44}^{2}))\right)$$
$$\left(\beta_{b,0} + \beta_{b,1}\,\triangle_{b,44} + \beta_{b,2}\,(\triangle_{b,14}\,\triangle_{b,41} + \triangle_{b,24}\,\triangle_{b,42} + \triangle_{b,34}\,\triangle_{b,43} + \triangle_{b,44}^{2}) + \beta_{b,3}\,(\triangle_{b,14}\,(\triangle_{b,11}\,\triangle_{b,41} + \triangle_{b,21}\,\triangle_{b,42} + \triangle_{b,31}\,\triangle_{b,43} + \triangle_{b,41}\,\triangle_{b,44}) + \triangle_{b,24}\,(\triangle_{b,12}\,\triangle_{b,41} + \triangle_{b,22}\,\triangle_{b,42} + \triangle_{b,32}\,\triangle_{b,43} + \triangle_{b,42}\,\triangle_{b,44}) + \right.$$
$$\left. \triangle_{b,34}\,(\triangle_{b,13}\,\triangle_{b,41} + \triangle_{b,23}\,\triangle_{b,42} + \triangle_{b,33}\,\triangle_{b,43} + \triangle_{b,43}\,\triangle_{b,44}) + \triangle_{b,44}\,(\triangle_{b,14}\,\triangle_{b,41} + \triangle_{b,24}\,\triangle_{b,42} + \triangle_{b,34}\,\triangle_{b,43} + \triangle_{b,44}^{2}))\right)$$

REFERENCES

[1]   J. B. Pendry, Physics 45, 191 (2004).

[2]   N.A. Spaldin, S. Cheong, R. Ramesh, "Physics today, October (2010).

[3]   D. W. Ward, E. Statz, K. J. Webb, and K. A. Nelson arXiv:cond-mat/0401046, (2004).

[4]   V. G. Veselago, Soviet Physics USPEKHI 10, 509 (1968).

[5]   R.A. Shelby, D.R. Smith, and S. Schultz, Science 292, 77-79 (2001).

[6]   F. Capolino, "Theory and Phenomana of Metamaterials", CRC Press: Boca Raton, Florida, (2009).

[7]   M. Wegener,S. Linden, Physics Today 63/10 (2010).

[8]   C. W. Nan et al., J. App. Phys. 103, 031101 (2008).

[9]   M. Vopsaroiu, J. Blackburn, M. Cain, J. Phys. D: Appl. Phys. 40 (2007).

[10]   W. Eerenstein, N.D. Mathur, J.F. Scott, Nature 442/7104 (2006).

[11]   I. E. Dzyaloshinskii, Soviet Phys. JETP 10, 628 (1960).

[12]   T. Kimura, T. Goto, H. Shintani, K. Ishizaka, T. Arima, Y. Tokura, Nature 426 (2003).

[13]   B. Lorenz, ISRN Condensed Matter Physics 2013, 497073 (2013).

[14]   D. Berreman, J. Opt. Soc. Am. 62, 502 (1972).

[15]   R. Azzam " Ellipsometry and Polarized Light," North Holland Publishing Company: Amsterdam, Netherlands, (1977).

[16]   P. D. Rogers, T. D. Kang, T. Zhou, M. Kotelyanskii, and A. A. Sirenko, Thin Solid Films, 519 (2011).

[17]   P. D. Rogers "Analysis of Mueller Matricies of Metamaterials and Multiferroics," PhD Dissertation, May (2011), NJIT.

[18]   P. Yeh, J. Opt. Soc. Am., Vol.69, No. 5, (1979).

[19]   M. Schubert, JOSA A, Vol. 15, Issue 10, 2769-2782 (1998).

[20]   J.-P. Rivera, Eur. Phys. J. B 71 (3), 299-313 (2009).

[21]   T. H. O'Dell, "The Electrodynamics of Magneto-Electric Media", North Holland: Amsterdam, Netherlands, (1970).

[22]   N. Kida, Y. Tokura, J. Mag. Mag. Mat. 324, 3512 (2012).

[23]   N. A. Spaldin and M. Fiebig, Science, 309, 391 (2005).

[24]   N. Hur, S. Park, P. A. Sharma, S. Guha, S-W. Cheong, Phys. Rev. Lett. 93, 207 (2004).

[25] H. Wohler, M. Fritsch, G. Haas, and D. A. Mlynski, J.Opt. Soc.Am. A 5, 1554, (1988).

[26] M. Abramowitz, I. Stegun, "Handbook of Mathematical Functions with Formulas, Graphs, and Mathematical Tables", Dover Publications: New York, NY (1972).

[27] H. Schmid, Ferroelectrics, 162, 317 (1994).

[28] C.W. Nan, M.I. Bichurin, S. Dong, D. Viehland, G. Srinivasan, J. Appl. Phys. 103, 031101 (2008).

[29] C.A.F. Vaz, J. Hoffman, C.H. Ahn, R. Ramesh, Adv. Mater. 22, 2900 (2010).

[30] B.G. Ueland, J.W. Lynn, M. Laver, Y.J. Choi, S.W. Cheong, Phys. Rev. Lett. 104, 147204 (2010).

[31] T. Goto, T. Kimura, G. Lawes, A. P. Ramirez, and Y. Tokura, Phys. Rev. Lett. 92, 257201(2004).

[32] Y. Tokunaga, N. Furukawa1, Hideaki Sakai, Y. Taguchi, T. Arima, and Y. Tokura1, Nature Materials 8, 558 (2009).

[33] T. Arima, Spin-Driven, J. Phys. Soc. Jpn. 80 (2011).

[34] W. S. Weiglhofer and A. Lakhtakia, SPIE Optical Engineering Press: Bellingham, Washington, (2003).

[35] Y. Takahashi, R. Shimano, Y. Kaneko, H. Murakawa, and Y. Tokura, Nature Physics 8, 121–125 (2012).

[36] S. Miyahara, and N. Furukawa, J. Phys. Soc. Jpn. 81, 023712 (2012).

[37] T. Arima, J. Phys.: Condens. Matter 20 434211 (2008).

[38] D. E. Aspnes, ''The accurate determination of optical properties by ellipsometry,'' in Handbook of Optical Constants of Solids, E. D. Palik, ed. Academic Press, Inc: New York, NY, (1985).

[39] M. Schubert, Theory and Application of Generalized Ellipsometry, Chapter 9 in "Handbook of Ellipsometry, edited by G. Irene and H. Tompkins" Noyes: Park Ridge, NJ, (2004).

[40] G. E. Jellison, Jr., Thin Solid Films 313-314, 33–39 (1998).

[41] U. Rossow and W. Richter, "Spectroscopic Ellipsometry", in Optical Characterization of Epitaxial Semiconductor Layers, Eds. G. Bauer and W. Richter, Springer (1996).

[42] H. Fujiwara, "Spectroscopic Ellipsometry: Principles and Applications" John Wiley & Sons: Tokyo, Japan (2007).

[43] T. Hofmann, U. Schade, C. M. Herzinger, P. Esquinazi, and M. Schubert, SPIE Vol.6120, 61200D (2006).

[44] T. Hofmann, C. M. Herzinger, A. Boosalis, T. E. Tiwald, J. A. Woollam, and M. Schubert, Rev. Sci. Instrum. 81, 023101 (2010).

[45] A. Röseler, "Infrared Spectroscopic Ellipsometry", Akademie: Berlin, (1992).

[46] M. Schubert, B. Rheinla¨nder, B. Johs, C. M. Herzinger, and J. A. Woollam, J. Opt. Soc. Am. A 13, 875–883 (1996).

[47] M. Schubert, T. E. Tiwald, and J. A. Woollam, Appl. Opt. 38, 177–187 (1999).

[48] M. Schubert, Phys. Rev. B 53, 4265–4274 (1996).

[49] T. E. Tiwald and M. Schubert, Optical Diagnostic Methods For Inorganic Materials II, L. M. Hanssen, ed., Proc. SPIE 4103, 19–29 (2000).

[50] M. Schubert, Another century of ellipsometry , Annalen der Physik 15, 480-497 (2006).

[51] M. Schubert, A. Kasic, T. Hofmann, V. Gottschalch, J. Off, F. Scholz, E. Schubert, H. Neumann, I. Hodgkinson, M. Arnold, W. Dollase, and C. M. Herzinger, SPIE Vol. 4806, 264 (2002).

[52] T. D. Kang, E. Standard, G. L. Carr, T. Zhou, M. Kotelyanskii, and A. A. Sirenko, Thin Solid Films, 519,2698(2011).

[53] M. Schubert, T. Hofmann, and C. M. Herzinger, J. Opt. Soc. Am. A, 20, No. 2 (2003).

[54] T. N. Stanislavchuk, T. D. Kang, P. D. Rogers, E. C. Standard, R. Basistyy, A. M. Kotelyanskii, G. Nita, T. Zhou, G. L. Carr, M. Kotelyanskii, and A. A. Sirenko, Rev. Sci. Instr. (2012).

[55] http://web.njit.edu/~sirenko/EllipsNJIT/index1.htm (accessed on 12/1/2014)

[56] http://www.nsls.bnl.gov/beamlines/beamline.asp?blid=U4IR (accessed on 12/1/2014)

[57] A. Pimenov, A. A. Mukhin, V. Yu. Ivanov, V. D. Travkin, A. M. Balbashov, and A. Loidl, Nat. Phys. 2, 97 (2006).

[58] A. Pimenov, A. Shuvaev, A. Loidl, F. Schrettle, A. A. Mukhin, V. D.Travkin, V. Yu. Ivanov, and A. M. Balbashov, Phys. Rev. Lett. 102, 107203 (2009).

[59] R. Schleck, R. L. Moreira, H. Sakata, and R. P. S. M. Lobo, Phys. Rev. B 82, 144309 (2010).

[60] A. Cano, Phys. Rev. B 80(18), 180416 (2009).

[61] R. Basistyy, T.N. Stanislavchuk, A.A. Sirenko, A.P. Litvinchuk, M. Kotelyanskii, G.L. Carr, N. Lee, X. Wang, S-W Cheong, Physical Review B 90, 024307 (2014).

[62] J. A. Alonso, M. J. Martinez-Lope, M. T. Casais, and M. T. Fernandez-Diaz, Inorg. Chem. 39, 917 (2000).

[63] J.-S. Zhou, J. B. Goodenough, J. M. Gallardo-Amores, E. Moran, M. A. Alario-Franco, R. Caudillo,   Phys. Rev. B 74, 014422 (2006).

[64] S. Petit, F. Moussa, M. Hennion, S. Pailhès, L. Pinsard-Gaudart, and A. Ivanov, Phys. Rev. Lett. 99, 266604 (2007).

[65] H. Katsura, N. Nagaosa, A. V. Balatsky, Phys. Rev. Lett. 95, 057205 (2005).

[66] I. A. Sergienko and E. Dagotto, Phys. Rev. B 73, 094434 (2006).

[67] M. Mostovoy, Phys. Rev. Lett. 96, 067601 (2006).

[68] Y. Tokura, J. Magn. Magn. Mat. 310, 1145 (2007).

[69] C. Kadlec, V. Goian, K. Z. Rushchanskii, P. Kužel, M. Ležaič, K. Kohn, R. V. Pisarev, and S. Kamba, Phys. Rev. B 84, 174120 (2011).

[70] D. Talbayev, A. D. LaForge, S. A. Trugman, N. Hur, A. J. Taylor, R. D. Averitt, D. N. Basov, Phys. Rev. Lett. 101, 247601 (2008).

[71] S. C. Abrahams, Acta Crystallogr., Sect. B: Struct. Sci. 57, 485 (2001).

[72] V. Goian, S. Kamba, C. Kadlec, D. Nuzhnyy, P. Kužel, J. Agostinho Moreira, A. Almeida, and P.B. Tavares, Phase Transitions 83, 931 (2010).

[73] M. N. Iliev, H.-G. Lee, V. N. Popov, M. V. Abrashev, A. Hamed, R. L. Meng, and C. W. Chu, Phys. Rev. B 56, 2488 (1997).

[74] I. Munawar and S. H. Curnoe, J. Phys.: Condens. Matter 18, 9575 (2006).

[75] S. H. Kim, S. H. Lee, T. H. Kim, T. Zyung, Y. H. Jeong, and M.S. Jang, Cryst. Res. Technol. 35, 19 (2000).

[76] H. Fukumura, S. Matsui, H. Harima, K. Kisoda, T. Takahashi, T. Yoshimura, and N. Fujimura, J. Phys. Condens. Matter 19, 365239 (2007).

[77] L. Martin-Carron and A. de Andres, Phys. Rev. Lett. 92, 175501 (2004).

[78] L Martín-Carrón, A de Andrés, M.J Martínez-Lope, M.T Casais, J.A Alonso, J. Alloys Compd 323, 494 (2001).

[79] H. Fukumura, N. Hasuike, H. Harima, K. Kisoda, K. Fukae, T. Takahashi, T. Yoshimura and N. Fujimura, Journal of Physics: Conference Series 92, 012126 (2007).

[80] H. Fukumura, N. Hasuike, H. Harima, K. Kisoda, K. Fukae, T. Yoshimura and N. Fujimura, J. Phys. Condens. Matter 21, 064218 (2009).

[81] J. Liu, C. Toulouse, P. Rovillain, M. Cazayous, Y. Gallais, M-A. Measson, N. Lee, S. W. Cheong, and A. Sacuto, Phys. Rev. B 86, 184410 (2012).

[82] A. Ghosh, J.Sahu, S. Venkataprasad Bhat, C.N.R. Rao, Solid State Sciences 11, 1639 (2009).

[83] J. Vermette, S. Jandl, A. A. Mukhin, V. Yu. Ivanov, A. Balbashov, M. M. Gospodinov and L. Pinsard-Gaudart, J. Phys.: Condens. Matter 22, 356002 (2010).

[84] A.P. Litvinchuk, M. N. Iliev, V. N. Popov and M. M. Gospodinov, J. Phys.: Condens. Matter 16, 809 (2004).

[85] N. Hien, X. Chen, L. Hoang, D. Lee, S.-Y. Jang, T. W. Noh and In-Sang Yang, J. Raman Spectrosc. 41, 983 (2010).

[86] N. Hien, S. Oh, X. Chen, D. Lee, S.-Y. Jang, T. W. Noh and I. Yang, J. Raman Spectrosc. 42, 1774 (2011).

[87] X. Chen, N. Hien, D. Lee, S-Y. Jang, T. W. Noh and Yang, New Journal of Physics 12, 073046 (2010).

[88] J. Vermette, S. Jandl and M. M. Gospodinov, J. Phys.: Condense. Matter 20, 425219 (2008).

[89] M. Zaghrioui, V. Ta Phuoc, R. A. Souza, and M. Gervais, Phys. Rev. B 78, 184305 (2008).

[90] B. Souchkov, J. R. Simpson, M. Quijada, H. Ishibashi, N. Hur, J. S. Ahn, S.W. Cheong, A. J. Millis, and H. D. Drew, Phys. Rev. Lett. 91, 027203 (2003).

[91] S. Lou, F. Zimmermann, R. Bartynski, N. Hur, and S.-W.Cheong, Phys. Rev. B 79, 214301 (2009).

[92] J. M. Wesselinowa and St. Kovachev, J. Phys.: Condens. Matter 19, 386218 (2007).

[93] St. Kovachev and J. M. Wesselinowa, J. Phys.: Condens. Matter 22, 255901 (2010).

[94] A. Prikockytė, D. Bilc, P. Hermet, C. Dubourdieu, and P. Ghosez, Phys. Rev. B 84, 214301 (2011).

[95] J. Varignon, S. Petit, and M.Lepetit, arXiv:1203.1752v1 8 March (2012).

[96] E. F. Bertaut and M. Mercier, Phys. Lett. 5, 27 (1963).

[97] P. A. Sharma, J. S. Ahn, N. Hur, S. Park, S.Kim, S. Lee, J.-G. Park, S. Guha, and S-W. Cheong, Phys. Rev. Lett. 93, 177202 (2004).

[98] S. G. Condran and M. L. Plumer, J. Phys. Condens. Matter 22, 162201 (2010).

[99] B. Lorenz, A.P. Litvinchuk, M.M. Gospodinov, and C.W. Chu. Phys. Rev. Lett. 92, 087204 (2004).

[100] B. Lorenz, F. Yen, M. M. Gospodinov, and C. W. Chu, Phys. Rev. B 71, 014438 (2005).

[101] A. Munoz, J. A. Alonso, M. J. Martinez-Lope, M. T. Casais, J. L. Martinez, and M. T. Fernandez-Diaz, Chem. Mater. 13, 1497 (2001).

[102] T. Lonkai, D. Hohlwein, J. Ihringer, and W. Prandl, Appl. Phys. A 74, S843 (2002).

[103] M. Fiebig, D. Frohlich, K. Kohn, S. Leute, T. Lottermoser, V.V. Pavlov, and R.V. Pisarev, Phys. Rev. Lett. 84, 5620 (2000).

[104] M. Fiebig, D. Frohlich, T. Lottermoser, and K. Kohn, Appl. Phys. Lett. 77, 4401 (2000).

[105] M. Fiebig, C. Degenhardt, and R.V. Pisarev, J. Appl. Phys. 91, 8867 (2002).

[106] M. Fiebig, D. Frohlich, T. Lottermoser, and M. Maat, Phys. Rev. B 66, 144102 (2002).

[107] B. G. Ueland, J. W. Lynn, M. Laver, Y. J. Choi, and S.-W. Cheong, Phys. Rev. Lett. 104, 147204 (2010).

[108] X. Fabrèges, I. Mirebeau, P. Bonville, S. Petit, G. Lebras-Jasmin, A. Forget, G. André, and S. Pailhès, Phys. Rev. B 78, 214422 (2008).

[109] H. A. Salama, and G. A. Stewart,J. Phys.: Condens. Matter 21, 386001 (2009).

[110] Y. Geng, N. Lee, Y. J. Choi, S-W. Cheong, W. Wu, Nano Lett. (accepted for publication Nov. 2012); arXiv:1201.0694v1.

[111] T. Moriya, Physical Review 120, 91 (1960).

[112] E. Standard, T. Stanislavchuk,A. Sirenko, N. Lee, S-W. Cheong, Phys. Rev. B 85, 144422 (2012).

[113] G.D. Gale, J. Chem. Soc. Faraday Trans. 93, 629 (1997).

[114] V.N. Popov, J. Phys.: Cond. Matter 7, 1625 (1995).

[115] M. N. Iliev, M. V. Abrashev, A. P. Litvinchuk, V.G. Hadjiev, H. Guo, and A. Gupta, Phys. Rev. B 75, 104118 (2007).

[116] G. E. Jellison, Jr. and J. S. Baba, J. Opt. Soc. Am. A 23, 468 (2006).

[117] P. D. Rogers, T. D. Kang, T. Zhou, M. Kotelyanskii, and A. A. Sirenko, Thin Solid Films, 519, 2668 (2011).

[118] J. Ménéndez and M. Cardona , Phys. Rev. B 29, 2051 (1984).

[119] A.P. Litvinchuk, J. Magn and Magn. Mat. 321, 2373 (2009).

[120] T. Penney, P. Berger, and K. Kritiyakirana,J. Appl. Phys. 40, 1234 (1969).

[121] J. Oh, M.Le, J. Jeong, J. Lee, H. Woo, W.-Y. Song, T. G. Perring, W. J. L. Buyers, S.-W. Cheong, and Je-Geun Park, Phys. Rev. Lett. 111, 257202 (2013).

[122] Y. J. Choi, N. Lee, P. A. Sharma, S. B. Kim, O. P. Vajk, J.W. Lynn, Y. S. Oh, and S-W. Cheong, Phys. Rev. Lett. 110, 157202 (2013).

[123] S. L. Shmakov, Int. J. of Pure and Applied Math., Volume 71 No. 2 2011, 251-259